Generalized Time-Frequency Representations and their Application to Quantum Control

by

André Marius Smit

Dissertation presented for the degree of Doctor of Philosophy
in the Faculty of Science, Department of Physics at
Stellenbosch University.

Pectora roborant cultus recti

Promoter: Dr. Hermann Uys

Co-promoter: Prof. Dr. Erich G. Rohwer

December 2015

DECLARATION

By submitting this thesis/dissertation electronically, I declare that the entirety of the work contained therein is my own, original work, that I am the sole author thereof (save to the extent explicitly otherwise stated), that reproduction and publication thereof by Stellenbosch University will not infringe any third party rights and that I have not previously in its entirety or in part submitted it for obtaining any qualification.

December 2015

Copyright © 2015 Stellenbosch University
All rights reserved

Abstract

We present here a new generalized Time-Frequency-Represenation (TFR) for use in describing ultra-fast laser pulses. The TFR is developed in terms of Fourier-Hermite-Gauss (FHG) polynomials on a von Neumann TFR lattice, by expanding the lattice in a third dimension, thus forming a lattice cube. The temporal and spectral coefficients of the Hermite-Gauss (HG) clearly are inherently functionally Fourier transform invariant. The enhanced numerical complexity of the FHG TFR is greatly reduced by exploiting the translation property of Hermite polynomials by means of Pascal matrices. Although the new FHG TFR represents an over complete basis set, it can be reduced by a subset selection to a complete basis. This method and the accompanying overlap integral is then developed and the complex orthogonality and similarity of the temporal and spectral overlap integral matrices is then analytically proved.

Numerically the Pascal matrices are unstable. The new two correlation FHG TFR lattice cubes present an improvement on the traditional TFRs in that they have the advantage that it is unnecessary to compute the undesirable inverse overlap matrix to reconstruct the signal, temporally and spectrally, i.e. they contain all the information necessary to reconstruct the signal. It is then proven that it is a digital requirement to double the original proposed bandwidths of the signal inputs, here and also for the von Neumann TFR.

The Hermite-Gauss polynomials correspond to the number states $\{n_{\mathbf{k}}\}$ of the Glauber-Sudarshan coherent states in Fock space. A classical correspondence analogy between Glauber-Sudarshan coherent states in Fock space and the temporal FHG TFR is then considered under certain conditions and thus allows for a comparison of the amplitudes between the two decompositions for each $\|\mathbf{k}\| = \omega_{\mathbf{k}}/c$, culminating in an optimization procedure to determine a “classical” coherent state correlation TFR. Application simulation results of quantum coherent control of IR ultra-short laser pulse interaction with octahedral molecules utilizing an optimal genetic algorithm are presented. A representative shaped laser pulse is used throughout to compare various TFRs.

Keywords: Coherent Quantum Control, Adaptive Feedback Control, Time-Frequency Representations, Ultrashort Laser Pulses, Spatial Light Modulator, Multilevel Molecules, von Neumann TFR, Anharmonic Rovibrational Levels, Genetic Algorithms

82. 53. Kp, 42. 55. -f, 31. 15. xv

Abstrak

Hier bied ons aan ’n nuwe veralgemende Tyd-Frekwensie-Voorstelling (TFV) vir die gebruik in die beskrywing van ultra-vinnige laser pulse. Die TFV word ontwikkel in terme van Fourier-Hermite-Gauss (FHG) polinome op ’n von Neumann TFV diskrete rooster, deur die normale rooster uit te brei in ’n derde dimensie, om ’n kubus rooster te vorm. Die temporale en spektrale koëffisiënte van die Hermite-Gauss (HG) polinome is duidelik inherent funksioneel Fourier transform invariant. Die verhoogde numeriese kompleksiteit van die FHG TFV word aansienlik verminder deur die ontginning van die translasie eienskap van Hermitiese polinome, deur gebruik te maak van Pascal matrikse. Hoewel die nuwe FHG TFV ’n oor volledige basis voorstel, kan dit deur ’n deelversameling selektief verminder word tot ’n volledige basis. Hierdie metode en die gepaardgaande oorvleuelings integrale word dan ontwikkel en die komplekse ortogonaliteit en similartieit van die temporale en spektrale oorvleueling integrale matrikse word dan analities bewys.

Numeries is die Pascal matrikse onstabiel. Die nuwe twee korrelasie FHG TFR kubus roosters bied ’n verbetering op die tradisionele TFV in dat hulle die voordeel inhou dat dit onnodig is om die ongewenste omgekeerde oorvleuelings matriks te bereken om die sein te herkonstrueer, temporaal en spektraal, d.w.s. dit bevat al die nodige inligting om die sein te herkonstrueer. Daar word dan bewys dat dit ’n digitale vereiste is om die oorspronklike voorgestelde bandwydtes van die sein insette te verdubbel, hier en ook vir die von Neumann TFV.

Die Hermite-Gauss polinome stem ooreen met die aantal getal toestande $\{n_{\mathbf{k}}\}$ van die Glauber-Sudarshan koherente toestande in die Fock ruimte. ’n Analogie tussen Glauber-Sudarshan koherente toestande in Fock ruimte en die temporale FHG TFV word dan beskou onder sekere omstandighede om gevolglik ’n vergelyking van die amplitudes tussen die twee ontbindings vir elke $\|\mathbf{k}\| = \omega_{\mathbf{k}}/c$, wat uiteindelik kulmineer in ’n optimalisering proses om ’n “klasieke” koherente toestand korrelasie TFV te bepaal. Simulasie resultate van ’n toepassing van kwantum koherente toestand beheer van IR ultra-kort laser pulse se interaksie met oktahedriese molekules, deur gebruik te maak van ’n optimale genetiese algoritme, word dan aangebied. ’n Verteenwoordigende gevormde laser puls word deurgaans gebruik om verskeie TFVs te vergelyk.

Sleutelwoorde: Koherente Kwantum Beheer, Aanpasbare Terugvoer Beheerlusse, Tyd-Frekwensie-Voorstelling, Ultra Kort Laser Pulse, Ruimtelike Lig Modulator, Multivlak Molekules, von Neumann TFV, Anharmonise Rovibrasionele Vlakke, Genetiese Algoritmes

82. 53. Kp, 42. 55. -f, 31. 15. xv

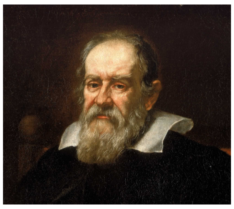

Mathematics is the Language with which God has written the Universe
Galileo Galilei

The True Logic of this World is in the Calculus of Probabilities
James Clerk Maxwell

Dedication

In memory of my parents, Sydney and Joey, my brother, Ethan, my twin daughters, Katlyn and Robyn, my daughter Rosemary, and my friend Lourens.

* * *

For the love of my daughters Celeste and Michelle

Deo Gloria

Contents

Declaration **II**

Abstract **III**

Abstrak **IV**

Dedication **VI**

Contents **i**

List of Figures **vii**

List of Tables **xi**

Foreword **1**

1. Introduction **7**
- 1.1. Quantum Control . . . 8
- 1.2. Quantum Coherent Control . . . 14
- 1.3. Dirac-Liouville-von Neumann Equation . . . 16
- 1.4. Octahedral Molecules . . . 17
  - 1.4.1. Irreducible Representations of Point Groups . . . 18
  - 1.4.2. Classification of irreducible representations . . . 18
  - 1.4.3. Character tables of point groups . . . 19
  - 1.4.4. XY_6 IR Active Transition Frequencies . . . 21
  - 1.4.5. XY_6 Dipole Moments . . . 24
- 1.5. Spatial Light Modulator . . . 28
- 1.6. Introduction to Time Frequency Representations . . . 30
- 1.7. Overview of the Thesis . . . 32

2. Time Frequency Representations **35**
- 2.1. Introduction . . . 35
- 2.2. Signal Localization . . . 36
- 2.3. Heisenberg-Gabor Inequality . . . 37

2.4. Analytical Signals 38
2.5. The Short-time Fourier Transform 40
2.6. Gabor TFR 42
2.7. Spectrogram 44
    2.7.1. Time-frequency Resolution 45
    2.7.2. Discrete Time-Frequency Representations 46
    2.7.3. The Short-Frequency Time Transform. 47
    2.7.4. Characteristic Function. 48
2.8. Wigner-Ville Distribution 48
    2.8.1. Properties of the Wigner Distribution 51
    2.8.2. Disadvantages 53
    2.8.3. Pseudo Wigner-Ville Distribution 54
    2.8.4. Ambiguity Function 54
2.9. The Kernel Methods 55
    2.9.1. Husimi Distribution 58
    2.9.2. Smoothed Pseudo Wigner-Ville distribution 58

3. The von Neumann TFR 59
3.1. Introduction 59
3.2. Derivation of Standard Gaussian Integrals 60
3.3. Gaussian Fourier Transform Invariance 64
3.4. Fourier Transform Properties of the Gaussian Function 66
    3.4.1. Scaling Condition 66
    3.4.2. Temporal and Spectral Shifting 66
    3.4.3. Gaussian Fourier Transform pair 67
3.5. The von Neumann Representations 68
    3.5.1. The von Neumann Basis 68
    3.5.2. The von Neumann Basis Lattice 69
    3.5.3. Principles of Signal Representation 71
    3.5.4. Derivation of the Overlap Integral 73
    3.5.5. The von Neumann Time-Frequency Representation 76
    3.5.6. Signal Reconstruction 77

4. Adaptive Quantum Coherent Control 79
4.1. Introduction 80
4.2. Interaction of the laser pulse with the multilevel system 81
4.3. Adaptive feedback control and the optimization process 83
4.4. Results 84
    4.4.1. Transform limited pulse 84
    4.4.2. SLM Results 85
    4.4.3. von Neumann Results 86

4.4.4. Comparison of the two methods 87
4.4.5. Robustness of the von Neumann solution 89
4.4.6. Topology of the optimization space 90
4.4.7. Excitation mechanism 93
4.5. Conclusion 95

5. The Generalized FHG TFR 97
5.1. Introduction 97
5.2. The Fourier Transform Eigenvalue Problem 98
5.2.1. Some properties of the Hermite polynomials 102
5.3. Extension to Fourier-Hermite-Gauss Polynomials 104
5.3.1. Generalized Fourier-Hermite-Gauss Polynomials 109
5.3.2. The Hermite Translation Expansion 110
5.4. The Fourier-Hermite-Gauss Representation 115
5.4.1. Temporal FHG Basis Functions 116
5.4.2. Spectral FHG Basis Functions 116
5.4.3. The FHG Overlap Integral 116
5.4.4. The Fourier-Hermite-Gauss TFR 117
5.4.5. The FHG Signal Reconstruction 117
5.4.6. The Fourier-Hermite-Gauss Overlap Integral 118
5.4.7. Spectral Overlap Integral 123
5.4.8. Validity of the Overlap Integral 124
5.5. Introduction to Frame Theory 130
5.6. Application Results 132

6. The Complete FHG TFR 139
6.1. Introduction 139
6.2. TFR Frames 140
6.3. Periodicity and Scaling 145
6.4. The Complete FHG TFR Cube 148
6.5. Unscaled FHG Signal Correlation 149
6.5.1. Alternative Derivation of the Unscaled Signals 154
6.6. The Complete FHG Overlap Matrices 156
6.6.1. Numerical Reconstruction of the Complete FHG Basis . . . 164
6.7. Signal Reconstruction with the Complete FHG TFR 176
6.8. The Complete FHG TFR 176

7. Coherent State FHG TFR Analogy 189
7.1. Introduction 189
7.2. A Brief Summary of Modern Light 190
7.2.1. Gaussian Laser Beams 192

7.2.2. Optical Phase Space . . . 196
7.3. Coherent States . . . 204
7.4. FHG Coherent State Analogy . . . 210
7.5. Conclusion . . . 217

8. Conclusion 219

Acknowledgments 225

A. The Fourier Series and Transform 229
A.1. Introduction . . . 229
A.1.1. Fourier Series . . . 230
A.2. Various Definitions of the Fourier Transform . . . 231
A.3. Properties . . . 232
A.3.1. Linearity . . . 232
A.3.2. Duality (Symmetry) . . . 233
A.3.3. Complex Conjugation . . . 233
A.3.4. Scaling (Reciprocity) . . . 233
A.3.5. Shifting . . . 234
A.3.6. Differentiation . . . 234
A.3.7. Real and Hermitian Functions . . . 234
A.3.8. Convolution . . . 237
A.3.9. Correlation . . . 238
A.3.10. Energy Theorem (Parseval-Plancherel) . . . 241
A.4. Common Functions . . . 242
A.4.1. Sign Function . . . 242
A.4.2. Step Function (Heaviside Function) . . . 242
A.4.3. Rectangular Function (Hat function) . . . 242
A.4.4. Triangular Function . . . 243
A.4.5. Sinc Function . . . 243
A.4.6. The Dirac-δ function . . . 244
A.4.7. Mirror Image Operator . . . 246
A.4.8. Translation Operator . . . 246
A.4.9. Modulation Operator . . . 247
A.4.10. Mirror Image and Complex Conjugation Commute . . . 247
A.4.11. Translation and $\mathcal{I}_c$ Commute . . . 248
A.5. Fourier Transforms . . . 249
A.6. Even and Odd Transforms . . . 249
A.7. Sampling Theory . . . 251
A.8. Properties of Bandlimited Functions . . . 253
A.9. Poisson Summation Formula . . . 254

A.10. Nyquist-Shannon Sampling Theorem 255
  A.10.1. Inverse Nyquist-Shannon Sampling Theorem 256

B. The FHG Spectral Overlap Matrix 257

C. Other Orthogonal Polynomials 263
C.1. Laguerre Polynomials 263
  C.1.1. Differential equation 263
  C.1.2. Rodrigues' formula 263
  C.1.3. Generating function 263
  C.1.4. Orthogonality 263
C.2. Associated Laguerre Polynomials 264
  C.2.1. Differential equation 264
  C.2.2. Rodrigues' formula 264
  C.2.3. Generating function 264
  C.2.4. Orthogonality 264
C.3. Ince Polynomials 264

D. Matlab Code 267
D.1. Main Molecule Function 267
D.2. von Neumann TFR Functions 272
  D.2.1. Spec2vNTFR.m 272
  D.2.2. Temp2vNTFR.m 274
  D.2.3. vNGrid.m 276
  D.2.4. vNOverlapAMS.m 278
  D.2.5. vNSpecB.m 279
  D.2.6. vNTempB.m 280
  D.2.7. vNTFR2Spec.m 281
  D.2.8. vNTFR2Temp.m 282
  D.2.9. vNTFRPlots.m 283
D.3. Coherent State Analogy Functions 287

Bibliography 291

List of Figures

1.1. Lev Pontryagin, E. T. Bellman and R. E. Kalman 9
1.2. (a) Open Loop Control (b) Adaptive Feedback Control (c) Measurement-based Real-Time Feedback Control (d) Coherent Real-Time Feedback Control 14
1.3. Quantum Coherent Control 15
1.4. Octahedral Molecule 22
1.5. ν_3-Rovibrational Levels of Octahedral Molecule 24
1.6. 4f-Spatial Light Modulator 29
1.7. Musical Score for Three Guitars 32

2.1. Eugene Wigner, John von Neumann and Dennis Gabor 36

3.1. The von Neumann Lattice 70
3.2. (a) The von Neumann TFR (b) von Neumann spectral reconstruction of the electric field 78

4.1. The level structure used in this study. Shown in the figure are the principal quantum numbers, n, as well as the anharmonic splitting of these levels for which there is a small difference in transition frequency. The broken lines represent forbidden transitions. 83
4.2. (a) The von Neumann transform of a 100fs Gaussian pulse (25×25) pixels. (b) Original Fourier transform (solid blue line) superimposed on the frequency domain pulse reconstructed from the von Neumann representation. The two vertical lines in (b) represent the bandwidth required to excite all the transitions in Figure 4.1. . 85
4.3. Interaction of a transform limited pulse with the polyatomic molecule. (a) Population dynamics, as can be seen approximately 20% of the population are in vibrational level $n = 2$ after the pulse has interacted with the molecule. (b) Transform limited electric field with a FWHM of 100fs. 86
4.4. Simulated AFC utilizing frequency domain shaping via an SLM. (a) Optimum time pulse obtained via a GA optimization process. (b) Population dynamics caused by the time pulse in (a). (c) Husimi plot of the pulse. 87

4.5. Simulated AFC the von Neumann time/frequency representation. (a) Optimum pulse obtained via a GA optimization process. (b) Population dynamics caused by this pulse. (c) Husimi plot of the optimum pulse (d) Fourier transform of the optimum pulse. 88
4.6. Fitness values obtained using the two processes described in the text. The von Neumann approach outperformed the SLM method significantly. 89
4.7. Influence of peak input pulse fluence on the calculated maximum population in vibrational level 2. 90
4.8. Maximum population in vibrational level 2 as a function of varying carrier frequency. 91
4.9. Husimi plots of two optimum pulses. Selective excitation of 97% (a) and 85% (b) were obtained for the right and left pulses respectively. 94

5.1. Carl Friedrich Gauss, Charles Hermite, Blaise Pascal 98
5.2. Fourier-Hermite-Gauss TFR Lattice 108
5.3. (a) Front face of cube von Neumann and FHG basis (b) Vertical diagonal slice of cube FHG basis (c) Horizontal diagonal slice of cube FHG basis 130
5.4. XF_6 rovibrational energy levels with forbidden transitions shown in dashed lines. (b) Selective excitation of the XY_6 second ν_3-rovibrational population level. 134
5.5. (a) Temporal electric field (b) Spectral electric field showing the transitions frequencies the XY_6 ν_3-rovibrational levels in circles . . . 135
5.6. (a) The Wigner-Ville TFR (b) The Husimi TFR 135
5.7. (a) The von Neumann TFR (b) von Neumann spectral reconstruction of the electric field 136
5.8. (a) FHG TFR Amplitude (b) FHG spectral reconstruction of the electric field 136
5.9. (a) FHG TFR Amplitude First 7 (b) FHG spectral phase reconstruction 137
5.10. (a) FHG temporal reconstruction (b) FHG temporal phase reconstruction 137
5.11. (a) FHG TFR Amplitude (b) FHG TFR Phase (c) FHG Spectral Amplitude Reconstruction (d) FHG Spectral Phase Reconstruction 138
5.12. (a) FHG Temporal Amplitude Reconstruction (b) FHG Temporal Phase Reconstruction 138

6.1. FHG TFR of the Spectral Frame 142
6.2. FHG TFR of the Temporal Frame (Bottom to Top) 143
6.3. FHG TFR of the Temporal Frame (Top to Bottom) 144

6.4. Time-Frequency Doubling 147
6.5. FHG TFR Spectral 6^{th} FHG basis and TF translation 6^{th} HG . . . 165
6.6. FHG TFR Spectral 6^{th} FHG basis and TF translation 14^{th} HG . . . 166
6.7. FHG TFR Spectral 6^{th} FHG basis reconstruction & TF translation 166
6.8. FHG TFR Temporal 6^{th} FHG basis and TF translation 6^{th} HG . . 167
6.9. FHG TFR Temporal 6^{th} FHG basis and TF translation 14^{th} HG . 168
6.10. FHG TFR Temporal 6^{th} FHG basis reconstruction & TF translation 169
6.11. FHG TFR Spectral HG complex inner product (All FHG Spectral bases) 171
6.12. FHG TFR Spectral HG inner product (1-12 FHG Spectral bases) . 172
6.13. FHG TFR Spectral HG inner product (13-24 FHG Spectral bases) . 173
6.14. FHG TFR Temporal HG inner product (1-12 FHG Temporal bases) 174
6.15. FHG TFR Temporal HG inner product (13-24 FHG Temporal bases) 175
6.16. FHG TFR case 2 Mean Spectral Signal with Spectral Amplitude and Phase Reconstruction 179
6.17. FHG TFR case 2 Mean Temporal Signal with Temporal Amplitude and Phase Reconstruction 179
6.18. FHG TFR case 3 Spectral and Temporal Signal Inner Product . . . 180
6.19. FHG TFR case 7 Spectral and Temporal HG Cube Inner Product . 180
6.20. FHG TFR symmetrical HG inner product (1-12 FHG bases) 181
6.21. FHG TFR symmetrical HG inner product (13-24 FHG bases) . . . 182
6.22. FHG TFR symmetrical HG inner product 183
6.23. The Spectral Overlap Matrices of the HG Planes 185
6.24. FHG TFR Spectral HG Planes multiplied by their Overlap Matrices 186
6.25. FHG TFR Temporal HG Planes multiplied by their Overlap Matrices 187
6.26. FHG TFR Spectral HG Planes x Overlap Matrices 188
6.27. FHG TFR Temporal HG Planes x Overlap Matrices 188

7.1. Roy Glauber and E. C. George Sudarshan 189
7.2. Phase Space Uncertainties 208
7.3. Coherent State TFR Analogy (First Representative Laser Pulse) . . 216
7.4. Coherent State TFR Analogy (Second Representative Laser Pulse) 217

List of Tables

1.1. XY_6 ν_3-rovibrational modes 23
1.2. 3^{rd}-level dipole transition moments 25
1.3. 4^{th}-level dipole transition moments 25
1.4. QC dipole transition moments 26

2.1. Kernel Cohen Classes 57

4.1. The fitness values (population in the chosen vibrational level) of different controls are shown in the second column. The norm of the masks of the different optimum solutions with respect to the origin(distance to origin) is shown in the first column and the distance of the other points with respect to a specific solution point are shown in the other columns. The norm was defined as $\|M_i\| = \sqrt{\sum_j^n M_{ij}^2}$. . 93

A.1. Fourier Transform Pairs 249

Foreword

Originally when I committed myself to do this dissertation, I was motivated and enticed by my supervisor, Dr. L. R. Botha, to extend his simulation work, which was essentially control of a closed quantum system, into to the bounds of open quantum systems. This was mainly due to my years of experience in classical stochastic nonlinear control and my exposure to quantum mechanics and quantum field theory, the natural extension is of course to maneuver into the field of quantum control. Thus my original dissertation was entitled **"Stochastic coherent control of quantum processes"**, which would have originally been summarized as follows.

The study of the coherent control of quantum systems via shaped ultra-short laser pulses is a very active field of research with various possible applications [1]. Currently deterministic optimal control techniques are utilized. Such a model was developed at the NLC which predicted preferential preparation of a pre-selected well defined quantum state [2]. Quantum mechanical systems must be regarded as open systems due to the fact that any real system will be subjected to a coupling to an uncontrolled environment which will influence it. Therefore in order to make meaningful predictions with regards to a control problem in the real world one needs to include stochastic processes in a simulation.

As a first step in this study stochastic variables will be included into the current NLC model. This will for example include stochastic modeling of the noise with regards to the laser center frequency, the influence of stochastic noise on the transition wavelengths of the molecule due to stochastic variability of the Doppler shifts. It is expected that these processes will introduce de-coherence into the process and possible reduced efficiency in producing the selected outcome. Various methods of introducing stochastic processes in coherent control problems and the possible countering of these effects will be investigated. The reduced-master equation will be derived for this specific model. Inclusion of stochastic processes in the model will give an indication of the robustness, stability and practical applicability of this particular quantum control problem. The predictions of the adapted model will be compared with that of the original deterministic model. As a second step the ap-

plicability of well-known stochastic control techniques applied to classical systems, such as extended Kalman filtering [3], to quantum coherent control will be investigated. In classical systems these techniques leads to great improvements in the control of the physical systems. It needs to be shown whether this is the case in a quantum system.

References:

[1] C Brif, R Chakrabati, H Rabitz, "Control of quantum phenomena: past, present and future", arxive:00912. 5121v2, May 2010, Submitted to New J. Physics.

[2] L de Clercq, "Numerical modeling of the excitation of a polyatomic molecule by femtosecond laser beams", M. Sc. Thesis, Univ. Of Stellenbosch, 2011.

[3] R F Strengel, "Optimal control and estimation", Dover Publications, 1996

I was well away into this study, of course firstly, the original closed system work and the method of representing a ultra-short laser pulse by means of the Time-Frequency Representations (TFR), such as the Wigner-Ville, Husimi and the von Neumann TFRs. The von Neumann TFR was the new method we wished to represent the ultra-fast laser pulses with. In the first year I even investigated new techniques to simplify the optimization process of the closed quantum control and was highly excited by the possibility of these new techniques, but struggled to convince my supervisor, who was concentrating on the von Neumann TFR, which I had already programmed.

Due to the persistence of my supervisor, I rethought the von Neumann TFR, and it dawned on me what aspects of the representation, being a representation in terms of Gaussian elementary pulses, was so desirable. The main feature is that a Gaussian pulse was Fourier transform invariant. The proverbial bulb lit up and I saw that the von Neumann representation could be extended to those general functions that are Fourier invariant, which happen to be the Hermite-Gauss polynomials, exactly the basis functions of the quantum harmonic oscillator. This happened almost one year to the day after starting this endeavor.

Well the morning after this insight, I explained it to my supervisor and my new supervisor, Dr. H. Uys, and they both unanimously agreed that I should stop all my work on the open quantum control optimization process, and pursue this novel idea, henceforth. Stopped in my tracks and off on a tangent.

Initially I investigated all the analytical aspects of the now novel Fourier-Hermite-Gauss TFR. I discovered beautiful properties concerning Pascal matrices and their interrelationship with the Hermite polynomials and exploited these aspects to simplify the calculation of the so-called overlap matrix that is required in these representations. After a year of struggling and developing this theory on my own I even discovered the relationship of the FHG temporal basis functions with the optical coherent state representations and because of the analogy (similarity) of these representations, that one could find a correlation TFR between the two representations.

This then was presented as a poster at the FEMTO11 Copenhagen Conference on Femtochemistry and Physics, in July 2013. I was extremely honored to be almost immediately accepted, especially seeing that 2013 was the centenary year of Niels Bohr discovery of the classical quantum theory of the Hydrogen atom, and his beloved city. Thereafter Niels Bohr established the Copenhagen Institute for quantum physics and developed the Copenhagen interpretation. The abstract is included hereafter.

All good and well, but this was all done analytically. Unfortunately, working with a simulation everything has to be sampled and digitized. The von Neumann TFR and the FHG TFR then soon become subfields of Digital Signal Processing (DSP). With DSP, the Digital Fourier Transform (DFT) and its associated digital algorithm, the Fast Fourier Transform (FFT), utilizing the so-called radix technique must be employed. Questions of sampling and the Nyquist-Shannon theorem, aliasing and anti-aliasing, z-transforms, causality and many other effects peculiar to DSP must be considered.

One of the first problems, that stuck out its head, was the high numerical instability of the Pascal matrices, which analytically are so fruitful, making their use digitally useless. Although, it was soon discovered that the temporal and spectral reconstruction of ultra-fast laser pulse can be amazingly well reconstructed by this novel FHG TFR in both amplitude and in phase, with the slight quirk, that two separate representations, one each for the temporal and spectral representations, but with the extraordinary feature that no overlap matrix is required in the signal reconstruction. It essentially proves their orthogonality. The FHG TFR signal lattice cube contains all the information. The one great disadvantage of using the von Neumann TFR is the construction of the overlap matrix and its inverse. The overlap matrix is highly ill-conditioned and one has to resort to Moore-Penrose pseudo inverse algorithms. Great effort and time was spent in constructing analytically and numerically the overlap matrix for the new FHG TFR, only to discover that one can actually by-pass its construction by using two separate TFRs and then using a special combination of the two to create a single TFR. Being correlation cubes, the one can be considered a translation of time and the other a translation in frequency, totally orthogonal.

I never knew, with its conception, that the invariance of the quantum oscillator, could digitally conceive a minimum content of digital information. This is still part of ongoing research and is not published here.

This is just a historical background reflection of the development of this new novel

FHG. The introductory Chapter 1 gives a thorough summary and an outline of this dissertation. This Chapter also concludes with an overview of the thesis, Section 1.7.

A New Hermite-Gauss Time-Frequency Representation on a von Neumann Lattice for Ultra Short Laser Pulses for Quantum Coherent Control

A.M. Smit[1], L.R. Botha[1], and E. Rohwer[2]

[1] *National Laser Centre, CSIR, P O Box 395, Pretoria 0001, South Africa*
[2]*University of Stellenbosch, Privatebag X1, Stellenbosch 7602, South Africa*

The Hermite-Gauss polynomials are the orthogonal eigenfunctions of the Fourier transform operator, and are thus functionally invariant under the Fourier transform. In the von Neumann picture [1][2], the basis functions are minimum uncertainty Gaussian functions which correspond to the zeroth order of the Gauss-Hermite polynomials. The new Hermite-Gauss Time-Frequency Representation (TFR) expands the von Neumann lattice in a third dimension with the Hermite-Gauss polynomials. In analogy with the von Neumann basis functions both temporal and spectral basis functions are defined, which are Fourier transform equivalent due to their Fourier translation properties. The dual equivalence of the temporal and spectral amplitudes of this TFR is clearly shown. Furthermore the Hermite polynomial translation property is beneficially utilized to facilitate the numerical algorithm of the TFR. The Hermite-Gauss polynomials correspond to the number states $\{n_{\mathbf{k}}\}$ of the Glauber-Sudarshan coherent states in Fock space [3] and thus allows for a comparison of the amplitudes between the two decompositions for each $\|\mathbf{k}\| = \omega_{\mathbf{k}}/c$. Results obtained from simulations of quantum coherent control of an octrahedral molecule's interaction with IR ultra short laser pulse are compared with various other TFRs, e.g. Wigner [4], von Neumann, Husimi etc.

References

[1] S. Fechner, F. Dimler, T. Brixner, G. Gerber and D. J. Tannor, *Opt. Express* **15**, 15387–15401 (2007).
[2] S. Ruetzel, C. Stolzenberger, F. Dimler, D.J. Tannor and T. Brixner, Phys. Chem. Chem. Phys., **13**, 8627–8636 (2011).
[3] R.J. Glauber, *OPhys. Rev.* **131**, 6, 2766–2788 (1963).
[4] W.P. Schleich , *Quantum Optics in Phase Space*, Wiley-VCH, (2001)

1. Introduction

Since the advent of lasers it has always been the dream of physicists and chemist to manipulate and control atomic and molecular processes and it was hoped that the new invention would deliver their wildest expectations. Almost immediately it became obvious that the laser did not meet all the far reaching expectations of the scientists. Nature was a bit more subtle and complicated. Modern control theory was also in its infancy and making enormous strides with the Apollo program, the space race and autonomous missile and aircraft guidance and control. In parallel these concepts flowed over to initiate the field of quantum control. Although the progress was slower than expected, the theory of quantum control steadily grew. In Brif et al. [1] an extensive overview can be found. It also contains a vast bibliography. This is also obvious in the introductory text book by d'Allessandro "Introduction to Quantum Control and Dynamics" [2], which has a similar enormous bibliography.

The hurdle of quantum control [2], [3] is that it has a myriad of multi-interdisciplinary fields, e.g.,

1. Quantum Mechanics [4, 5, 6, 7, 8]
2. Nonlinear Stochastic Control Theory [9, 10, 11, 12, 13, 14, 15, 16, 17]
3. Laser Theory and Optics [18, 19, 20, 21, 22, 23, 24]
4. Molecular Group Representation Theory [25, 26, 27, 28, 29, 30, 31]
5. Lie Groups and Algebra [32, 2]
6. Time Frequency Analysis (TFA) [33, 34]
7. Correlation and Coherent States [35, 36, 37, 38]
8. etc.

One can now expect that the time required for a single researcher to master all of the above fields is a great trek, with many hardships. This is confirmed by d'Allessandro. The simpler route is of course to combine a team of specialists. This also has its advantages and disadvantages. The greatest of which is the communication between the various fields. Nonetheless, successes have been accomplished by various groups.

In this introductory Chapter, we refer to modern control theory as classical control theory as opposed to quantum control theory.

In Section 1.1 an almost too brief overview of quantum control theory is given. In Section 1.2 gives a general overview of Quantum Coherent Control with femtosecond lasers as the major application of this research. It is necessary, for the great simplification that is obtained, to rather work in Dirac-interaction picture. The derivation of a interaction Hamiltonian is given in Section 1.3. This derivation is also done in [39], but in a round about way. Section 1.4 discusses octahedral molecules, which is the molecule under investigation for our quantum coherent control application. Due to the symmetry of the molecule and Emmy Noether's theorem, a short overview of irreducible representations of point groups is given in Subsection 1.4.1, the classification of them in Subsection 1.4.2 and the character tables of the point groups, specifically for the relevant octahedron group in Subsection 1.4.3. The IR active transitions for octahedral molecules is discussed in Subsection 1.4.4. For our specific XY_6 octahedral molecule under investigation, the IR dipole moments are given Subsection 1.4.5, as well as the corresponding interaction IR dipole moment matrix for our interaction Hamiltonian matrix, that is required for our simulations.

A brief overview of spatial light modulators that is used to manipulate the ultrashort IR laser pulses for the coherent quantum control of the octahedral molecule, is given in Section 1.5. Finally to prepare the reader for the presentation on Time-Frequency-Representations (TFR) we have included a short introduction in Section 1.6. Finally, in Section 1.7 an overview of the thesis is presented.

1.1. Quantum Control

Historically, probably the first instance of control (cybernetics), was the automatic opening of Egyptian temple doors invented by the Greek, Hero of Alexandria, c.10 – c.70 AD, using the pneumatics of steam. In the nineteenth century, with the invention of the steam engine, Watt invented a spinning regulator to regulate the speed of the engine. Classical control theory really kicked off in World War 2, especially in the design of the German V1 and V2 rockets. At the allied front an automatic target predictor was invented by the American Norbert Wiener and also independently by the Russian A. Kolmogorov, now known as the Wiener-Hopf filter. In the ensuing Cold war years, this independent development continued. The blind Russian mathematician Lev Pontryagin introduced the sufficient conditions for optimal control, known as the Pontryagin Maximum Principle (PMP). In the USA similar equations were developed by E. T. Bellman that lead to the Hamilton-Jacobi-Bellman equation and dynamic programming. With so many matrices and matrix integrations involved, it is obvious that as the dimension of the system increases, that the numerical load on the computer exponentially explodes. The phrase *"The curse of dimensionality"* was coined by Bellman [9]. Early in the 1960, R. E. Kalman, introduced stochastic estimation, and many required definitions conditions in optimal control, that were intensively utilized in the Apollo Lunar program. Introductory textbooks in linear control theory are usually [13, 12]. The classic text books on optimal control are [9, 10, 11]. On stochastic estimation and control theory [40, 14, 15, 16, 41]. Applied nonlinear control is well introduced by Slotine and Li [17] and Isidori [42]. By far the favourite is Stengel [9], since it actually covers all the topics (The first edition was actually published as "Stochastic optimal control: theory and application" [43]). Robert Stengel was also the principle design engineer of the Apollo Lunar Module[1]. This book would best be supplemented by the nonlinear control books [17, 42].

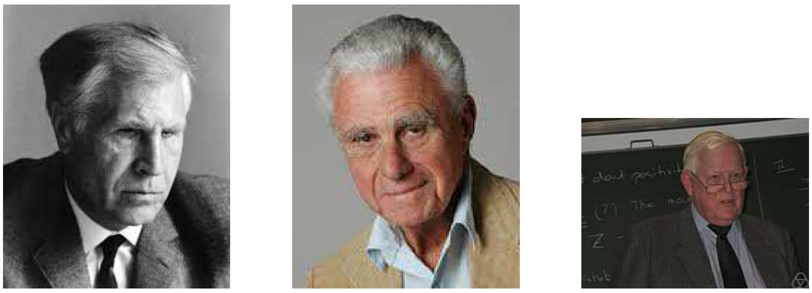

Figure 1.1.: Lev Pontryagin, E. T. Bellman and R. E. Kalman

When walking over to the terrain of quantum control all the classical and modern control theory methods are applicable. What is important is to correctly define the various quantum dynamical system equations and the quantum mechanical measurement equations of the system to which these techniques may be applied. We only define these techniques on closed quantum systems, (cf. [2]). The main purpose of this section is to introduce and formally define the most general quantum control problem, and the concept of quantum controllability.

In any Hilbert space, $\mathbb{H}$, it is always possible to find a set of countable or denumerable orthonormal basis vectors, in the Dirac notation, $|e_i\rangle$, where, i, is in some index set, $\mathcal{I}$, such that a state vector of the quantum system, $|\psi\rangle$, can be expanded in terms of these basis vectors as,

$$|\psi\rangle = \sum_{i\in\mathcal{I}} \alpha_i \, |e_i\rangle \qquad \alpha_i \in \mathbb{C}. \tag{1.1}$$

---

[1] All digital reproductions, photographs and paintings, of persons in this thesis were obtained from www.wikipedia.com

We associate a **completeness relation** to the basis vectors by,

$$\sum_{i\in\mathcal{I}} |e_i\rangle \langle e_i| = \mathbf{I}, \tag{1.2}$$

where, $\mathbf{I}$, is the identity operator. For a dynamical quantum state we have to introduce the time, so that the state vector is given by,

$$|\psi(t)\rangle = \sum_{i\in\mathcal{I}} \alpha_i(t) |e_i\rangle . \tag{1.3}$$

Note that the time dependence enters through the coefficients, for it is assume that the basis vectors are stationary. In the case of a uncountable infinite dimensional Hilbert space, an orthonormal basis is replaced by a basis, $|x\rangle$, where, x, varies over an appropriate measurable set, Ω, with measure, dx, such that,

$$\langle x|x_1\rangle = \delta(x - x_1), \tag{1.4}$$

where, $\delta(x - x_1)$, is the generalized Dirac-δ function centered at, x_1. The quantum state, $|\psi\rangle$, is then expanded as,

$$|\psi\rangle = \int_\Omega \psi(x) |x\rangle dx, \tag{1.5}$$

for some function,$\psi(x)$, defined on, Ω. The completeness relation is then given by,

$$\int_\Omega |x\rangle \langle x| dx = \mathbf{I}. \tag{1.6}$$

If we ignore all possible dependencies, except the time, t, the Schrödinger equation can be written in vector notation[2], for a closed quantum system as,

$$i\hbar\frac{\partial}{\partial t}\vec{\psi}(t) = H(u(t))\vec{\psi}(t), \quad \vec{\psi}(0) = \vec{\psi}_0, \tag{1.7}$$

where, $\vec{\psi}(t) \in \mathbb{C}^n$, if the Hilbert space, $\mathbb{H}$, has dimension, n, and $u(t) \in \mathbb{C}^m$, is the control input and, H, is the quantum Hamiltonian. The general solution of the above equation is given by,

$$\vec{\psi}(t) = X(t)\vec{\psi}_0, \tag{1.8}$$

---

[2] The equivalence between the abstract Dirac notation and vector algebra is given by: $|\psi\rangle \leftrightarrow \vec{\psi}$ and $\langle\psi| \leftrightarrow \vec{\psi}^T$, where T denotes the transpose operation. In abstract algebra they are known as **dual vector spaces**.

is called the **Schrödinger Operator Equation**, where the, $X(t) \in \mathbb{C}^n \times \mathbb{C}^n$, is called the **evolution operator**, which of course is a matrix. Here we used the shorthand notation commonly used if the initial time, $t = 0$. More generally, if the initial time is given by, $t = t_0$, with initial state still presented as, $\vec{\psi}(t_0) = \vec{\psi}_0$, then the evolution operator is given by,

$$\vec{\psi}(t) = X(t, t_0)\vec{\psi}_0. \tag{1.9}$$

$X(t, t_0)$, therefore propagates the state vector from its initial state, $\vec{\psi}_0$, to its final state, $\vec{\psi}(t)$. In control literature it is often referred to as the **state propagator**. The evolution operator, $X(t, t_0)$, satisfies a similar differential equation to the Schrödinger equation and is given by,

$$i\hbar\frac{d}{dt}X(t, t_0) = H(u(t))X(t, t_0), \quad X(t_0, t_0) = \mathbf{I}. \tag{1.10}$$

Noticing that in a sense this equation is a first order differential equation, we could simply write the solution as,

$$X(t_1, t_0) = e^{-\frac{i}{\hbar}\int_{t_0}^{t_1} H(u(\tau))d\tau}. \tag{1.11}$$

Since the problem is multi-dimensional, this, however, will only be approximately valid if, $t_1 - t_0 = \delta t$, is very small. It does allow for a numerical calculation method. The true solution was developed by F. Dyson and is known as the **Dyson Series** (once again employing the shorthand notation and assuming, $\hbar = 1$, for simplicity),

$$X(t) = \mathbf{I} + \sum_{n=1}^{\infty} D_n(t), \tag{1.12}$$

with

$$D_n(t) = (-i)^n \int_0^t \int_0^{t_1} \cdots \int_0^{t_n} \tilde{H}_1(t_1)\tilde{H}_1(t_2)\cdots\tilde{H}_1(t_n)dt_n \cdots dt_1, \tag{1.13}$$

where, $\tilde{H}_1(t)$, is the Dirac interaction picture Hamiltonian (to be discussed later).

The mathematician John von Neumann introduced the concept of a quantum **density matrix**, $\rho(t)$, to work with an ensemble of identical quantum systems, as is necessary for quantum statistics. If, using the Dirac notation, given that there is a fraction, $0 < w_j(t) \leq 1$, of systems in the ensemble with state, $|\psi_j(t)\rangle$, and j, in some index set, $\mathcal{I}$, such that, $\sum_{j\in\mathcal{I}} w_j(t) = 1$, then the density operator describing the state of the state of the ensemble is defined by,

$$\rho(t) = \sum_{j\in\mathcal{I}} w_j(t) \left|\psi_j(t)\right\rangle \left\langle\psi_j(t)\right| = \vec{\psi}(t)\mathcal{W}(t)\vec{\psi}^{\dagger}(t), \tag{1.14}$$

and the † is the Hermitian conjugate operator and $\mathcal{W}(t) = \mathrm{diag}\{w_j(t)\}_{j\in\mathcal{I}}$. It is a linear operator, $\rho(t) : \mathbb{H} \rightarrow \mathbb{H}$. The density matrix satisfies the **von Neumann-Liouville equation**,

$$i\hbar\frac{d}{dt}\rho(t) = [H(t), \rho(t)] \quad \rho(0) = \rho_0, \tag{1.15}$$

where, $[\cdot, \cdot]$, is the normal commutator bracket. The solution is given by the **Liouvillian Superoperator** equation,

$$\rho(t) = X(t)\rho_0 X^\dagger(t). \tag{1.16}$$

In the **Schrödinger picture** the state vectors are dynamical wavefunctions, $\psi(\mathbf{r}, t)$, and the operators, A, are stationary Hermitian observables. In direct contrast, in the **Heisenberg picture**, the state vectors, $|\psi_j\rangle$, are stationary state vectors and the Hermitian observable operators, $A(t)$, are dynamical. Intermediate between these two pictures lies the **Dirac interaction picture**. This is the quantum picture we prefer to work in, because of its many desirable properties.

One of the fundamental principles of quantum mechanics that had many consequences, is the probability nature of quantum mechanics and from the Copenhagen interpretation the strange consequences of measurement on a quantum system. A measurement has the effect of projecting the quantum state into one of its eigenvalue and eigenvector states of the quantum operator. This is best summarized in the following postulate.

Postulate 1.1.1. von Neumann-Lüders Measurement Postulate. When an observable (operator), A, is measured the result is an eigenvalue of A.

$$\langle A\rangle_\psi = \sum_j \lambda_j Pr(\lambda_j) = \sum_j \lambda_j \langle\psi|P_j|\psi\rangle = \left\langle \psi|\sum_j \lambda_j P_j|\psi \right\rangle = \langle\psi|A|\psi\rangle . \tag{1.17}$$

For any controllable system, measurement is essential. You have got to know in which state a system is to be able to control it to another desired state. Given the formalism we have just introduced we are now in a position to define the various concepts of closed quantum controllability.

Definition 1.1.2. The Schrödinger equation,

$$\frac{d}{dt}\vec{\psi}(t) = -iH(u(t))\vec{\psi}(t), \tag{1.18}$$

is **pure state controllable** if for every pair of initial states, $\vec{\psi}_0$ and $\vec{\psi}_1$, there exist a control functions, u, and a time, $T \geq 0$, such that the solution of Eq. (1.18) at time, T, with initial condition, $\vec{\psi}_0$, is, $\vec{\psi}(T) = \vec{\psi}_1$. Here, $\vec{\psi}_0$ and $\vec{\psi}_1$, are two vectors on the complex sphere of radius, 1, $S_{\mathbb{C}}^{n-1}$.

All the quantum states that can be obtained from the solution of Eq. (1.18) with initial condition, $\vec{\psi}(0) = \vec{\psi}_0$, are referred to as the orbit of a quantum state,

$$\mathcal{O}_{\psi_0} := \left\{ X(t)\vec{\psi}_0 | X \in e^{\mathcal{L}} \right\}, \tag{1.19}$$

where, $\mathcal{L}$, is the associated Lie algebra with the Lie group, $e^{\mathcal{L}}$.

Since for any vector, $\vec{\psi}_0$, and, $e^{i\phi}\vec{\psi}_0$, represent the same physical state, for any, $\phi \in \mathbb{R}$, from a physics viewpoint, the following property, equivalent state controllable, is equivalent to pure state controllable.

Definition 1.1.3. The system Eq. (1.7) is **equivalent state controllable** if, for every pair of initial and final states, $\vec{\psi}_0$ and $\vec{\psi}_1$, in $S_{\mathbb{C}}^{n-1}$, there exist control, u, and a phase factor, ϕ, such that the solution, $\vec{\psi}(t)$, of Eq. (1.18), with, $\vec{\psi}(0) = \vec{\psi}_0$, satisfies, $\vec{\psi}(T) = e^{i\phi}\vec{\psi}_1$, at some time, $T \geq 0$.

Definition 1.1.4. The system Eq. (1.15) is **density matrix controllable** if, for each pair of unitarily equivalent matrices, ρ_1, and ρ_2, there exist a control, u, and a time, $T \geq 0$, such that the solution, $\rho(t)$, of Eq. (1.15), with initial condition equal to, ρ_1,

$$\rho(T) = \rho_2. \tag{1.20}$$

For density matrix controllability, the orbit of density matrices are given by,

$$\mathcal{O}_{\mathcal{L}}(\rho_0) := \left\{ X\rho_0 X^{\dagger} | X \in e^{\mathcal{L}} \right\}. \tag{1.21}$$

The Lie algebra is called **the dynamical Lie algebra** associated with the system. This is always a subalgebra of, $\mathfrak{u}(n)$. In this case, $\dim(\mathcal{L}) = n^2 = \dim(\mathfrak{u}(n))$, which is equivalent to, $\mathcal{L} = \mathfrak{u}(n)$ and $e^{\mathcal{L}} = U(n)$, the system is said to be **controllable**. In this case, $\mathcal{R} = U(n)$, which means that every unitary matrix can be obtained by choosing an appropriate control in Eq. (1.7). We shall say that the system is controllable even in the case where, $\dim(\mathcal{L}) = n^2 - 1 = \dim(\mathfrak{su}(n))$, which is equivalent to, $\mathcal{L} = \mathfrak{su}(n)$ and $e^{\mathcal{L}} = SU(n)$. Sometimes we use the terminology **operator controllability** or **complete controllability** to distinguish this case (controllability of system Eq. (1.15)) from the case where we have controllability of the state, $|\psi\rangle$.

Theorem 1.1.5. *A quantum control system with dynamical Lie algebra, $\mathcal{L}$, is density matrix controllable, if and only if, $\mathcal{L} = \mathfrak{su}(n)$ or $\mathcal{L} = \mathfrak{u}(n)$, i.e., it is operator controllable.*

1.2. Quantum Coherent Control

It has long been the dream of physicists and chemists alike to accomplish proper quantum coherent control of complex quantum systems such as multi-level molecules. The methodologies were quite generally boosted by the following two schemes:

- Two-pathway control scheme, invented by Brumer and Shapiro [44, 45, 46].
- Pump-dump control scheme, also known as Stimulated Raman scattering involving Adiabatic Passage (STIRAP), invented by Tannor, Kosloff and Rice [47, 48].

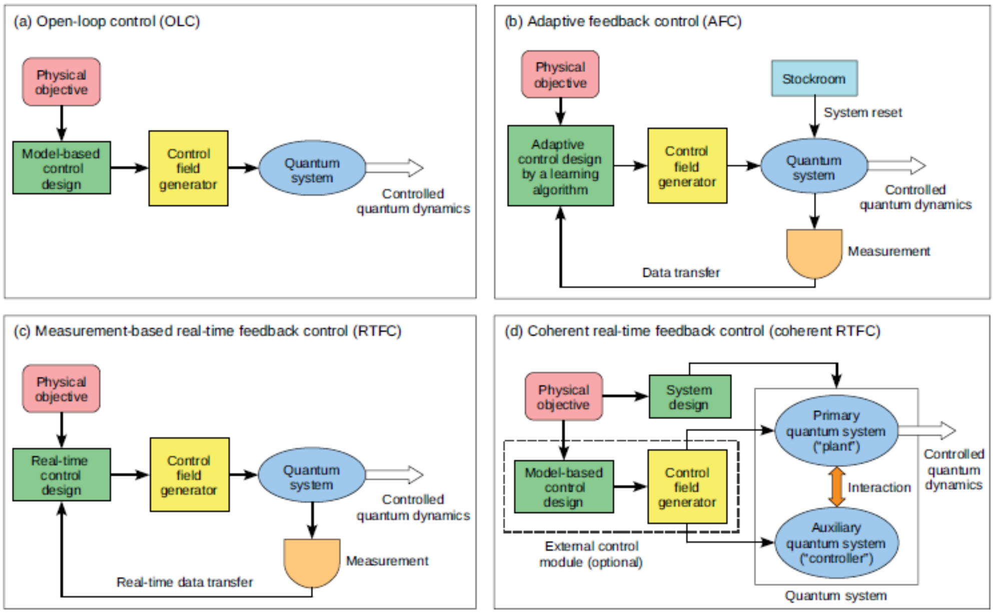
(a) Open-loop control (OLC)
Physical objective
Model-based control design
Control field generator
Quantum system
Controlled quantum dynamics
(b) Adaptive feedback control (AFC)
Physical objective
Stockroom
System reset
Adaptive control design by a learning algorithm
Control field generator
Quantum system
Controlled quantum dynamics
Measurement
Data transfer
(c) Measurement-based real-time feedback control (RTFC)
Physical objective
Real-time control design
Control field generator
Quantum system
Controlled quantum dynamics
Measurement
Real-time data transfer
(d) Coherent real-time feedback control (coherent RTFC)
Physical objective
System design
Primary quantum system ("plant")
Controlled quantum dynamics
Model-based control design
Control field generator
Interaction
Auxiliary quantum system ("controller")
External control module (optional)
Quantum system

Figure 1.2.: (a) Open Loop Control (b) Adaptive Feedback Control (c) Measurement-based Real-Time Feedback Control (d) Coherent Real-Time Feedback Control

The Russians were always in the background, behind the iron curtain, but never behind, and already in 1985, Bagratashvili et al. published, *"Multiple photon* *infrared laser photophysics and photochemistry"* [49][3]. Only in 1991 did Tannor and Yin publish [50] "Mode selective Chemistry". General unifying features are given in Pechen at at. [51]. An authoritative and extensive review is given by Brif et al. [1]. It also contains a vast bibliography. Optimal control of quantum systems is discussed in [52]. Rabitz even speculates in [53]. The interested reader is advised to consult these articles, because it is our opinion that we cannot give a better overview. As a summary, in Figure 1.2 the four main quantum control techniques are outlined, namely:

1. Open Loop Control (OLC)
2. Adaptive Feedback Control (AFC)
3. Measurement-based Real-Time Feedback Control (RTFC)
4. Coherent Real-Time Feedback Control

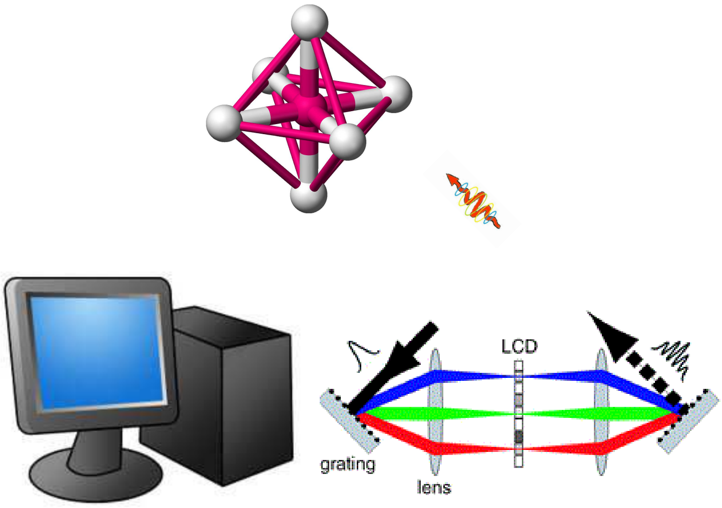

Figure 1.3.: Quantum Coherent Control

Of course our goal is to use lasers to coherently control molecules and Tannor [50] and Judson and Rabitz article describes this quite well [54]. Our simulated quantum coherent control is abstractly represented in Figure 1.3, and falls in the class of Adaptive Feedback Control of Figure 1.2(b).

---

[3] V.S. Letokhov held the first patent on Laser cooling. The Nobel Prize in Physics 1997 was awarded jointly to Steven Chu, Claude Cohen-Tannoudji and William D. Phillips "for development of methods to cool and trap atoms with laser", without recognition of Letokov's precedence. In his own words "probably because I am Russian". Another Nobel Prize controversy.

Firstly, we use a IR femtosecond ultra short laser pulse with a Gaussian envelope that then enters a 4f-SLM (Spatial Light Modulator, see Section 1.5) that shapes the pulse in the spatial frequency domain by means of a Liquid Crystal Display, which is programmed by an optimization program running in the computer to optimally shape the laser pulse for a specific purpose. XY_6 octahedral molecules (see Section 1.4 for a brief outline of the physics involved) are then bombarded by the shaped IR laser pulse. The IR interaction is described in terms of the Dirac-Louiville-von Neumann interaction picture which is derived in Section 1.3. Accordingly, the octahedral molecule is selectively excited in the first few rovibrational for further physical manipulation. This could be for selective isotope separation by means of kinetic reaction of energy and momentum as derived in [35], or for further molecular or atomic reactions. At the CSIR NLC the first article that was published relating to this work was [55].

At present, the simulation program uses a genetic algorithm to optimize the laser pulse shape in a open loop control (OLC) scheme. It is ideally suited, by measuring the spectroscopic transmitted pulse, for adaptive feedback control (AFC).

1.3. Dirac-Liouville-von Neumann Equation

It is by far easier, for our specific quantum system, to rather work in the interaction picture. The Hamiltonian of the Octahedral (see Section 1.4) $\mathbf{O}_h$ molecule in the presence of an interacting EM field (ignoring the field contribution) is given by,

$$H = H_m + H_I, \tag{1.22}$$

where,

$$\begin{aligned} H_m &= \text{The Hamiltonian of the } \nu_3\text{-rovibrational levels } = \operatorname{diag}\left(\hbar\omega_i\right)_{i=1}^{17} \\ H_I &= \text{The interaction Hamitonian of the EM field} \end{aligned}$$

where the time independent molecular equation satisfy, (H_m and H_I are Hermitian operators, i.e., $H_m = H_m^\dagger$, $H_I = H_I^\dagger$),

$$H_m\psi_n(\mathbf{r}) = E_n\psi_n(\mathbf{r}), \quad E_n = \hbar\omega_n, \quad n = 1,\ldots,17. \tag{1.23}$$

This is related to the time-dependent solution by,

$$\psi_n(\mathbf{r},t) = e^{-\frac{i}{\hbar}E_n t}\psi_n(\mathbf{r}). \tag{1.24}$$

The Louiville-von Neumann density matrix equation is given by,

$$i\hbar\frac{d}{dt}\rho(t) = \left[H(t),\rho(t)\right]. \tag{1.25}$$

Define the Dirac-interaction picture by means of the unitary time transformation,

$$U(t) = \exp\left(\frac{i}{\hbar} H_m t\right),$$

so that in the Dirac-interaction picture we have,

$$\begin{aligned} \rho_I(t) &= U(t)\rho(t)U^\dagger(t), && (1.26) \\ H_{ID}(t) &= U(t)H_I(t)U^\dagger(t). && (1.27) \end{aligned}$$

Then the time derivative of Eq. (1.26), and using Eq. (1.27), gives us,

$$\begin{aligned} \frac{d}{dt}\rho_I(t) &= \frac{i}{\hbar} H_m \rho_I(t) - \rho_I(t)\frac{i}{\hbar} H_m + U(t)\frac{d}{dt}\rho(t)U^\dagger(t) \\ &= \frac{i}{\hbar}\left[H_m, \rho_I(t)\right] - \frac{i}{\hbar} U(t)\left[H_m + H_I(t), \rho(t)\right]U^\dagger(t) \\ &= \frac{i}{\hbar}\left[H_m, \rho_I(t)\right] - \frac{i}{\hbar}\left[H_m, \rho_I(t)\right] - \frac{i}{\hbar}\left[H_{ID}(t), \rho_I(t)\right]. \qquad (1.28) \end{aligned}$$

This leaves us with the Dirac-interaction picture Louiville-von Neumann equation,

$$i\hbar\frac{d}{dt}\rho_I(t) = \left[H_{ID}(t), \rho_I(t)\right], \qquad (1.29)$$

where, $H_{ID}(t) = H^\dagger_{ID}(t)$ and diag$[H_{ID}(t)] = \mathbf{0}$. This reduces the *curse of dimensionality* that we are confronted with.

In Subsection 1.4.5, the dipole moments χ are defined for the Dirac-interaction picture and we find that the Hamiltonian is then given by,

$$H_{ID}(t) = H_{ij}(t) = \chi_{ij} e^{i\omega_{ij}t} \varepsilon_o(t), \qquad (1.30)$$

where, $\omega_{ij} = \omega_i - \omega_j$, and, $\varepsilon_o(t)$, is the real component of the electric field of the input femtosecond laser pulse.

1.4. Octahedral Molecules

Nuclei of molecules can of course vibrate as discussed in the Born-Oppenheimer approximation [56]. The first analytical solution of a homonuclear diatomic molecule was given in terms of the approximate Morse potential [57]. One of the first textbooks on molecular vibrations is [31]. A very good read is “Molecular symmetry and spectroscopy” [30]. The importance of group theory and symmetry in quantum mechanics was first recognized by E.P. Wigner and collected in his book [25], (just for this contribution he could have won the Nobel prize), and Hermann Weyl [26]. These are classical textbooks on quantum group theory, but a modern version is given by Tinkham [28].

The various elements in a point group are labeled according to its symmetry operations, e.g., in the cyclic point groups, $\mathbf{C}_n$, the elements are rotations through angles of, $2\pi k/n$, about the symmetry axis, with $k = 1, 2, \ldots, n$. The group is a cyclic group of order n, with a generating element given by the rotation matrix, C_n, i.e., $\mathbf{C}_n = \{C_n, C_n^2, \ldots, C_n^n = E\}$[4]. The rotations dependent on the rational factor, k/n. In denoting the elements of the point group, this rational factor must be written in its lowest prime form, so that for example, $\mathbf{C}_6 = \{C_6, C_6^2, C_6^3, C_6^4, C_6^5, C_6^6 = E\} = \{C_6, C_3, C_2, C_3^2, C_6^5, E\}$. The classes of the groups are labeled using calligraphic text of the generating symmetry element of the class, so that, $\mathbf{C}_6 = \mathcal{E} \cup \mathcal{C}_6 \cup \mathcal{C}_3 \cup \mathcal{C}_2 \cup \mathcal{C}_3^2 \cup \mathcal{C}_6^5$. If two inequivalent classes $\mathcal{C}_2$ appear in the decomposition of the group then they are labeled, $\mathcal{C}_2$ and $\mathcal{C}_2^{'}$. An additional inequivalent class, $\mathcal{C}_2$ would be labeled, $\mathcal{C}_2^{''}$, etc. Sometimes the labels of the symmetry axes to which the distinct equivalent classes refer are used as superscripts, e.g., $\mathcal{C}_2^x$, $\mathcal{C}_2^y$, and, $\mathcal{C}_2^z$. In the dihedral, $\mathbf{D}_n$, groups (these are symmetry groups with additional reflection symmetry) a problem arises in denoting the n twofold axes perpendicular to the axis of highest symmetry. To denote these rotations we write, $C_{2_\perp}$, for the elements and the class as, $\mathcal{C}_{2_\perp}$.

1.4.1. Irreducible Representations of Point Groups

The great majority of molecules in physical problems has axes of symmetry only of the second, third, fourth and sixth orders. The cyclic groups are the simplest and it is rather straight forward to determine their irreducible representations. Each element in a cyclic group is in its own class. The number of irreducible representations is equal to the number of classes. Therefore the number of irreducible representations of a cyclic group is equal to the order of the group. The cyclic group has only one-dimensional irreducible representations. Therefore the cyclic subgroups of a group all have one-dimensional irreducible representations. Irreducible representations play a far reaching effect on physics and a very good text book is [29].

1.4.2. Classification of irreducible representations

The origin of the classification of irreducible representations of abstract groups is not clear, but most books adhere to the following notation. The irreducible representations are all labeled by a capital letter with a subscript usually denoting its specific multiplicity. If there is parity (inversion-i) symmetry then the subscripts (g, e, s - *gerade*, even, symmetric or u, o, a - *ungerade*, odd, asymmetric) are used:

---

[4] The convention of using, E, for the the identity operator, I, is from German *"Einheit"*.

1. A and B denote the one-dimensional irreducible representations.

   Those having a character, $+1$, under the principal rotation symmetry class, $\mathbf{C}_n$, are labeled, A, and those with a character, -1, are labeled, B. If the inversion symmetry operator, i, is present in the class structure of the group, then the subscript labels, g or u, are used depending on whether the character is either, $+1$ or -1, respectively in the inversion class column of the character table.

2. E denotes the two-dimensional irreducible representations.

   This, E, must not be confused with the identity element.

3. F denotes the three-dimensional irreducible representations.

4. G denotes the four-dimensional irreducible representations.

The fact that the letters, C and D, are already used to describe the symmetry point groups could possibly explain their exclusion in the classification of irreducible representation and the natural order of the alphabet.

When the irreducible representations refer to the electron wavefunctions of molecules, such as the well-known homonuclear diatomic molecule H_2, then the notation of the electron molecular wavefunctions are related to the atomic orbital angular momentum spherical harmonics, which are given by, s, p, d, f (sharp, principal, diffuse, fundamental), but for molecules the equivalent Greek capitals are used, i.e., Σ, Π, Δ, Φ.

1.4.3. Character tables of point groups

There are 32 crystallographic point groups. The orders of the first 22 point groups, those point groups that are isomorphic to one another are listed in the same rows, are listed in the following Table:[5]

Point group	Order
$\mathbf{C}_1$	1
$\mathbf{S}_2 = \mathbf{C}_i$, $\mathbf{C}_2$, $\mathbf{C}_s$	2
$\mathbf{C}_3$	3
$\mathbf{C}_{2h}$, $\mathbf{C}_{2v}$, $\mathbf{D}_2 = \mathcal{V}$	4
$\mathbf{C}_4$, $\mathbf{S}_4$	4
$\mathbf{C}_{3v}$, $\mathbf{D}_3$	6
$\mathbf{C}_6$	6
$\mathbf{C}_{4v}$, $\mathbf{D}_4$, $\mathbf{D}_{2d}$	8
$\mathbf{D}_6$, $\mathbf{C}_{6v}$, $\mathbf{D}_{3h}$	12
$\mathbf{T}$	12
$\mathbf{O}$, $\mathbf{T}_d$	24

The other ten symmetry point groups can all be constructed by direct products of those already considered with the group, $\mathbf{C}_i$ (or $\mathbf{C}_s$).

$$\begin{array}{lclcl}
\mathbf{C}_{3h} = \mathbf{C}_3 \otimes \mathbf{C}_s & ; & \mathbf{D}_{2h} = \mathbf{D}_2 \otimes \mathbf{C}_i & ; & \mathbf{D}_{3d} = \mathbf{D}_3 \otimes \mathbf{C}_i \\
\mathbf{C}_{4h} = \mathbf{C}_4 \otimes \mathbf{C}_i & ; & \mathbf{D}_{4h} = \mathbf{D}_4 \otimes \mathbf{C}_i & ; & \mathbf{D}_{6h} = \mathbf{D}_6 \otimes \mathbf{C}_i \\
\mathbf{C}_{6h} = \mathbf{C}_6 \otimes \mathbf{C}_i & ; & \mathbf{S}_6 = \mathbf{D}_3 \otimes \mathbf{C}_i & ; & \mathbf{T}_h = \mathbf{T} \otimes \mathbf{C}_i \\
 & & & & \mathbf{O}_h = \mathbf{O} \otimes \mathbf{C}_i
\end{array} \tag{1.31}$$

In this notation our example group is the, $\mathbf{D}_3$, point group, i.e., it has a threefold symmetry axis and three twofold axes perpendicular to the symmetry axis. The character table can then be written as,

$\mathbf{D}_3$	$\mathcal{E}$	$3\mathcal{C}_{2\perp}$	$2\mathcal{C}_3$
A_1	1	1	1
A_2	1	-1	1
E	2	0	-1

(1.32)

The octahedron group,[6] $\mathbf{O}$, of proper rotations of a cube has direct bearing on the XY_6 molecule which has the full octahedron symmetry, $\mathbf{O}_h$. The full octahedron symmetry group is the direct product of the octahedron group and the inversion operator, $\mathbf{O}_h = \mathbf{O} \otimes \mathbf{C}_i$. To study the full octahedron group $\mathbf{O}_h$, we first obtain the character table of the octahedron group, $\mathbf{O}$, from which we can obtain the character table of the, $\mathbf{O}_h$ group.

---

[5] $\mathbf{C}$ are the cyclic groups, $\mathbf{D}$ are the dihedral groups, $\mathbf{D}_2 = \mathcal{V}$ is the German "vierengruppen", $\mathbf{S}$ are the symmetric groups, $\mathbf{T}$ is the tetrahedron group, $\mathbf{O}$ is the octahedron group.

[6] Note that when referring to the group it is known as the octahedron group, but when applied to the symmetry of molecules, the molecule is known as an octahedral molecule.

$\mathbf{O}$	$\mathcal{E}$	$8\mathcal{C}_3$	$3\mathcal{C}_2$	$6\mathcal{C}_2$	$6\mathcal{C}_4$
A_1	1	1	1	1	1
A_2	1	1	1	-1	-1
E	2	-1	2	0	0
F_1	3	0	-1	-1	1
F_2	3	0	-1	1	-1

(1.33)

This group is isomorphic to the regular tetrahedron group, $\mathbf{T}_d$. The only differences being that the classes are labeled, $\mathcal{E}$, $8\mathcal{C}_3$, $3\mathcal{C}_2$, $6\sigma_d$, $6\mathcal{S}_4$. The classes of the full octahedron group, $\mathbf{O}_h$, can be obtained from the direct products of the classes of the regular octahedron group, $\mathbf{O}$, with the class of the inversion operator, $\mathcal{I} = \mathcal{S}_2$.

$\mathbf{O}$	$\mathcal{E}$	$8\mathcal{C}_3$	$3\mathcal{C}_2$	$6\mathcal{C}_2$	$6\mathcal{C}_4$
$\otimes\mathbf{S}_2$	$\downarrow$	$\downarrow$	$\downarrow$	$\downarrow$	$\downarrow$
	$\mathcal{I}$	$8\mathcal{S}_6$	$3\sigma_h$	$6\sigma_d$	$6\mathcal{S}_4$

(1.34)

The character table of the full octahedron symmetry group, $\mathbf{O}_h$, is given below (this can also be found in Barrow [58]),

$\mathbf{O}_h$	$\mathcal{E}$	$8\mathcal{C}_3$	$3\mathcal{C}_2$	$6\mathcal{C}_2$	$6\mathcal{C}_4$	$\mathcal{I}$	$6\mathcal{S}_4$	$8\mathcal{S}_6$	$3\sigma_h$	$6\sigma_d$
A_{1g}	1	1	1	1	1	1	1	1	1	1
A_{1u}	1	1	1	1	1	-1	-1	-1	-1	-1
A_{2g}	1	1	1	-1	-1	1	-1	1	1	-1
A_{2u}	1	1	1	-1	-1	-1	1	-1	-1	1
E_g	2	-1	2	0	0	2	0	-1	2	0
E_u	2	-1	2	0	0	-2	0	1	-2	0
F_{1g}	3	0	-1	-1	1	3	1	0	-1	-1
F_{1u}	3	0	-1	-1	1	-3	-1	0	1	1
F_{2g}	3	0	-1	1	-1	3	-1	0	-1	1
F_{2u}	3	0	-1	1	-1	-3	1	0	1	-1

(1.35)

1.4.4. XY_6 IR Active Transition Frequencies

The rovibrational energy spectrum of a polyatomic molecule has a complex structure. For our octahedral, XY_6, we have, $3N - 6 = 15$, where, $N = 7$, the number of atoms, natural vibrational modes ($6 = 3 + 3$ for translational and rotational freedom). A change of variables of the Hamiltonian, in the Born-Oppenheimer approximation 1927, to mass weighted coordinate are usually referred to as normal coordinates with their associated normal vibrational modes. This assures that the normal modes contain no net translation or rotation about the center of mass of

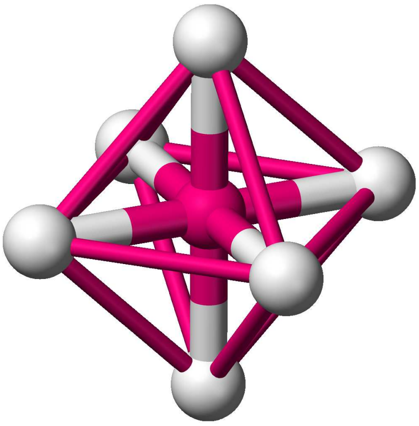

Figure 1.4.: Octahedral Molecule

the molecule. The potential energy function of the intramolecular vibration harmonic oscillator are diagonal, i.e., contain no cross terms in the normal coordinate representation. The octahedral symmetry of the XY_6 molecule reduces the number of active normal vibrational modes to 6, usually referred to as, $\nu_1, \nu_2, \ldots, \nu_6$. For a thorough understanding of the methods employed consult the classic of Wilson, Decius, Cross [31] and the up to date Bunker and Jensen [30]. Specifically for octahedral molecules the 1934 article by Nath [59] which directly applies the GF Matrix method of Wilson et al [31]. The importance of determining the force constants of octahedral molecules by this method and improvements thereof, is shown in the number of articles relating to the technique, even as recent as 2005, cf. Fatih Ucun and M. Gökhan Sengül [60]. This is also an excellent paper that summarizes all the aspects quite well. It also contains a list of the common octahedral XY_6 molecules, namely, SF_6, SeF_6, MoF_6, TeF_6, WF_6, OsF_6, IrF_6, NpF_6, UF_6, and PuF_6. It calculates the 7 force constants of all these molecules.

Of the 6 vibrational frequency modes, ν_1, is a single mode, ν_2, is a double degenerate mode, and ν_3,ν_4, ν_5, and ν_6, are triply degenerate modes. Multiplied with there degeneracies, these add up to their original 15 natural modes. Not all the normal modes are Raman or infrared (IR) active, i.e., modes that can be directly excited by a single frequency EM field. We concentrate only on the IR-active ν_3 mode. The energy spectrum is discrete in the first few IR-active rovibrational levels of the ν_3 normal mode. The statistical density of rovibrational states increases rapidly with energy. For a polyatomic molecule a point is reached where the density of the states is so high that the energy states are in a quasi-continuum. As we climb further up the ν_3 ladder we eventually reach the dissociation energy where the molecule dissociates into the continuum. An interesting effect occurs at the onset of the quasi-continuum. In a high intensity monochromatic electromagnetic field, i.e., a laser pulse, the polyatomic molecule is excited in a dipole active normal mode. This absorbed energy redistributes itself quite rapidly into the other available vibrational modes to establish a statistical equilibrium among the modes. The agent of the intramolecular redistribution of energy can qualitatively be explained by intramode coupling at the heart of which lies the nonlinear spectroscopic anharmonicities. This process is called intramolecular vibrational redistribution or relaxation (IVR). The onset is called the stochastization energy. In analogy with classical Hamiltonian systems one could say the molecular rovibrations find themselves in a quantum chaos. IVR induces statistical inhomogeneous broadening in the rovibrational spectrum. A quantitative theory for the IVR has been developed by Makarov et al. [49]. There are numerous theories to model the IR multiphoton excitation of a polyatomic molecule. The overtone of eigenvalue modes listed in the Table 1.1 below are given in Halonen and Child [61]. The infra-red active ν_3 rovibrational modes of the $\mathbf{O}_h$-symmetry of the octahedral molecule are listed in Table 1.1.

No	**Frequency**	**Level**	**Group Symmetry**
1	$\omega_1 = 0$	0	A_{1g}
2	$\omega_2 = 627.71$	1	F_{1u}
3	$\omega_3 = 2\omega_2 - 2.6080$	2	E_g
4	$\omega_4 = 2\omega_2 - 2.3560$	2	A_{1g}
5	$\omega_5 = 2\omega_2 + 0.2120$	2	F_{1g}
6	$\omega_6 = \omega_5 + \omega_2 - 7.7916$	3	F_{1u}
7	$\omega_7 = \omega_5 + \omega_2 - 2.3960$	3	F_{2u}
8	$\omega_8 = \omega_5 + \omega_2 - 2.2204$	3	F_{1u}
9	$\omega_9 = \omega_5 + \omega_2 + 0.3330$	3	A_{2u}
10	$\omega_{10} = 2495.75$	4	A_{1g}
11	$\omega_{11} = 2495.76$	4	E_g
12	$\omega_{12} = 2503.73$	4	F_{1g}
13	$\omega_{13} = 2504.20$	4	F_{2g}
14	$\omega_{14} = 2506.60$	4	E_g
15	$\omega_{15} = 2506.87$	4	A_{1g}
16	$\omega_{16} = 2509.42$	4	F_{2g}
17	$\omega_{17} = 3132.17$	QC	None

Table 1.1.: XY_6 ν_3-rovibrational modes

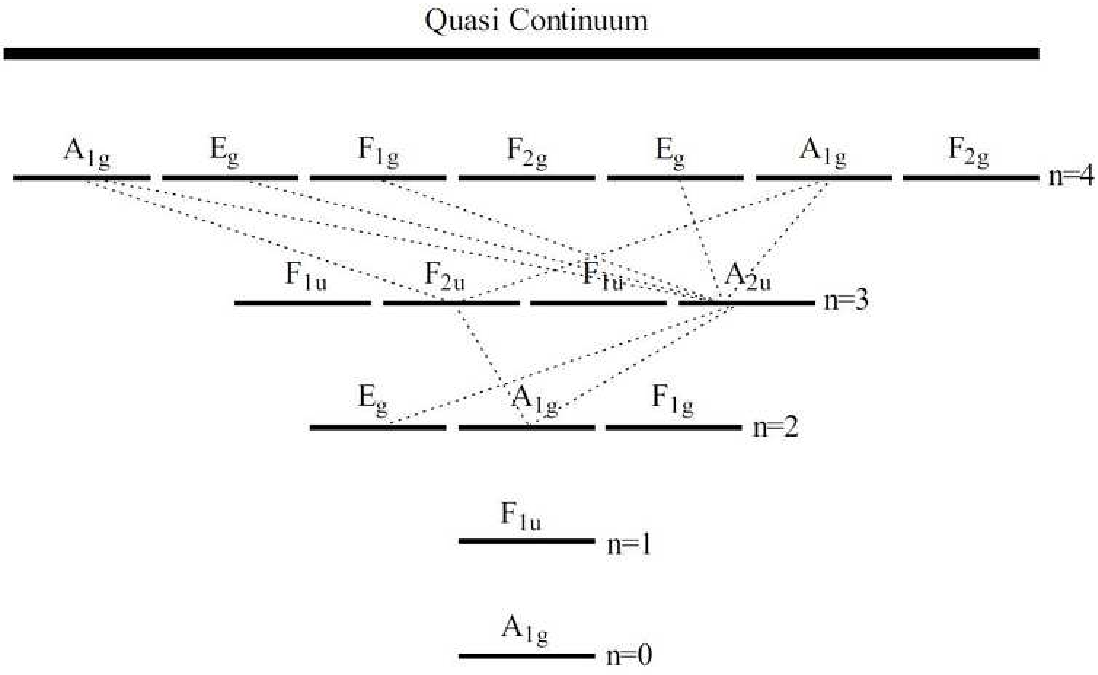
Quasi Continuum
A1g
Eg
F1g
F2g
Eg
A1g
F2g
n=4
F1u
F2u
F1u
A2u
n=3
Eg
A1g
F1g
n=2
F1u
n=1
A1g
n=0

Figure 1.5.: ν_3-Rovibrational Levels of Octahedral Molecule

1.4.5. XY$_6$ Dipole Moments

Transition dipole moments are measured in units of Debye and is given by,

$$\text{Debye} = 3.3356 \times 10^{-30}\text{Cm}$$

.

The dipole moment of the first rovibrational transition moment of XY$_6$ is given by,

$$S_1 = (0.394 * \text{Debye})/e = 8.202759 \times 10^{-12}\text{m},$$

where, $e = 1.602176 \times 10^{-19}$ C, is the charge of the electron. The first transition dipole moments can be rounded off to,

$$S_2 = 8 \times 10^{-12}.$$

Transition Dipole Moment Matrix, χ, is symmetrical with zero diagonal. Define only the upper triangular nonzero transition dipole moments, X. Adding the transpose to the matrix completes the lower triangular matrix,

$$\chi = X + X^T \tag{1.36}$$

Dipole constants $\mathbf{XY}_6$

1. The first-level dipole transition moment is given by,

$$\chi_{1,2} = S_2.$$

2. The second-level dipole transition moment is given by,

$$\begin{aligned} \chi_{2,3} &= S_2\sqrt{0.444}, \\ \chi_{2,4} &= S_2\sqrt{0.222}, \\ \chi_{2,5} &= S_2\sqrt{0.666}. \end{aligned}$$

3. The third-level dipole transition moment is given by,

$\chi_{3,6} = S_2\sqrt{1.029}$	$\chi_{4,6} = S_2\sqrt{0.939}$	$\chi_{5,6} = S_2\sqrt{0.009}$
$\chi_{3,7} = S_2\sqrt{0.500}$	$\chi_{4,7} = S_2\sqrt{0.372 \times 10^{-27}}$	$\chi_{5,7} = S_2\sqrt{0.667}$
$\chi_{3,8} = S_2\sqrt{0.137}$	$\chi_{4,8} = S_2\sqrt{0.7274}$	$\chi_{5,8} = S_2\sqrt{0.6658}$
$\chi_{3,9} = S_2\sqrt{0.278 \times 10^{-31}}$	$\chi_{4,9} = S_2\sqrt{0.5434 \times 10^{-31}}$	$\chi_{5,9} = S_2\sqrt{0.333}$

Table 1.2.: 3rd-level dipole transition moments

4. The fourth-level dipole transition moment is given by,

$\chi_{6,10} = S_2\sqrt{0.095}$	0	$\chi_{8,10} = S_2\sqrt{0.095}$	0
$\chi_{6,11} = S_2\sqrt{0.190}$	$\chi_{7,11} = S_2\sqrt{0.2198}$	$\chi_{8,11} = S_2\sqrt{0.190}$	0
$\chi_{6,12} = S_2\sqrt{0.2857}$	$\chi_{7,12} = S_2\sqrt{0.3297}$	$\chi_{8,12} = S_2\sqrt{0.2857}$	0
$\chi_{6,13} = S_2\sqrt{0.2857}$	$\chi_{7,13} = S_2\sqrt{0.3297}$	$\chi_{8,13} = S_2\sqrt{0.2857}$	$\chi_{9,13} = S_2\sqrt{0.7143}$
$\chi_{6,14} = S_2\sqrt{0.190}$	$\chi_{7,14} = S_2\sqrt{0.2198}$	$\chi_{8,14} = S_2\sqrt{0.190}$	0
$\chi_{6,15} = S_2\sqrt{0.095}$	0	$\chi_{8,15} = S_2\sqrt{0.095}$	0
$\chi_{6,16} = S_2\sqrt{0.2857}$	$\chi_{7,16} = S_2\sqrt{0.3297}$	$\chi_{8,16} = S_2\sqrt{0.2857}$	$\chi_{9,16} = S_2\sqrt{0.7143}$

Table 1.3.: 4th-level dipole transition moments

5. The quasi-continuum dipole transition moment is given by,

$\chi_{10,17} = S_2\sqrt{11/36}$
$\chi_{11,17} = S_2\sqrt{11/36}$
$\chi_{12,17} = S_2\sqrt{11/36}$
$\chi_{13,17} = S_2\sqrt{11/36}$
$\chi_{14,17} = S_2\sqrt{11/36}$
$\chi_{15,17} = S_2\sqrt{11/36}$
$\chi_{16,17} = S_2\sqrt{11/36}$

Table 1.4.: QC dipole transition moments

In the following representation (on the next page) of the interaction Hamiltonian matrix the coefficients are denoted by, $a = \chi$.

Dirac interaction Hamiltonian is then given by,

$$H_{ij}(t) = \chi_{ij} e^{i\omega_{ij} t} \varepsilon(t), \tag{1.37}$$

where, $\omega_{ij} = \omega_i - \omega_j$, and $\varepsilon(t)$, is the real component of the electric field of the input femtosecond IR laser pulse.

$$
\boldsymbol{\chi} = \begin{pmatrix}
0 & a_{1,2} & 0 & 0 & 0 & 0 & 0 & 0 & 0 & 0 & 0 & 0 & 0 & 0 & 0 & 0 & 0 \\
a^*_{1,2} & 0 & a_{2,3} & a_{2,4} & a_{2,5} & 0 & 0 & 0 & 0 & 0 & 0 & 0 & 0 & 0 & 0 & 0 & 0 \\
0 & a^*_{2,3} & 0 & 0 & 0 & a_{3,6} & a_{3,7} & a_{3,8} & a_{3,9} & 0 & 0 & 0 & 0 & 0 & 0 & 0 & 0 \\
0 & a^*_{2,4} & 0 & 0 & 0 & a_{4,6} & a_{4,7} & a_{4,8} & a_{4,9} & 0 & 0 & 0 & 0 & 0 & 0 & 0 & 0 \\
0 & a^*_{2,5} & 0 & 0 & 0 & a_{5,6} & a_{5,7} & a_{5,8} & a_{5,9} & 0 & 0 & 0 & 0 & 0 & 0 & 0 & 0 \\
0 & 0 & a^*_{3,6} & a^*_{4,6} & a^*_{5,6} & 0 & 0 & 0 & 0 & a_{6,10} & a_{6,11} & a_{6,12} & a_{6,13} & a_{6,14} & a_{6,15} & a_{6,16} & 0 \\
0 & 0 & a^*_{3,7} & a^*_{4,7} & a^*_{5,7} & 0 & 0 & 0 & 0 & 0 & a_{7,11} & a_{7,12} & a_{7,13} & a_{7,14} & 0 & a_{7,16} & 0 \\
0 & 0 & a^*_{3,8} & a^*_{4,8} & a^*_{5,8} & 0 & 0 & 0 & 0 & a_{8,10} & a_{8,11} & a_{8,12} & a_{8,13} & a_{8,14} & a_{8,15} & a_{8,16} & 0 \\
0 & 0 & a^*_{3,9} & a^*_{4,9} & a^*_{5,9} & 0 & 0 & 0 & 0 & 0 & 0 & 0 & a_{9,13} & 0 & 0 & a_{9,16} & 0 \\
0 & 0 & 0 & 0 & 0 & a^*_{6,10} & 0 & a^*_{8,10} & 0 & 0 & 0 & 0 & 0 & 0 & 0 & 0 & a_{10,17} \\
0 & 0 & 0 & 0 & 0 & a^*_{6,11} & a^*_{7,11} & a^*_{8,11} & 0 & 0 & 0 & 0 & 0 & 0 & 0 & 0 & a_{11,17} \\
0 & 0 & 0 & 0 & 0 & a^*_{6,12} & a^*_{7,12} & a^*_{8,12} & 0 & 0 & 0 & 0 & 0 & 0 & 0 & 0 & a_{12,17} \\
0 & 0 & 0 & 0 & 0 & a^*_{6,13} & a^*_{7,13} & a^*_{8,13} & a^*_{9,13} & 0 & 0 & 0 & 0 & 0 & 0 & 0 & a_{13,17} \\
0 & 0 & 0 & 0 & 0 & a^*_{6,14} & a^*_{7,14} & a^*_{8,14} & 0 & 0 & 0 & 0 & 0 & 0 & 0 & 0 & a_{14,17} \\
0 & 0 & 0 & 0 & 0 & a^*_{6,15} & 0 & a^*_{8,15} & 0 & 0 & 0 & 0 & 0 & 0 & 0 & 0 & a_{15,17} \\
0 & 0 & 0 & 0 & 0 & a^*_{6,16} & a^*_{7,16} & a^*_{8,16} & a^*_{9,16} & 0 & 0 & 0 & 0 & 0 & 0 & 0 & a_{16,17} \\
0 & 0 & 0 & 0 & 0 & 0 & 0 & 0 & 0 & a^*_{10,17} & a^*_{11,17} & a^*_{12,17} & a^*_{13,17} & a^*_{14,17} & a^*_{15,17} & a^*_{16,17} & 0
\end{pmatrix} \tag{1.38}
$$

1.5. Spatial Light Modulator

The 4-f SLM configuration is used to modulate the femtosecond laser pulse to control the molecular transition level. The SLM consists of 640 pixel amplitude and phase modulators. The modulation occurs in spatial frequency domain, but it can easily be shown to be equivalent to time-frequency modulation. Given an input electric field IR femtosecond laser pulse, with a Gaussian modulation modeled as,

$$\begin{aligned} \varepsilon_i(t) &= A_i \frac{1}{\sqrt{2\pi}\sigma} e^{-\frac{(t-t_0)^2}{2\sigma^2}} \cos\omega_i(t-t_0) \\ &= A_i \frac{1}{\sqrt{2\pi}\sigma} e^{-\frac{(t-t_0)^2}{2\sigma^2}} \frac{e^{i\omega_i(t-t_0)} + e^{-i\omega_i(t-t_0)}}{2}, \end{aligned} \tag{1.39}$$

where, A_i, is the input amplitude, ω_i, is the IR angular frequency, t_0, is the center time (usually taken to be zero) and σ, is the standard deviation of the Gaussian pulse, respectively. We are only interested in the analytic signal with positive frequencies,

$$\varepsilon_i(t) = A_i \frac{1}{\sqrt{2\pi}\sigma} e^{-\frac{(t-t_0)^2}{2\sigma^2}} e^{i\omega_i(t-t_0)}. \tag{1.40}$$

Note also that it is the standard Gaussian normalized to one, i.e.,

$$\int_{-\infty}^{\infty} \frac{1}{\sqrt{2\pi}\sigma} e^{-\frac{(t-t_0)^2}{2\sigma^2}} = 1. \tag{1.41}$$

This is then transformed to the frequency domain by standard Fourier optics by means of a grating and mirrors. For, $t_0 = 0$,

$$\tilde{\varepsilon}_i(\omega) = A_i \frac{1}{\sqrt{2\pi}} e^{-\frac{\sigma^2(\omega-\omega_i)^2}{2}} = \tilde{A}_i e^{-\frac{\sigma^2(\omega-\omega_i)^2}{2}}. \tag{1.42}$$

A N-discretization of a transform limited pulse in the frequency domain can therefore be written as,

$$\tilde{\varepsilon}_N(\omega) = \sum_{n=-\frac{N}{2}}^{\frac{N}{2}-1} \operatorname{rect}\left[\frac{\omega-\omega_n}{\triangle\omega}\right] \tilde{\varepsilon}_n(\omega) = \sum_{n=-\frac{N}{2}}^{\frac{N}{2}-1} \tilde{A}_n e^{i\Phi_n}, \tag{1.43}$$

where, rect$(\cdot)$, is the normal rectangular function defined in Subsection A.4.3.

This is easily obtained from the Fourier transform and Fourier transform properties (cf. Table A.1 in Section A.5),

$$\mathcal{F}\left\{\frac{1}{\sqrt{2\pi}\sigma}e^{-\frac{t^2}{2\sigma^2}}\right\} = \frac{1}{\sqrt{2\pi}}e^{-\frac{\sigma^2\omega^2}{2}}. \tag{1.44}$$

The masking function associated with the pixellated device with N-pixels is given by,

$$M(x) = \sum_{n=-\frac{N}{2}}^{\frac{N}{2}-1} \text{rect}\left[\frac{x-x_n}{\triangle x_p - \triangle x_g}\right] M_n e^{-i\phi_n} + \sum_{k=-\frac{N}{2}}^{\frac{N}{2}-1} \text{rect}\left[\frac{x-x_k+\frac{\triangle x_p}{2}}{\triangle x_p - \triangle x_g}\right] M_k e^{-i\phi_k}, \tag{1.45}$$

where,

$$\begin{aligned}
\triangle x_p &= \text{Width of a single pixel.}\\
\triangle x_g &= \text{Separation between pixels.}\\
M_n &= \text{Amplitude modulation of the pixels.}\\
M_k &= \text{Amplitude modulation of the gaps.}\\
\phi_n &= \text{Phase modulation of the pixels.}\\
\phi_k &= \text{Phase modulation of the gaps}
\end{aligned}$$

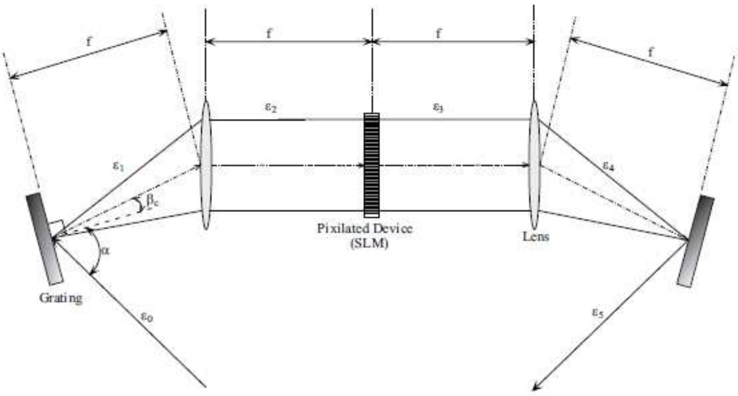

Figure 1.6.: 4f-Spatial Light Modulator

A complete analysis can be found in various articles Trebino [62] and the MSc thesis [55]. The effect of the SLM in the frequency domain for a transform limited bandwidth is the following discretization,

$$M(\omega) = \sum_{n=-\frac{N}{2}}^{\frac{N}{2}-1} \text{rect}\left[\frac{\omega-\omega_n}{\triangle\omega}\right] M_n e^{-i\phi_n}. \tag{1.46}$$

The product with the input electric pulse then gives,

$$\tilde{E}_N(\omega) = M(\omega)\tilde{\varepsilon}_N(\omega) = \sum_{n=-\frac{N}{2}}^{\frac{N}{2}-1} \operatorname{rect}\left[\frac{\omega-\omega_n}{\triangle\omega}\right] M_n\tilde{A}_n e^{i\Phi_n - i\phi_n}. \tag{1.47}$$

The second set of lens and grating inverse Fourier transforms the electric field of the femtosecond pulse back into time domain,

$$\varepsilon_N(t) = \Re\left[\boldsymbol{\mathcal{F}}^{-1}\{\tilde{E}_N(\omega)\}\right], \tag{1.48}$$

and of course it is only real part that interacts with Hamiltonian of the molecule.

1.6. Introduction to Time Frequency Representations

Time-frequency Representations (TFR) and analysis (TFA) was originally introduced in a seminal paper by E. P. Wigner for quantum statistical mechanics [63], in quantum phase space, (q, p), known as the Wigner distribution. In 1946, D. Gabor was researching communication theory [64] and immediately saw that the quantum wave mechanics was also applicable to TFA of sound. He modified the von Neumann phase space representation to TFA and represented the signal with Gaussian pulses on the time-frequency domain. These pulses would later be known as Gabor atoms. Ville 1948 [65] adapted the bilinear Wigner representation to a TFR which is now commonly known as the Wigner-Ville distribution. Since then a myriad of TFR have been invented, mainly due to some short comings of the Wigner-Ville distribution. In 1966 Leon Cohen [66] "Generalized phase-space distribution functions", came up with a classification scheme for the various TFRs, known as **Cohen Classes**.

Essentially there are two main classes:

1. The Atomic Decompositions
    a) Short Time Frequency Transform (STFT)
    b) Gabor Representation
    c) Time-scale analysis and wavelet transforms
    d) Spectrogram
    e) Scalogram
2. The Energy Distributions (Cohen classes)

a) The Wigner-Ville Distribution

b) The Ambiguity function - Symmetrical Sussman ambiguity function

c) Generalized phase-space distribution functions

One of the most popular methods to analyze a non-stationary time signal would probably be the original short-time Fourier transform developed by Gabor.

The simplicity of the concept behind it, directly displays the shortcomings of the Fourier transform technique. Imagine we are lying down and absorbing the sounds of a beautiful classical piece of music, which lasts an hour. The opus starts with slow violins, cello's with harps and slowly builds up were the woodwinds enter. Then the brass and drums come in building up to a crescendo climax. If we were to have any idea of the frequency content of the music, we simply Fourier analyze it. In the spectrum we could localize the frequency contents of the violin or the drum, but alas we will have no indication of when the instruments were played. Ah, but to accomplish this, it would be much better to break down the hour into five minute intervals and to Fourier analyze them individually. At least this would give us some indication of when the violins or drums were played. This is of course a coarse scaling and to achieve a better localization it would be straightforward to break it down into one minute intervals. This is the concept behind the short-time Fourier transform. Just chop up the signal and individually Fourier analyze the small intervals to obtain a combined time-frequency picture of the signal.

Of course, we can continue and just make the intervals smaller and smaller to get an ever improved representation of the music. Unfortunately, this is were we run into a mathematical conundrum. We cannot and the reason is that, when the time intervals become so narrow, then the spectrum looses any relationship to our music. What has happened? And this is one of the fundamental limitations of Fourier transforms. We have taken the original score and dissected it into short time signals, but according to Fourier analyzes, short signals have broad bandwidths, so much so, that they do not properly represent the frequency content of the original signal. Buried in the underlying Fourier technique is an uncertainty principle, almost similar to the Heisenberg uncertainty principle of quantum mechanics and they have the same mathematical foundations (cf. Appendix A "The Fourier Integral and Delta Functions" of Gasiorowicz [5]). Irrespective, this technique can work well, if the right discretization is chosen for the specific signal. But in other specific cases this might not be possible. Although, we see that it sometimes works and at other times doesn't and that we are aware that there is a fundamental uncertainty principle underlying the technique, we must also bear in mind that it maybe the process of breaking down our signal in smaller pieces that might cause the failure of the method. Therefore, the plethora of various time-frequency representations. One technique may just work better for a specific signal than another. The best analogy to TFR is a musical score, depicted in Figure 1.7, where the horizontal lines denote direction of time and the vertical direction the frequency content. Without this type of musical representation, musicians would not have been able to play each other's compositions, without having listened to the piece.

Larghetto
from Divertimento No. 2
W. A. Mozart
Arranged by Andrew Forrest (1986)
gtr1
gtr2
gtr3
p dolce
p dolce
p dolce
5
V

Figure 1.7.: Musical Score for Three Guitars

1.7. Overview of the Thesis

In this introductory Chapter 1, short overviews of various relevant topics were already presented, such as classical control theory, quantum control, quantum coherent control, the derivation of the Dirac-Liouville-von Neumann interaction picture equation, octahedral molecules, with their irreducible representations, group theory, etc., spatial light modulators, and an introduction to time-frequency representations, specifically discussing the short time Fourier transform.

No discussion about lasers is given in the introductory Chapter 1. A short discussion about EM waves, Gaussian beams, Fourier optics, optical phase space, EM quantization and Lagrangians and coherent states is lastly overviewed in Chapter 7.

An overview relating to Time-Frequency-Representation (TFR) is given in Chapter 2. Here the two main types are characterized. It is worthy to note that the original Cohen classes were meant as a classification scheme for the then known quantum mechanical TFRs.

It seems that the preferred Time-Frequency-Representation (TFR) for scientists, i.e., physicists and chemists, as opposed to engineers, is the von Neumann TFR, Chapter 3, to represent ultra-short laser pulses. Here the von Neumann TFR is defined and some features are highlighted. The derivations relating to the overlap integral or matrix is also given and found to differ from that given in an important article.

Chapter 4 is a prepublished article concerning the adaptive quantum coherent control of a multi-level molecular system in the von Neumann time-frequency domain. Here we explore the use of the von Neumann TFR specifically for our quantum coherent control of an octahedral molecule. We discover that the von Neumann representation greatly reduces the search time of the optimization algorithm. With the speed advantage we explore the quantum topology of the laser interaction with octahedral molecule.

Given the advantages that we gained from the use of the von Neumann it was discovered that certain of the great features of the von Neumann spectral and temporal bases could be extended into the Hermite-Gauss polynomials. For TFRs this is a novel discovery andChapter 5 describes in detail the derivation of the generalized Fourier-Hermite-Gauss (FHG) time-frequency representation. Much of this Chapter is unique to this dissertation. The discovery and application of Pascal matrices to Hermite translations is also new. Whole new Lemmas, Corollaries and a Theorem, specifically pertaining to this representation are also presented.

Although the Pascal matrices perform marvels analytically there numerical calculation and stability leave much to be desired. This necessitated a deep research in Chapter 6, concerning the complete FHG spectral and temporal lattice cubes. Being a direct consequence of the FHG TFR this Chapter in its entirety is novel and unique to this dissertation. The complete lattice cube is investigated and even new functions are defined to facilitate in the development.

The very nature of the FHG temporal and spectral bases are very reminiscent to the solution of the quantum harmonic oscillator. The subsequent step to coherent states, which can also be expanded in terms of quantum harmonic oscillator states, is cautiously analyzed in Chapter 7. It is discovered, that at least for the temporal FHG TFR bases that there exists an analogy between these states and a correspondence “classical” coherent state harmonic oscillator representation. This is then developed in terms of a correlation function between these FHG temporal representation of laser shaped ultrafast pulses. This is what we call the coherent state TFR analogy, which in essence, is a correlation between the respective state representations.

Finally, in Chapter 8, the dissertation is once again summarized in the conclusion. The main discoveries are highlighted. A short description of outstanding work relating to this thesis, that should be completed in the future, is given. Then future research is outlined.

There are quite a few appendices which we include here to ensure that the reader has a rather complete reference handy on all the mathematics relevant to this thesis. There is a serious Appendix A on Fourier transforms. One on the derivation of the FHG spectral overlap matrix, and another on orthogonal polynomials, and then lastly just some Matlab© programs.

2. Time Frequency Representations

2.1. Introduction

Time Frequency Representations (TFR) originated with Eugene Wigner and John von Neumann to represent the quantum mechanical wave functions in phase space (q, p) and then only recognized to be just as applicable for sound waves by Denis Gabor. The forefathers are shown in Figure 2.1.

To get a better idea of wave signal analysis, we firstly introduce a few common definitions like signal localization Section 2.2, the Heisenberg-Gabor Inequality Section 2.3, the concept of an analytical signal Section 2.4, before venturing into a discussion of some atomic decompositions, starting with the mathematical analysis of the Short-Time-Fourier-Transform Section 2.5. Thereafter, in Section 2.6, we discuss the Gabor transform, which was the first STFT, and was actually originally conceived by Denis Gabor from the von Neumann TFR. The von Neumann TFR is discussed in detail in Chapter 3. The widely used spectrogram, in signal analysis, is given in Section 2.7, its characteristic function and its relationship with the so called ambiguity function. In Subsection 2.7.1 a short discussion of the inherent barrier of time-frequency resolution is outlined. Subsection 2.7.2 gives an all to brief discussion on discrete time signal analysis (this is a field all on its own [67]) for the STFT. An extremely good classical review of the various time-frequency distributions is given by Cohen [68]. Although a bit outdated 1989, it reviews the historical developments quite nicely.

Section 2.8 discusses the prototype of the TFR kernel methods, namely the Wigner-Ville distribution. In Subsection 2.8.1, some properties of the Wigner-Ville distribution are given, Subsection 2.8.2, disadvantages, Subsection 2.8.3, the Pseudo-Wigner-Ville distribution and in Subsection 2.8.4, the related ambiguity is discussed, respectively.

Finally, in Section 2.9, the all important kernel methods developed by Leon Cohen are presented. Only a brief history and summary is given, but in Subsection 2.9.1 the Husimi distribution, which has quantum mechanical implementations and also used herein, is presented and in Subsection 2.9.2 the Smoothed-Pseudo-Wigner-Ville Distribution is given.

Figure 2.1.: Eugene Wigner, John von Neumann and Dennis Gabor

2.2. Signal Localization

In Appendix A an overview of Fourier transforms is presented. There we see that the Fourier transform can be defined in various ways. It is essential for anybody working in this field to be able to use any of these definitions, and to be able to revert from one to another. It is also common in electrical engineering and Digital Signal Processing (DSP) to rather use, $j = \sqrt{-1}$, for the imaginary symbol to avoid possible confusion with symbol used for electrical current, i. However, for this paragraph we define (t, is time and, ν, is frequency)

$$\boldsymbol{\mathcal{F}}\left\{g\left(t\right)\right\} = G\left(\nu\right) = \int_{-\infty}^{\infty} g\left(t\right) e^{-2\pi i\nu t}\,\mathrm{d}t, \tag{2.1}$$

$$\boldsymbol{\mathcal{F}}^{-1}\left\{G\left(\nu\right)\right\} = g\left(t\right) = \int_{-\infty}^{\infty} G\left(\nu\right) e^{2\pi i\nu t}\,\mathrm{d}\nu. \tag{2.2}$$

The advantage of this definition is that we do not have any normalization constants, and its immediate disadvantage of continuesly writting the 2π in the exponent. To avoid this, we can transform to angular frequency, $\omega = 2\pi\nu$, (which then corresponds to the quantum mechanical Fourier transform definitions between phase space, (q, p)), but unfortunately this introduces the normalization constants. This is also discussed in excellent classic book of Cohen [33].

If we consider that the *energy*, E_x, is assumed to be finite, of a signal, $x(t)$[1], is related through Parseval's theorem (cf. Subsection A.3.10 and Eq. (A.72)) by,

$$E_x = \int_{-\infty}^{\infty} \left|x(t)\right|^2\,\mathrm{d}t = \int_{-\infty}^{\infty} \left|X(\nu)\right|^2\,\mathrm{d}\nu. \tag{2.3}$$

---

[1] We shall either refer to time signals as $s(t)$ or as $x(t)$.

Since, $|x(t)|^2$, and, $|X(\nu)|^2$, are positive and can be normalized to unity it is tempting to consider these functions as probability density distribution functions, namely, $p_x(t) = \frac{1}{E_x}|x(t)|^2$, and $p_X(\nu) = \frac{1}{E_x}|X(\nu)|^2$. This is exactly what Cohen does. Then, in analogy with probability theory, we can define the following averages[2]:

- Time average.

$$t_m = \langle t \rangle = \bar{t} = \frac{1}{E_x}\int_{-\infty}^{\infty} t\,|x(t)|^2 \,\mathrm{d}t \tag{2.4}$$

- Frequency average.

$$\nu_m = \langle \nu \rangle = \bar{\nu} = \frac{1}{E_x}\int_{-\infty}^{\infty} \nu\,|X(\nu)|^2 \,\mathrm{d}\nu \tag{2.5}$$

- Time spreading (Temporal covariance, Time duration).

$$T^2 = (\Delta t)^2 = \frac{4\pi}{E_x}\int_{-\infty}^{\infty} (t - t_m)^2\,|x(t)|^2 \,\mathrm{d}t \tag{2.6}$$

- Frequency spreading (Spectral covariance, Frequency bandwidth).

$$B^2 = (\Delta \nu)^2 = \frac{4\pi}{E_x}\int_{-\infty}^{\infty} (\nu - \nu_m)^2\,|X(\nu)|^2 \,\mathrm{d}\nu \tag{2.7}$$

- Characteristic function (Given a “probability density”, $p_x(t) = \frac{1}{E_x}|x(t)|^2$.)

$$P_x(\theta) = \int_{-\infty}^{\infty} p_x(t)e^{i\theta t}\,\mathrm{d}t$$

A signal can then be characterized in the time-frequency domain by its average position, (t_m, ν_m), and its average location of energy given by the area of the *time-bandwidth product,* $T \times B$.

2.3. Heisenberg-Gabor Inequality

A consequence of the scaling property of the the Fourier transform pairs (see Subsection A.3.4) reveals an interesting constraint,

$$\boxed{T \times B \geq 1} \tag{2.8}$$

---

[2] The bracket $\langle\cdot\rangle$ denotes an integral probability average or expectation

or,

$$\Delta t \Delta \nu \geq 1.$$

This constraint is known as the *Heisenberg-Gabor inequality* (in honour of the Heisenberg uncertainty relationship in Quantum Mechanics which Denis Gabor accredited to Heisenberg, in his original article [64], cf. also [33, 34]). This manifests, that it is impossible to simultaneously represent a signal in the time and in the frequency domain with arbitrarily small support. The lower bound or equality in Eq. (2.8) is reached for a *Gaussian function,*

$$x(t) = C \exp\left[-\alpha(t-t_m)^2 + 2\pi i \nu_m (t-t_m)\right], \qquad C \in \mathbb{R},\ \alpha \in \mathbb{R}^+. \tag{2.9}$$

2.4. Analytical Signals

Gabor recognized that in Fourier transforms *negative* frequencies naturally occur, as mathematical artifacts of the complex representation, but physically that they hard to interpret. Mirror images of the Fourier spectrum about the zero frequency to reflect physical real signals is common. If a signal can somehow be transformed so that it generally shows only positive frequencies, these signals would be considered more *physical.* This is also closely related to the commonly upheld *principle of causality*, that the future cannot effect the present and that from cause and effect, we establish that only causes in the past can effect the present. Just like chirality is broken by some elementary particles, there may be reasons to believe that this principle also, may not be as fundamental as we would hope it to be.

For any real valued signal, $s(t)$, we associate a complexed valued signal, $s_a(t)$, called an *analytical signal* by (cf. [69, 33]),

$$\boxed{s_a(t) = s(t) + i\boldsymbol{\mathcal{H}}\left\{s(t)\right\} = s(t) + i\check{s}(t)} \tag{2.10}$$

where, $\boldsymbol{\mathcal{H}}\left\{\cdot\right\}$ the *Hilbert transform* defined by (cf. [69, 70, 33]),

$$\boxed{\boldsymbol{\mathcal{H}}\left\{s(t)\right\} = \check{s}(t) = \frac{1}{\pi}\int_{-\infty}^{\infty} \frac{s(\tau)}{t-\tau}\,\mathrm{d}\tau = \frac{1}{\pi t} * s(t)} \tag{2.11}$$

where the * denotes the convolution operator (cf. Subsection A.3.8 for the definition). A common use of the Hilbert transform in the communication industry is to generate single side band signals (SSB). The Fourier transform of, $s_a(t)$, is a single sided Fourier transform of which the negative frequencies have been removed and the positive frequencies have been doubled, and the DC component is kept unchanged,

$$S_a(\nu) = \begin{cases} 0 & \text{if} \quad \nu < 0 \\ S(0) & \text{if} \quad \nu = 0 \\ 2S(\nu) & \text{if} \quad \nu > 0 \end{cases}, \tag{2.12}$$

where, $S(\nu) = \boldsymbol{\mathcal{F}}\{s(t)\}$, and, $S_a(\nu) = \boldsymbol{\mathcal{F}}\{s_a(t)\}$. Thus,

$$s_a(t) = \int_0^\infty S(\nu) e^{2\pi i \nu t}\, d\nu, \tag{2.13}$$

where,

$$S(\nu) = \int_{-\infty}^{\infty} s(t) e^{-2\pi i \nu t}\, dt. \tag{2.14}$$

For a real signal, $s(t)$, we have, $S(-\nu) = S^*(\nu)$, therefore by zeroing the negative frequencies in the analytical signal, we do not alter the real information content of the signal. The relationship between the Hilbert transform definition of the analytical signal and the single sided frequency definition can be obtained from the Fourier transform pair,

$$\mathcal{P}\frac{1}{\pi t} \overset{\mathcal{F}}{\Longleftrightarrow} -i\,\mathrm{sgn}\,(\nu), \tag{2.15}$$

where, $\mathcal{P}$, denotes the Cauchy principal value of the function. Using the convolution theorem, (see Subsection A.3.8), we have (in Section A.4 we list all the common functions and in Table A.1 we have a list of their Fourier transform pairs),

$$\boldsymbol{\mathcal{F}}\{i\check{s}(t)\} = \boldsymbol{\mathcal{F}}\{i\boldsymbol{\mathcal{H}}\{s(t)\}\} = i\boldsymbol{\mathcal{F}}\{\frac{1}{\pi t} * s(t)\} = \mathrm{sgn}\,(\nu)S(\nu), \tag{2.16}$$

thus,

$$S_a(\nu) = S(\nu) + \mathrm{sgn}\,(\nu)S(\nu) = \begin{cases} 0 & \text{if} \quad \nu < 0 \\ S(0) & \text{if} \quad \nu = 0 \\ 2S(\nu) & \text{if} \quad \nu > 0 \end{cases}. \tag{2.17}$$

In our analysis of our quantum control problem, we model an incoming Gaussian femtosecond IR laser pulse as an analytical signal. Also important is the even and odd functions of Fourier transforms presented in Section A.6. This emphasizes the reality of a the signal content. In the numerical or digital implementation it is known that the Hilbert transform should not be directly implemented, because it exhibits undesirable numerical properties. A modern trick of the trade is to rather use Noble identities or Noble transform that remedies these inconsistencies. This is an indication of the intricacies of numerical or digital methods that, even a simple operation like as a sign function, may lead to problems.

2.5. The Short-time Fourier Transform

In the analysis of nonstationary signals, probably the most widely used method is the short-time Fourier transform (STFT) and its related spectrogram. A short introduction for the general necessity of TFR was given in Section 1.6.

Mathematically, the STFT is treated as follows: To study the properties of the signal at a specific time, t, one simply emphasizes the signal at that time and suppresses the signal at other times. This is achieved by multiplying the signal by a so called window function, $w(t)$, centered at, t, to snatch a piece of the signal to produce a modified signal,

$$s_{w(t)}(\tau) = s(\tau)w(\tau - t). \tag{2.18}$$

The modified signal is a function of two times. We have a fixed time we are concentrating on, t, and the running time, τ. The window function is chosen specifically to leave the signal more or less unmodified around the time, t, but distant from the time of interest τ, to suppress the signal. That is,

$$s_{w(t)}(\tau) = \begin{cases} s(\tau) & \text{for } \tau \text{ near } t \\ 0 & \text{for } \tau \text{ far away from } t \end{cases} . \tag{2.19}$$

The window function is actually a way of taking a running or moving average of the signal. This is the chopping up of the signal described in the introduction. However, in studying the STFT, one must always bear in mind that the properties of the signal are inextricably intertwined with the properties of the window function. Unscrambling or inverting the process is required for the proper interpretation and estimation of the original signal.

Notwithstanding the above difficulties, the STFT method is ideal in many respects. Based on reasonable physical principles, consistent with our intuition, it is well defined and for many signals it gives an excellent TFR. However, for certain situations and signals it may not be the best method available. Other techniques may give a clearer picture for the particular situation. Thus other methods have been developed, which are discussed here and in subsequent Chapters.

Since the modified signal emphasizes the signal around, t, the Fourier transform will of course reflect the distribution of frequencies around time, t,

$$\begin{aligned} F_s(t,\nu;w) &= \int s_w(\tau)e^{-2\pi i\nu\tau}d\tau \\ &= \int s(\tau)w(\tau-t)e^{-2\pi i\nu\tau}d\tau. \end{aligned} \tag{2.20}$$

This is generally referred to as the atomic decompositions method of the signal, where the short time window function, $w(t)$, is considered as an atom. They are elementary parts that are used to reconstruct the total signal as a moving average of elementary waveforms. More generally we define the window function,

$$w_{t,\nu}(\tau) = w(\tau-t)e^{2\pi i\nu\tau}. \tag{2.21}$$

The additional dependence on the time, t, and frequency, ν, are subscripted. Each atom is obtained from a translation in time, $(\tau-t)$, and a shifting (translation) in frequency (modulation), $e^{2\pi i\nu\tau}$ (See Subsection A.3.5). The *Weyl-Heisenberg group* incorporates all translation in time and frequency transformations.

The short time Fourier transform (STFT) is now generally defined by,

$$\boxed{F_s(t,\nu;w) = \int_{-\infty}^{\infty} w^*(\tau-t)s(\tau)e^{-2\pi i\nu\tau}\,d\tau} \tag{2.22}$$

where the function, $w(t)$, has finite extend (localized about $t=0$), mathematically defined as the support of the function and we allowed the window function to complex, where $*$ denotes the complex conjugate operation.

The STFT can also be defined in terms of its Fourier transforms as, if $s(t) \overset{\mathcal{F}}{\Longleftrightarrow} S(\nu)$ and window, $w(t) \overset{\mathcal{F}}{\Longleftrightarrow} W(\nu)$, spectra, then,

$$F_s(t,\nu;w) = \int_{-\infty}^{\infty} S(u)\,W^*(u-\nu)\,e^{2\pi i(u-\nu)t}\,\mathrm{d}u. \tag{2.23}$$

This last form illustrates quite a unique feature, if we rewrite it as a convolution (see Subsection A.3.8 and Eq. (A.41)),

$$\boxed{F_s(t,\nu;w) = W_t(\nu) * S(\nu)} \tag{2.24}$$

where, notationally we have specifically written, $W_t(\nu)$, to highlight the dependent variable, ν, of the convolution, and still display the dependence of the variable, t,

$$W_t(\nu) = W^*(\nu)e^{2\pi it\nu}. \tag{2.25}$$

It is quite instructive to highlight a physical analogy of this equation with filtering theory. In the language of signal analysis, the STFT can be considered as passing the signal, $s(t)$, through a band-pass filter with frequency response, $W^*(u-\nu)$. This band pass filter is obtained from a filter, $W(u)$, by frequency translation, ν. Thus the short-time Fourier transform, $F_s(t,\nu;w)$, is analogous to passing the signal, $s(u)$, through a continuous filterbank, $W^*(u-\nu)$, with parameter, ν.

If, $h(t)$, is the *analysis window* of the STFT, then generally the signal, $s(t)$, can be reconstructed (synthesized) from, $F_s(t,\nu;h)$, by a different *synthesis window,* $g(t)$,

$$s(t)=\int_{-\infty}^{\infty}\int_{-\infty}^{\infty}F_s(\tau,\nu;h)g(t-\tau)e^{2\pi it\nu}\,d\tau d\nu, \tag{2.26}$$

provided that the analysis window, $h(t)$, and synthesis window, $g(t)$, are functionally orthogonal or inverses,

$$\int_{-\infty}^{\infty}g(t)h^*(t)\,dt=1. \tag{2.27}$$

The results we will obtain are revealing when expressed in terms of the amplitudes and phases of the signal and window and their transforms. The notation we use is,

$$s(t)=A(t)e^{j\varphi(t)}. \tag{2.28}$$

2.6. Gabor TFR

The Gabor TFR is a specific implementation of the STFT. Initially, this was how Gabor modified ideas of the von Neumann TFR to be applicable to the analysis of sound. The first modern day use of the Gabor-von Neumann TFR can be found in Helstrom [71] "An expansion of a signal in Gaussian elementary signals (Corresp.)", 1966. Then it was again recognized by Bastiaans in 1980 and 1981, [72, 73]. The first discrete Gabor expansion only appear in 1990, Wexler [74] and Orr contributed as well, in 1990 and 1991 [75, 76]. Bastiaans [77] recognized that the inverse of the discrete Gabor transform is a discrete Zac transform.

Lately it has also been used for signal compression, Shimshovitz and Tannor [78] "Periodic Gabor Functions with Biorthogonal Exchange: A Highly Accurate and Efficient Method for Signal Compression" 2012.

It was soon recognized that the window function could be replaced by other functions, e.g., a hat function etc. all with the feature of having a short or confined domain, which gave rise to the general STFT method. The term atom arose from the so-called *Gabor atoms*, where Gabor used the *Gaussian function* as a window function (which he named fundamental atoms to construct the signal),

$$h(t;\sigma) = \frac{1}{\sqrt{2\pi}\sigma} e^{-\frac{t^2}{2\sigma^2}}. \tag{2.29}$$

If we define the window function as,

$$w(t-\tau) = e^{-\pi(t-\tau)^2}, \tag{2.30}$$

or

$$w(t) = e^{-\pi t^2}, \tag{2.31}$$

the Gabor transform can be considered as a special case of the short-time Fourier transform,

$$G_s(\tau,\nu) = F_s(\tau,\nu;w). \tag{2.32}$$

The *Gabor Transform* is defined as,

$$G_s(\tau,\nu) = \int_{-\infty}^{\infty} s(t)\, e^{-\pi(t-\tau)^2} e^{-i2\pi vt}\, \mathrm{d}t. \tag{2.33}$$

The STFT can be inverted, provided, $E_w < \infty$, according to,

$$s(t) = \frac{1}{E_w} \int_{-\infty}^{\infty} \int_{-\infty}^{\infty} F_s(\tau,\nu;w) w(t-\tau) e^{2\pi it\nu}\, d\tau d\nu. \tag{2.34}$$

The Gabor transform is invertible and the original signal can be retrieved by the *inverse Gabor transform,*

$$s(t) = \frac{1}{E_g} \int_{-\infty}^{\infty} \int_{-\infty}^{\infty} G_s(u,\nu)\, e^{-\pi(u-t)^2} e^{i2\pi vt}\, \mathrm{d}u\mathrm{d}\nu. \tag{2.35}$$

The Gabor transform has some very valuable properties, which we list below without proving.

- Linearity.

$$as_1(t) + bs_2(t) \overset{\mathcal{G}}{\longleftrightarrow} aG_{s_1}(t,\nu) + bG_{s_2}(t,\nu) \tag{2.36}$$

- Shifting property.

$$s(t-t_o) \overset{\mathcal{G}}{\longleftrightarrow} G_s(t-t_o,\nu) e^{-i2\pi vt_o} \tag{2.37}$$

- Modulation property.

$$s(t)e^{i2\pi v_o t} \xleftrightarrow{\mathcal{G}} G_s(t, \nu - \nu_o) \tag{2.38}$$

Strictly, the inverse digital Gabor transform is performed by a *Zac transform*, another physicist [79, 77]. This is related to the synthesis window, described in *Eq. (2.26)*.

2.7. Spectrogram

The spectrogram, which is so often used in signal analysis, is in fact just a glorified special STFT of which we only take the square of the TFR to obtain the the energy density of spectrum or the signal probability distribution. The energy density is always the square of the spectrum. This is directly related to the square of the electric field being equal to the energy or intensity of a electromagnetic field or signal. Here we quickly reproduce the STFT definition with a different notation to emphasize that it is just a Fourier transform of a moving average of a windowed function. The window function, $w(t)$, is just multiplied to the signal to generate,

$$s_{w(t)}(\tau) = s(\tau)w(\tau - t). \tag{2.39}$$

The window function has limited support, i.e., it is defined only on a finite time, e.g., $t \in [-\frac{T}{2}, \frac{T}{2}]$, so that generally for a *hat function* (cf. Eq. (A.76) and Eq. (A.80)),

$$w_T(t) = \pi_T(t) = \begin{cases} 1 & \text{if} \quad t \in [-\frac{T}{2}, \frac{T}{2}] \\ 0 & \quad \text{otherwise} \end{cases} . \tag{2.40}$$

The *Fourier transform* will reproduce the frequency content of the small window of the signal,

$$\boldsymbol{\mathcal{F}}\left\{s_{w(t)}(\tau)\right\} = S_{w(t)}(\nu) = F_s(t, \nu; w). \tag{2.41}$$

The STFT contains both amplitude and phase information in the time-frequency domain.

The energy density spectrum at time t, also known as the ***spectrogram***, is simply given by,

$$P(t, \nu) = |S_t(\nu)|^2 . \tag{2.42}$$

This operation essentially destroys the phase information contained in the STFT. The energy density of the window function is given by,

$$E_w = \int_{-\infty}^{\infty} |w(t)|^2 \, \mathrm{d}t.$$

The **characteristic function** is straightforwardly obtained from the definition,

$$M(\theta,\tau)=\int\int |S_t(\nu)|^2\, e^{i\theta t+i\tau\nu}\, \mathrm{d}\nu \mathrm{d}t, \tag{2.43}$$

$$=\mathcal{A}_s(\theta,\tau)\mathcal{A}_w(-\theta,\tau), \tag{2.44}$$

where,

$$\mathcal{A}_s(\theta,\tau)=\int s^*(t-\frac{1}{2}\tau)s(t+\frac{1}{2}\tau)e^{i\theta t}\, \mathrm{d}t, \tag{2.45}$$

$$\mathcal{A}_w(\theta,\tau)=\int w^*(t-\frac{1}{2}\tau)w(t+\frac{1}{2}\tau)e^{i\theta t}\, \mathrm{d}t, \tag{2.46}$$

are the **ambiguity functions** (see Subsection 2.8.4) of the signal and the window.

2.7.1. Time-frequency Resolution

Having considered the analogy with filtering theory we can extend these thoughts further by using the Dirac-δ (See Subsection A.4.6) time signal and frequency inputs to obtain the characteristics of the filter, i.e.,

- Dirac-δ time signal.

$$s(t)=\delta(t-t_o)\overset{\mathcal{F}}{\Longleftrightarrow} F_s(t,\nu;w)=w(t-t_o)\, e^{-2\pi i\nu t_o} \tag{2.47}$$

- Dirac-δ frequency signal (Modulation).

$$s(t)=e^{2\pi i\nu_o t}\overset{\mathcal{F}}{\Longleftrightarrow} F_s(t,\nu;w)=W(\nu-\nu_o)\, e^{-2\pi i\nu_o t} \tag{2.48}$$

Here we clearly notice that the temporal resolution of the STFT is dependent on the duration, $h(t)$, of the analysis window, and the frequency resolution is proportional on the effective bandwidth, H, of the analysis window, h. Thus we are confronted with a reciprocal *trade-off* between temporal and frequency resolution which is directly inherited from the corresponding Fourier relationship and the Heisenberg-Gabor inequality.

2.7.2. Discrete Time-Frequency Representations

Alas all of the above is defined for continuous signals. In the calculation of these transforms the signal had to be discretized. This is the field of Digital Signal Processing (DSP) [80, 81]. For an example of a discrete Gabor TFR consult [74]. As some background reference, the important sampling theorem is given in Section A.7 along with some properties of band-limited signals in Section A.8. Related to the sampling theorem is the Poisson summation theorem and the Nyquist-Shannon sampling theorem given in Section A.9 and Section A.10. The sampling of a signal is accomplished by a so-called Dirac comb defined in Subsection A.4.6.5. A discrete sampled signal[3], $s[n]$, with sampling period, Δt, the sampling period of the discrete STFT must chosen such that, $T = k\Delta t$, with $k \in \mathbb{N}$. The discrete STFT for a discrete rectangular window, $m, n \in \mathbb{Z}$, with sampling steps sizes, T, and, Ω, becomes,

$$\boxed{F_s[n, m; h] = F_s(nT, m\Omega; h) = \int_{-\infty}^{\infty} h^*(\tau - nT)s(\tau)e^{-2\pi i m\Omega\tau}\, d\tau} \tag{2.49}$$

For discrete time-frequency representations Gabor suggested that an arbitrary time signal can be decomposed as,

$$s(t) = \sum_{n,m} c_{n,m} h_{n,m}(t) \qquad\qquad h_{n,m}(t) = h(t - mT)e^{in\Omega t}, \tag{2.50}$$

where the time-frequency domain, $(t, \omega) \in \mathbb{R}^2$, is discretized in a lattice were, T and Ω, are the time and frequency lattice intervals. Gabor proposed that the function, $h(t)$, should coincide with the minimum variance function that is most compact for the time-frequency bandwidth product which is of course the Gaussian function,

$$h(t) = (\alpha/\pi)^{1/4} e^{-\alpha t^2/2}. \tag{2.51}$$

The Gabor atoms, $h_{n,m}(t) = h(t - mT)e^{in\Omega t}$, with both, T and Ω, small, collectively form an oversampled overcomplete non-orthgonal basis, which is called a frame. It has been shown that such an expansion is possible, if,

$$\Omega \times T \geq 1. \tag{2.52}$$

Without loosing any signal information, the problem reduces to choosing the values of, T and Ω, so as to minimize the redundancy (overlapping of atoms). The Balian-Low theorem, however, proves that it is impossible to have a window function, h, that is well localized in both frequency and time, and is appropriately named the Balian-Low obstruction. A well localized window, h, (for example a Gaussian window), the reconstruction (synthesis) formula will be *numerically unstable.*

---

[3] The $[\cdot]$ is common notation for discrete signals in DSP

In the discrete case the reconstruction (synthesis) of the signal can generally be written as,

$$s(t) = \sum_{n,m} F_s[n,m;h] g_{n,m}(t) \qquad\qquad g_{n,m}(t) = g(t-mT)e^{in\Omega t}, \tag{2.53}$$

with, h, g, and, T, Ω, subject to

$$\frac{1}{\Omega}\sum_n g(t+\frac{k}{\Omega}-nT)h^*(t-nT) = \delta_k \qquad \forall t, \tag{2.54}$$

where, $\delta_k = 0 \quad \forall k \neq 0$ and $\delta_o = 1$. This discrete condition on the analysis and synthesis window functions is a much more severe condition than the compliance of the continuous condition.

2.7.3. The Short-Frequency Time Transform.

In motivating the short-time Fourier transform we emphasized the desire to study frequency properties at time t. Conversely, we may wish to study time properties at a particular frequency. We just multiply the spectrum, $S(\nu)$, with a frequency window, $W(\nu)$, and take the time transform, which of course, is the inverse Fourier transform. In particular, we define the short-frequency time transform by,

$$s_\nu(t) = \int_{-\infty}^{\infty} e^{2\pi i\theta t} S(\theta) W(\nu-\theta) d\theta \tag{2.55}$$

where of course, $w \overset{\mathcal{F}}{\Longleftrightarrow} W$ and $s \overset{\mathcal{F}}{\Longleftrightarrow} S$, then,

$$S_t(\nu) = e^{-2\pi i\nu t} s_\nu(t). \tag{2.56}$$

Only the modulation phase factor, $e^{-2\pi i\nu t}$, separates the the short-frequency time transform from short-time Fourier transform. Since the distribution is the absolute square, the phase factor does not enter into it and either the short-time Fourier transform or the short-frequency time transform can be used to define the joint distribution,

$$P(t,\nu) = |S_t(\nu)|^2 = |s_\nu(t)|^2 . \tag{2.57}$$

This exhibits the desirable fact that the spectrogram can be used to study the behavior of time properties at a particular frequency. This is done by choosing an, $H(\nu)$, that is narrow, or equivalently, due to reciprocity, by taking an, $h(t)$, that is broad.

2.7.3.1. Narrowband and Wideband Spectrogram.

Due to the reciprocity theorem of Fourier transform (cf. Subsection A.3.4), which manifests itself in the Heisenberg-Gabor uncertainty, if the time window is of short duration, the frequency window, $H(\nu)$, is broad; in that case the spectrogram is called a **broadband spectrogram**. Conversely, if the window is of long duration, then, $H(\nu)$, is narrow, and we say we have a **narrowband spectrogram**.

2.7.4. Characteristic Function.

The characteristic function of the spectrogram is straightforwardly obtained,

$$\begin{aligned} M_{SP}(\theta,\tau) &= \int\int |S_t(\omega)|^2 \, e^{j\theta t + j\tau\omega} dt d\omega && (2.58)\\ &= \mathcal{A}_s(\theta,\tau)\mathcal{A}_h(-\theta,\tau), && (2.59) \end{aligned}$$

where,

$$\mathcal{A}_s(\theta,\tau) = \int s^*(t - \frac{1}{2}\tau)s(t + \frac{1}{2}\tau)e^{j\theta t}dt, \qquad (2.60)$$

is the **ambiguity function** (see Subsection 2.8.4) of the signal [69], and, $\mathcal{A}_h$, is the ambiguity function of the window defined in the identical manner, except that we use, $h(t)$, instead of $s(t)$. Note that the ambiguity function has the following property, $\mathcal{A}(-\theta,\tau) = \mathcal{A}^*(\theta,-\tau)$.

2.8. Wigner-Ville Distribution

In 1932 E. P. Wigner invented his quasi-probability distribution for quantum statistical purposes [63]. The wave mechanics of quantum mechanics, represent particles as waves and Ville (1948) recognized by analogy that it could also be utilized for any wave of signal analysis[4] [65]. Wigner's original motivation for introducing the distribution was to calculate the quantum contributions of the second virial coefficient for a gas, to indicate how it deviates from the ideal gas law. Classically, to calculate the second virial coefficient one needs a joint distribution of position and momentum. So Wigner devised a joint distribution that gave, as marginal probabilities distributions, the quantum mechanical distributions of position and momentum. Quantum mechanics motivated the distribution, but the distribution was used in a classical manner. It was a hybrid method. Also Wigner was motivated in part by the work of Kirkwood and Margenau which had previously calculated this quantity, but Wigner improved on it. Kirkwood subsequently developed what is now the standard theory of nonlinear statistical mechanics, the BBGKY Hierarchy (the theory was independently developed by Bogoluibov, Born, Green, Kirkwood and Yvon). Kirkwood attempted to extend the classical theory to the quantum case and devised the distribution which is commonly called the Rihaczek or Margenau-Hill distribution to do that. Many years later Margenau and Hill rederived the Margenau-Hill distribution. The importance of Margenau-Hill work is not the distribution, but the derivation. They were also the first to consider joint distributions involving spin. The Wigner-Ville TFR still remains one of the great methods in optics, as can be seen in Bastiaans [86].

---

[4] This we would like to call the Ville correspondence, which is just an example of the Copenhagen correspondence. We are aware that it may be confused with the Weyl correspondence. Even Feynman contributed to this quantum-classical correspondence, his 1948 and 1949, path integrals [82, 83], with Kac (1949) in stochastic theory [84], which resulted in the Feynman-Kac formula. It is widely used, even in finance, see Rouah [85].

The Wigner-Ville distribution of a signal, $s(t)$, or its Fourier transform, $S(\omega)$, is defined as, i.t.o. angular frequency, ω,

$$\mathcal{W}_s(t,\omega) = \frac{1}{2\pi}\int s^*(t-\frac{1}{2}\tau)s(t+\frac{1}{2}\tau)e^{-i\omega\tau}\,\mathrm{d}\tau, \tag{2.61}$$

$$\mathcal{W}_s(t,\omega) = \frac{1}{2\pi}\int S^*(\omega+\frac{1}{2}\theta)S(\omega-\frac{1}{2}\theta)e^{-i\theta t}\,\mathrm{d}\theta. \tag{2.62}$$

In what follows, we define the Wigner-Ville TFR in terms of ordinary frequency, ν. Given a time signal, $s(t)$,

$$\boxed{\mathcal{W}_s(t,\nu) = \int_{-\infty}^{\infty} s^*(t-\frac{\tau}{2})s(t+\frac{\tau}{2})e^{-2\pi i\nu\tau}\,d\tau} \tag{2.63}$$

The only difference is the, $\frac{1}{2\pi}$, factor. It is important to note that,

$$\mathcal{W}_s(t,\nu) = \boldsymbol{\mathcal{F}}_\tau\left\{s^*(t-\frac{\tau}{2})s(t+\frac{\tau}{2})\right\},$$

were we have used the notation, $\boldsymbol{\mathcal{F}}_\tau$, to indicate explicitly that the Fourier transform is to be taken over the variable, τ. The frequency, ν, appears due to the Fourier transform.

Using the correlation theorem of Fourier transforms Eq. (A.41) with, $s(t) = g(t)$ and $s^*(t) = f(t)$, we obtain the auto-correlation of, $s(t)$, as,

$$C_s(t) = s^*(t) * s(t) = \int_{-\infty}^{\infty} s^*(t-\tau)s(\tau)\,d\tau,$$

a simple change of integration variable to, $\tau =\frac{t}{2} + \frac{\tau'}{2}$,

$$C_s(t) = s^*(t) * s(t) = \frac{1}{2}\int_{-\infty}^{\infty} s^*(\frac{t}{2} - \frac{\tau'}{2})s(\frac{t}{2} + \frac{\tau'}{2})\, d\tau'.$$

Thus,

$$2C_s(2t) = 2s^*(2t) * s(2t) = \int_{-\infty}^{\infty} s^*(t - \frac{\tau}{2})s(t + \frac{\tau}{2})\, d\tau.$$

From the relationship between convolution and correlation Eq. (A.58) and Eq. (A.59) with, $s(t) = g(t)$ and $s^*(t) = f(t)$, so that $f^*(-t) = s(-t)$, we obtain the auto-convolution of, $s(t)$, as,

$$s^*(t) * s(t) = s(-t) \star s(t).$$

This shows that integrand of Wigner transform, $\mathcal{W}_s(t, \nu)$, is related to the integrand of the convolution, $2s^*(2t) * s(2t)$, or to the integrand of the correlation of, $2s(-2t) \star s(2t)$.

The Wigner-Ville distribution can also be calculated in terms of the spectral signal. For this purposes we substitute the inverse Fourier transforms of, $s(t + \frac{\tau}{2})$, and, $s^*(t - \frac{\tau}{2})$, utilizing the Fourier time translation property (cf. Subsection A.3.5),

$$s(t + \frac{\tau}{2}) = \boldsymbol{\mathcal{F}}^{-1}\{e^{2\pi i\frac{\tau}{2}\nu}S(\nu)\} = \int_{-\infty}^{\infty} S(\nu)e^{2\pi i\nu(t+\frac{\tau}{2})}\, d\nu, \tag{2.64}$$

$$s^*(t - \frac{\tau}{2}) = \boldsymbol{\mathcal{F}}^{-1}\{e^{2\pi i\frac{\tau}{2}\nu}S^*(\nu)\} == \int_{-\infty}^{\infty} S^*(\nu)e^{-2\pi i\nu(t-\frac{\tau}{2})}\, d\nu, \tag{2.65}$$

into the Wigner-Ville distribution Eq. (2.63) and with dummy transform variables, η, in Eq. (2.64) and, ξ, in Eq. (2.65) we obtain

$$\mathcal{W}_s(t, \nu) = \int_{-\infty}^{\infty} \left[\int_{-\infty}^{\infty} S^*(\eta)e^{-2\pi i\eta(t-\frac{\tau}{2})}\, d\eta\right] \left[\int_{-\infty}^{\infty} S(\xi)e^{2\pi i\xi(t+\frac{\tau}{2})}\, d\xi\right] e^{-2\pi i\nu\tau}\, d\tau, \tag{2.66}$$

and with a little manipulation this becomes,

$$\mathcal{W}_s(t, \nu) = \int_{-\infty}^{\infty} \int_{-\infty}^{\infty} S^*(\eta)S(\xi)e^{-2\pi it(\eta-\xi)} \left[\int_{-\infty}^{\infty} e^{2\pi i\tau(\frac{\eta}{2}+\frac{\xi}{2}-\nu)}\, d\tau\right] d\eta\, d\xi. \tag{2.67}$$

The integral in the square parenthesis is equal to the Dirac-δ, therefore,

$$\mathcal{W}_s(t,\nu) = \int_{-\infty}^{\infty}\int_{-\infty}^{\infty} S^*(\eta)S(\xi)e^{-2\pi i t(\eta-\xi)}\delta(\frac{\eta}{2}+\frac{\xi}{2}-\nu)\,d\eta\,d\xi. \tag{2.68}$$

The Dirac-δ obeys, $\delta(ax) = \delta(x)/|a|$, (cf. Eq. (A.96)) so that the integration over, η, results in,

$$\mathcal{W}_s(t,\nu) = \int_{-\infty}^{\infty}\int_{-\infty}^{\infty} 2S^*(2\nu-\xi)S(\xi)e^{-2\pi i t(2\nu-2\xi)}\,d\xi. \tag{2.69}$$

Now substitute, $\xi = \nu + \frac{\theta}{2}$, thus, $d\xi = d\theta/2$, into Eq. (2.69) and we obtain the Wigner-Ville distribution in terms of the Spectral signal, $S(\nu)$, by means of the inverse Fourier transform,

$$\boxed{\mathcal{W}_s(t,\nu) = \int_{-\infty}^{\infty} S^*(\nu-\frac{\theta}{2})S(\nu+\frac{\theta}{2})e^{2\pi i\theta t}\,d\theta} \tag{2.70}$$

that is,

$$\mathcal{W}_s(t,\nu) = \boldsymbol{\mathcal{F}}_\theta^{-1}\left\{S^*(\nu-\frac{\theta}{2})S(\nu+\frac{\theta}{2})\right\}.$$

The time t is a result of the inverse Fourier transform. Now instead, by simply substituting, $\xi = \nu - \frac{\theta}{2}$, thus, $d\xi = d\theta/2$, into Eq. (2.69), we obtain the Wigner-Ville distribution in terms of the Spectral signal, $S(\nu)$, by means of the Fourier transform (direct), but with the signs reversed in Spectral signals, $\nu + \frac{\theta}{2}$,

$$\mathcal{W}_s(t,\nu) = \int_{-\infty}^{\infty}\int_{-\infty}^{\infty} S^*(\nu+\frac{\theta}{2})S(\nu-\frac{\theta}{2})e^{-2\pi i t\theta}\,d\theta. \tag{2.71}$$

This is equivalent to the definition in Eq. (2.62). That is,

$$\mathcal{W}_s(t,\nu) = \boldsymbol{\mathcal{F}}_\theta\left\{S^*(\nu+\frac{\theta}{2})S(\nu-\frac{\theta}{2})\right\}.$$

2.8.1. Properties of the Wigner Distribution

The Wigner have several unique properties which we state here without proof.

- Energy conservation.

$$\boxed{E_s = \int_{-\infty}^{\infty}\int_{-\infty}^{\infty} \mathcal{W}_s(t,\nu)\,dt\,d\nu} \tag{2.72}$$

- Marginal Properties.

$$\boxed{|S(\nu)|^2 = \int_{-\infty}^{\infty} \mathcal{W}_s(t,\nu)\, dt} \tag{2.73}$$

$$\boxed{|s(t)|^2 = \int_{-\infty}^{\infty} \mathcal{W}_s(t,\nu)\, d\nu} \tag{2.74}$$

- Real valued (Reality).

$$\boxed{\mathcal{W}_s(t,\nu) \in \mathbb{R} \quad \forall\, t,\nu \in \mathbb{R}^2} \tag{2.75}$$

- Translation covariance (Time and Frequency Shifts).

$$\boxed{x(t) = s(t-t_o) \implies \mathcal{W}_x(t,\nu) = \mathcal{W}_s(t-t_o,\nu)} \tag{2.76}$$

$$\boxed{x(t) = s(t)e^{2\pi i \nu_o t} \implies \mathcal{W}_x(t,\nu) = \mathcal{W}_s(t,\nu-\nu_o)} \tag{2.77}$$

- Dilation covariance (scale).

$$\boxed{x(t) = \sqrt{k}s(kt);\ k>0 \implies \mathcal{W}_x(t,\nu) = \mathcal{W}_s(kt,\frac{\nu}{k})} \tag{2.78}$$

- Compatibility with filtering

$$\boxed{x(t) = \int_{-\infty}^{\infty} h(t-u)s(u)\, du \implies \mathcal{W}_x(t,\nu) = \int_{-\infty}^{\infty} \mathcal{W}_h(t-u,\nu)\mathcal{W}_s(u,\nu)\, du} \tag{2.79}$$

- Compatibility with modulation.

$$\boxed{x(t) = m(t)s(t) \implies \mathcal{W}_x(t,\nu) = \int_{-\infty}^{\infty} \mathcal{W}_m(t,\nu-\xi)\mathcal{W}_s(t,\xi)\, d\xi} \tag{2.80}$$

- Wide-sense support conservation.

$$\boxed{s(t) = 0\ \ |t|>T \implies \mathcal{W}_s(t,\nu) = 0\ \ |t|>T} \tag{2.81}$$

$$\boxed{S(\nu) = 0\ \ |\nu|>B \implies \mathcal{W}_s(t,\nu) = 0\ \ |\nu|>B} \tag{2.82}$$

- Unicity (Moyal's formula)

$$\boxed{\left|\int_{-\infty}^{\infty} x^*(t)y(t)\,dt\right|^2 = \int_{-\infty}^{\infty}\int_{-\infty}^{\infty} \mathcal{W}_x^*(t,\nu)\mathcal{W}_y(t,\nu)\,dt\,d\nu} \tag{2.83}$$

- Instantaneous frequency (where $\check{s}$ is the analytic signal of, s.)

$$\boxed{f_s(t) = \frac{\int_{-\infty}^{\infty} \nu\mathcal{W}_{\check{s}}(t,\nu)\,d\nu}{\int_{-\infty}^{\infty} \mathcal{W}_{\check{s}}(t,\nu)\,d\nu}} \tag{2.84}$$

- Group delay (where $\check{s}$ is the analytic signal of, s.)

$$\boxed{t_s(\nu) = \frac{\int_{-\infty}^{\infty} t\mathcal{W}_{\check{s}}(t,\nu)\,dt}{\int_{-\infty}^{\infty} \mathcal{W}_{\check{s}}(t,\nu)\,dt}} \tag{2.85}$$

- Perfect localization of linear chirp.

$$s(t) = e^{2\pi i\nu_s(t)t};\ \nu_s(t) = \nu_o + \beta t \Longrightarrow\ \mathcal{W}_s(t,\nu) = \delta(\nu - (\nu_o + \beta t)) \tag{2.86}$$

2.8.2. Disadvantages

With so many desirable properties one can easily be deceived into believing that we have the ultimate time-frequency distribution, but unfortunately the underlying problems must also be highlighted.

The Wigner-Ville distribution is a bilinear function of the signal $s(t)$, which implies the *quadratic superposition principle* and therefore exhibits the artifact of interference terms between different pulses. Consider the Wigner-Ville distribution of the sum of two signals,

$$s(t) = s_1(t) + s_2(t). \tag{2.87}$$

We obtain,

$$\mathcal{W}_s(t,\nu) = \mathcal{W}_{11}(t,\nu) + \mathcal{W}_{22}(t,\nu) + 2\Re e\{\mathcal{W}_{12}(t,\nu)\}. \tag{2.88}$$

which clearly shows the interference term, also known as the cross Wigner distribution, that arises and where,

$$\mathcal{W}_{12}(t,\nu) = \int_{-\infty}^{\infty} s_1^*(t - \frac{\tau}{2})s_2(t + \frac{\tau}{2})e^{-2\pi i\nu\tau}\,d\tau. \tag{2.89}$$

Strictly the Wigner-Ville distribution is only called a *quasi-probability distribution*, since the interference terms can be negative. According to probability definition a probability distribution must be positive semi-definite. It may only be zero on sets of measure zero.

Although the Wigner suffers from this problem, the marginal property in the previous Subsection 2.8.1 shows that the marginal densities are probability densities, Eq. (2.73) and Eq. (2.74). Wigner was the first to be aware of these negative probabilities. That there might be merit in considering negative probabilities, can be appreciated if one notices that even the great Richard Feynman wrote an article [87] on negative probabilities, and that other important physicists like Scully and Schleich [88] take him seriously. Maybe we must sit up and take notice.

2.8.3. Pseudo Wigner-Ville Distribution

The pseudo Wigner-Ville distribution is just a windowed version of the Wigner-Ville distribution,

$$\boxed{PW_s(t,\nu) = \int_{-\infty}^{\infty} h(\tau) s^*(t-\frac{\tau}{2}) s(t+\frac{\tau}{2}) e^{-2\pi i\nu\tau}\, d\tau} \tag{2.90}$$

where $h(t)$ is just a regular window function. The spectral equivalent given by,

$$\boxed{PW_s(t,\nu) = \int_{-\infty}^{\infty} H(\nu-\theta)\mathcal{W}(t,\theta)\, d\theta} \tag{2.91}$$

clearly shows that it is just the frequency convolution and consequently frequency smoothing of the Wigner-Ville function. The pseudo-Wigner-Ville distribution comes to its own in its representation of nonstationary signals.

2.8.4. Ambiguity Function

The narrow band ambiguity function, also known as as the *symmetric Sussman ambiguity function* is defined as,

$$\boxed{\mathcal{A}(\tau,\theta) = \int_{-\infty}^{\infty} s^*(t-\frac{\tau}{2}) s(t+\frac{\tau}{2}) e^{-2\pi i\theta t}\, dt} \tag{2.92}$$

In the Wigner-Ville distribution the variables, t, and, ν, are true or absolute coordinates. Notice that the difference in this definition with Wigner-Ville distribution is that the Fourier transform is with respect to, t, rather than, τ. In the ambiguity function the variable, τ, refers to the relative time or *delay* in the signal, and, θ, refers to relative frequency or the *Doppler* in the signal. This is extensively used in Radar, where the delay, τ, is a measure of the relative distance to the target, and the Doppler, θ, is a measure of the relative velocity of the target. (See [69])

It is generally complex and satisfies the Hermitian even symmetry,

$$\mathcal{A}(\tau,\theta) = \mathcal{A}^*(-\tau,-\theta). \tag{2.93}$$

The ambiguity function is the **two-dimensional Fourier transform** of the Wigner-Ville distribution,

$$\mathcal{A}(\tau,\theta) = \int_{-\infty}^{\infty}\int_{-\infty}^{\infty} \mathcal{W}(t,\nu)e^{2\pi i(\nu\tau-\theta t)}dt\,d\nu \tag{2.94}$$

Mathematically, $A(\tau,\theta)$, is the *dual* of, $W(t,\nu)$, with respect to the Fourier transform.

Being a pseudo-probability density, we can, from probability theory, calculate the **characteristic function** of the Wigner Distribution as,

$$M(\theta,\tau) = \int\int \mathcal{W}(t,\omega)e^{i\theta t+i\tau\omega}\,\mathrm{d}t\mathrm{d}\omega \tag{2.95}$$

$$= \frac{1}{2\pi}\int\int\int s^*(t-\frac{1}{2}\tau')s(t+\frac{1}{2}\tau')e^{-i\omega(\tau-\tau')}e^{i\theta t}\,\mathrm{d}\tau'\mathrm{d}t\mathrm{d}\omega$$

$$= \int\int \delta(\tau-\tau')s^*(t-\frac{1}{2}\tau')s(t+\frac{1}{2}\tau')e^{i\theta t}\,\mathrm{d}\tau'\mathrm{d}t$$

$$= \int s^*(t-\frac{1}{2}\tau)s(t+\frac{1}{2}\tau)e^{i\theta t}\,\mathrm{d}t = \mathcal{A}(\theta,\tau). \tag{2.96}$$

This is just the ***symmetric ambiguity function***.

2.9. The Kernel Methods

In 1966, Leon Cohen characterized the time frequency approach by means of Kernel functions [66]. This then actually classified all the then known quasi probability distributions developed by physicists for the quantum thermodynamics and statistics, see the introduction of Section 2.8. Cohen also named a quasi probability distribution in honour of Born-Jordan, which he created. Later, 1969, contributing to his work, another paper was published by Summerfeld and Zweifel [89]. The properties of the distribution are reflected by simple constraints on the kernel function and vice versa.

According to Cohen, all kernel time-frequency distributions can be obtained from the time signal, $s(t)$,

$$\boxed{\mathcal{C}(t,\omega) = \frac{1}{4\pi^2} \int\int\int s^*(u - \frac{1}{2}\tau)s(u + \frac{1}{2}\tau)\mathcal{K}(\theta,\tau)e^{-i\theta t - i\tau\omega + i\theta u}\, \mathrm{d}u\mathrm{d}\tau\mathrm{d}\theta} \tag{2.97}$$

or its related Fourier transform spectrum, $S(\omega)$,

$$\boxed{\mathcal{C}(t,\omega) = \frac{1}{4\pi^2} \int\int\int S^*(u + \frac{1}{2}\theta)S(u - \frac{1}{2}\theta)\mathcal{K}(\theta,\tau)e^{-i\theta t - i\tau\omega + i\tau u}\, \mathrm{d}\theta\mathrm{d}\tau\mathrm{d}u} \tag{2.98}$$

In terms of the characteristic function we get,

$$\mathcal{C}(t,\omega) = \frac{1}{4\pi^2} \int\int M(\theta,\tau)e^{-i\theta t - i\tau\omega}\, \mathrm{d}\theta\mathrm{d}\tau, \tag{2.99}$$

where,

$$M(\theta,\tau) = \mathcal{K}(\theta,\tau) \int s * (u - \frac{1}{2}\tau)s(u + \frac{1}{2}\tau)e^{i\theta u}\, \mathrm{d}u \tag{2.100}$$

$$= \mathcal{K}(\theta,\tau)\mathcal{A}(\theta,\tau). \tag{2.101}$$

Thus the characteristic function may then be called the **generalized ambiguity function**.

The energy density may be written as the Fourier transform of the autocorrelation function. Now consider the energy density of the time frequency distribution as the Fourier transform of a local autocorrelation function,

$$\mathcal{C}(t,\omega) = \frac{1}{2\pi} \int R_t(\tau)e^{-i\omega\tau}\, \mathrm{d}\tau. \tag{2.102}$$

Then the deterministic generalized local autocorrelation function is defined by,

$$R_t(\tau) = \frac{1}{2\pi} \int\int s * (u - \frac{1}{2}\tau)s(u + \frac{1}{2}\tau)\mathcal{K}(\theta,\tau)e^{i\theta(u-t)}\, \mathrm{d}u\mathrm{d}\theta. \tag{2.103}$$

Name	Kernel	Distribution
General Cohen Class	$\mathcal{K}(\theta,\tau)$	$\frac{1}{4\pi^2}\int\int\int s*(u-\frac{1}{2}\tau)s(u+\frac{1}{2}\tau)$ $\mathcal{K}(\theta,\tau)e^{-i\theta t-i\tau\omega+i\theta u}\,\mathrm{d}u\mathrm{d}\tau\mathrm{d}\theta$
Wigner-Ville	1	$\frac{1}{2\pi}\int s*(t-\frac{1}{2}\tau)s(t+\frac{1}{2}\tau)e^{-i\omega\tau}\,\mathrm{d}\tau$
Margenau-Hill	$\cos(\frac{1}{2}\theta\tau)$	$\Re\{\frac{1}{\sqrt{2\pi}}s(t)S^*(\omega)e^{-i\omega t}\}$
Kirkwood-Rihaczek	$e^{i\theta\tau/2}$	$\frac{1}{\sqrt{2\pi}}s(t)S^*(\omega)e^{-i\omega t}$
Born-Jordan (Cohen)	$\mathrm{sinc}(\frac{1}{2}\theta\tau)$	$\frac{1}{2\pi}\int\frac{1}{\lvert\tau\rvert}e^{-i\tau\omega}\int_{t-\lvert\tau\rvert/2}^{t+\lvert\tau\rvert/2}$ $s*(u-\frac{1}{2}\tau)s(u+\frac{1}{2}\tau)e^{-i\omega\tau}\,\mathrm{d}u\mathrm{d}\tau$
Page	$e^{i\theta\lvert\tau\rvert}$	$\frac{\partial}{\partial t}\left\lvert\frac{1}{\sqrt{2\pi}}\int_{-\infty}^{t}s(t')e^{-i\omega t'}\,\mathrm{d}t'\right\rvert^2$
Choi-Williams	$e^{-\theta^2\tau^2/\sigma}$	$\frac{1}{4\pi^{3/2}}\int\int\frac{1}{\sqrt{\tau^2/\sigma}}e^{-\sigma(u-t)^2/\tau^2-i\tau\omega}$ $s*(u-\frac{1}{2}\tau)s(u+\frac{1}{2}\tau)e^{-i\omega\tau}\,\mathrm{d}u\mathrm{d}\tau$
Spectrogram	$\int w^*(u-\frac{1}{2}\tau)e^{-i\theta u}$ $w(u+\frac{1}{2}\tau)\,\mathrm{d}u$	$\left\lvert\frac{1}{\sqrt{2\pi}}\int e^{-i\omega\tau}s(\tau)w(\tau-t)\,\mathrm{d}\tau\right\rvert^2$
Zhao-Atlas-Marks	$g(\tau)\lvert\tau\rvert\mathrm{sinc}(a\theta\tau)$	$\frac{1}{4\pi a}\int g(\tau)e^{-i\tau\omega}\int_{t-\lvert\tau\rvert a}^{t+\lvert\tau\rvert a}$ $s*(u-\frac{1}{2}\tau)s(u+\frac{1}{2}\tau)e^{-i\omega\tau}\,\mathrm{d}u\mathrm{d}\tau$
Positive		$\lvert S(\omega)\rvert^2\lvert s(t)\rvert^2\Omega(u,v)$

Table 2.1.: Kernel Cohen Classes

A first class of such time-frequency representations is given by the atomic decompositions (also known as the linear time-frequency representations). Table 2.1 gives a short list of the kernel Cohen classes.

A signal independent approach to time-frequency representations is the inclusion of a *kernel function,* $\Phi(\theta,\tau)$, (sometimes also called the *parametrization function*) so that,

$$\boxed{D_s(t,\nu;\Phi)=\int\int\int_{-\infty}^{\infty}e^{2\pi i\theta(u-t)}\Phi(\theta,\tau)s^*(u-\frac{\tau}{2})s(u+\frac{\tau}{2})e^{-2\pi i\nu\tau}d\theta\,du\,d\tau} \tag{2.104}$$

A whole set of bilinear time-frequencies can be defined by, in terms of the Wigner distribution, by means of a double convolution integral of the Wigner distribution

$$\boxed{D_s(t,\nu;F)=\int_{-\infty}^{\infty}\int_{-\infty}^{\infty}F(u-t,\theta-\nu)W_s(u,\theta)\,dud\theta} \tag{2.105}$$

where,

$$F(t,\nu)=\int_{-\infty}^{\infty}\int_{-\infty}^{\infty}\Phi(\zeta,\tau)e^{-2\pi i(\zeta t+\nu\tau)}d\zeta\,d\tau. \tag{2.106}$$

is just the double Fourier transform of the Kernel function. We now only briefly discuss two related TFR distributions, in the next two Subsection 2.9.1 and Subsection 2.9.2. This is only for reference purposes, since later we use the Husimi TFR distribution.

2.9.1. Husimi Distribution

The Japanese physicist Kôdi Husimi in 1940 in “Some Formal properties of the Density Matrix” [90] developed what is called the *Q-function* in quantum optics. The Husimi distribution is essentially a two-dimensional convolution (cf. Subsection A.3.8) by a phase-space Gaussian distribution of the Wigner-Ville quasi-probability distribution,

$$\boxed{H_s(t,\nu;\alpha,\gamma) = \int_{-\infty}^{\infty}\int_{-\infty}^{\infty} G_{\alpha\gamma}(u-t,\theta-\nu))\mathcal{W}_s(u,\theta)\,du d\theta} \tag{2.107}$$

where,

$$F(t,\nu) = G_{\alpha\gamma}(t,\nu) = \frac{4}{\alpha}\exp\left[-\frac{1}{\alpha}\left(\frac{\nu^2}{\gamma^2}+4\gamma^2t^2\right)\right]. \tag{2.108}$$

For, $\alpha = 0$, then, $G_0(t,\nu) = \delta(t)\delta(\nu)$, is the double Dirac-$\delta$ thus the Wigner function, $W_s(t,\nu)$, is returned.

2.9.2. Smoothed Pseudo Wigner-Ville distribution

Rather than taking a convolution with Wigner-Ville distribution, we can also consider a separable smoothing function for the Kernel function. We then get the smoothed pseudo Wigner-Ville distribution,

$$F(t,\nu) = g(t)H(-\nu), \tag{2.109}$$

that is,

$$\boxed{SPW_s(t,\nu) = \int_{-\infty}^{\infty} h(\tau)\int_{-\infty}^{\infty} g(u-t)s^*(u-\frac{\tau}{2})s(u+\frac{\tau}{2})\,du\,e^{-2\pi i\nu\tau}\,d\tau} \tag{2.110}$$

3. The von Neumann TFR

3.1. Introduction

The Wigner quasi-probability distribution was originally developed by Eugene Wigner as a bilinear representation of classical and quantum phase space, (q, p), in 1932. “On the quantum correction for thermodynamic equilibrium” [63]. In 1949 Jean-André Ville recognized that this distribution can also be used as a time-frequency “phase space” representation [65].

Although several people, notably Nyquist (1928), Shannon (1949), Wiener and Kolmogoroff (1941), worked on related topics, the advent of the modern day time-frequency analysis really occurred with the publication of “Theory of Communication” in 1946 by Denis Gabor [64]. (The inventor of the hologram and recipient of the 1971 Nobel Prize in Physics). In this work he extends his admiration to the founding fathers of quantum mechanics and expressed the idea to treat sound analogous to quantum wave mechanics. In analogy of the Gabor atom decomposition (1946) of a sound time signal can then be seen as a quantum of sound and is closely related to the von Neumann representation. The Gabor transform is the first instance of a Short-Time-Fourier-Transform (STFT). In this same paper the idea of an analytic signal is formally established. The von Neumann representation [91] was also originally developed for quantum mechanical phase space, i.e., (q, p). One of the first modern application is given in [92], and it has become quite popular in the scientific community, as can be seen by the various articles of late, [93, 94, 95, 96, 97, 98, 99, 100, 101, 102, 103, 104].

In this Chapter we present the von Neumann TFR, which is an indispensable stepping stone to the generalized Fourier-Hermite Gauss (FHG) TFR that is the main contribution of this thesis. Indeed, the von Neumann TFR may be seen as a zeroth order subset of the FHG TFR. Before we eventually present the von Neumann TFR we state a few mathematical preliminaries that will assist the reader in understanding it. In Section 3.2 we derive the standard Gaussian integral by a few different methods. In Section 3.3 we prove the extremely important fact that Gaussian function are Fourier transform invariant, i.e., functionally the Gaussian function remains a Gaussian function under a Fourier transform. This fact is what gives the von Neumann TFR basis functions basically all its various properties.

In Appendix A the Fourier transform is summarized in general. In Section 3.4 the Fourier transform properties of Gaussian functions are given, so when presented later, the properties are there for convenience. In Section 3.5 the von Neumann Representation is outlined. In Subsection 3.5.1 the basis functions are presented with the Fourier transform invariance. In Subsection 3.5.2 the important von Neumann basis lattice is presented. In Subsection 3.5.3 we state the principles of what would be required of basis functions to perform this task. We introduce the so-called overlap integral (Matrix). In Subsection 3.5.4 the overlap integral is derived. The result differs from that given in [94] and explained. The derivation has an obvious way to confirm and the results herein coincide. Then finally, the definitions of the von Neumann TFR and the signal reconstruction is given in Subsection 3.5.5 and Subsection 3.5.6, respectively. These preliminaries are all known results. However, they will be essential in deriving the generalized representation which is to follow in Chapter 5.

3.2. Derivation of Standard Gaussian Integrals

Theorem 3.2.1. *If, $\Re(a) > 0$, i.e., a, might be complex, the integral of a Gaussian function or normal curve is,*

$$I(a) = \int_{-\infty}^{\infty} e^{-ax^2}\, dx = \sqrt{\frac{\pi}{a}}. \tag{3.1}$$

Proof. This can be shown by taking the square of the above integral,

$$I^2(a) = \left[\int_{-\infty}^{\infty} e^{-ax^2}\, \mathrm{d}x\right]\left[\int_{-\infty}^{\infty} e^{-ay^2}\, \mathrm{d}y\right] = \int_{-\infty}^{\infty}\int_{-\infty}^{\infty} e^{-a(x^2+y^2)}\, \mathrm{d}x\mathrm{d}y, \tag{3.2}$$

and transforming to polar coordinates, $x = r\cos\theta$ and $y = r\sin\theta$, so that,

$$I^2(a) = \int_0^{2\pi}\int_0^{\infty} re^{-ar^2}\, \mathrm{d}r\mathrm{d}\theta = \frac{\pi}{a}. \tag{3.3}$$

Giving,

$$\boxed{\int_{-\infty}^{\infty} e^{-ax^2}\, \mathrm{d}x = \sqrt{\frac{\pi}{a}}} \tag{3.4}$$

□

This is for, $a \in \mathbb{C}$. It has a direct Corollary if, $a = i\beta$. From Euler's formula, $e^{ix} = \cos x + i \sin x$, we have, $i = e^{i\pi/2}$.

Corollary 3.2.2. *Generally for, $\beta \in \mathbb{C}$,*

$$\int_{-\infty}^{\infty} e^{i\beta x^2}\, dx = \sqrt{\frac{i\pi}{\beta}} = \sqrt{\frac{\pi}{\beta}} e^{i\pi/4}. \tag{3.5}$$

We now state and proof a Theorem that is quite relevant to this thesis.

Theorem 3.2.3. *For, $a = \alpha + i\beta \qquad \alpha > 0$, and, $\omega \in \mathbb{R}$, we have,*

$$\int_{-\infty}^{\infty} e^{-at^2 \pm i\omega t}\, dt = \sqrt{\frac{\pi}{a}} e^{-\frac{\omega^2}{4a}}.$$

Proof. We begin by showing that for any, a, $c \in \mathbb{C}$,

$$\boxed{\int_{-\infty}^{\infty} e^{-a(x+c)^2}\, \mathrm{d}x = \sqrt{\frac{\pi}{a}}, \qquad a = \alpha + i\beta \qquad \alpha > 0} \tag{3.6}$$

Although the integrand does not tend to zero as $x \to 0$, this can be justified because the integral exists for, $a = \alpha + i\beta$ and $\alpha \to 0$. Let, $c = g + ih$. This is accomplished by complex contour path integration with a rectangle with a line segment containing the real axis and the other line segment, $z = c$, the two other joining sides a distance, $k \in \mathbb{R} \ni |k| > |g|$, and since, e^{-az^2}, is analytic we obtain by Cauchy's theorem,

$$\oint e^{-az^2}\, \mathrm{d}z = 0. \tag{3.7}$$

The transformation, $z = x + c$, maps the real, x axis into a complex line, L_c, and results in a complex line integral,

$$\int_{-\infty}^{\infty} e^{-a(x+c)^2}\, \mathrm{d}x = \int_{L_c} e^{-az^2}\, \mathrm{d}z. \tag{3.8}$$

The contribution of the joining sides on the contour integral can be shown to tend to zero and we are left with,

$$\int_{L_c} e^{-az^2}\, \mathrm{d}z - \int_{-\infty}^{\infty} e^{-ax^2}\, \mathrm{d}x = 0, \tag{3.9}$$

or Eq. (3.6),

$$\int_{-\infty}^{\infty} e^{-a(x+c)^2}\, \mathrm{d}x = \sqrt{\frac{\pi}{a}}. \tag{3.10}$$

As a corollary consider the integral,

$$\int_{-\infty}^{\infty} e^{-at^2 \pm i\omega t} \,\mathrm{d}t. \tag{3.11}$$

By completing the square we have,

$$-at^2 \pm i\omega t = -a(t \mp \frac{i\omega}{2a})^2 - \frac{\omega^2}{4a}, \tag{3.12}$$

thus,

$$\int_{-\infty}^{\infty} e^{-at^2 \pm i\omega t} \,\mathrm{d}t = e^{-\frac{\omega^2}{4a}} \int_{-\infty}^{\infty} e^{-a(t \mp i\frac{\omega}{2a})^2} \,\mathrm{d}t, \tag{3.13}$$

but by setting, $c = \mp i\frac{\omega}{2a}$, we see that the above right hand integral is equal to, $\sqrt{\frac{\pi}{a}}$, Eq. (3.6) and Eq. (3.10), thus,

$$\boxed{\int_{-\infty}^{\infty} e^{-at^2 \pm i\omega t} \,\mathrm{d}t = \sqrt{\frac{\pi}{a}} e^{-\frac{\omega^2}{4a}}} \tag{3.14}$$

□

Not everybody is comfortable with contour integration, but fortunately the above standard integral can be derived by an alternative method using Fourier transform properties. This is directly related to the characteristic function methods of stochastic analysis.

Alternative Proof

Proof. The n^{th}**-moment of a function** $f(t)$, is defined by the following integral,

$$m_n = \int_{-\infty}^{\infty} t^n f(t) \,\mathrm{d}t \qquad n = 0, 1, 2, \dots \tag{3.15}$$

Now if we are given the Fourier transform pair,

$$f(t) \overset{\mathcal{F}}{\Longleftrightarrow} F(\omega), \tag{3.16}$$

then it is easy to see from the differentiation property of Fourier transforms, Subsection A.3.6 cf. A.27, that,

$$F(\omega) = \int_{-\infty}^{\infty} f(t)\, e^{-i\omega t}\, \mathrm{d}t \tag{3.17}$$

$$\frac{d^n F(\omega)}{d\omega^n} = (-i)^n \int_{-\infty}^{\infty} t^n f(t)\, e^{-i\omega t}\, \mathrm{d}t \tag{3.18}$$

$$\frac{d^n F(0)}{d\omega^n} = (-i)^n \int_{-\infty}^{\infty} t^n f(t)\, \mathrm{d}t = (-i)^n m_n \tag{3.19}$$

that is,

$$\boxed{(-i)^n m_n = \frac{d^n F(0)}{d\omega^n}} \tag{3.20}$$

With, $f(t) = e^{-at^2}$, differentiating,

$$\int_{-\infty}^{\infty} f(t)\, \mathrm{d}t = \int_{-\infty}^{\infty} e^{-at^2}\, \mathrm{d}t = \sqrt{\frac{\pi}{a}}, \tag{3.21}$$

n times w. r. t. a, we obtain (!! denotes the double factorial, see [105])

$$(-1)^n \int_{-\infty}^{\infty} t^{2n} e^{-at^2}\, \mathrm{d}t = (-1)^n \frac{(2n-1)!!}{2^n} \sqrt{\frac{\pi}{a^{2n+1}}}. \tag{3.22}$$

Thus, from Eq. (3.20) and Eq. (3.20), we obtain,

$$m_n = \frac{(2n-1)!!}{2^n} \sqrt{\frac{\pi}{a^{2n+1}}}. \tag{3.23}$$

Due to the evenness of the Gaussian function the odd moments are zero, thus using the double factorial formula [105],

$$(2n-1)!! = \frac{(2n)!}{n! 2^n}. \tag{3.24}$$

We find,

$$m_k = \left\{ \begin{array}{lll} 0 & k & \text{odd} \\ \frac{(k)!}{(k/2)! 2^k} \sqrt{\frac{\pi}{a^{k+1}}} & k & \text{even} \end{array} \right\}. \tag{3.25}$$

Now the (non-unitary Eq. (A.11)) Fourier transform of $f(t)$, is given by,

$$F(\omega) = \int_{-\infty}^{\infty} e^{-at^2} e^{-i\omega t}\, \mathrm{d}t = \int_{-\infty}^{\infty} e^{-at^2 - i\omega t}\, \mathrm{d}t. \tag{3.26}$$

Expanding the Taylor series about zero we obtain,

$$F(\omega) = \sum_{n=0}^{\infty} \frac{\omega^n}{n!} \frac{d^n F(0)}{d\omega^n} = \sum_{k=0}^{\infty} \frac{(-i\omega)^k}{k!} m_k, \tag{3.27}$$

$$F(\omega) = \sum_{n=0}^{\infty} \frac{(-i\omega)^{2n}}{(2n)!} m_{2n} = \sqrt{\frac{\pi}{a}} \sum_{n=0}^{\infty} \frac{\left(-\frac{i\omega}{2\sqrt{a}}\right)^{2n}}{(2n)!} \frac{(2n)!}{n!}, \tag{3.28}$$

$$F(\omega) = \sqrt{\frac{\pi}{a}} \sum_{n=0}^{\infty} \frac{\left(-\frac{\omega^2}{4a}\right)^{n}}{n!} = \sqrt{\frac{\pi}{a}} e^{-\frac{\omega^2}{4a}}. \tag{3.29}$$

The standard integral relationship is then given by,

$$\boxed{\int_{-\infty}^{\infty} e^{-at^2 - i\omega t}\, \mathrm{d}t = \sqrt{\frac{\pi}{a}} e^{-\frac{\omega^2}{4a}}} \tag{3.30}$$

□

3.3. Gaussian Fourier Transform Invariance

Let $f(t) = e^{-at^2}$, then if we define the Fourier transform as a unitary transform in terms of the angular frequency ω, Eq. (A.9), i.e.,

$$\boldsymbol{\mathcal{F}}\left\{f(t)\right\} = \frac{1}{\sqrt{2\pi}} \int_{-\infty}^{\infty} f(t) e^{-i\omega t}\, \mathrm{d}t = F(\omega), \tag{3.31}$$

where $F(\omega) = \frac{1}{\sqrt{2a}} e^{-\frac{\omega^2}{4a}}$ and,

$$\boldsymbol{\mathcal{F}}^{-1}\left\{F(\omega)\right\} = \frac{1}{\sqrt{2\pi}} \int_{-\infty}^{\infty} F(\omega) e^{i\omega t}\, \mathrm{d}\omega = f(t), \tag{3.32}$$

then the standard integral, Eq. (3.30), immediately has the following corollaries,

$$\boldsymbol{\mathcal{F}}\left\{e^{-at^2}\right\} = \frac{1}{\sqrt{2a}} e^{-\frac{\omega^2}{4a}}, \tag{3.33}$$

$$\boldsymbol{\mathcal{F}}^{-1}\left\{e^{-b\omega^2}\right\} = \frac{1}{\sqrt{2b}} e^{-\frac{t^2}{4b}}. \tag{3.34}$$

Notice that the forward ***and*** the inverse unitary Fourier transforms, transform the same. Note also,

$$\boldsymbol{\mathcal{F}}\left\{\frac{1}{\sqrt{2\pi}\sigma} e^{-\frac{t^2}{2\sigma^2}}\right\} = \frac{1}{\sqrt{2\pi}} \int_{-\infty}^{\infty} \frac{1}{\sqrt{2\pi}\sigma} e^{-\frac{t^2}{2\sigma^2} \pm i\omega t}\, \mathrm{d}t = \frac{1}{\sqrt{2\pi}} e^{-\frac{\sigma^2\omega^2}{2}}. \tag{3.35}$$

If the Fourier transform pair is defined symmetrically (or unitary, cf. Eq. (A.9)) we have the following relationship,

$$\boldsymbol{\mathcal{F}}\left\{f(t)\right\} = F(\omega) = \frac{1}{\sqrt{2\pi}} \int_{-\infty}^{\infty} f(t) e^{-i\omega t}\, \mathrm{d}t, \tag{3.36}$$

$$\boldsymbol{\mathcal{F}}^{-1}\left\{F(\omega)\right\} = f(t) = \frac{1}{\sqrt{2\pi}} \int_{-\infty}^{\infty} F(\omega) e^{i\omega t}\, \mathrm{d}t. \tag{3.37}$$

The standard normal Gaussian distribution with zero mean, $\langle x \rangle$, and unit standard deviation, σ, and normalized to 1 is defined as,

$$\mathcal{N}(0,1) = \frac{1}{\sqrt{2\pi}} e^{-\frac{x^2}{2}}. \tag{3.38}$$

More generally this is defined as,

$$\mathcal{N}(\langle x \rangle, \sigma) = \frac{1}{\sqrt{2\pi}\sigma} e^{-\frac{(x-\langle x \rangle)^2}{2\sigma^2}} = \frac{1}{\sqrt{2\pi}\sigma} e^{-\frac{1}{2}\left(\frac{x-\langle x \rangle}{\sigma}\right)^2}. \tag{3.39}$$

This is the standard definition of Gaussian function, normally used for probability theory[1] and statistics. For our purposes we will modify this slightly to explicitly denote the dependent variable and the shifting and scaling

$$N(x - \langle x \rangle, \sigma) = \frac{1}{\sqrt{2\pi}\sigma} e^{-\frac{1}{2}\left(\frac{x-\langle x \rangle}{\sigma}\right)^2} := \mathcal{N}(\langle x \rangle, \sigma). \tag{3.40}$$

Thus we write, $\mathcal{N}(x) = \mathcal{N}(0,1)$. Thus a symmetrical Fourier transform of a Gaussian function can be defined as,

$$\left(\frac{2\alpha}{\pi}\right)^{\frac{1}{4}} e^{-\alpha t^2} \overset{\mathcal{F}}{\Longleftrightarrow} \left(\frac{2\alpha}{\pi}\right)^{\frac{1}{4}} \sqrt{\frac{\pi}{\alpha}} e^{-\frac{(\pi\nu)^2}{\alpha}}, \left(\frac{2\alpha}{\pi}\right)^{\frac{1}{4}} e^{-\alpha t^2} \overset{\mathcal{F}}{\Longleftrightarrow} \left(\frac{1}{2\alpha\pi}\right)^{\frac{1}{4}} e^{-\frac{\omega^2}{4\alpha}}. \tag{3.41}$$

for Fourier transforms Eq. (A.5) and Eq. (A.7), respectively. Or equivalently,

$$\frac{1}{\sqrt{2\pi}} \int_{-\infty}^{\infty} \left[\frac{1}{\sqrt{2\pi}} e^{-\frac{t^2}{2}}\right] e^{-i\omega t}\, \mathrm{d}t = \frac{1}{\sqrt{2\pi}} e^{-\frac{\omega^2}{2}} \tag{3.42}$$

$$\boldsymbol{\mathcal{F}}\left\{\mathcal{N}(t)\right\} \to \mathcal{N}(\omega), \tag{3.43}$$

in other words the normal Gaussian distribution with zero mean and standard deviation 1 is functionally its own Fourier transform!!!!!!! Mathematically this functional form is invariant under the Fourier transform.

---

[1] Historically Laplace is the father of classical probability theory (Pascal, Huygens et al.). Einstein, Norbert Wiener, von Mises, Markov, Kolmogorov all contributed, but at present, Edwin Jaynes, yes the Jaynes-Cumming model, with his treatise "Probability theory: the logic of science" is the preferred book [106].

3.4. Fourier Transform Properties of the Gaussian Function

In this Section we derive a few Fourier transform properties of Gaussian functions for convenience for later use.

3.4.1. Scaling Condition

Using the linearity of the Fourier transform and the standard Gaussian integral derived in Eq. (3.30),

$$\frac{1}{\sqrt{2\pi}}\int_{-\infty}^{\infty}\left[\frac{1}{\sqrt{2\pi}}e^{-\frac{ax^2}{2}}\right]e^{-i\omega x}\,\mathrm{d}x=\frac{1}{\sqrt{2\pi a}}e^{-\frac{\omega^2}{2a}}=\mathcal{N}(\omega,\sqrt{a}), \tag{3.44}$$

$$\frac{1}{\sqrt{2\pi}}\int_{-\infty}^{\infty}\left[\frac{\sqrt{a}}{\sqrt{2\pi}}e^{-\frac{ax^2}{2}}\right]e^{-i\omega x}\,\mathrm{d}x=\sqrt{a}\mathcal{N}(\omega,\sqrt{a}), \tag{3.45}$$

which gives the scaling condition for Fourier transforms,

$$\mathcal{F}\left\{\mathcal{N}(x,\frac{1}{\sqrt{a}})\right\}=\sqrt{a}\mathcal{N}(\omega,\sqrt{a}). \tag{3.46}$$

3.4.2. Temporal and Spectral Shifting

The Fourier Temporal and Spectral Shifting Theorem states (cf. Eq. (A.22) and Eq. (A.23)),

$$\boldsymbol{\mathcal{F}}\left\{f(t-a)\right\} \rightarrow e^{-ia\omega}F(\omega), \tag{3.47}$$

$$\boldsymbol{\mathcal{F}}\left\{e^{ia\omega}f(t)\right\} \rightarrow F(\omega-a), \tag{3.48}$$

and applied on the normal distribution,

$$\boldsymbol{\mathcal{F}}\left\{\mathcal{N}(t-a,\sigma)\right\} \rightarrow e^{-ia\omega}\frac{1}{\sigma}\mathcal{N}(\omega,\frac{1}{\sigma}), \tag{3.49}$$

$$\boldsymbol{\mathcal{F}}\left\{e^{iat}\mathcal{N}(t,\sigma)\right\} \rightarrow \frac{1}{\sigma}\mathcal{N}(\omega-a,\frac{1}{\sigma}). \tag{3.50}$$

3.4.3. Gaussian Fourier Transform pair

Combining both the Fourier scaling and shifting Theorems Subsection A.3.4 and Subsection A.3.5 we find,

$$\mathcal{F}\left\{\mathcal{N}(t-t_m,\sigma)\right\} \to e^{-it_m\omega}\frac{1}{\sigma}\mathcal{N}(\omega,\frac{1}{\sigma}) = P(\omega), \tag{3.51}$$

$$P(\omega-\omega_n) = e^{-it_m(\omega-\omega_n)}\frac{1}{\sigma}\mathcal{N}(\omega-\omega_n,\frac{1}{\sigma}), \tag{3.52}$$

$$\mathcal{F}^{-1}\left\{P(\omega-\omega_n)\right\} = e^{i\omega_n t}\mathcal{N}(t-t_m,\sigma). \tag{3.53}$$

We arrive at this transform pair

$$\boxed{\mathcal{F}\left\{e^{i\omega_n t}\mathcal{N}(t-t_m,\sigma)\right\} = e^{-it_m(\omega-\omega_n)}\frac{1}{\sigma}\mathcal{N}(\omega-\omega_n,\frac{1}{\sigma})} \tag{3.54}$$

which will play a central role in the von Neumann TFR discussed in the next Section 3.5. Replacing, σ, with, $\sqrt{2\alpha}$,

$$\mathcal{F}\left\{e^{i\omega_n t}\frac{1}{\sqrt{4\pi\alpha}}e^{-\frac{(t-t_m)^2}{4\alpha}}\right\} = e^{-it_m(\omega-\omega_n)}\frac{1}{\sqrt{2\pi}}e^{-\alpha(\omega-\omega_n)^2}. \tag{3.55}$$

To obtain the von Neumann basis coefficient (cf. Subsection 3.5.1) multiply both sides with, $(8\alpha\pi)^{\frac{1}{4}}$,

$$\boxed{\mathcal{F}\left\{\left(\frac{1}{2\alpha\pi}\right)^{\frac{1}{4}}e^{-\frac{(t-t_m)^2}{4\alpha}+i\omega_n t}\right\} = \left(\frac{2\alpha}{\pi}\right)^{\frac{1}{4}}e^{-\alpha(\omega-\omega_n)^2-it_m(\omega-\omega_n)}} \tag{3.56}$$

or in terms of the normal function,

$$\boxed{\mathcal{F}\left\{(8\alpha\pi)^{\frac{1}{4}}e^{i\omega_n t}\mathcal{N}(t-t_m,\sqrt{2\alpha})\right\} = \left(\tfrac{2\pi}{\alpha}\right)^{\frac{1}{4}}e^{-it_m(\omega-\omega_n)}\mathcal{N}(\omega-\omega_n,\frac{1}{\sqrt{2\alpha}}).} \tag{3.57}$$

3.5. The von Neumann Representations

As discussed in Tannor et al. [94], the original idea that was proposed by von Neumann, was to represent a discrete $K-$point time signal on a discrete time-frequency grid or lattice of exactly the same dimension, i.e., $K-$points. According to von Neumann, given a discrete $K-$point time signal, which one can also transform by means of a Discrete Fourier Transform (DFT) to the frequency domain, to obtain a discrete $K-$point frequency signal, implies that all the available information of the signal is contained in a discrete set of $K-$points. To retain the total information content of the signal in a time-frequency representation, he proposed to decompose the signal in terms of K-Gaussian functions (or Gabor atoms) over the time-frequency domain, i.e., each Gaussian function is centered around a discrete time-frequency point, say, (t_i, ω_j), with $i, j = 1, 2, \ldots, \sqrt{K}$. Now, $\sqrt{K} \in \mathbb{N}$, which implies that, $K \in \mathbb{N}$, must be quadratic. If it is not, the signal must be resampled or zero-padded so that it is. He stated that in quantum mechanics the minimum uncertainty wave function is a Gaussian function. This was originally shown by Schrödinger in 1926. Both von Neumann and Cohen include derivations of this statement in their books.

3.5.1. The von Neumann Basis

Originally it was shown by Erwin Schrödinger (1926) that to comply with the Heisenberg uncertainty principle, $\triangle x \triangle p \geq \frac{\hbar}{2}$, the normalized minimum uncertainty quantum wave packet (this is derived in many textbooks, [4, 7, 107, 108]), is given by,

$$\psi(x) = \left[\frac{1}{2\pi\,(\triangle x)^2}\right]^{\frac{1}{4}} \exp\left[-\frac{(x - \langle x\rangle)^2}{4(\triangle x)^2} + \frac{i\,\langle p\rangle\, x}{\hbar}\right]. \tag{3.58}$$

Utilizing these minimum uncertainty wave packets, von Neumann originally presented the von Neumann representation to decompose a general wave packet in quantum mechanics. For TFR we make the following analogy, equivalent to the Ville correspondence for the Wigner-Ville TFR, namely, $x \to t$, and, $p/\hbar \to \omega$. Comparing Eq. (3.58) with Eq. (3.60), we see, $(\triangle x)^2 \to \sigma$, $\langle x\rangle \to t_m$ and, $\langle p\rangle/\hbar \to \omega_n$, then $\psi(x) \to \alpha_{t_m,\omega_n}(t)$. The analogy is plainly mathematical using a tool to represent waves.

The von Neumann basis representations in the frequency (spectral) domain is given by an evenly spaced lattice in time frequency phase space,

$$\tilde{\alpha}_{t_m,\omega_n}(\omega) = \tilde{\alpha}_{m,n}(\omega) = \left(\frac{2\sigma}{\pi}\right)^{\frac{1}{4}} \exp\left[-\sigma(\omega-\omega_n)^2 - it_m(\omega-\omega_n)\right]. \tag{3.59}$$

The inverse Fourier transform of the basis gives the time (temporal) von Neumann basis,

$$\alpha_{t_m,\omega_n}(t) = \alpha_{m,n}(t) = \left(\frac{1}{2\sigma\pi}\right)^{\frac{1}{4}} \exp\left[-\frac{1}{4\sigma}(t-t_m)^2 + it\omega_n\right]. \tag{3.60}$$

This inverse relationship can easily be computed with the observation that the conjugate of the time representation of the von Neumann basis can be written as,

$$\alpha_{m,n}(t) = (8\sigma\pi)^{\frac{1}{4}}\, e^{it\omega_n}\mathcal{N}(t-t_m,\sqrt{2\sigma}), \tag{3.61}$$

and the frequency representation as,

$$\tilde{\alpha}_{m,n}(\omega) = \left(\tfrac{2\pi}{\sigma}\right)^{\frac{1}{4}} e^{-it_m(\omega-\omega_n)}\mathcal{N}(\omega-\omega_n,\sqrt{\frac{1}{2\sigma}}). \tag{3.62}$$

We then note that,

$$\boxed{\mathcal{F}\left\{\alpha_{m,n}(t)\right\} = \tilde{\alpha}_{m,n}(\omega)} \tag{3.63}$$

or,

$$\boxed{\alpha_{m,n}(t) \overset{\mathcal{F}}{\Longleftrightarrow} \tilde{\alpha}_{m,n}(\omega)} \tag{3.64}$$

3.5.2. The von Neumann Basis Lattice

The von Neumann basis can be represented as a square lattice of evenly spaced points in time and frequency phase space. Originally, von Neumann wanted to represent the quantum mechanical wave function in terms of the minimum uncertainty wavefunction determined by Erwin Schrödinger in 1926. The subsequent development of time-frequency analysis and the Gabor limit, also known as the Heisenberg-Gabor uncertainty, specifies that the limit of the uncertainty, namely 1 is only reached for a Gaussian envelope time signal. This is proven in L. Cohen's book, "Time Frequency Analysis. " The concept behind the von Neumann TFR is to retain the maximum or similar information contained in the discrete sampled time signal. This places the condition on TFRs that, given an N point time signal, $E(t_i)$, $i = 1, \ldots, N$, then the time-frequency representation must also contain N points. Thus the time-frequency lattice must be divided as, $N = \sqrt{N} \times \sqrt{N}$.

In taking a Fourier transform on a digital computer, the so called discrete Fourier transform must be calculated and inadvertently the ubiquitous Fast Fourier Transform (FFT) is implemented (in one of its myriad of algorithms). For an ultra-short laser pulse, when one wants to zoom into a spectral window of interest and reconstruct the time signal using these Fourier coefficients, one quickly finds idiosyncrasies in the results, that mainly pertain to fact that all the digital data must be used in the reconstruction. The von Neumann representation bridges this shortcoming. It allows the user to zoom in on the spectral portion of interest of the spectral signal, and discarding the null-support[2] in the spectral domain.

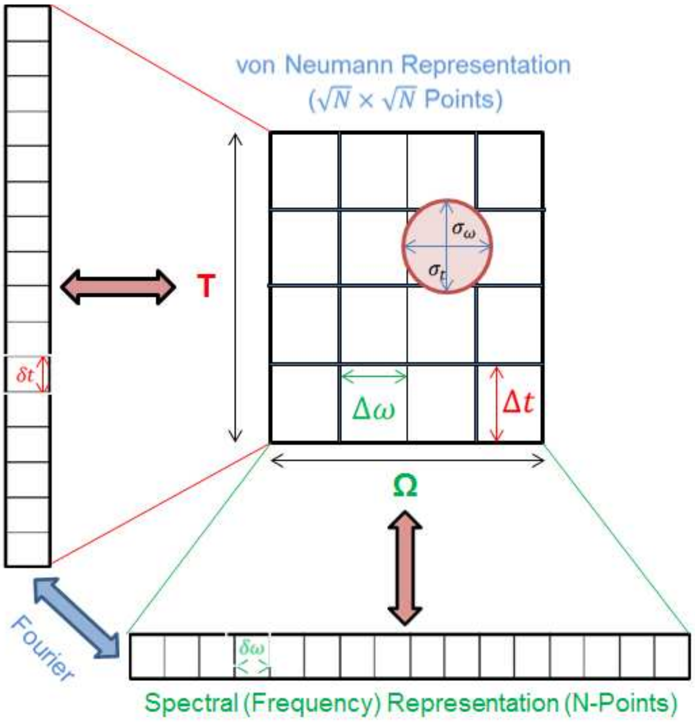
von Neumann Representation
($\sqrt{N} \times \sqrt{N}$ Points)
σ_ω
σ_t
T
δt
$\Delta\omega$
Δt
Ω
Fourier
$\delta\omega$
Spectral (Frequency) Representation (N-Points)

Figure 3.1.: The von Neumann Lattice

Consider the spectral electric field, $E(\omega)$, of a signal sampled at, M, complex data points. The analytical signal will, however, only have a non-null support over the bandwidth, $\Omega = \omega_{max} - \omega_{min}$. In this bandwidth of interest the electric field, $E(\omega)$, will have, N points, ω_{min}, $\omega_{min} + \delta\omega$, $\ldots$, $\omega_{min} + (N-1)\delta\omega = \omega_{max}$. By Nyquist sampling theorem (See Section A.10) (actually the reciprocal theorem of Fourier transforms) the timespan, T, of the original signal must correspond to, $T = 2\pi/\delta\omega$. The temporal electrical field, $E(t)$, will correspond to the inverse Fourier transform of $E(\omega)$, that will also have, M, data points.

The von Neumann lattice is defined on, $N = \sqrt{N} \times \sqrt{N}$, points equally and uniformly distributed between the time and frequency domains, (T, Ω). For each lattice square, the equivalent von Neumann point, (t_k, ω_l), is defined at the center of the square, i.e., given the incremental von Neumann time step, $\Delta t = T/K$, then,

---

[2] Null-support is defined for instance on the real line for a real function,$f(x)$, as a set, $\mathscr{N} = \{x \in \mathbb{R} \,|\, f(x) = 0\}$

$$t_m = -T/2 + (m - \frac{1}{2})\Delta t \quad m = 1, \cdots, K = \sqrt{N}, \tag{3.65}$$

and similarly the von Neumann frequency increment, $\Delta\omega = \Omega/K$, then,

$$\omega_n = \omega_{min} + (n - \frac{1}{2})\Delta\omega \quad n = 1, \cdots, K = \sqrt{N}. \tag{3.66}$$

The subscripts, (m, n), coincide with subscripts of the von Neumann basis functions, α_{t_m,ω_n}, and, $\tilde{\alpha}_{t_m,\omega_n}(\omega)$. It is important to note that, $K = \sqrt{N}$, and this can always be accomplished by zero-padding the original signal.

The temporal, $\alpha_{t_m,\omega_n}(t)$, and spectral, $\tilde{\alpha}_{t_m,\omega_n}(\omega)$, Gaussian functions all have the same full-width half-maximums (FWHM) given by, $\beta_t = \sqrt{\sigma 16 \ln 2}$, and $\beta_\omega = \sqrt{4\ln 2/\sigma}$, respectively. The Fourier scaling theorem, Subsection A.3.4, establishes a reciprocity between the two FWHMs given by,

$$\beta_t \beta_\omega = 8 \ln 2. \tag{3.67}$$

The σ parameter defines a constant ratio between the two FWHMs,

$$\sigma = \frac{\beta_t}{2\beta_\omega} = \frac{T}{2\Omega}. \tag{3.68}$$

J. von Neumann, “Der Eindeutigkeit der Schödingerschen Operatoren”, Math. Ann **104**, 570 (1931), [91]

3.5.3. Principles of Signal Representation

The objective of the von Neumann basis is to represent an arbitrary signal time signal, $\varepsilon(t)$, in terms of the von Neumann temporal basis, $\alpha_{m,n}(t)$, or equivalently Fourier transform of the signal, $\tilde{\varepsilon}(\omega)$, in terms of the von Neumann spectral basis, i.e., can we represent, $\varepsilon(t)$, such that,

$$\varepsilon(t) \sim \sum_{m,n} \mathcal{V}_{m,n} \alpha_{m,n}(t), \tag{3.69}$$

or equivalently as,

$$\tilde{\varepsilon}(\omega) \sim \sum_{m,n} \tilde{\mathcal{V}}_{m,n} \tilde{\alpha}_{m,n}(\omega). \tag{3.70}$$

The question now is: What is the relationship between, $\mathcal{V}_{m,n}$ and $\tilde{\mathcal{V}}_{m,n}$? This would be simplicity itself if the basis vectors were orthogonal, that is if (this also definition of the inner product in this abstract space, using the Dirac bra and ket notation),

$$\langle \alpha_{m,n}(t) | \alpha_{k,l}(t) \rangle = \int_{-\infty}^{\infty} \alpha^*_{m,n}(t) \alpha_{k,l}(t) \, \mathrm{d}t = \delta_{m,k} \delta_{n,l}, \tag{3.71}$$

$$\langle \tilde{\alpha}_{m,n}(\omega) | \tilde{\alpha}_{k,l}(\omega) \rangle = \int_{-\infty}^{\infty} \tilde{\alpha}^*_{m,n}(\omega) \tilde{\alpha}_{k,l}(\omega) \, \mathrm{d}\omega = \delta_{m,k} \delta_{n,l}, \tag{3.72}$$

where, $\delta_{m,k}$, are usual Kronecker delta function defined in Eq. (A.84). Then as in Fourier Series analysis (Subsection A.1.1) we would have,

$$\int_{-\infty}^{\infty} \alpha^*_{m,n}(t) \varepsilon(t) \, \mathrm{d}t = \sum_{k,l} \mathcal{V}_{k,l} \int_{-\infty}^{\infty} \alpha^*_{m,n}(t) \alpha_{k,l}(t) \, \mathrm{d}t = \sum_{k,l} \mathcal{V}_{k,l} \delta_{m,k} \delta_{n,l} = \mathcal{V}_{m,n}, \tag{3.73}$$

and,

$$\int_{-\infty}^{\infty} \tilde{\alpha}^*_{m,n}(\omega) \tilde{\varepsilon}(\omega) \, \mathrm{d}\omega = \sum_{k,l} \tilde{\mathcal{V}}_{k,l} \int_{-\infty}^{\infty} \tilde{\alpha}^*_{m,n}(\omega) \tilde{\alpha}_{k,l}(\omega) \, \mathrm{d}\omega = \sum_{k,l} \tilde{\mathcal{V}}_{k,l} \delta_{m,k} \delta_{n,l} = \tilde{\mathcal{V}}_{m,n}. \tag{3.74}$$

Thus we see that,

$$\mathcal{V}_{m,n} = \tilde{\mathcal{V}}_{m,n}, \tag{3.75}$$

if and only if,

$$\int_{-\infty}^{\infty} \alpha^*_{m,n}(t) \alpha_{k,l}(t) \, \mathrm{d}t = \int_{-\infty}^{\infty} \tilde{\alpha}^*_{m,n}(\omega) \tilde{\alpha}_{k,l}(\omega) \, \mathrm{d}\omega, \tag{3.76}$$

or (using the Dirac Bra-Ket notation is common in physics articles to denote the *functional integral inner product*, Eq. (3.76), see e.g., Fechner et al. [94])[3],

$$\langle \alpha_{m,n}(t) | \alpha_{k,l}(t) \rangle = \langle \tilde{\alpha}_{m,n}(\omega) | \tilde{\alpha}_{k,l}(\omega) \rangle \, . \tag{3.77}$$

---

[3] This notation implies that the basis vectors are $|\alpha_{k,l}(t)\rangle \in \mathbb{H}$, in a mathematical functional Hilbert space, with their associated dual basis vectors $\langle \alpha_{k,l}(t)|$. In fact in any abstract Hilbert space, i.e., a complete inner product space, this notation is applicable. It is just a mathematical shorthand notation inherited from quantum mechanics.

The above equations define the so-called overlap matrix (integral) and unfortunately, Eq. (3.71) and Eq. (3.72) do not hold and we have a non-zero overlap integral, which implies that the basis vectors are non-orthogonal, i.e.,

$$\langle \alpha_{m,n}(t)|\alpha_{k,l}(t)\rangle = \langle \tilde{\alpha}_{m,n}(\omega)|\tilde{\alpha}_{k,l}(\omega)\rangle = \mathbb{S}^{k,l}_{m,n} \neq \delta_{m,k}\delta_{n,l}. \tag{3.78}$$

The following relationship is required to impose orthogonality and for uniqueness of an expansion for non-unitary overlap integrals. This is the principle of signal representation,

$$\sum_{k,l}\sum_{m,n} |\alpha_{m,n}(t)\rangle \left[\mathbb{S}^{k,l}_{m,n}\right]^{-1} \langle \alpha_{k,l}(t)| = \delta_{m,k}\delta_{n,l}, \tag{3.79}$$

or

$$\sum_{k,l}\sum_{m,n} |\tilde{\alpha}_{m,n}(\omega)\rangle \left[\mathbb{S}^{k,l}_{m,n}\right]^{-1} \langle \tilde{\alpha}_{k,l}(\omega)| = \delta_{m,k}\delta_{n,l}. \tag{3.80}$$

More generally, because of the continuous time t and angular frequency ω domains, we actually have,

$$\sum_{k,l}\sum_{m,n} |\alpha_{m,n}(t)\rangle \left[\mathbb{S}^{k,l}_{m,n}\right]^{-1} \langle \alpha_{k,l}(\tau)| = \delta_{m,k}\delta_{n,l}\delta(t-\tau), \tag{3.81}$$

or

$$\sum_{k,l}\sum_{m,n} |\tilde{\alpha}_{m,n}(\omega\rangle \left[\mathbb{S}^{k,l}_{m,n}\right]^{-1} \langle \tilde{\alpha}_{k,l}(\omega')| = \delta_{m,k}\delta_{n,l}\delta(\omega-\omega'). \tag{3.82}$$

Here $\delta(t-\tau)$ is the Dirac-δ-function defined in Subsection A.4.6.

3.5.4. Derivation of the Overlap Integral

The overlap integral of the von Neumann is defined as an inner product of the various basis, i.e., for the angular frequency basis as

$$\mathbb{S}^{k,l}_{m,n} = \langle \tilde{\alpha}_{m,n}(\omega)|\tilde{\alpha}_{k,l}(\omega)\rangle = \int_{-\infty}^{\infty} \tilde{\alpha}^{*}_{m,n}(\omega)\tilde{\alpha}_{k,l}(\omega)\,\mathrm{d}\omega, \tag{3.83}$$

and also for the time basis.

$$\mathbb{S}^{k,l}_{m,n} = \langle \alpha_{m,n}(t)|\alpha_{k,l}(t)\rangle = \int_{-\infty}^{\infty} \alpha^{*}_{m,n}(t)\alpha_{k,l}(t)\,\mathrm{d}t. \tag{3.84}$$

where equality is assured by the Parseval-Plancherel theorem for energy densities (cf. Subsection A.3.10). Inserting the angular frequency basis, Eq. (3.59), into the overlap integral inner product we arrive at,

$$\mathbb{S}^{k,l}_{m,n} = \left(\frac{2\sigma}{\pi}\right)^{\frac{1}{2}} \int_{-\infty}^{\infty} \exp\left[-\sigma(\omega-\omega_n)^2 - \sigma(\omega-\omega_l)^2 + it_m(\omega-\omega_n) - it_k(\omega-\omega_l)\right] \mathrm{d}\omega. \tag{3.85}$$

The evaluation of this integral is essentially an exercise in converting the exponent of the exponential into a similar form as the standard normal integral. This entails completing the square of the exponent, which, after some algebra, reduces the exponent of the integrand of Eq. (3.85) to,

$$\left[-\frac{\sigma}{2}\left(\omega_n-\omega_l\right)^2 + i\left(t_k\omega_l - t_m\omega_n\right)\right] + \left\{-2\sigma\left[\omega - \frac{1}{2}\left(\omega_n+\omega_l\right)\right]^2 + i\left(t_m-t_k\right)\omega\right\}. \tag{3.86}$$

The exponential of the square bracket can be factored out of the integral and after substituting,

$$\omega' = \omega - \frac{1}{2}\left(\omega_n+\omega_l\right), \tag{3.87}$$

into Eq. (3.86) and after some simplifications we obtain,

$$\left[-\frac{\sigma}{2}\left(\omega_n-\omega_l\right)^2 - \frac{1}{2}i\left(t_m+t_k\right)\left(\omega_n-\omega_l\right)\right] + \left\{-2\sigma\omega^2 + i\left(t_m-t_k\right)\omega\right\}. \tag{3.88}$$

The curly brackets is now in the form of the standard normal integral, $-a\omega^2+ib\omega$, namely, Eq. (3.30)

$$\begin{aligned}\int_{-\infty}^{\infty} e^{-a\omega^2+ib\omega}\,\mathrm{d}\omega &= \sqrt{\frac{\pi}{a}}e^{-\frac{b^2}{4a}} \\ &= \left(\frac{\pi}{2\sigma}\right)^{\frac{1}{2}} e^{-\frac{(t_m-t_k)^2}{8\sigma}}.\end{aligned} \tag{3.89}$$

The overlap integral (substituting Eq. (3.88) in the exponent of Eq. (3.85) and using Eq. (3.89)) can thus be written as,

$$\boxed{\mathbb{S}^{k,l}_{m,n} = \exp\left[-\frac{\sigma}{2}\left(\omega_n-\omega_l\right)^2 - \frac{1}{2}i\left(t_m+t_k\right)\left(\omega_n-\omega_l\right) - \frac{1}{8\sigma}\left(t_m-t_k\right)^2\right]} \tag{3.90}$$

This result can be confirmed by doing the temporal basis integral, which gives the same result, i.e.,

$$\langle\alpha_{m,n}(t)|\alpha_{k,l}(t)\rangle = \mathbb{S}^{k,l}_{m,n} = \langle\tilde{\alpha}_{m,n}(\omega)|\tilde{\alpha}_{k,l}(\omega)\rangle\,. \tag{3.91}$$

The unit constant in front of the overlap integral, i.e., $A = 1$, explains the choice of the normalization constants of the von Neumann representation basis.

Exploring some of the aspects of the overlap integral, we notice first of all, that it represents some kind of matrix indexed in the rows by, (m, n), and in the columns by, (k, l). To place the time and the angular frequency on the same footing we set, $\sigma = 1/2$,

$$\mathbb{S}_{m,n}^{k,l} = \exp\left[-\frac{1}{4}\left(\omega_n - \omega_l\right)^2 - \frac{1}{2}i\left(t_m + t_k\right)\left(\omega_n - \omega_l\right) - \frac{1}{4}\left(t_m - t_k\right)^2\right]. \tag{3.92}$$

This can be written in complex polar form as,

$$\mathbb{S}_{m,n}^{k,l} = A_{mn,kl}e^{i\phi_{mn,kl}}, \tag{3.93}$$

where,

$$A_{mn,kl} = \exp\left[-\frac{1}{4}\left(\omega_n - \omega_l\right)^2 - \frac{1}{4}\left(t_m - t_k\right)^2\right], \tag{3.94}$$

$$\phi_{mn,kl} = -\frac{1}{2}\left(t_m + t_k\right)\left(\omega_n - \omega_l\right). \tag{3.95}$$

What follows is just a comment and an errata of Fechner et al. [109]. They define the spectral von Neumann bases as (exactly as in the article as Eq. (1)),

$$\tilde{\alpha}_{\omega_n t_m}(\omega) = \left(\frac{2\alpha}{\pi}\right)^{1/4} \exp\left[-\alpha(\omega - \omega_n)^2 - it_m(\omega - \omega_n)\right].$$

This corresponds to our Eq. (3.59) except that our variance has been changed to σ to avoid notational ambiguity and a change in our subscript order. Their definition of their temporal von Neumann bases is (exactly as in the article as Eq. (2))

$$\alpha_{\omega_n t_m}(t) = \left(\frac{1}{2\alpha\pi}\right)^{1/4} \exp\left[-\frac{1}{4\alpha}(t - t_m)^2 - it\omega_n\right].$$

This differs from our definition Eq. (3.60) by a change in the sign of the phase, i.e., $-it\omega_n$. From Eq. (3.64) this implies that, for their von Neumann bases, that,

$$\alpha^*_{\omega_n t_m}(t) \overset{\mathcal{F}}{\Longleftrightarrow} \tilde{\alpha}_{\omega_n t_m}(\omega). \tag{3.96}$$

In this subsection we state that Eq. (3.83) is equal to Eq. (3.84), which is true. In their article they then calculate the overlap matrix as (their Eq. (10)),

$$\begin{aligned} S_{(n,m),(i,j)} = \sqrt{\frac{2\alpha}{\pi}} \exp\Bigg[&-\frac{\alpha}{2}\left(\omega_n - \omega_i\right)^2 - \frac{1}{8\alpha}\left(t_j - t_m\right)^2 \\ &+\frac{i}{2}\left(\omega_i - \omega_n\right)\left(t_j + t_m\right)\Bigg]. \end{aligned}$$

Now this corresponds to our Eq. (3.90), except for the notational difference, but they include a constant factor, $\sqrt{\frac{2\alpha}{\pi}}$, which we do not find. The scaling of the bases cancels this factor exactly. We assume the correct equation should have been

$$S_{(n,m),(i,j)} = \exp\left[-\frac{\alpha}{2}\left(\omega_n - \omega_i\right)^2 - \frac{1}{8\alpha}\left(t_j - t_m\right)^2 \right.$$
$$\left. + \frac{i}{2}\left(\omega_i - \omega_n\right)\left(t_j + t_m\right)\right]. \tag{3.97}$$

Now, because of the phase difference in, $\alpha_{\omega_n t_m}(t)$, compared to our Eq. (3.60), if we calculate the overlap matrix with them we find,

$$T_{(n,m),(i,j)} = \exp\left[-\frac{\alpha}{2}\left(\omega_n - \omega_i\right)^2 - \frac{1}{8\alpha}\left(t_j - t_m\right)^2 \right.$$
$$\left. - \frac{i}{2}\left(\omega_i - \omega_n\right)\left(t_j + t_m\right)\right]. \tag{3.98}$$

Notice the phase change in the bottom half of Eq. (3.98) compared with Eq. (3.97). The constant factor that appears in this calculation is also, $\sqrt{\frac{1}{2\alpha\pi}}$, but it is also exactly canceled by the scaling of the temporal bases. Thus,

$$S_{(n,m),(i,j)} = T^{*}_{(n,m),(i,j)}. \tag{3.99}$$

It is our belief that this minor phase difference would not effect any of their results, except for the temporal phases. The equality of Eq. (3.90) lead us to our choice of temporal von Neumann bases Eq. (3.60) and the extensions that are to be revealed in Chapter 5, these notational definitions are continued.

3.5.5. The von Neumann Time-Frequency Representation

The von Neumann TFR representation is then given by,

$$\boldsymbol{\mathcal{Q}}_{m,n} = \sum_{k,l}\left[\mathbb{S}^{k,l}_{m,n}\right]^{-1}\int_{-\infty}^{\infty}\alpha^{*}_{k,l}(t)\varepsilon(t)\,dt, \tag{3.100}$$

$$\boldsymbol{\mathcal{Q}}_{m,n} = \sum_{k,l}\left[\mathbb{S}^{k,l}_{m,n}\right]^{-1}\int_{-\infty}^{\infty}\tilde{\alpha}^{*}_{k,l}(\omega)\tilde{\varepsilon}(\omega)\,d\omega. \tag{3.101}$$

Expansion of the signal in either the temporal or spectral basis with their accompanying respective signals result in the same TFR. This is only possible because of the Fourier invariance of the von Neumann basis functions shown in Eq. (3.63).

Notice that in the calculation of the von Neumann representation the inverse of the overlap matrix, $\mathbb{S}^{k,l}_{m,n}$, is required. The matrix is invertible, since it contains no non-zero eigenvalues and therefore, $\det\left(\mathbb{S}^{k,l}_{m,n}\right) \neq 0$. Unfortunately the overlap matrix is ill-conditioned and sparse so that, even at very modest dimensions, it becomes necessary to numerically calculate the inverse with the pseudo-inverse Moore-Penrose technique. This rather places a question mark on the relative numerical accuracy of the technique, but we assume that the inverse technique is accurate enough.

3.5.6. Signal Reconstruction

The reconstruction of the temporal signal and spectral signals are then given by the expansion of the von Neumann representation into their respective temporal or spectral von Neumann bases,

$$\varepsilon(t) = \sum_{m,n} \boldsymbol{Q}_{m,n} \alpha_{m,n}(t), \tag{3.102}$$

$$\tilde{\varepsilon}(\omega) = \sum_{m,n} \boldsymbol{Q}_{m,n} \tilde{\alpha}_{m,n}(\omega). \tag{3.103}$$

This is simply derived by inserting the von Neumann TFR, Eq. (3.100) and Eq. (3.101) into Eq. (3.102) and Eq. (3.103), respectively, and then employing the orthogonality conditions, Eq. (3.81) and Eq. (3.82), respectively, e.g., the temporal reconstruction expansion,

$$\begin{aligned}
\sum_{m,n} \boldsymbol{Q}_{m,n} \alpha_{m,n}(t) &= \sum_{m,n} \left(\sum_{k,l} \left[\mathbb{S}^{k,l}_{m,n}\right]^{-1} \int_{-\infty}^{\infty} \alpha^*_{k,l}(\tau) \varepsilon(\tau)\, d\tau \right) \alpha_{m,n}(t) \\
&= \sum_{m,n} |\alpha_{m,n}(t)\rangle \left(\sum_{k,l} \left[\mathbb{S}^{k,l}_{m,n}\right]^{-1} \int_{-\infty}^{\infty} \langle \alpha_{k,l}(\tau)|\, \varepsilon(\tau)\, d\tau \right) \\
&= \int_{-\infty}^{\infty} \left(\sum_{m,n} \sum_{k,l} |\alpha_{m,n}(t)\rangle \left[\mathbb{S}^{k,l}_{m,n}\right]^{-1} \langle \alpha_{k,l}(\tau)| \right) \varepsilon(\tau)\, d\tau \\
&= \int_{-\infty}^{\infty} \left(\delta_{m,k} \delta_{n,l} \delta(t-\tau) \right) \varepsilon(\tau)\, d\tau \\
&= \varepsilon(t).
\end{aligned}$$

In the last step of this derivation, we note the importance of the inclusion of the Dirac-δ function, which is also absent in Fechner et al [109].

In Figure 3.2(a) we present a von Neumann TFR. The von Neumann grid was, $25 \times 25 = 625$ pixels, which is the closest square to 640 pixel SLM. The colour represents the relative amplitude of the signal. In Figure 3.2(b) the reconstructed spectral signal (red) along with the true signal (blue) is depicted. Notice that there are small errors in the reconstruction. Comparing this with the vertical axis of the von Neumann TFR, we see they are in good agreement.

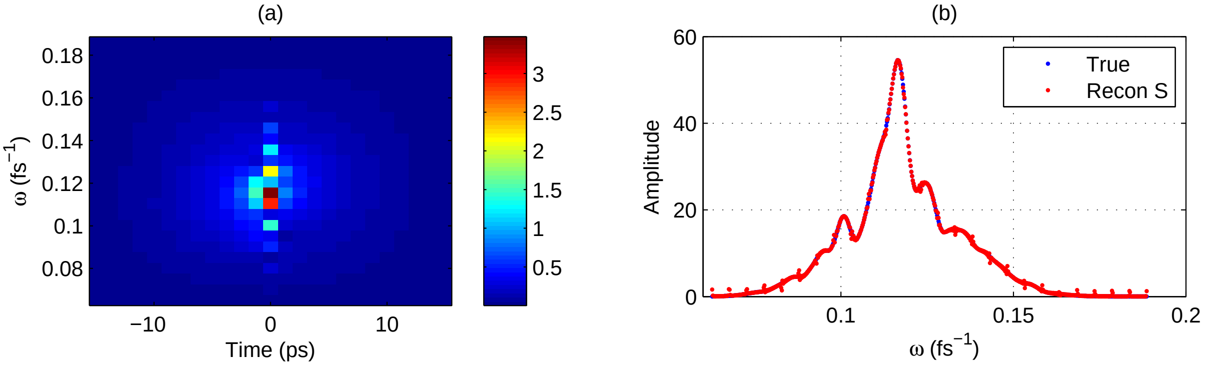

Figure 3.2.: (a) The von Neumann TFR (b) von Neumann spectral reconstruction of the electric field

In the next Chapter 4 an Article is presented giving an application of the von Neumann TFR to ultrashort laser pulse optimal control on an octahedral molecule and there various results are obtained and discussed.

4. Adaptive Quantum Coherent Control

Adaptive quantum coherent control of a multi-level molecular system in the von Neumann time-frequency domain

L R Botha, [1, 2] A M Smit, [1, 2] L E de Clercq, [3] R Madigoe[1, 2] and E R Rohwer[2]

1 *CSIR National Laser Centre, CSIR Campus, Pretoria, South Africa*
2 *Laser Research Institute, Department of Physics, Stellenbosch University, South Africa*
3 *Institute of Quantum Electronics, ETH Zürich, Zürich, Switzerland*
asmit1@csir. co. za

Abstract

A numerical model of the coherent interaction of a shaped femtosecond pulse with a multilevel quantum system was developed. This model was used with a learning algorithm to optimize the population in an arbitrarily chosen quantum level within the multi-level system in the von Neumann time-frequency representation. It was found that optimization in the von Neumann space outperformed optimization in the frequency domain. It was found that optimum solutions are robust with regards to variation in laser energy and frequency as well as to random variation in phase and amplitude of the pulse. The topology of the optimization space was investigated and the results are not in disagreement with published predictions.

Keywords: Coherent Quantum Control, Adaptive Feedback Control, Time-Frequency Representations, Ultrashort Laser Pulses, Spatial Light Modulator, Multi-Level

Molecules, von Neumann TFR, Anharmonic Rovibrational Levels, Genetic Algorithms

82. 53. Kp, 42. 55. -f, 31. 15. xv

4.1. Introduction

Adaptive Feedback Control (AFC) of quantum systems is a well-known technique with applications ranging from femtochemistry to quantum logic gates [110, 46, 111, 54, 112, 51]. The object of this study is to apply AFC to optimize the population of an arbitrarily chosen higher vibrational level in a specific vibrational mode of a molecule utilizing a joint time-frequency description of a femtosecond laser pulse. The time-frequency representation used is the von Neumann representation introduced in [94, 96]. AFC using the von Neumann basis has been reported in [113]. They compared the speed and efficiency of an adaptive coherent control process to reproduce given pulse shapes. It was found the AFC utilizing the von Neumann basis (VN method) outperformed AFC utilizing frequency domain shaping via a Spatial Light Modulator (SLM) (SLM method). The subject of our investigation is the excitation of a particular vibrational mode of a molecule in which anharmonicity causes a red shift in the resonant frequencies of the higher vibrational levels compared to the ground state. In the vibrational ladder climbing process a molecule is excited from the ground state to some higher vibrational state via various in-between vibrational states. In such a process the pulse should initially be resonant with the first vibrational state and then at a later stage, when the population has been transferred from the ground state to some higher vibrational level it should again be resonant with the transition frequency from that level to the next. It seems logical that such a pulse should have a specific time-frequency structure, similar to the pulses used in [113] and hence based on the results obtained in [113] it can be expected that the VN method would also outperforms the SLM method.

Selective optimization of an arbitrarily chosen higher vibrational level utilizing the SLM method was previously reported [114]. This study expands the previous work to include optimization in the time-frequency domain using the von Neumann basis. In this study AFC of the excitation of a molecule via a shaped femtosecond laser pulse was numerically simulated. The multilevel system used was a polyatomic molecule and a specific vibrational mode of the molecule. The objective was to show that an arbitrarily chosen upper vibrational level, in the ground electronic state of the molecule, could be preferentially populated. This could then, for example, allow mode selective chemistry by applying a second laser that interacts with the excited population but not with the ground state population or alternatively, the enhanced reactivity of the excited molecule could be utilized for selective chemistry.

The control of the vibrational excitation of molecules has been studied by various authors. Solving the time-dependent Schrödinger equation of the interaction of an HCN molecule with intense, ultrashort, chirped laser pulse was reported in [115]. It was shown that controlling the chirping rate and the area of a laser pulse allows selective vibrational excitation and dissociation of a particular bond of a molecule. Vibrational ladder climbing in NO utilizing ultrafast frequency chirped laser pulses has been reported in [116]. They demonstrated experimentally that the transfer of population up to vibrational state 3 of NO shows strong enhancement when the frequency chirp of the laser pulses follows the consecutive vibrational transitions [117]. It was shown that quantum gates based on molecular vibrational qubits can be implemented utilizing shaped femtosecond pulses and selectively exiting different vibrational modes [112, 117]. Energy deposition via vibrational ladder climbing in the ground electronic state and the ability to control a ground state unimolecular dissociation was demonstrated [118]. They chose the cleavage of CO from $\mathrm{Cr(CO)_6}$ and excited the molecule up to vibrational level $n = 7$ within a fs pulse. Control over the reaction by applying a linearly chirped pulse was demonstrated. It was found that there is a clear reactivity dependence on the chirp of the excitation pulse. The influence of the number of control parameters on the fidelity of obtaining certain logical quantum gates utilizing the vibrational levels of $\mathrm{SCCl_2}$ was investigated and it was found that fidelity of ~ 0.999 is possible [119]. In addition it was reported that these transformations show robustness with regards to errors in the phase and amplitudes of the shaping system. Therefore, selective excitation of specific vibrational modes of molecules is a well-studied field, however frequency chirping was the predominant mechanism employed in most studies. In this study the bandwidth of the laser pulse was significantly wider that the bandwidth required to excite all the different levels of the specific vibrational mode investigated. It was thus at the onset of the investigation not clear whether chirping the pulse would have the same effect as that reported previously.

4.2. Interaction of the laser pulse with the multilevel system

Here we briefly present our physical model of a laser's interaction with an octahedral molecule. This leads to the dynamical von Neumann equation in the interaction picture for the process. Assume that the laser light that interacts with the molecule is linearly polarized in the $\vec{e}$-direction, the field can then be written as,

$$E(t) = E_0 \varepsilon(t)\vec{e}. \tag{4.1}$$

With, E_0, the amplitude of the electric field and the time dependence of the field is given by, $\varepsilon(t)$. The total Hamiltonian is given by,

$$H = H_0 + H_I. \tag{4.2}$$

H_o, represents the molecule in its unperturbed state and, H_I, is the interaction Hamiltonian which is due to the molecule interacting with the laser light. For concreteness we choose to work with an octahedral spherical top molecule, XY_6. The molecule has $3N-6$ modes of vibration, but we restrict our analysis to the, ν_3, infrared active vibrational mode. Even so each excitation of this mode may contain several near-degenerate levels with a number of forbidden couplings as dictated by the molecular symmetries. As such this choice provides us with a non-trivial quantum system to work with. The level structure is indicated in Figure 4.1. The unperturbed Hamiltonian is diagonal with regards to the frequencies associated with each vibrational level. Thus is given by,

$$H_0 = \sum_j \omega_j \left|\psi_j\right\rangle \left\langle\psi_j\right| \tag{4.3}$$

where, ω_j, are the frequencies associated with the vibrational levels within the specific vibrational mode. In this study the energy levels of XY_6 for which the spectroscopy of the higher vibrational levels are available in the literature [49, 61] were used. The spectroscopy of the model included anharmonicities as well as anharmonic splitting of the levels, see Figure 4.1. In this study it was assumed that the onset of the vibrational quasi-continuum was at level 5, i.e., 5 vibrational quanta [49]. It was assumed that once the molecule was excited into the vibrational quasi-continuum its energy would be re-distributed via inter-vibrational relaxation to all the other vibrational modes according to equilibrium statistics and would no longer be available for selective excitation of a particular chosen level. The dipole approximation of the interaction Hamiltonian was used. The model considered only single photon transitions. The von Neumann equation was used to describe the dynamics of density matrix elements, of the different levels and can be written as,

$$\frac{d\rho}{dt} = \frac{-i}{\hbar}\left[H, \rho\right], \tag{4.4}$$

in the interaction picture this can be written as [114],

$$\frac{d\rho}{dt} = \frac{-i}{\hbar}\sum_{l=1}^{n}\left(\rho_{lb}e^{i\omega_{bl}t}I_{al} - \rho_{al}e^{i\omega_{bl}t}I_{lb}\right), \tag{4.5}$$

with,

$$\omega_{ij} = \omega_i - \omega_j, \tag{4.6}$$

and,

$$I_{ab} = \varepsilon(t) E_0 X_{ab}, \tag{4.7}$$

where, X_{ab}, is the transition dipole moment strength from level, a to b. The set of simultaneous differential equation given in Eq. (7.87), for the 16 levels shown in Figure 4.1, was solved numerically.

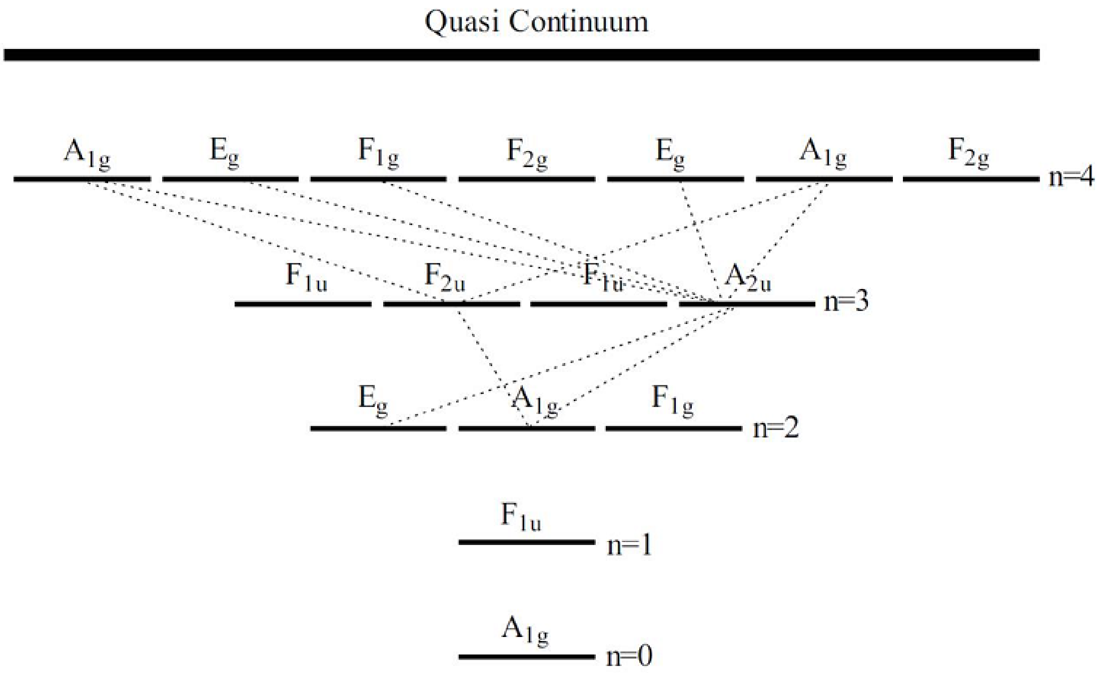

Figure 4.1.: The level structure used in this study. Shown in the figure are the principal quantum numbers, n, as well as the anharmonic splitting of these levels for which there is a small difference in transition frequency. The broken lines represent forbidden transitions.

4.3. Adaptive feedback control and the optimization process

The electric field used in the simulation was a shaped ultra-short laser pulse. A genetic algorithm based process was utilized to obtain an optimum pulse shape.

The objective function used in this study was the population in an arbitrarily chosen upper vibrational level of the molecule. The goal of the GA was to optimize the population in this specific vibrational level.

As mentioned previously, two different approaches were used to obtain an optimum population in a specific vibrational level, i.e., SLM and VN. In the SLM approach a Gaussian pulse in the time domain was Fourier transformed to the frequency domain. Shaping of this pulse via a 640 pixel SLM was simulated. Shaping was done via discrete amplitude and phase modulation in the frequency domain. This was done by applying a shaping mask to the SLM. The pulse was then transformed back to the time domain resulting in a pulse shaped in the time domain. The interaction of this shaped pulse with the vibrational energy levels was then calculated. The shaping mask was used by the GA to optimize the population in the chosen vibrational level. Therefore the structure of the system (genotype) consists of two strings of 640 different features (genes) that can take values from zero to 1 in the case of the amplitude and $-\pi$ to π in the case of the phase, thus a total of 1280 genes were used by the GA. A Matlab© genetic algorithm was used to optimize the pulse shape.

In the second approach, the so-called VN process, modulation is done in the von Neumann time-frequency domain i.e. applying a mask to the $Q_{m,n}$ values, defined in Eq. (3.100) or Eq. (3.101). This was done via modulating the amplitude and phase of the von Neumann coefficients. In this particular case the von Neumann space chosen was 25x25 pixels as mentioned previously, giving 625 numbers. The gene values at these points varied between 0 and 1 for the amplitude and $-\pi$ to π for the phase. The same algorithm used in the SLM method was used to optimize the population in a specific level. An experimental implementation of this process would be to apply the mask in the von Neumann space, transforming back to the frequency domain utilizing Eq. (3.103). The mask required in the frequency domain to produce this from the input Gaussian pulse can then be calculated and applied to a 4-f type shaper.

4.4. Results

4.4.1. Transform limited pulse

A transform limited 100fs pulse was used as a benchmark for comparing the effect of shaped femtosecond pulses on the system. A fluence of 700mJ/cm^2 was used in all cases, and the energy of the shaped pulse was normalized with respect to the total energy in the transform limited case. This ensured that results obtained

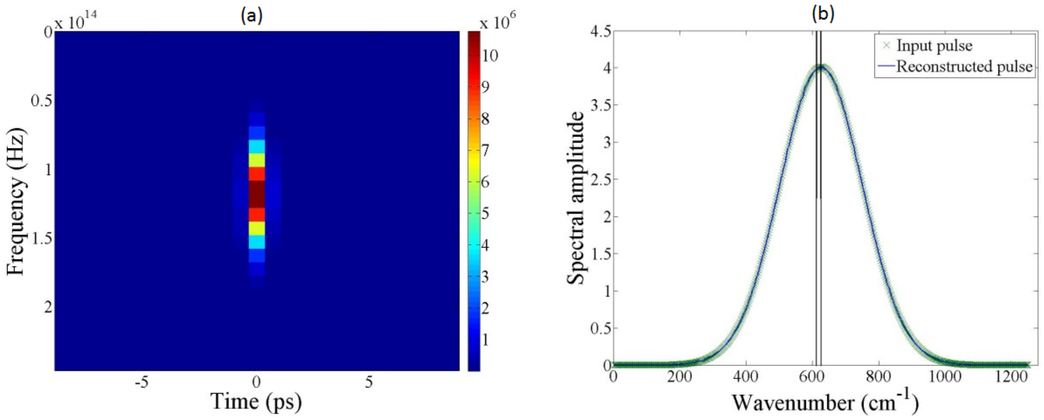

Figure 4.2.: (a) The von Neumann transform of a 100fs Gaussian pulse (25 × 25) pixels. (b) Original Fourier transform (solid blue line) superimposed on the frequency domain pulse reconstructed from the von Neumann representation. The two vertical lines in (b) represent the bandwidth required to excite all the transitions in Figure 4.1.

with pulses with equivalent energy were compared. It was assumed that the carrier frequency is that of the $n = 0$ to $n = 1$ transition in Figure 4.1 and it was assumed that at the start of the pulse 100% of the population was in the vibrational ground state, the $n = 0$ state. The levels shown in Figure 4.3 are those with the same principal quantum number, therefore, the sum of the population in the various anharmonic splittings at a particular principal quantum number after interacting with the transform limited pulse. As can be seen the percentage of population after the interaction with the standard Gaussian laser pulse, in level 2, i.e., vibrational state, $n = 2$, is 20% of the initial population. Now we choose to optimize level 2 with our various techniques.

4.4.2. SLM Results

In the SLM method pulse shaping was obtained by modulating the phase and amplitude in the frequency domain. The input pulse was the same 100fs transform limited pulse as in the previous section. A 640 pixel SLM capable of phase and amplitude modulation was assumed. Therefore, the optimization space consisted of 1280 (phase and amplitude) parameters that could be individually varied between 0 and 1 for amplitude and $-\pi$ to π for the phase. It was decided to optimize the population in the arbitrary chosen$n = 2$ vibrational level. The shaped pulses were used to numerically calculate the population in a specific level and this population was optimized using a Matlab© genetic algorithm. Typical results obtained are

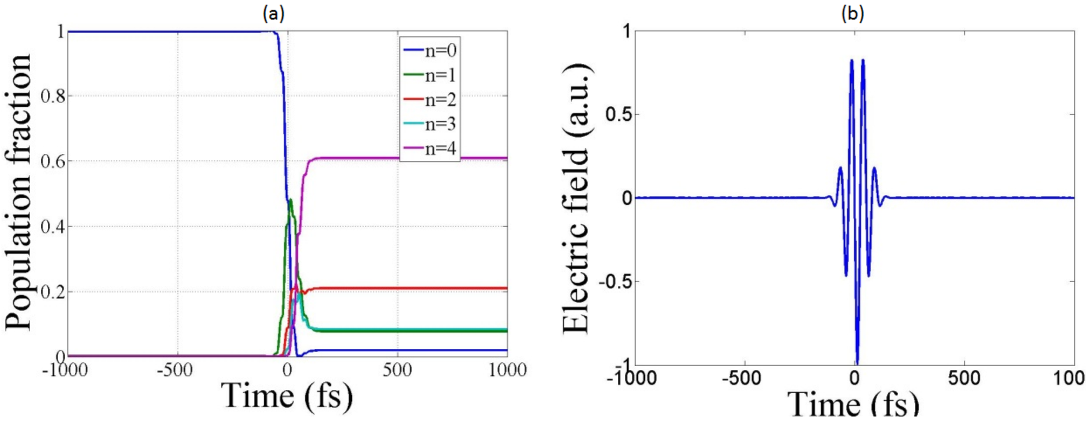

Figure 4.3.: Interaction of a transform limited pulse with the polyatomic molecule. (a) Population dynamics, as can be seen approximately 20% of the population are in vibrational level $n = 2$ after the pulse has interacted with the molecule. (b) Transform limited electric field with a FWHM of 100fs.

shown in Figure 4.4. Optimum population values obtained for the$n = 2$ vibrational level varied between 70% and 80%. Thus significant selectivity compared to the 20% obtained by the transform limited pulse. It was also noted that the optimum pulses showed limited structure in the time-frequency domain as can be seen in Figure 4.4(a, c).

4.4.3. von Neumann Results

Shaping using the VN method was done by modulating the von Neumann amplitude and phase in the von Neumann time-frequency domain. Again a 100fs transform limited pulse was used as the input pulse. A 25×25 von Neumann grid was used since 625 is the closest square to 640 and we wanted to compare the results to the SLM method utilizing 640 pixels. In addition, the parameter space was limited to only those von Neumann coefficients in the time-frequency space that had a non-zero von Neumann amplitude, similar to [113]. This resulted in a reduced optimization space with approximately 75 points, therefore, the input to the genetic algorithm was 75 von Neumann coefficients. Thus a total of 150 (phase and amplitude) parameters compared to the 1280 of the SLM case. The modulated pulse in the von Neumann space was then transformed to the frequency domain using Eq. (3.103) and then transformed to the time domain via a Fourier transform. A typical optimization result is shown in Figure 4.5. The optimum values obtained using the VN method varied between 77% and 99%. This is significantly higher than that obtained with the SLM method.

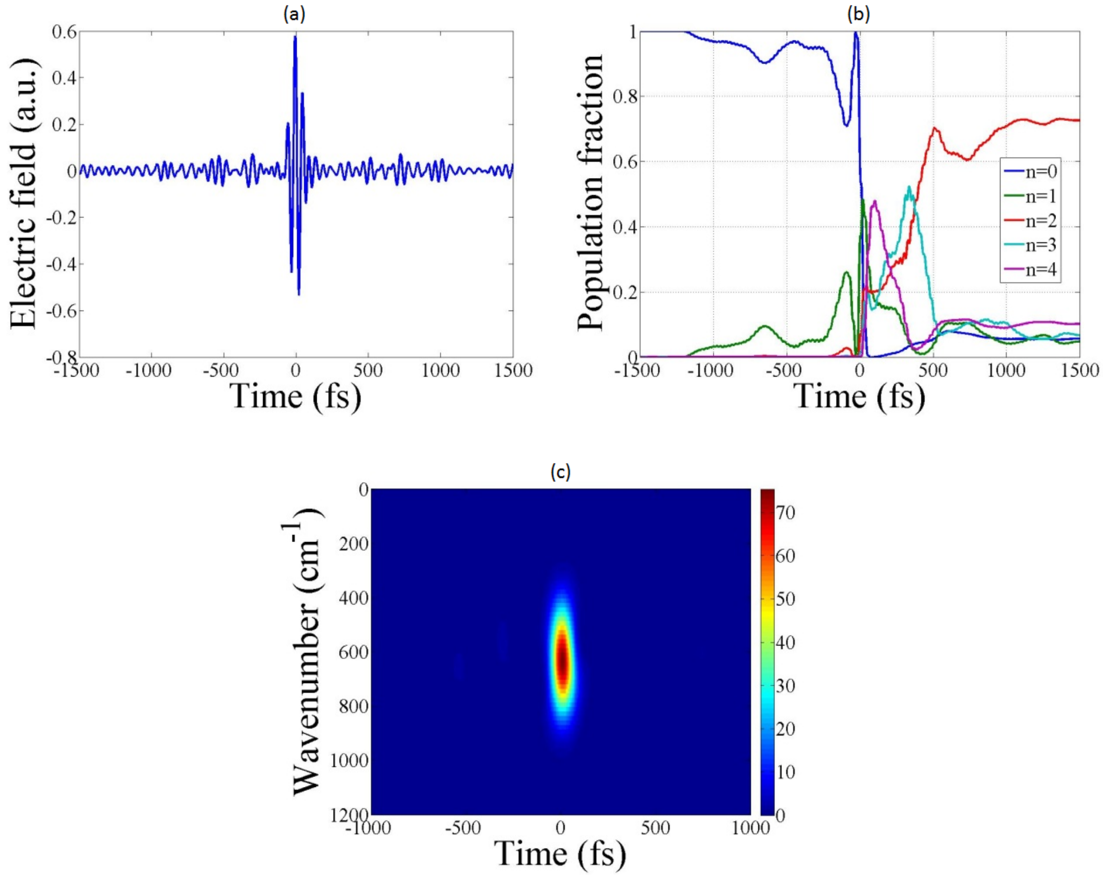

Figure 4.4.: Simulated AFC utilizing frequency domain shaping via an SLM. (a) Optimum time pulse obtained via a GA optimization process. (b) Population dynamics caused by the time pulse in (a). (c) Husimi plot of the pulse.

4.4.4. Comparison of the two methods

Three typical optimization results obtained with the SLM and VN methods are shown in Figure 4.6. As can be seen optimizing in the von Neumann space produced significantly higher population fractions in the selected vibrational level than that obtained using the SLM method. In addition, in most instances, the von Neumann method achieved relatively high population fraction very soon. This would have a great advantage for experiments where individual runs can tedious. In our opinion, the reason for the improved performance of the VN method is the fact that the "control knobs" in the von Neumann time-frequency domain affects the electric field in a tightly confined area of phase space and even more so if a reduced space is used where only the non-negative frequency values are considered. Conversely, to achieve control in a specific phase-space using shaping in the frequency domain

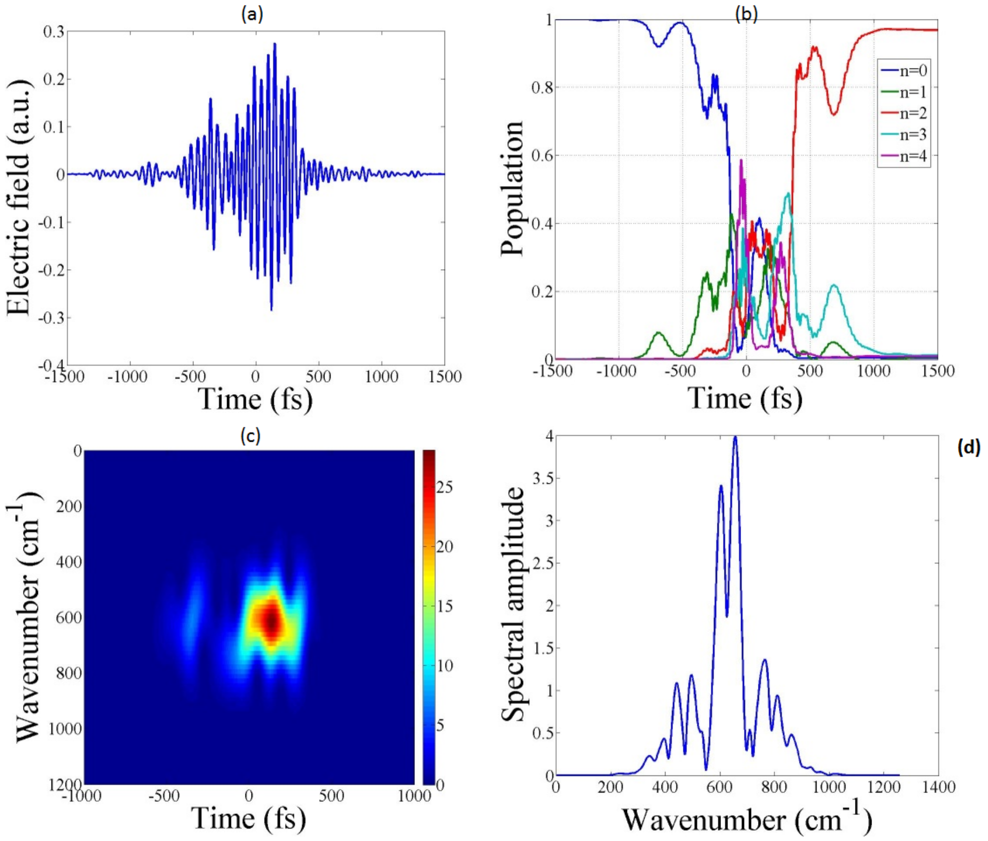

Figure 4.5.: Simulated AFC the von Neumann time/frequency representation. (a) Optimum pulse obtained via a GA optimization process. (b) Population dynamics caused by this pulse. (c) Husimi plot of the optimum pulse (d) Fourier transform of the optimum pulse.

only would require the simultaneous changing of many "control knobs". This also explains why, in the VN method, the optimization graph displays "jumps" while in the SLM method the improvement is very gradual. Since the two representations, i.e. Fourier and von Neumann contain the same information, it can be expected that the SLM method would eventually approach the values obtained using the VN method but that the number of generations required to achieve this will be significantly higher. Another noteworthy difference between the two methods can be seen if the Husimi plots of the optimum pulses obtained by both methods are investigated. In all instances investigated the VN method produced a much richer time-frequency structure than that obtained using the SLM method after the 100 generations. The Husimi graphs shown in Figure 4.4 and Figure 4.5 are typical of the results obtained for the SLM and VN methods respectively.

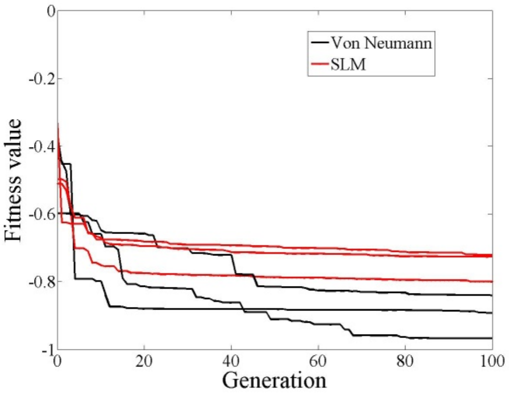

Figure 4.6.: Fitness values obtained using the two processes described in the text. The von Neumann approach outperformed the SLM method significantly.

4.4.5. Robustness of the von Neumann solution

Robustness of the optimum solution is important for the eventual experimental implementation of the process. If small changes in the shaped pulses produced large changes in the expected optimum values then the process will have only limited practical usefulness. Therefore, various tests of the robustness of the solutions were done. The robustness of the solution was investigated in the following manner: (i) The carrier frequency was varied but the shape was kept constant, (ii) the shape was kept constant but the peak fluence of the pulse was varied and (iii) random phase and amplitude values were added to the Fourier transform of the optimum pulse. In all three cases the influence of the variation of the parameters on the calculated maximum population values was determined. The optimum pulse used in these calculations produced a population of approximately 83% in the $n = 2$ vibrational level.

The impact of varying the peak fluence of the laser pulse on the calculated population in vibrational level 2 is shown in Figure 4.7. As can be seen the population is relatively insensitive to a change in the peak fluence of the laser pulse. A change of 10% in the laser fluence produces a maximum population level of approximately 80% compared to the best value of 83%. The influence of changing the carrier frequency on the expected maximum population is shown in Figure 4.8. Changing the carrier frequency is equivalent to changing the frequency of the excitation laser. Again, the maximum population obtained is remarkably insensitive to a change in the laser carrier frequency. A change in carrier frequency of 10cm^{-1}produces a reduction in the expected maximum population value of less than 10%. Due to the fact that every experiment will have some noise the influence of random amplitude and phase noise on the expected maximum value was investigated. Random amplitude and phase noise was added to the Fourier transform of the optimum pulse and this new pulse was then used to calculate the maximum population value in a specific vibrational level. Two different scenarios were investigated: i.e., random noise was varied from [-10%; 10%] and [-20%, 20%] both in amplitude and phase. The first produced negligible effects on the maximum population, the second reduced the maximum population from 83% to 81%. It therefore seems that this process is remarkably robust. A similar robustness to changes in amplitude and phase for the SLM method was reported in [114, 115] and [120] predicted that an optimally controlled quantum system will have a degree of robustness around full control solutions.

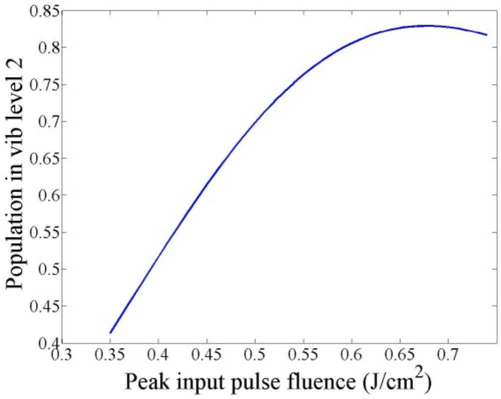

Figure 4.7.: Influence of peak input pulse fluence on the calculated maximum population in vibrational level 2.

4.4.6. Topology of the optimization space

The topology of optimally controlled quantum mechanical transition landscapes was investigated in [120], the findings were (a) the transition probability extrema landscape consists of values corresponding to no control or full control, (b) approaching full control involves climbing a gentle slope with no false traps in the control space and (c) there is an inherent degree of robustness around any full control solution. In a later paper [121] it was shown that some systems can show trapping behavior thus contradicting the findings of [120]. In this study the control variables is a high dimensional space consisting of the various von Neumann mask values, separated into phase and amplitude, in our case a 150 dimensional space. In order to investigate whether the optimum points obtained by various different runs were also different points in the optimization space an Euclidean

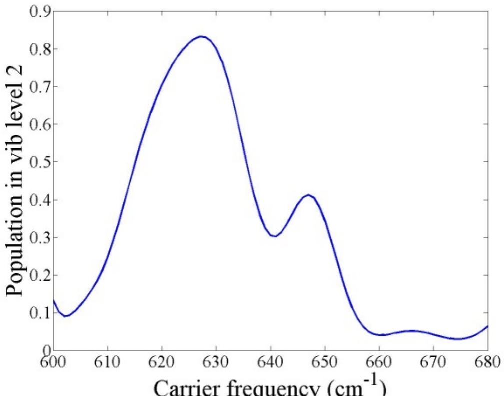

Figure 4.8.: Maximum population in vibrational level 2 as a function of varying carrier frequency.

norm was applied to the various von Neumann parameters of which the mask is comprised. The norm was taken with respect to the origin (i.e., no mask) and also between the different optimal solutions that were obtained. Results obtained for 14 different runs of the optimization algorithm are shown in table 1. The optimum values obtained by the different runs varied between 99. 5% and 77. 4%. The fitness values are shown in the second column. The third column gives the value of the norm of the various solutions with respect to zero. As can be seen the norms of the different optima are all approximately the same, therefore, suggesting that they either all lie on a hyperdimensional spherical surface (n-sphere) centered at the origin or that they are all the same point. However, the other columns gives the norm (or distance in hyperdimensional space) between the first solution and others. If the points were the same then this norm would have been zero. As can be seen this is not zero, but again an approximately constant value. These values are very close to each other also suggesting that they are all an equal “distance “ from the specific optimum point used as a reference. Similar results were obtained for the distance of the other solutions, calculated examples for the distance between the 4th and the other and the 10th and the other, are shown in the table. The solutions seems to be a constant distance from zero and all the solutions seems to be approximately a constant distance from each other thus forming a hyperdimensional spherical surface in all cases investigated.

In an n-dimensional Hilbert space, $\mathcal{H}^n$, the unitary time-evolution operator (propagator), $U(t_1, t_0)$, of a state vector, $\psi(t)$, in any of the quantum pictures is given by [6],

$$\psi(t_1) = U(t_1, t_0)\psi(t_0) \quad \text{with} \quad U(t_1, t_0)U^\dagger(t_1, t_0) = \mathbf{1}, \tag{4.8}$$

where the unitary time-evolution operator, $U(t_1, t_0)$, satisfies the original Schrödinger-

Hamiltonian equation associated with the interaction picture,

$$i\hbar\frac{d}{dt}U(t,t_0) = H_I(t)U(t,t_0) \quad \text{with} \quad U(t_0,t_0) = \mathbf{1}. \tag{4.9}$$

In essence the unitary condition restricts the state vector trajectory to some hyperspherical surface in the $\mathcal{H}^n$ space. Now placing a SLM mask, $M(\omega)$, in the spectral domain of a laser pulse, $\tilde{\varepsilon}(\omega)$, can be written as,

$$\varepsilon_M(t) = \mathcal{F}^{-1}\left\{M(\omega)\tilde{\varepsilon}(\omega)\right\}. \tag{4.10}$$

The interaction Hamiltonian of our system is given by,

$$H_I(t) = X(t)\Re\left[\varepsilon_M(t)\right] = X(t)\Re\left[\mathcal{F}^{-1}\left\{M(\omega)\tilde{\varepsilon}(\omega)\right\}\right]. \tag{4.11}$$

where $X(t)$ is the dipole interaction Hamiltonian (in the interaction picture) of the molecule and $\Re$ denotes the real part. Since the input laser $\tilde{\varepsilon}(\omega)$ is a non-varying function and the inverse Fourier operator $\mathcal{F}^{-1}$ is a linear operator, we conclude that for infinitesimal time maps the unitary map

$$U(t+\delta t) \simeq e^{-\frac{i}{\hbar}\int_t^{t+\delta t} X(\tau)\Re\left[\mathcal{F}_\tau^{-1}\left\{M(\omega)\tilde{\varepsilon}(\omega)\right\}\right]d\tau} \tag{4.12}$$

is approximately a linear map of the mask function $M(\omega)$ and therefore due to successive application of infinitesimal unitary operators, $U(t_{n+1},t_n)$, will be approximately a linear map of the mask function. Therefore, since there is a linear relation between, $M(\omega)$ and $U(t_1,t_0)$, we suspect similar behavior in the domain, $M(\omega)$, as that implied by the restriction of the unitary transformation, i.e., some confinement on a hyperspherical surface in the vicinity of the optimal solution. The above is of course by no means a formal mathematical secure footing and must only be considered as heuristic explanation of some of our observations.

It is clear that there are many different optimal points as can be seen by investigating the norms and also visually inspecting the shapes of the pulses. The maximum fitness values at all the points were quite similar and were all obtained after only 100 generations via a GA. If more generations, e.g., 200 are used the optimum values reached are closer to each other and at higher generations the approach to the optimal value is gradual, as can be seen in Figure 4.7, as is also predicted by [120]. The solutions are all robust as was also predicted by [120]. In our particular problem gradient based methods are extremely slow, however, a limited number of runs were performed utilizing gradient based optimization techniques. Gradient based techniques are generally known to be easily trapped in a local maxima. The number of runs was not sufficient to give a confident indication of whether local traps in the optimization landscape do exist. However, no traps were found during any of our runs.

Table 4.1.: The fitness values (population in the chosen vibrational level) of different controls are shown in the second column. The norm of the masks of the different optimum solutions with respect to the origin(distance to origin) is shown in the first column and the distance of the other points with respect to a specific solution point are shown in the other columns. The norm was defined as $\|M_i\| = \sqrt{\sum_j^n M_{ij}^2}$.

i	Fitness Value (%)	$\|M_i\|$	$\|M_1 - M_{1i}\|$	$\|M_2 - M_i\|$	$\|M_3 - M_i\|$	$\|M_4 - M_i\|$
M_1	92. 4	8. 0	0	5. 0	5. 5	4. 6
M_2	96. 3	7. 6	5. 0	0	4. 9	4. 9
M_3	80. 7	7. 2	4. 9	4. 8	4. 7	4. 5
M_4	90. 3	7. 5	5. 5	4. 9	0	5. 0
M_5	99. 5	8. 8	4. 9	5. 5	5. 3	5. 3
M_6	83. 0	7. 3	5. 2	4. 5	4. 5	4. 7
M_7	88. 7	8. 2	4. 5	4. 6	4. 7	4. 5
M_8	96. 1	8. 5	5. 4	5. 4	5. 2	5. 1
M_9	89. 7	8. 4	4. 9	4. 8	5. 1	5. 0
M_{10}	95. 1	8. 1	4. 6	4. 8	5. 0	0
M_{11}	77. 4	7. 3	5. 3	5. 4	4. 9	5. 3
M_{12}	80. 3	7. 5	4. 9	5. 2	4. 7	4. 8
M_{13}	98. 5	8. 6	5. 1	5. 2	5. 0	4. 8
M_{14}	94. 6	9. 2	4. 9	5. 1	5. 6	4. 8
Average	90. 2	8. 0	5. 0	4. 7	4. 7	4. 6

4.4.7. Excitation mechanism

A chirped femtosecond laser was used to excite the vibrational levels of $Cr(CO)_6$ up to vibrational level $n > 7$ in [118]. It was found that the excitation mechanism was population transfer up the vibrational ladder caused by a series of chirped adiabatic passages. In their case the anharmonic vibrational ladder consists of energies, thus the anharmonic shift for the transition from $n = 7$ to $n = 8$ is 195cm^{-1} which is significant compared to their laser bandwidth of 150cm^{-1}. In their case the maximum anharmonic shift is larger than their laser bandwidth. In our case the bandwidth of the 100 fs pulse (FWHM) is 146cm^{-1} and the maximum anharmonic shift, i.e., $n = 1$ to 2 compared to $n = 3$ to 4 is less than 15cm^{-1}, and therefore, negligible compared to the pulse bandwidth. This is graphically illustrated in Figure 4.2(b) where the total bandwidth required to excite all the transitions shown in Figure 4.1 lie between the two vertical lines. It can thus be expected that chirping of the pulse would have a negligible effect in our case because even if the pulse is chirped, all the levels will still be resonant with some frequency component of the laser. The influence of chirp on the excitation was investigated by including chirp in the interaction model. The chirp of the laser pulse was varied over a broad range and it was found that chirp had a negligible influence on the excitation probabilities of the various levels. In our case the optimum pulses obtained did not have any noticeable chirp or a specific time structure and we believed that neither an adiabatic process nor pulse sequences shifted in frequency and time were responsible for the high level of selectivity of the process. The robustness of the solutions also seems to rule out π-pulse dependent processes. One of the motivations for utilizing the von Neumann time/frequency representation was because it was felt that due to the fact that it could be expected that the excitation of the various higher levels of the vibrational ladder will be time and frequency dependent. This means that a time-frequency based optimization process would be well suited to this process and might elucidate the excitation mechanism. However, even though the time-frequency based process outperformed the frequency only process it is difficult to discern the excitation mechanism. Optimum pulses obtained are vastly different making it very difficult to understand the underlying mechanism, for example, Figure 4.9 shows the Husimi plots of two optimum pulses. The pulse shown in Figure 4.9(a) produced a population of 85% and that shown in Figure 4.9(b) 97%. Both were obtained after utilizing the same laser parameters and after 100 generations of a GA based optimization process. The two pulses are clearly different with some time structure. Both pulses were stretched from 100fs to approximately 1ps. These are typical of the results obtained i.e. stretched to 1ps with some time structure. Multiple pass interference is a possible mechanism.

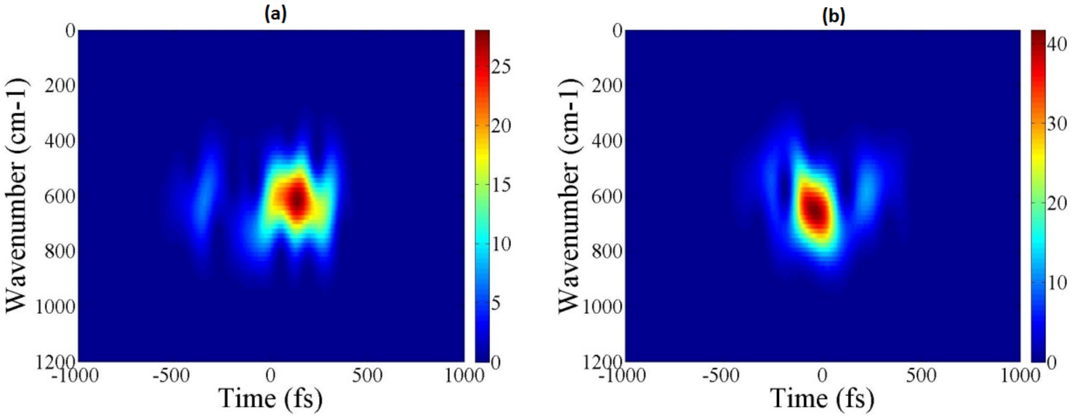

Figure 4.9.: Husimi plots of two optimum pulses. Selective excitation of 97% (a) and 85% (b) were obtained for the right and left pulses respectively.

4.5. Conclusion

A simulated AFC based on the von Neumann time-frequency representation for the selective excitation of an arbitrary vibrational level in a polyatomic molecule was developed. The results obtained were compared to that obtained via a previously developed process based on shaping only in the frequency domain the so-called SLM method.

The VN time-frequency method outperformed the SLM based one by a significant margin. The parameters space in the von Neumann method is much smaller than that of an equivalent SLM based method. This should be very attractive from an experimental point of view.

It was found that the optimum solution obtained using the von Neumann method, similar to what was found for the SLM method, is a very robust solution and this should also be favorable from an experimental implementation point of view.

Utilizing the von Neumann method selective excitation of a specific vibrational level of up to 97% was achieved. However the excitation mechanism is not clear but multiple path interference is a possibility.

The topology of the optimization space was investigated and even though the results are not conclusive it was found that the results are not in disagreement with the predictions made in [120], i.e., (a) the transition probability extrema landscape consists of values corresponding to no control or full control, (b) approaching full control involves climbing a gentle slope with no false traps in the control space and (c) an inherent degree of robustness around any full control solution.

5. The Generalized FHG TFR

5.1. Introduction

This Chapter presents the new generalized Fourier-Hermite-Gauss (FHG) TFR in its entirety. The methods and **analytical** derivations can all be found here. Whereas the von Neumann TFR only uses Fourier-Gauss basis functions, which are the zeroth order Fourier-Hermite-Gauss polynomials, we generalize the method on the same von Neumann representation lattice to a discrete FHG basis functions. The importance of the Fourier transform invariance of these functions is once again the crux to the success of the representation.

Considering the value of invariant Fourier transform functions, we extend the problem to the general Fourier transform eigenvalue problem in Section 5.2. The eigenvalue problem is solved there, in some detail, and the resulting general Fourier Transform eigenfunctions are the well-known Hermite-Gauss polynomials. In the derivation a few of the properties of the Hermite functions are utilized. In Subsection 5.2.1 some properties of Hermite polynomials are summarized for easy access and convenience.

In Subsection 5.3.1 the von Neumann TFR is generalized and extended to Fourier-Hermite-Gauss polynomials. We explore the possibilities of expanding a signal with this additional freedom of the generalized Hermite polynomials. Being orthogonal polynomials we note that it is possible to expand a signal over the Hermite-Gauss polynomials, but that the spectral and temporal shifting, $e^{i\omega_n t}$ and $e^{-it_m(\omega-\omega_n)}$, the Fourier component of the expansion, have essentially no role. The coefficients of this expansion are written vectorially for easy representation. We do show that they have the desired Fourier transform independence.

Perelemov [122] proved that the von Neumann lattice representation is complete but not over complete. Obviously, this new generalization is overcomplete, but can be made complete by the the theory of frames [123]. The theory of frames is then exploited to address the ill-conditioning of the von Neumann overlap matrix. By the correct choice of the basis functions of the FHG TFR an overlap matrix can be obtained with much better conditioning. The immense power of the Hermite polynomial expansion is exploited to greatly benefit the calculation of the various

HG polynomial necessary occurring in the new representation. This is shown in Subsection 5.3.2. Temporal and spectral HG polynomials are then defined in a new manner with the aid of the, so-called, lower and upper triangular Pascal matrices. Portraits of Gauss, Hermite and Pascal are shown in Figure 5.1. Fourier is not included because he has a whole, Appendix A, dedicated to him.

Thereafter, a summary of the analytical generalized FHG representation is given in Section 5.4 in which the FHG TFR is presented in generalized format for the first time. The signal reconstruction is also shown for the generalized FHG TFR. The FHG overlap matrix is then derived in detail for the temporal FHG basis. It is shown that the spectral overlap matrix does not directly equal the temporal overlap matrix. The verification and the similarity between the two overlap matrices is then derived, with some rather novel mathematics, and is unique to this thesis.

In the generalized FHG TFR use is made of a coefficient matrix, which is specifically left for later determination. This is then the strength of the technique. In Section 5.5 a very brief introduction of the theory of frames to show how this coefficient matrix can be chosen. Finally in Section 5.6, some applications to quantum control theory is given.

Figure 5.1.: Carl Friedrich Gauss, Charles Hermite, Blaise Pascal

5.2. The Fourier Transform Eigenvalue Problem

The Fourier transform is a linear operator on the square integral functions [124, 125, 126, 127]. Being a linear operator we can conceive an eigenvalue problem for the Fourier transform operator. Then a general invariant function under the Fourier transform will be an eigenfunction of the linear operator. This naturally invites the question: ***"What is the most general function that is invariant under the Fourier transform?"***, i.e.,

$$\mathcal{F}\left\{f(t)\right\} = \lambda f(\omega), \tag{5.1}$$

where, $\lambda \in \mathbb{C}$. This is essentially an operator eigenvalue problem, because the Fourier transform is a linear functional operator. In Appendix A, the Fourier transforms, $f(t) \overset{\mathcal{F}}{\Longleftrightarrow} F(\omega)$, of derivatives, Eq. (A.26) and Eq. (A.27), are given by,

$$\mathcal{F}\{\frac{d^n}{dt^n}f(t)\} = (i\omega)^n F(\omega), \qquad \mathcal{F}^{-1}\{\frac{d^n}{d\omega^n}F(\omega)\} = (-it)^n f(t). \tag{5.2}$$

The similarity of these Fourier properties leads us firstly to the preliminary differential equation,

$$\frac{d^2 g\left(t\right)}{dt^2} - t^2 g(t) = 0 = \frac{d^2 G\left(\omega\right)}{d\omega^2} - \omega^2 G\left(\omega\right), \tag{5.3}$$

the solution of which is a Gaussian function, $g(t) = \frac{1}{\sqrt{2\pi}} e^{-\frac{t^2}{2}}$, which we know is Fourier transform invariant, Eq. (3.33) and Eq. (3.34). Since we are in search of the most general function that is invariant under the Fourier transform, we generalize this differential equation, Eq. (5.3). We note that including the function, $g\left(t\right) = f(t)$, with an integer constant, i.e.,

$$\boxed{\frac{d^2 f\left(t\right)}{dt^2} - t^2 f(t) = -\left(2n+1\right) f\left(t\right) \quad n \in \mathbb{Z}^+} \tag{5.4}$$

will still be Fourier transform invariant, which we now prove. Fourier transforming this differential equation, Eq. (5.4), results in,

$$\boxed{\frac{d^2 F\left(\omega\right)}{d\omega^2} - \omega^2 F\left(\omega\right) = -\left(2n+1\right) F\left(\omega\right) \quad n \in \mathbb{Z}^+} \tag{5.5}$$

But this is the exactly the same differential equation as Eq. (5.4). This shows that the differential equation, Eq. (5.4) and Eq. (5.5), remains invariant under the Fourier transform. I suppose that the mathematicians arrived at the above differential equation by trial and error. Now consider the trial solution, in which we include the original Gaussian function, $e^{-\frac{t^2}{2}}$,

$$x\left(t\right) = e^{-\frac{t^2}{2}} H_n\left(t\right), \tag{5.6}$$

for some unknown function, $H_n(t)$, to be evaluated. Inserting this into the time differential equation, Eq. (5.4), results in the following differential equation,

$$\frac{d}{dt}\left[e^{-\frac{t^2}{2}} H_n\left(t\right)\right] \quad = \quad e^{-\frac{t^2}{2}} \frac{dH_n}{dt} - t e^{-\frac{t^2}{2}} H_n,$$

$$\frac{d^2}{dt^2}\left[e^{-\frac{t^2}{2}}H_n(t)\right] = e^{-\frac{t^2}{2}}\frac{d^2H_n}{dt^2} - 2te^{-\frac{t^2}{2}}\frac{dH_n}{dt} + \left(t^2-1\right)e^{-\frac{t^2}{2}}H_n, \tag{5.7}$$

$$e^{-\frac{t^2}{2}}\frac{d^2H_n}{dt^2} - 2te^{-\frac{t^2}{2}}\frac{dH_n}{dt} + \left(t^2-1\right)e^{-\frac{t^2}{2}}H_n - t^2e^{-\frac{t^2}{2}}H_n = -\left(2n+1\right)e^{-\frac{t^2}{2}}H_n. \tag{5.8}$$

Canceling the Gaussian function, $e^{-\frac{t^2}{2}}$, in Eq. (5.8), we find our trial unknown function, from Eq. (5.6), satisfies the following differential equation,

$$\boxed{\frac{d^2H_n}{dt^2} - 2t\frac{dH_n}{dt} + 2nH_n = 0} \tag{5.9}$$

To solve the differential equation we use the common series expansion technique of Frobenius, M. Boas [128],

$$H_n(t) = \sum_{k=0}^{n} a_k t^k. \tag{5.10}$$

Inserting this in Eq. (5.9) the differential equation results in the following recursion relationship for the polynomial coefficients, a_k,

$$\frac{a_k}{a_{k-2}} = \frac{2(k-n-2)}{k(k-1)}. \tag{5.11}$$

This is exactly the recursion relationship that satisfies the *Hermite polynomials*, i.e., $H_n(t)$, is a Hermite polynomial (See Subsection 5.2.1 for a summary of their properties).

Define the unnormalized Hermite-Gauss polynomials by,

$$\boxed{g_n(t,1) = \mathcal{N}(t,1)H_n(t)} \tag{5.12}$$

where, $H_n(t)$, is a Hermite polynomial. Then our Fourier eigenvalue problem is given by,

$$\boxed{\boldsymbol{F}\left\{g_n(t,1)\right\} = \frac{1}{\sqrt{2\pi}}\int_{-\infty}^{\infty} g_n(t,1)e^{-i\omega t}\,\mathrm{d}t = \lambda_n g_n(\omega,1)} \tag{5.13}$$

with eigenvalues, $\lambda_n = (-i)^n$. An orthonormal basis for, $L^2(\mathbb{R})$, (quadratically Lebesgue integrable functions) is given by,

$$\boxed{\psi_n(x) = 2^{-\frac{n}{2}}(n!)^{-\frac{1}{2}}\pi^{-\frac{1}{4}}e^{-\frac{x^2}{2}}H_n(x)} \tag{5.14}$$

This conforms to the so-called physicist's choice, with the *Rodrigues' generating function*, for the Hermite polynomials given by (cf. [129, 130] and Eq. (5.28)),

$$e^{2tx-t^2} = \sum_{n=0}^{\infty} H_n(x)\frac{t^n}{n!}, \tag{5.15}$$

or

$$H_n(x) = \left[\frac{d^n}{dt^n}e^{2tx-t^2}\right]_{t=0} = (-1)^n e^{x^2}\frac{d^n}{dx^n}e^{-x^2}. \tag{5.16}$$

Now it is easy to show that,

$$\frac{dH_n}{dx} = 2xH_n - H_{n+1}, \tag{5.17}$$

$$\frac{d^2H_n}{dx^2} = 2H_n + 4x^2H_n - 4xH_{n+1} + H_{n+2}. \tag{5.18}$$

Inserting this into the differential equation, Eq. (5.9), gives as the following recursion relationship (cf. Eq. (5.33)),

$$\boxed{H_{n+1} = 2xH_n - 2nH_{n-1}} \tag{5.19}$$

Now insert this into, $\frac{dH_n}{dx}$, Eq. (5.17), and we obtain (cf. Eq. (5.31)),

$$\frac{dH_n}{dx} = 2nH_{n-1}. \tag{5.20}$$

This last relationship shows that the Hermite polynomials constitute an *Appell sequence*. Multiple application of the formula, Eq. (5.20), gives us,

$$\frac{d^kH_n}{dx^k} = \frac{2^k n!}{(n-k)!}H_{n-k}. \tag{5.21}$$

Under the frequency convention, Eq. (A.5) and Eq. (A.6), (as opposed to the unitary transform for the angular frequency) for the Fourier transform, i.e.,

$$\boldsymbol{F}\{f(t)\} = \int_{-\infty}^{\infty} f(t)e^{-2\pi i\nu t}\,\mathrm{d}t = F(\nu), \tag{5.22}$$

and

$$\boldsymbol{F}^{-1}\{F(\nu)\} = \int_{-\infty}^{\infty} F(\nu)e^{2\pi i\nu t}\,\mathrm{d}\nu = f(t), \tag{5.23}$$

we have that the following *eigenvalue problem,*

$$\boxed{\boldsymbol{\mathcal{F}}\left\{\psi_n(t)\right\} = (-i)^n \psi_n(\nu)} \tag{5.24}$$

The Hermite polynomials form a complete orthonormal system of eigenfunctions for the Fourier transform on, $L^2(\mathbb{R})$. The *general Fourier eigenfunction* is thus given by,

$$\boxed{\psi_n(x) = 2^{-\frac{n}{2}} \left(n!\right)^{-\frac{1}{2}} \pi^{-\frac{1}{4}} e^{-\frac{x^2}{2}} H_n(x)} \tag{5.25}$$

However, this choice of eigenfunctions is not unique. The eigenvalue problem for the Fourier transform only has four distinct eigenvalues (± 1 and $\pm i$). Any linear combination of eigenfunctions with the same eigenvalue gives another eigenfunction.

The eigenvalues of the Discrete Fourier Transform (DFT) matrix are simple and well-known. The eigenvectors, however, are complicated, not unique, and are the subject of ongoing research.

5.2.1. Some properties of the Hermite polynomials

Although we did derive some of the properties of Hermite polynomials in the previous Section 5.2, the remainder we merely list for easy reference. These properties are derived in various books [130, 129].

5.2.1.1. Differential equation

$$\frac{d^2 H_n}{dx^2} - 2x\frac{dH_n}{dx} + 2nH_n = 0 \tag{5.26}$$

5.2.1.2. Rodrigues' formula

For $n = 0, 1, \ldots$ then,

$$H_n(x) = (-1)^n e^{x^2} \frac{d^n}{dx^n}\left(e^{-x^2}\right) \tag{5.27}$$

5.2.1.3. Generating function

$$e^{2tx-t^2} = \sum_{n=0}^{\infty} H_n(x)\frac{t^n}{n!} \tag{5.28}$$

5.2.1.4. Recurrence formulae

Differentiating Rodrigues' formula Eq. (5.27) we find,

$$\begin{aligned}\frac{dH_n(x)}{dx} &= (-1)^n \frac{d}{dx}\left[e^{x^2}\frac{d^n}{dx^n}\left(e^{-x^2}\right)\right] \\ &= 2x\left[(-1)^n e^{x^2}\frac{d^n}{dx^n}\left(e^{-x^2}\right)\right] - \left[(-1)^{n+1}e^{x^2}\frac{d^{n+1}}{dx^{n+1}}\left(e^{-x^2}\right)\right].\end{aligned}$$

Reinserting Eq. (5.27) in the above equation we obtain,

$$\frac{dH_n(x)}{dx} = 2xH_n(x) - H_{n+1}(x), \tag{5.29}$$

or

$$H_{n+1}(x) = 2xH_n(x) - \frac{dH_n(x)}{dx}. \tag{5.30}$$

Now inserting Eq. (5.29) into the second derivative of the Hermite differential equation Eq. (5.26) for $n-1$. Performing the second derivative and simplifying we obtain the following recurrence relation,

$$\frac{dH_n(x)}{dx} = 2nH_{n-1}(x). \tag{5.31}$$

From the above Eq. (5.31) we generalize by repeated application,

$$\frac{d^kH_n(x)}{dx^k} == \begin{cases}\frac{2^k n!}{(n-k)!}H_{n-k}(x) & k \leq n \\ 0 & k > n\end{cases}. \tag{5.32}$$

Using Eq. (5.31) in Eq. (5.30) we find the following recurrence relation,

$$H_{n+1}(x) = 2xH_n(x) - 2nH_{n-1}(x). \tag{5.33}$$

5.2.1.5. Translation formulae

The Taylor series expansion of

$$H_n(x+y) = \sum_{k=0}^{\infty}\left(\frac{d^kH_n(\xi)}{d\xi^k}\right)_{\xi=x}\frac{y^k}{k!}$$

,Applying Eq. (5.32) we find,

$$\begin{aligned} H_n(x+y) &= \sum_{k=0}^{n} \frac{2^k n!}{k!(n-k)!} H_{n-k}(x) y^k \\ &= \sum_{k=0}^{n} \begin{pmatrix} n \\ n-k \end{pmatrix} H_{n-k}(x)(2y)^k. \end{aligned} \tag{5.34}$$

A change of the dummy variable k to $n-k$, since $\binom{n}{k} = \binom{n}{n-k}$, finally gives the **Hermite translation formula**,

$$\boxed{H_n(x+y) = \sum_{k=0}^{n} \begin{pmatrix} n \\ k \end{pmatrix} (2y)^{n-k} H_k(x)} \tag{5.35}$$

or in a more symmetrical form,

$$H_n(x+y) = \sum_{k=0}^{n} \frac{1}{2^{n/2}} \begin{pmatrix} n \\ k \end{pmatrix} H_k(\sqrt{2}x) H_{n-k}(\sqrt{2}y). \tag{5.36}$$

5.2.1.6. Hermite Polynomials

$$\begin{aligned} H_0(x) &= 1 \\ H_1(x) &= 2x \\ H_2(x) &= 4x^2 - 2 \\ H_3(x) &= 8x^3 - 12x \\ H_4(x) &= 16x^4 - 48x^2 + 12 \\ &\vdots \\ &\vdots \end{aligned}$$

5.3. Extension to Fourier-Hermite-Gauss Polynomials

In Section 5.2 we derived the fact that the eigenfunctions of the Fourier transform linear operator correspond to the unnormalized Hermite-Gauss (HG) polynomials,

$$\boxed{\boldsymbol{F}\left\{\phi_p(t)\right\} = \lambda_p \phi_p(\nu)} \tag{5.37}$$

Let, $C_p = 2^{-\frac{p}{2}}(p!)^{-\frac{1}{2}}\pi^{-\frac{1}{4}}$, $p \in \mathbb{Z}^+$, be an normalization constant then the general Fourier eigenfunction is given by,

$$\boxed{\phi_p(x) = C_p e^{-\frac{x^2}{2}} H_p(x)} \tag{5.38}$$

where, $H_p(x)$, is a p-th order Hermite polynomial and, $e^{-x^2/2}$, is a Gaussian function (ergo **Hermite-Gauss polynomials**). Because the Hermite-Gauss functions, $\phi_k(x)$, are all symmetrical or anti-symmetrical depending on $k = 1, ..., N$, i.e., $k = p + 1$, so that

$$\phi_k(-x) = \begin{cases} \phi_k(x) & \text{, if } k \text{ odd} \\ -\phi_k(x) & \text{, if } k \text{ even} \end{cases}$$

or simply,

$$\phi_k(-x) = (-1)^{(k-1)}\phi_k(x). \tag{5.39}$$

Suppose we now extend the usual basis functions of the von Neumann TFR, Eq. (3.59) and Eq. (3.60), to Hermite-Gauss polynomials, actually due to the translation exponential, $e^{i\omega_n t}$, they are Fourier-Hermite-Gauss polynomials, i.e.,

$$\alpha_{mn}(t) \longmapsto e^{i\omega_n t}\phi_p[(t - t_m)/\sqrt{2\sigma}], \tag{5.40}$$

and

$$\tilde{\alpha}_{mn}(\omega) \longmapsto e^{-it_m(\omega-\omega_n)}\phi_p[\sqrt{2\sigma}(\omega - \omega_n)], \tag{5.41}$$

where the HG polynomials with proper normalization are given by,

$$\boxed{\phi_p[(t - t_m)/\sqrt{2\sigma}] = (2\sigma)^{-\frac{1}{4}}\, 2^{-\frac{p}{2}}(p!)^{-\frac{1}{2}}\pi^{-\frac{1}{4}} e^{-\frac{(t-t_m)^2}{4\sigma}} H_p[(t - t_m)/\sqrt{2\sigma}]} \tag{5.42}$$

and

$$\boxed{\phi_p[\sqrt{2\sigma}(\omega - \omega_n)] = (2\sigma)^{\frac{1}{4}}\, 2^{-\frac{p}{2}}(p!)^{-\frac{1}{2}}\pi^{-\frac{1}{4}} e^{-\sigma(\omega-\omega_n)^2} H_p[\sqrt{2\sigma}(\omega - \omega_n)]} \tag{5.43}$$

If we shift and modulate on a time-frequency lattice (t_m, ω_n), we retain the desired functional invariance of the Fourier transform,

$$\boxed{\mathcal{F}\{\alpha_{mn}(t)\} = \tilde{\alpha}_{mn}(\omega)} \tag{5.44}$$

but with N functions available in the index p (the Hermite-Gauss polynomials). Whereas we saw that the von Neumann basis functions are not orthogonal, we might be able to construct orthogonal basis functions from these Hermite-Gauss functions with this additional extension of having N polynomials available. Now let us venture down the road and explore the possibilities of expanding an electric signal with this additional freedom. To simplify the notation we introduce the following vector notation,

$$\mathbf{h}(t) = \begin{bmatrix} H_0(t) \\ H_1(t) \\ \vdots \\ H_{N-1}(t) \end{bmatrix}. \tag{5.45}$$

Then,

$$\mathbf{\Phi}(t) = e^{-\frac{t^2}{2}}\mathbf{Ch}(t), \tag{5.46}$$

where,

$$\mathbf{C} = \operatorname{diag}\left(C_p = 2^{-\frac{p}{2}}(p!)^{-\frac{1}{2}}\pi^{-\frac{1}{4}}\right)_{p=0}^{N-1}, \tag{5.47}$$

is a the constant diagonal matrix and spectrally,

$$\tilde{\mathbf{\Phi}}(\omega) = e^{-\frac{\omega^2}{2}}\mathbf{Ch}(\omega). \tag{5.48}$$

Here we present the new FHG generalization of the von Neumann TFR. The general shifted FHG TFR basis vectors are then given by,

$$\mathbf{\Psi}_{m,n}(t) = e^{it\omega_n}\mathbf{\Phi}(t-t_m) \overset{\mathcal{F}}{\Longleftrightarrow} \tilde{\mathbf{\Psi}}_{m,n}(\omega) = e^{-it_m(\omega-\omega_n)}\tilde{\mathbf{\Phi}}(\omega-\omega_n), \tag{5.49}$$

where the new **Fourier-Hermite-Gauss polynomials** are, in vector notation with proper scaling, given by,

$$\begin{aligned}\mathbf{\Psi}_{m,n}(t) &= e^{it\omega_n}\left\{(2\sigma)^{-\frac{1}{4}}e^{-\frac{(t-t_m)^2}{4\sigma}}\mathbf{Ch}[(t-t_m)/\sqrt{2\sigma}]\right\}, \\ &= e^{it\omega_n}\mathbf{\Phi}(t-t_m)\end{aligned} \tag{5.50}$$

and

$$\begin{aligned}\tilde{\mathbf{\Psi}}_{m,n}(\omega) &= e^{-it_m(\omega-\omega_n)}\left\{(2\sigma)^{\frac{1}{4}}e^{-\sigma(\omega-\omega_n)^2}\mathbf{Ch}[\sqrt{2\sigma}(\omega-\omega_n)]\right\}. \\ &= e^{-it_m(\omega-\omega_n)}\tilde{\mathbf{\Phi}}(\omega-\omega_n)\end{aligned} \tag{5.51}$$

Note that all that has happened is the inclusion of the Fourier phase translations, $e^{it\omega_n}$, $e^{-it_m(\omega-\omega_n)}$, with HG $\mathbf{\Phi}$ polynomials. In Eq. (5.42) and Eq. (5.43), please notice that no tilde appears on the ϕ_p polynomials, because they remain invariant under Fourier transform and are correctly scaled. Utilizing the notation of Subsection A.4.9 and Eq. (A.107) (cf. the definitions of the modulation, $\mathcal{M}_x$, and translation, $\mathcal{T}_x$, functional operators, therein), then Eq. (5.49), in terms of ***unscaled units***, i.e., $\sigma = \frac{1}{2}$, can be succinctly rewritten as,

$$\boxed{\mathcal{M}_{\omega_n}\mathcal{T}_{t_m}\mathbf{\Phi}(t) \overset{\mathcal{F}}{\Longleftrightarrow} \mathcal{T}_{\omega_n}\mathcal{M}_{-t_m}\mathbf{\Phi}(\omega)} \tag{5.52}$$

In this functional operator notation, we have removed ~ from the Fourier transform of $\mathbf{\Phi}$, because in this notation it is just a change in the dependent variable, $t \to \omega$. This is a magnificent method of truly understanding the real nature of the FHG polynomial bases. It is emphasized in the interchange of the functional operators (and a sign change), and as we know operators do not commute. This leads to all the difficulties. Unfortunately, I only discovered this notation myself right in the end. This would have simplified this thesis tremendously.

The electric field of the laser pulse, $\varepsilon(t)$, can be represented with a set of over-complete Fourier-Hermite-Gauss (FHG) functions on a similar discrete von Neumann lattice, as defined in Subsection 3.5.2,

$$\varepsilon(t) = \sum_{p=0}^{K-1} a^p_{m,n} e^{i\omega_n t}\phi_p[(t - t_m)/\sqrt{2\sigma}]. \tag{5.53}$$

The choice of the dimension K is rather open, and only constrained by the digital conversion of Eq. (5.53). Here we choose K to equal one of the TF dimensions. The expansion coefficients $a^p_{m,n}$ are obtained from,

$$\begin{aligned}
a^p_{m,n} &= \int_{-\infty}^{\infty} e^{-i\omega_n t}\phi_p[(t - t_m)/\sqrt{2\sigma}]\,\varepsilon(t)\,dt \qquad (5.54)\\
&= \int_{-\infty}^{\infty} e^{-i\omega_n t}\phi_p[(t - t_m)/\sqrt{2\sigma}]\sum_{k=0}^{K-1} a^p_{m,n} e^{i\omega_n t}\phi_k[(t - t_m)/\sqrt{2\sigma}]\,dt\\
&= \sum_{k=0}^{K-1} a^k_{m,n}\int_{-\infty}^{\infty} \phi_p[(t - t_m)/\sqrt{2\sigma}]\,\phi_k[(t - t_m)/\sqrt{2\sigma}]\,dt\\
&= \sum_{k=0}^{K-1} a^k_{m,n}\delta^p_k.
\end{aligned}$$

In vector notation (where all vectors are denoted in math bold are column vectors and where the superscript, T, denotes the transpose operation), this can be written concisely as an inner product as,

$$\varepsilon(t) = \mathbf{a}^T_{m,n}\mathbf{\Psi}_{m,n}(t). \tag{5.55}$$

where,

$$\mathbf{a}_{i,,j} = \begin{bmatrix} a^1_{i,j} \\ a^2_{i,j} \\ \vdots \\ a^N_{i,j} \end{bmatrix}, \tag{5.56}$$

and

$$\mathbf{a}_{m,n} = \int_{-\infty}^{\infty} \mathbf{\Psi}^*_{m,n}(t)\, \varepsilon(t)\, dt. \tag{5.57}$$

The signal representation then becomes,

$$\boxed{\varepsilon(t) = \mathbf{a}^T_{m,n} e^{it\omega_n} \mathbf{\Phi}(t - t_m) \overset{\mathcal{F}}{\Longleftrightarrow} \tilde{\varepsilon}(\omega) = \mathbf{a}^T_{m,n} e^{-it_m(\omega-\omega_n)} \tilde{\mathbf{\Phi}}(\omega - \omega_n)} \tag{5.58}$$

This insures that the TFR coefficients $\mathbf{a}_{m,n}$ defined in Eq. (5.57) are also Fourier transform invariant. It is worthy to note that in the continuum the electric field can be represented solely by a HG orthonormal expansion, but then the time-frequency interpretation is lost. The numerical discreteness of the problem allows for this finite expansion. The various frames can also be viewed as a movie of picture frames.

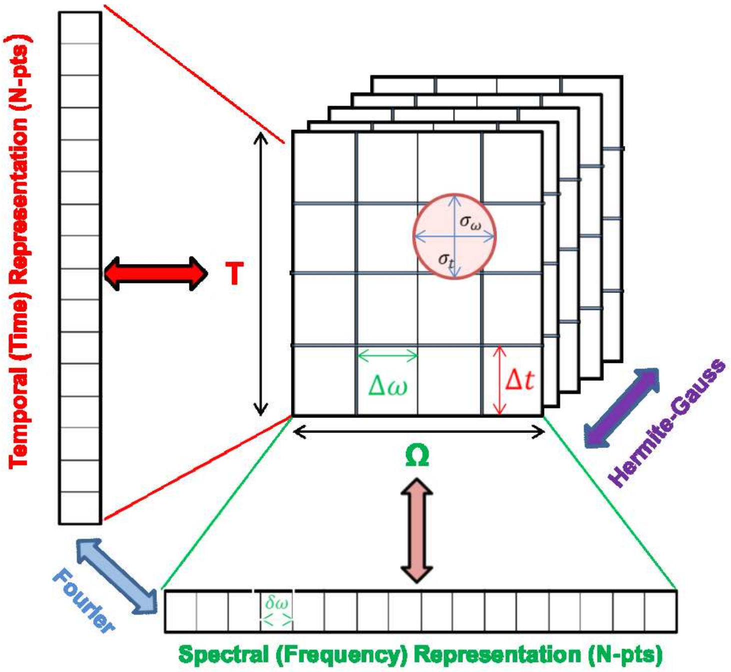
Temporal (Time) Representation (N-pts)
T
σ_ω
σ_t
$\Delta\omega$
Δt
Ω
Hermite-Gauss
Fourier
$\delta\omega$
Spectral (Frequency) Representation (N-pts)

Figure 5.2.: Fourier-Hermite-Gauss TFR Lattice

5.3.1. Generalized Fourier-Hermite-Gauss Polynomials

We are aware that we have an overcomplete functional bases for the FHG TFR. To allow for the reduction in the dimensions, we now introduce an arbitrary selection coefficient, $c^n_{i,j}$, into the expansion of the temporal and spectral translations FHG bases and some over the HG functions. So we now re-express a set of basis vectors as a linear expansion of these FHG polynomials as,

$$\beta_{i,j}(t) = \sum_{n=1}^{N} c^n_{i,j} \mathbf{\Psi}^n_{i,j}(t) \qquad \text{where} \quad c^n_{i,j} \in \mathbb{C},\ n = 1, \ldots, N\ \forall i, j \tag{5.59}$$

i.e., we seek a subset, $\beta_{i,j}(t)$, of basis functions of the full FHG set, which still fulfill the conditions of completeness and orthogonality. The main challenge is to find an appropriate set of selection coefficients, $c^n_{i,j}$, that allows us to construct, $\beta_{i,j}(t)$, that comply to the required conditions. From the linearity of the Fourier transform we note that,

$$\boxed{\boldsymbol{\mathcal{F}}\left\{\beta_{i,j}(t)\right\} = \tilde{\beta}_{i,j}(\omega)} \tag{5.60}$$

Let us investigate the orthogonality of a set of these basis functions leaving the coefficients, $c^n_{i,j}$, unspecified, but bearing in mind that they may be manipulated later to accomplish our goal of constructing a complete, but not overcomplete orthonormal basis set. Before we proceed, we rather rewrite the basis functions in vector notation as,

$$\beta_{i,j}(t) = \begin{bmatrix} c^1_{i,j} & c^2_{i,j} & \cdots & c^N_{i,j} \end{bmatrix} \begin{bmatrix} \mathbf{\Psi}^1_{i,j}(t) \\ \mathbf{\Psi}^2_{i,j}(t) \\ \vdots \\ \mathbf{\Psi}^N_{i,j}(t) \end{bmatrix} = \begin{bmatrix} \mathbf{\Psi}^1_{i,j}(t) & \mathbf{\Psi}^2_{i,j}(t) & \cdots & \mathbf{\Psi}^N_{i,j}(t) \end{bmatrix} \begin{bmatrix} c^1_{i,j} \\ c^2_{i,j} \\ \vdots \\ c^N_{i,j} \end{bmatrix}, \tag{5.61}$$

or

$$\beta_{m,n}(t) = \mathbf{c}^T_{m,n} \mathbf{\Psi}_{m,n}(t) = \mathbf{\Psi}^T_{m,n}(t)\mathbf{c}_{m,n} = e^{it\omega_n} \mathbf{\Phi}^T(t - t_m)\mathbf{c}_{m,n}. \tag{5.62}$$

Notice that,

$$\beta^*_{m,n}(t) = \mathbf{c}^\dagger_{m,n} e^{-it\omega_n} \mathbf{\Phi}(t - t_m), \tag{5.63}$$

and that

$$\mathbf{\Psi}^T_{k,l}(t) = \left[\mathbf{\Psi}^*_{k,l}(t)\right]^\dagger, \tag{5.64}$$

and the superscript, T, denotes the transpose of the vector and the † the complex conjugate transpose operation or Hermitian operation. A temporal overlap integral then becomes,

$$\mathbb{T}^{k,l}_{m,n} = \langle \beta_{m,n}(t) | \beta_{k,l}(t) \rangle = \int_{-\infty}^{\infty} \beta^*_{m,n}(t)\beta_{k,l}(t)\,\mathrm{d}t, \tag{5.65}$$

$$\boxed{\mathbb{T}_{(m,n),(k,l)} = \mathbf{c}_{m,n}^{\dagger}\left(\int_{-\infty}^{\infty} \mathbf{\Psi}_{m,n}^{*}(t)\mathbf{\Psi}_{k,l}^{T}(t)\,\mathrm{d}t\right)\mathbf{c}_{k,l}} \tag{5.66}$$

Similarly, a spectral overlap matrix can be defined as,

$$\mathbb{W}_{m,n}^{k,l} = \langle\tilde{\beta}_{m,n}(\omega)|\tilde{\beta}_{k,l}(\omega)\rangle = \int_{-\infty}^{\infty} \tilde{\beta}_{m,n}^{*}(\omega)\tilde{\beta}_{k,l}(\omega)\,\mathrm{d}\omega, \tag{5.67}$$

$$\boxed{\mathbb{W}_{(m,n),(k,l)} = \mathbf{c}_{m,n}^{\dagger}\left(\int_{-\infty}^{\infty} \tilde{\mathbf{\Psi}}_{m,n}^{*}(\omega)\tilde{\mathbf{\Psi}}_{k,l}^{T}(\omega)\,\mathrm{d}\omega\right)\mathbf{c}_{k,l}} \tag{5.68}$$

5.3.2. The Hermite Translation Expansion

To numerically calculate all the Hermite-Gaussian bases functions in FHG TFR is a numerical extensive load. Fortunately, the translated Hermite functions that occur in the FHG expansion, have a translation property that can be exploited to our benefit to reduce the numerical load. This is now explained in detail. Using the translation formulae for Hermite polynomials, Eq. (5.35), we can write the time shifted polynomials as,

$$H_p\left(t - t_m\right) = \sum_{k=0}^{p} \begin{pmatrix} p \\ k \end{pmatrix} (-2t_m)^{p-k} H_k(t). \tag{5.69}$$

This allows us to expand the time shifted Hermite polynomial vector as (Note that the final index of the Hermite polynomials has been extended by one to $n+1$ for notational convenience),

$$\mathbf{h}(t-t_m) = \begin{bmatrix} H_0\left(t-t_m\right) \\ H_1\left(t-t_m\right) \\ \vdots \\ H_n\left(t-t_m\right) \end{bmatrix} = \mathbf{L}(-2t_m)\begin{bmatrix} H_0\left(t\right) \\ H_1\left(t\right) \\ \vdots \\ H_n\left(t\right) \end{bmatrix} = \mathbf{L}(-2t_m)\mathbf{h}(t), \tag{5.70}$$

where the lower diagonal matrix, $\mathbf{L}(x)$, is defined as,

$$\mathbf{L}(x) = \begin{bmatrix} 1 & 0 & 0 & \cdots & 0 & 0 \\ x & 1 & 0 & \cdots & 0 & 0 \\ x^2 & 2x & 1 & \cdots & 0 & 0 \\ x^3 & 3x^2 & 3x & 1 & \vdots & \vdots \\ \vdots & \vdots & \vdots & \ddots & \ddots & 0 \\ x^n & nx^{n-1} & \frac{n(n-1)}{2}x^{n-1} & \cdots & nx & 1 \end{bmatrix}. \tag{5.71}$$

The specific form of this lower diagonal matrix is not just reminiscent of the binomial expansion and *Pascal's triangle*, it is exactly just that! and this is an extreme coincidence. The lower triangular matrix, $\mathbf{L}$, and upper triangular matrix, $\mathbf{U} = \mathbf{L}^T$, and the symmetric, $\mathbf{S} = \mathbf{L}\mathbf{L}^T = \mathbf{L}\mathbf{U}$, (Known as *Pascal's Matrices*, [131] due to the similarity with Pascal's triangle since they all contain the binomial coefficients). If, $x = 1$, then we obtain Pascal's triangle in the lower diagonal of the matrix,

$$\mathbf{L}(1) = \begin{bmatrix} 1 & 0 & 0 & 0 & 0 & \cdots & 0 \\ 1 & 1 & 0 & 0 & 0 & \cdots & 0 \\ 1 & 2 & 1 & 0 & 0 & \cdots & 0 \\ 1 & 3 & 3 & 1 & 0 & \cdots & 0 \\ 1 & 4 & 6 & 4 & 1 & \ddots & \vdots \\ \vdots & \vdots & \vdots & \vdots & \ddots & \ddots & 0 \\ 1 & n & \binom{n}{2} & \binom{n}{3} & \cdots & n & 1 \end{bmatrix}. \tag{5.72}$$

This matrix has the following beautiful property,

$$\mathbf{L} = \mathbf{L}(1) = \exp \mathbf{D}, \tag{5.73}$$

where,

$$\mathbf{D} = \begin{bmatrix} 0 & 0 & 0 & 0 & 0 & \cdots & 0 \\ 1 & 0 & 0 & 0 & 0 & \cdots & 0 \\ 0 & 2 & 0 & 0 & 0 & \cdots & 0 \\ 0 & 0 & 3 & 0 & 0 & \cdots & 0 \\ 0 & 0 & 0 & 4 & 0 & \ddots & \vdots \\ \vdots & \vdots & \vdots & \vdots & \ddots & \ddots & 0 \\ 0 & 0 & 0 & 0 & \cdots & n & 0 \end{bmatrix}, \tag{5.74}$$

in other words, it is equal to an $(n+1) \times (n+1)$ matrix with $1, 2, \ldots, n$ in the first subdiagonal. In addition,

$$\mathbf{L}(x) = [\exp \mathbf{D}]^x = \exp(x\mathbf{D}), \tag{5.75}$$

so that,

$$\mathbf{L}(x) = \mathbf{L}^x, \tag{5.76}$$

$\mathbf{D} = \operatorname{subdiag}\left(\begin{bmatrix} 1 & 2 & 3 & \cdots & n \end{bmatrix}\right)$ and $\mathbf{D}^T = \operatorname{superdiag}\left(\begin{bmatrix} 1 & 2 & 3 & \cdots & n \end{bmatrix}\right)$, $\dim \mathbf{D} = n+1$, which are both nilpotent, i.e., $\mathbf{D}^{n+1} = \mathbf{0}$. Also note that, $\det \mathbf{L}(x) = \det \mathbf{U}(y) = \det \mathbf{S}(z) = 1$, and are therefore all unimodular. All lower triangular matrices commute with each other and all upper triangular matrices commute as well, so that addition of the exponents are allowed. However, the product of a lower and upper triangular matrix does not commute so that the addition of the exponents is forbidden. Whereas,

$$\mathbf{L}(x) = \exp\left[x\mathbf{D}\right] = \left[\exp\mathbf{D}\right]^{x} = \left[\mathbf{L}\right]^{x}, \tag{5.77}$$

and

$$\mathbf{U}(x) = \mathbf{L}^{T}(x) = \exp\left[x\mathbf{D}^{T}\right] = \left[\exp\mathbf{D}^{T}\right]^{x} = \left[\mathbf{U}\right]^{x}, \tag{5.78}$$

We note that,

$$\mathbf{P} = \mathbf{L}\mathbf{L}^{T} = \mathbf{L}\mathbf{U}, \tag{5.79}$$

but,

$$\mathbf{P}(x) = \mathbf{L}(x)\mathbf{U}(x) = \left[\mathbf{L}\right]^{x}\left[\mathbf{U}\right]^{x} \neq \left[\mathbf{L}\mathbf{U}\right]^{x} = \mathbf{P}^{x}. \tag{5.80}$$

because the matrices do not commute $[\mathbf{L}, \mathbf{U}] \neq 0$. This is a very important result used in the numerical calculation of the various matrix exponents

$$\boxed{\mathbf{P}(x) \neq \mathbf{P}^{x}} \tag{5.81}$$

The Hermite polynomial vector Eq. (5.70), using Eq. (5.75), can therefore be expanded as,

$$\boxed{\mathbf{h}(t-t_m) = \left[e^{-2t_m\mathbf{D}}\right]\mathbf{h}(t)} \tag{5.82}$$

$$\mathbf{h}^{T}(t+t_k) = \mathbf{h}^{T}(t)\left[e^{2t_k\mathbf{D}^{T}}\right]$$

.

Employing the time translation property of the Hermite polynomials Eq. (5.31) with Eq. (5.106) and noting that, $\mathbf{\Phi}(t)$, are the HG polynomials also includes the Gaussian functions, i.e., with proper scaling the temporal FHG polynomials can be written in terms of this notation as,

$$\begin{aligned} \mathbf{\Psi}_{m,n}(t) &= e^{it\omega_n}\mathbf{\Phi}(t-t_m) \\ &= e^{it\omega_n}(2\sigma)^{-\frac{1}{4}}e^{-\frac{(t-t_m)^2}{4\sigma}}\mathbf{Ch}[(t-t_m)/\sqrt{2\sigma}] \end{aligned} \tag{5.83}$$

$$\boxed{\mathbf{\Phi}(t-t_m) = e^{-\frac{t_m^2}{4\sigma}+\frac{t_m t}{2\sigma}}\mathbf{L}^{-2t_m/\sqrt{2\sigma}}\mathbf{\Phi}(t)} \tag{5.84}$$

Our Fourier-Hermite-Gauss atom polynomials in vector notation is given by,

$$\mathbf{\Psi}_{m,n}(t) = e^{it\omega_n}\mathbf{\Phi}(t-t_m). \tag{5.85}$$

Of course we also have the transpose of, $\mathbf{\Phi}(t - t_m)$, which can similarly be expanded as,

$$\boxed{\mathbf{\Phi}^T(t - t_m) = e^{-\frac{t_m^2}{4\sigma} + \frac{t_m t}{2\sigma}} \mathbf{\Phi}^T(t) \left(\mathbf{L}^{-2t_m/\sqrt{2\sigma}}\right)^T} \tag{5.86}$$

which gives us the following relationship amongst the representation expansion coefficients, from Eq. (5.110) and Eq. (5.111),

$$\mathbf{a}_{o,n}^T = e^{-\frac{t_m^2}{4\sigma} + \frac{t_m t}{2\sigma}} \mathbf{a}_{m,n}^T \mathbf{L}^{-2t_m/\sqrt{2\sigma}}. \tag{5.87}$$

One can now argue that we have just replaced the numerical cost with the equally costly calculation of the Pascal's matrix. But not so if you recognize that, since we have equally spaced time steps say, Δt, and that each time step in the program is just an integer multiple of this increment, i.e., $t_k = k\Delta t$ then we only have to calculate two Pascal's matrices, namely, $\mathbf{L}_{\pm t} = \mathbf{L}(\pm 2\Delta t/\sqrt{2\sigma})$, (actually only one, since by Corollary 5.4.7, $\mathbf{L}_{-t} = \mathbf{L}^{-2\Delta t/\sqrt{2\sigma}} = \mathbf{G}\mathbf{L}_t\mathbf{G} = \mathbf{L}_t^{-1}$) and all other required matrices are just integer multiples of these matrices.

5.3.2.1. Temporal HG polynomials

Let (note that this expansion is with respect to the center angular frequency, ω_o),

$$\mathbf{A}_m(t) = \begin{bmatrix} \mathbf{a}_{m,K/2}^T e^{i\omega_{K/2} t} \\ \vdots \\ \mathbf{a}_{m,1}^T e^{i\omega_1 t} \\ \mathbf{a}_{m,o}^T e^{i\omega_o t} \\ \mathbf{a}_{m,-1}^T e^{i\omega_{-1} t} \\ \vdots \\ \mathbf{a}_{m,-K/2}^T e^{i\omega_{-K/2} t} \end{bmatrix}; \qquad \mathbf{A}_o(t) = \begin{bmatrix} \mathbf{a}_{o,K/2}^T e^{i\omega_{K/2} t} \\ \vdots \\ \mathbf{a}_{o,1}^T e^{i\omega_1 t} \\ \mathbf{a}_{o,o}^T e^{i\omega_o t} \\ \mathbf{a}_{o,-1}^T e^{i\omega_{-1} t} \\ \vdots \\ \mathbf{a}_{o,-K/2}^T e^{i\omega_{-K/2} t} \end{bmatrix}, \tag{5.88}$$

and that the subindex, m, is with respect to the time lattice. Now defining,

$$\mathbf{L}_t = \mathbf{L}(2\Delta t/\sqrt{2\sigma}). \tag{5.89}$$

Then by Eq. (5.87), with,

$$\boxed{\mathbf{A}_o(t) = e^{-\frac{t_m^2}{4\sigma} + \frac{t_m t}{2\sigma}} \mathbf{A}_m(t)\mathbf{L}_t^{-m}} \tag{5.90}$$

The signal representation Eq. (5.58) then becomes ($t_o = 0$),

$$\begin{aligned}\varepsilon(t) &= \sum_{m=-K/2}^{K/2} \hat{\mathbf{e}}_n^T \mathbf{A}_m(t)\mathbf{\Phi}(t-t_m) \\ &= \sum_{m=-K/2}^{K/2} \hat{\mathbf{e}}_n^T e^{-\frac{t_m^2}{4\sigma}+\frac{t_m t}{2\sigma}} \mathbf{A}_m(t)\mathbf{L}_t^{-m}\mathbf{\Phi}(t) \\ &= \sum_{m=-K/2}^{K/2} \hat{\mathbf{e}}_n^T \mathbf{A}_o(t)\mathbf{\Phi}(t),\end{aligned} \tag{5.91}$$

where, $\hat{\mathbf{e}}_n$, is the standard orthonormal basis vector (zero everywhere with 1 in the n^{th}-position).

5.3.2.2. Spectral HG polynomials

Similarly the spectral HG polynomials can be recast into the following form,

$$\begin{aligned}\tilde{\mathbf{\Phi}}(\omega-\omega_o) &= (2\sigma)^{\frac{1}{4}}\, e^{-\sigma(\omega-\omega_o)^2}\mathbf{Ch}[\sqrt{2\sigma}(\omega-\omega_o)] \\ \tilde{\mathbf{\Phi}}(\omega-\omega_n) &= (2\sigma)^{\frac{1}{4}}\, e^{-\sigma(\omega-\omega_n)^2}\mathbf{Ch}[\sqrt{2\sigma}(\omega-\omega_n)] \\ &= (2\sigma)^{\frac{1}{4}}\, e^{-\sigma(\omega-\omega_o-\omega_{no})^2}\mathbf{Ch}[\sqrt{2\sigma}(\omega-\omega_o-\omega_{no})].\end{aligned} \tag{5.92}$$

A similar argument and calculation can be used to generate the equivalent frequency coefficients. For numerical purposes the expansion must be taken over the central angular frequency, ω_o (or $\omega_o = \omega_{min}$ as is done in the von Neumann basis. The choice must then just be consistently adhered to). We specifically refer to these central frequency as, $\omega_o = \omega_c$, since it then corresponds to the time center as does, $t = 0$. For numerical purposes it is desirable to keep the exponents on the Pascal matrices as small as possible. The maximum exponents in the temporal domain is then equivalent, $\pm T/2$. Referencing to the central frequency the maximum exponents in the spectral basis is then equivalent to, $\pm\Omega/2$. The angular frequency formula are given by,

$$\boxed{\tilde{\mathbf{\Phi}}(\omega-\omega_n) = e^{-\sigma\omega_{no}^2+2\sigma(\omega-\omega_o)\omega_{no}}\mathbf{L}^{-2\sqrt{2\sigma}\omega_{no}}\tilde{\mathbf{\Phi}}(\omega-\omega_o)} \tag{5.93}$$

where, $\omega_{no} = \omega_n - \omega_o$, which gives us the following relationship amongst the expansion coefficients of the representation

$$\mathbf{a}_{m,o}^T = \mathbf{a}_{m,n}^T e^{-\sigma\omega_{no}^2+2\sigma(\omega-\omega_o)\omega_{no}}\mathbf{L}^{-2\sqrt{2\sigma}\omega_{no}}. \tag{5.94}$$

Let,

$$\mathbf{B}_n(\omega) = \begin{bmatrix} \mathbf{a}^T_{K/2,n} e^{-it_{K/2}(\omega-\omega_n)} \\ \vdots \\ \mathbf{a}^T_{-1,n} e^{-it_{-1}(\omega-\omega_n)} \\ \mathbf{a}^T_{o,n} e^{-it_0(\omega-\omega_n)} \\ \mathbf{a}^T_{-1,n} e^{-it_{-1}(\omega-\omega_n)} \\ \vdots \\ \mathbf{a}^T_{-K/2,n} e^{-it_{-K/2}(\omega-\omega_n)} \end{bmatrix}; \qquad \mathbf{B}_o(\omega) = \begin{bmatrix} \mathbf{a}^T_{K/2,o} e^{-it_{K/2}(\omega-\omega_o)} \\ \vdots \\ \mathbf{a}^T_{-1,o} e^{-it_{-1}(\omega-\omega_o)} \\ \mathbf{a}^T_{o,o} e^{-it_0(\omega-\omega_o)} \\ \mathbf{a}^T_{-1,o} e^{-it_{-1}(\omega-\omega_o)} \vdots \\ \vdots \\ \mathbf{a}^T_{-K/2,o} e^{-it_{-K/2}(\omega-\omega_o)} \end{bmatrix}, \tag{5.95}$$

and that the subindex, n, is with respect to the frequency lattice. Notice that we have defined the above matrices, $\mathbf{B}_n$, $n = -\frac{K}{2}, \ldots, -1, 0, 1, \ldots, \frac{K}{2}$, with respect to the central frequency, ω_o.

Then defining,

$$\mathbf{L}_\omega = \mathbf{L}(2\sqrt{2\sigma}\Delta\omega), \tag{5.96}$$

and inserting this new notation we obtain,

$$\boxed{\mathbf{B}_n(\omega) = e^{\sigma\omega_{no}^2 - 2\sigma(\omega-\omega_o)\omega_{no}} \mathbf{B}_o(\omega)\mathbf{L}^n_\omega} \tag{5.97}$$

The spectral signal representation Eq. (5.126) then becomes ($\omega_o = \omega_c$)

$$\begin{aligned} \tilde{\varepsilon}(\omega) &= \sum_{n=-K/2}^{K/2} \hat{\mathbf{e}}^T_m \mathbf{B}_n(\omega)\tilde{\mathbf{\Phi}}(\omega-\omega_n) \qquad (5.98) \\ &= \sum_{n=-K/2}^{K/2} \hat{\mathbf{e}}^T_m \mathbf{B}_o(\omega)\tilde{\mathbf{\Phi}}(\omega-\omega_o). \end{aligned}$$

5.4. The Fourier-Hermite-Gauss Representation

As was proven by Perelomov in [122], the von Neumann basis is complete but not over complete. The over-completeness of FHG polynomials does present an unnecessary complication. Let us investigate the orthogonality of a set of these basis functions leaving the coefficients unspecified, but bearing in mind that they may be manipulated to accomplish our goal of establishing a reduced complete basis TFR.

5.4.1. Temporal FHG Basis Functions

Before proceeding, we rather rewrite the basis functions Eq. (5.62) in vector notation as,

$$\beta_{m,n}(t) = \mathbf{c}_{m,n}^T e^{it\omega_n} \mathbf{\Phi}(t - t_m) \qquad \text{where} \quad \mathbf{c}_{m,n}^T \in \mathbb{C}^K. \tag{5.99}$$

Remember this set, $\beta_{m,n}(t)$, is a selected subset (by means of $\mathbf{c}_{m,n}^T$) of the full FHG basis set, reduced to satisfy the conditions of completeness and orthogonality. Using the Hermite translation formula, Eq. (5.84), with the correct scaling we have,

$$\boxed{\beta_{m,n}(t) = \mathbf{c}_{m,n}^T e^{it\omega_n} e^{-\frac{t_m^2}{4\sigma} + \frac{t_m t}{2\sigma}} \mathbf{L}^{-2t_m/\sqrt{2\sigma}} \mathbf{\Phi}(\frac{t}{\sqrt{2\sigma}})} \tag{5.100}$$

The total dimension of the temporal FHG basis functions $K \times K = K^2$.

5.4.2. Spectral FHG Basis Functions

From the linearity of the Fourier transform we note that, $\boldsymbol{\mathcal{F}}\{\beta_{m,n}(t)\} = \tilde{\beta}_{m,n}(\omega)$,

$$\tilde{\beta}_{m,n}(\omega) = \mathbf{c}_{m,n}^T e^{-it_m(\omega - \omega_n)} \tilde{\mathbf{\Phi}}(\omega - \omega_n) \qquad \text{where} \quad \mathbf{c}_{m,n}^T \in \mathbb{C}^K \tag{5.101}$$

Using the Hermite translation formula, Eq. (5.93), with the scaling specifically included, we have,

$$\boxed{\tilde{\beta}_{m,n}(\omega) = \mathbf{c}_{m,n}^T e^{-it_m(\omega - \omega_n)} e^{-\sigma\omega_{no}^2 + 2\sigma(\omega - \omega_o)\omega_{no}} \mathbf{L}^{-2\sqrt{2\sigma}\omega_{no}} \tilde{\mathbf{\Phi}}[\sqrt{2\sigma}(\omega - \omega_o)]} \tag{5.102}$$

The total dimension of the spectral FHG basis functions $K \times K = K^2$.

5.4.3. The FHG Overlap Integral

As discussed earlier an **FHG overlap integral** can then be defined as, similar to the von Neumann TFR, Eq. (3.84), as,

$$\mathbb{T}_{m,n}^{k,l} = \langle \beta_{m,n}(t) | \beta_{k,l}(t) \rangle \triangleq \int_{-\infty}^{\infty} \beta_{m,n}^*(t) \beta_{k,l}(t) \, \mathrm{d}t \tag{5.103}$$

The dimension of the FHG overlap matrix is $K^2 \times K^{2\cdot}$.

$$\boxed{\mathbb{T}_{(m,n),(k,l)} = \mathbf{c}_{m,n}^\dagger \left(\int_{-\infty}^{\infty} \mathbf{\Psi}_{m,n}^*(t) \mathbf{\Psi}_{k,l}^T(t) \, \mathrm{d}t \right) \mathbf{c}_{k,l}} \tag{5.104}$$

where, the † denotes the complex conjugate transpose operation or Hermitian operation. This is derived completely in Subsection 5.4.6 with the result,

$$\boxed{\mathbb{T}^{k,l}_{m,n} = \mathbf{c}^{\dagger}_{m,n} e^{-\frac{1}{8\sigma}t^2_{mk}-\frac{\sigma}{2}\omega^2_{ln}-\frac{1}{2}i\omega_{ln}(t_m+t_k)} \mathbf{L}^{-\frac{t_{mk}}{\sqrt{2\sigma}}-i\sqrt{2\sigma}\omega_{ln}} \mathbf{U}^{\frac{t_{mk}}{\sqrt{2\sigma}}-i\sqrt{2\sigma}\omega_{ln}} \mathbf{c}_{k,l}} \tag{5.105}$$

The dimension of the lower and upper Pascal matrices is $K \times K$, while $\dim(\mathbb{T}) = K^2 \times K^{2}$. Remember that, $\mathbb{T}^{k,l}_{m,n}$, is just a component of this matrix.

Equivalently, this can also be calculated with FHG spectral basis, Eq. (B.30), with the result,

$$\boxed{\mathbb{W}^{k,l}_{m,n} = \mathbf{c}^{\dagger}_{m,n} e^{-\frac{1}{8\sigma}t^2_{mk}-\frac{\sigma}{2}\omega^2_{ln}-\frac{1}{2}i\omega_{ln}(t_m+t_k)} \mathbf{L}^{-\sqrt{2\sigma}\omega_{ln}-i\frac{t_{mk}}{\sqrt{2\sigma}}} \mathbf{U}^{\sqrt{2\sigma}\omega_{ln}-i\frac{t_{mk}}{\sqrt{2\sigma}}} \mathbf{c}_{k,l}} \tag{5.106}$$

Although there is an unexpected difference between the two methods of calculation Theorem 5.4.8 actual proves that the two matrices are similar.

5.4.4. The Fourier-Hermite-Gauss TFR

Similar to the von Neumann TFR, Eq. (3.100), we have a **Fourier-Hermite-Gauss Time-Frequency-Representation** given by,

$$\boxed{\boldsymbol{\mathcal{A}}_{m,s} = \sum_{k,l} \left[\mathbb{T}^{k,l}_{m,s}\right]^{-1} \int_{-\infty}^{\infty} \beta^*_{k,l}(t)\varepsilon(t)\, dt} \tag{5.107}$$

Or, equivalently (cf. Eq. (3.101)) in terms of the FHG spectral basis,

$$\boxed{\boldsymbol{\mathcal{A}}_{m,s} = \sum_{k,l} \left[\mathbb{W}^{k,l}_{m,s}\right]^{-1} \int_{-\infty}^{\infty} \tilde{\beta}^*_{k,l}(\omega)\tilde{\varepsilon}(\omega)\, d\omega} \tag{5.108}$$

5.4.5. The FHG Signal Reconstruction

The **signal reconstruction**, similar to Eq. (3.102) and Eq. (3.103), is then given by,

$$\boxed{\varepsilon(t) = \sum_{m,s} \boldsymbol{\mathcal{A}}_{m,s}\beta_{m,s}(t) \overset{\mathcal{F}}{\Longleftrightarrow} \tilde{\varepsilon}(\omega) = \sum_{m,s} \boldsymbol{\mathcal{A}}_{m,s}\tilde{\beta}_{m,s}(\omega)} \tag{5.109}$$

5.4.6. The Fourier-Hermite-Gauss Overlap Integral

We fully derive the temporal overlap matrix in this subsection. Considering that the whole concept of FHG TFR is novel, this to also unique to this dissertation. The overlap integral Eq. (5.104) will be developed in three parts. We, firstly, note the Hermite polynomials are all time shifted,

$$\begin{aligned}\mathbb{T}^{k,l}_{m,n} &= \mathbf{c}^{\dagger}_{m,n}\left(\int_{-\infty}^{\infty} e^{-it\omega_n}\boldsymbol{\Phi}(t-t_m)\, e^{it\omega_l}\boldsymbol{\Phi}^T(t-t_k)\,\mathrm{d}t\right)\mathbf{c}_{k,l}\\ &= \mathbf{c}^{\dagger}_{m,n}\left(\int_{-\infty}^{\infty} \boldsymbol{\Phi}(t-t_m)\,\boldsymbol{\Phi}^T(t-t_k)e^{-it\omega_{nl}}\,\mathrm{d}t\right)\mathbf{c}_{k,l} \qquad (5.110)\end{aligned}$$

where have made use of the shorthand,

$$\omega_{nl} \triangleq \omega_n - \omega_l. \qquad (5.111)$$

The generalized FHG spectral basis is defined by,

$$\tilde{\beta}_{m,n}(\omega) = \mathbf{c}^T_{m,n}e^{-it_m(\omega-\omega_n)}\tilde{\boldsymbol{\Phi}}(\omega-\omega_n) \qquad \text{where} \quad \mathbf{c}^T_{m,n} \in \mathbb{C}^K. \qquad (5.112)$$

The spectral overlap matrix is given by,

$$\begin{aligned}\mathbb{W}^{k,l}_{m,n} &= \mathbf{c}^{\dagger}_{m,n}\left(\int_{-\infty}^{\infty} e^{it_m(\omega-\omega_n)}\tilde{\boldsymbol{\Phi}}(\omega-\omega_n)\, e^{-it_k(\omega-\omega_l)}\tilde{\boldsymbol{\Phi}}^T(\omega-\omega_l)\,\mathrm{d}\omega\right)\mathbf{c}_{k,l}\\ &= \mathbf{c}^{\dagger}_{m,n}e^{it_k\omega_l-it_m\omega_n}\left(\int_{-\infty}^{\infty} \tilde{\boldsymbol{\Phi}}(\omega-\omega_n)\,\tilde{\boldsymbol{\Phi}}^T(\omega-\omega_l)e^{it_{mk}\omega}\,\mathrm{d}\omega\right)\mathbf{c}_{k,l}, \qquad (5.113)\end{aligned}$$

where, $t_{mk} = t_m - t_k$. The results of this spectral overlap matrix are given in Eq. (B.30).

Part I

We are now in a position to evaluate the integral of the overlap matrix *Eq.* (5.110),

$$\int_{-\infty}^{\infty} \boldsymbol{\Psi}^*_{m,n}(t)\boldsymbol{\Psi}^T_{k,l}(t)\,\mathrm{d}t = \int_{-\infty}^{\infty} \boldsymbol{\Phi}^*(t-t_m)\,\boldsymbol{\Phi}^T(t-t_k)e^{-it\omega_{nl}}\,\mathrm{d}t, \qquad (5.114)$$

with the integrand given by, (ignoring the HG normalization constants, $2^{-\frac{p}{2}}(p!)^{-\frac{1}{2}}\pi^{-\frac{1}{4}}$, which is p dependent and also neglecting the time scaling, which we shall include at a later stage),

$$\boldsymbol{\Psi}^*_{m,n}(t)\boldsymbol{\Psi}^T_{k,l}(t) = e^{-\frac{1}{2}(t-t_m)^2-\frac{1}{2}(t-t_k)^2-i\omega_{nl}t}\mathbf{h}(t-t_m)\mathbf{h}^T(t-t_k). \tag{5.115}$$

Subsection 5.3.2 showed that it is possible to handle the two time translations, t_m and t_k, for the Hermitian polynomial vectors, $\mathbf{h}$. The quadratics in the exponential still represent a bother. Remembering that this is an integrand we transform to an averaged translation time,

$$\tau = t - \frac{t_m + t_k}{2} \tag{5.116}$$

so that,

$$t - t_m = \tau - \frac{t_{mk}}{2} \text{ and } t - t_k = \tau + \frac{t_{mk}}{2}. \tag{5.117}$$

Inserting Eq. (5.116) and Eq. (5.117) into the integrand of Eq. (5.115) the quadratic exponent then becomes,

$$\begin{aligned} -\frac{1}{2}\left(\tau - \frac{t_{mk}}{2}\right)^2 - \frac{1}{2}\left(\tau + \frac{t_{mk}}{2}\right)^2 - i\omega_{nl}\left(\tau + \frac{t_m + t_k}{2}\right) = \\ -\tau^2 - i\omega_{nl}\tau - \left(\frac{t_{mk}}{2}\right)^2 - i\omega_{nl}\left(\frac{t_m + t_k}{2}\right) \end{aligned} \tag{5.118}$$

With the aid of Eq. (5.116), Eq. (5.117) and Eq. (5.118) the overlap matrix transforms to,

$$\int_{-\infty}^{\infty} \boldsymbol{\Psi}^*_{m,n}(t)\boldsymbol{\Psi}^T_{k,l}(t)\,\mathrm{d}t = e^{-\left(\frac{t_{mk}}{2}\right)^2 - i\omega_{nl}\left(\frac{t_m+t_k}{2}\right)} \int_{-\infty}^{\infty} \mathbf{h}(\tau - \frac{t_{mk}}{2})\mathbf{h}^T(\tau + \frac{t_{mk}}{2})e^{-\tau^2 - i\omega_{nl}\tau}\,\mathrm{d}\tau. \tag{5.119}$$

Using the translation property of the Hermite polynomials Eq. (5.82), the above integral becomes,

$$\boxed{e^{-\left(\frac{t_{mk}}{2}\right)^2 - i\omega_{nl}\left(\frac{t_m+t_k}{2}\right)}\mathbf{L}^{-t_{mk}} \int_{-\infty}^{\infty} \mathbf{h}(\tau)\mathbf{h}^T(\tau)e^{-\tau^2 - i\omega_{nl}\tau}\,\mathrm{d}\tau\,\mathbf{U}^{t_{mk}}} \tag{5.120}$$

Part II

Now, secondly, let's just focus on the remaining integral of Eq. (5.120), namely,

$$\int_{-\infty}^{\infty}\left[e^{-\frac{\tau^2}{2}}\mathbf{h}(\tau)\right]\left[e^{-\frac{\tau^2}{2}}\mathbf{h}^T(\tau)\right]e^{-i\omega_{nl}\tau}\,\mathrm{d}\tau. \tag{5.121}$$

Now,

$$\mathbf{h}(\tau)\mathbf{h}^T(\tau)=\begin{bmatrix} H_0\left(\tau\right) \\ H_1\left(\tau\right) \\ \vdots \\ H_N\left(\tau\right)\end{bmatrix}\begin{bmatrix} H_0\left(\tau\right) & H_1\left(\tau\right) & \cdots & H_N\left(\tau\right)\end{bmatrix} \tag{5.122}$$

We present this here in detail, because this could not be found in standard reference books. So generally, we like to evaluate the Fourier transform of the product of two quantum harmonic oscillator polynomials,

$$\mathbb{J}_{nm}(\omega)=\int_{-\infty}^{\infty}\left[e^{-\frac{\tau^2}{2}}H_n\left(\tau\right)\right]\left[e^{-\frac{\tau^2}{2}}H_m\left(\tau\right)\right]e^{-i\omega\tau}\,\mathrm{d}\tau. \tag{5.123}$$

The generating function of the Hermite polynomials is given by Eq. (5.28). Taking a second generating function with dummy variable, y, and multiplying the two we obtain,

$$e^{2t(x+y)-\left(x^2+y^2\right)}=\sum_{n=0}^{\infty}\sum_{m=0}^{\infty}H_n(t)H_m(t)\frac{x^n y^m}{n!m!}. \tag{5.124}$$

Multiplying the Eq. (5.124) by, e^{-t^2},

$$e^{-t^2+2t(x+y)-\left(x^2+y^2\right)}=\sum_{n=0}^{\infty}\sum_{m=0}^{\infty}\left[e^{-\frac{t^2}{2}}H_n(t)\right]\left[e^{-\frac{t^2}{2}}H_m(t)\right]\frac{x^n y^m}{n!m!}. \tag{5.125}$$

Now, multiplying by, $e^{-i\omega t}$, and integrating with respect to, t,

$$\int_{-\infty}^{\infty}\exp\left[-t^2+2t\left(x+y\right)-\left(x^2+y^2\right)\right]e^{-i\omega t}\,\mathrm{d}t= \tag{5.126}$$

$$=\sum_{n=0}^{\infty}\sum_{n=0}^{\infty}\left\{\int_{-\infty}^{\infty}\left[e^{-\frac{t^2}{2}}H_n\left(t\right)\right]\left[e^{-\frac{t^2}{2}}H_m\left(t\right)\right]e^{-i\omega t}\,\mathrm{d}t\right\}\frac{x^n y^m}{n!m!} \tag{5.127}$$

$$=\sum_{n=0}^{\infty}\sum_{m=0}^{\infty}\mathbb{J}_{nm}(\omega)\frac{x^n y^m}{n!m!}. \tag{5.128}$$

Consider the left hand integral in Eq. (5.126) and complete the square of the exponent of the exponential,

$$-t^2+2t\left(x+y\right)-\left(x^2+y^2\right)=-\left[t-\left(x+y\right)\right]^2+2xy \tag{5.129}$$

and substitute into Eq. (5.126) and change the integration variable,

$$\tau = t - (x+y)\,, \qquad d\tau = dt, \tag{5.130}$$

then the integral transforms to,

$$e^{-i\omega(x+y)+2xy} \int_{-\infty}^{\infty} e^{-\tau^2 - i\omega\tau}\,\mathrm{d}\tau. \tag{5.131}$$

The integral in Eq. (5.131) is once again in the form of our standard Gaussian integral Eq. (3.14), so that Eq. (5.128) becomes,

$$\boxed{\left[\sqrt{\pi}e^{-\frac{\omega^2}{4}}\right] e^{-i\omega(x+y)+2xy} = \sum_{n=0}^{\infty}\sum_{m=0}^{\infty} \mathbb{J}_{nm}(\omega)\frac{x^n y^m}{n!m!}} \tag{5.132}$$

Expanding the left hand exponentials of Eq. (5.132) in terms of a Taylor series,

$$e^{x(2y-i\omega)}e^{-i\omega y} = \sum_{n=0}^{\infty}\frac{x^n(2y-i\omega)^n}{n!}\sum_{q=0}^{\infty}\frac{y^q}{q!}(-i\omega)^q, \tag{5.133}$$

and using the binomial theorem for $(2y - i\omega)^n$ in Eq. (5.133) (Notice the addition of $(p+q)!$ above and below),

$$e^{x(2y-i\omega)}e^{-i\omega y} = \sum_{n=0}^{\infty}\frac{x^n}{n!}\sum_{q=0}^{\infty}\sum_{p=0}^{n} 2^p\binom{n}{p}\frac{y^{p+q}}{(p+q)!}\frac{(p+q)!}{q!}(-i\omega)^{n+q-p}. \tag{5.134}$$

The binomial factorial becomes,

$$\binom{p+q}{p} = \frac{(p+q)!}{p!q!}, \tag{5.135}$$

thus,

$$e^{x(2y-i\omega)}e^{-i\omega y} = \sum_{n=0}^{\infty}\frac{x^n}{n!}\sum_{q=0}^{\infty}\sum_{p=0}^{n} 2^p p!\binom{n}{p}\binom{p+q}{p}\frac{y^{p+q}}{(p+q)!}(-i\omega)^{n+q-p}. \tag{5.136}$$

Now substitute $m = p + q$ in the above equation,

$$e^{x(2y-i\omega)}e^{-i\omega y} = \sum_{n=0}^{\infty}\sum_{m=0}^{\infty}\left\{\sum_{p=0}^{\min(n,m)} 2^p p!\binom{n}{p}\binom{m}{p}(-i\omega)^{n+m-2p}\right\}\frac{x^n}{n!}\frac{y^m}{m!}. \tag{5.137}$$

Comparing the coefficients Eq. (5.137) with Eq. (5.132) we obtain,

$$\boxed{\mathbb{J}_{nm}(\omega) = \sqrt{\pi}e^{-\frac{\omega^2}{4}} \sum_{p=0}^{\min(n,m)} 2^p p! \binom{n}{p}\binom{m}{p}(-i\omega)^{n+m-2p}} \tag{5.138}$$

$$\mathbb{J}_{nm}(\omega) = \int_{-\infty}^{\infty} \left[e^{-\frac{\tau^2}{2}} H_n\left(\tau\right)\right] \left[e^{-\frac{\tau^2}{2}} H_m\left(\tau\right)\right] e^{-i\omega\tau}\, \mathrm{d}\tau \tag{5.139}$$

$$\Downarrow \tag{5.140}$$

$$\boxed{\mathbb{J}_{nm}(\omega) = \sqrt{\pi}e^{-\frac{\omega^2}{4}} \sum_{p=0}^{\min(n,m)} 2^p p! \binom{n}{p}\binom{m}{p}(-i\omega)^{n+m-2p}} \tag{5.141}$$

Remembering that, $\mathbb{J}_{nm}$, Eq. (5.139), is just an element of a matrix, the structure of this element with the presence with two binomial coefficients is reminiscent of the triangular Pascal matrix that we previously investigated in Eq. (5.71). Let us rewrite this element as,

$$\mathbb{J}_{nm}(\omega) = e^{-\frac{\omega^2}{4}} \sum_{p=0}^{\min(n,m)} \left[\pi^{\frac{1}{4}} 2^{\frac{p}{2}} \sqrt{p!}\binom{n}{p}(-i\omega)^{n-p}\right] \left[\pi^{\frac{1}{4}} 2^{\frac{p}{2}} \sqrt{p!}\binom{m}{p}(-i\omega)^{m-p}\right]. \tag{5.142}$$

This is just the product of two of Pascal's triangles except for the $\pi^{\frac{1}{4}} 2^{\frac{p}{2}} \sqrt{p!}$ factor. It is still, however, possible to factorize this matrix as

$$\boxed{\int_{-\infty}^{\infty} \left[e^{-\frac{\tau^2}{2}} \mathbf{h}(\tau)\right] \left[e^{-\frac{\tau^2}{2}} \mathbf{h}^T(\tau)\right] e^{-i\omega\tau}\, \mathrm{d}\tau = e^{-\frac{\omega^2}{4}} \mathbf{L}^{-i\omega} \mathbf{N}^{\frac{1}{2}} \mathbf{N}^{\frac{1}{2}} \left[\mathbf{L}^{-i\omega}\right]^T} \tag{5.143}$$

where, $\mathbf{N} = \operatorname{diag}\left(\sqrt{\pi}\left[\begin{array}{ccccccc} 2^0 0! & 2^1 \cdot 1! & 2^2 \cdot 2! & 2^3 \cdot 3! & 2^4 \cdot 4 & \cdots & 2^n \cdot n! \end{array}\right]\right)$ or,

$$\mathbf{N} = \sqrt{\pi} \begin{bmatrix} 2^0 0! & 0 & 0 & 0 & 0 & \cdots & 0 \\ 0 & 2^1 \cdot 1! & 0 & 0 & 0 & \cdots & 0 \\ 0 & 0 & 2^2 \cdot 2! & 0 & 0 & \cdots & 0 \\ 0 & 0 & 0 & 2^3 \cdot 3! & 0 & \cdots & 0 \\ 0 & 0 & 0 & 0 & 2^4 \cdot 4! & \vdots & \vdots \\ 0 & 0 & 0 & 0 & 0 & \ddots & 0 \\ 0 & 0 & 0 & 0 & 0 & 0 & 2^n \cdot n! \end{bmatrix}. \tag{5.144}$$

Fortunately, we must still include HG normalization constants for the product in Eq. (5.143), which just serendipitously happens to be the inverse!

$$\mathbf{C}^2 = \operatorname{diag}\left(2^{-p}(p!)^{-1}\pi^{-\frac{1}{2}}\right)_{p=0}^{n} = \mathbf{N}^{-1}$$

. Because we have an imaginary power, it is easy to see that, if $\omega \in \mathbb{R}$,

$$\left[\mathbf{L}^{i\omega}\right]^{\dagger} = \mathbf{U}^{-i\omega}. \tag{5.145}$$

and in general we have for, $z \in \mathbb{C}$,

$$[\mathbf{L}^{z}]^{\dagger} = \mathbf{U}^{z^*}. \tag{5.146}$$

Therefore the above equation becomes,

$$\boxed{\int_{-\infty}^{\infty} \Phi(\tau)\Phi^T(\tau)e^{-i\omega\tau}\,\mathrm{d}\tau = e^{-\frac{\omega^2}{4}}\mathbf{L}^{-i\omega}\mathbf{U}^{-i\omega}} \tag{5.147}$$

Part III

The overlap matrix element Eq. (5.110), with $\omega = \omega_{nl}$, can thus be written as,

$$\mathbb{T}^{k,l}_{m,n} = \mathbf{c}^{\dagger}_{m,n} e^{-\frac{1}{4}t^2_{mk}-\frac{1}{4}\omega^2_{ln}-\frac{1}{2}i\omega_{nl}(t_m+t_k)}\mathbf{L}^{-t_{mk}-i\omega_{nl}}\mathbf{U}^{t_{mk}-i\omega_{nl}}\mathbf{c}_{k,l} \tag{5.148}$$

With the correct time scaling, we have,

$$\boxed{\mathbb{T}^{k,l}_{m,n} = \mathbf{c}^{\dagger}_{m,n} e^{-\frac{1}{8\sigma}t^2_{mk}-\frac{\sigma}{2}\omega^2_{ln}-\frac{1}{2}i\omega_{nl}(t_m+t_k)}\mathbf{L}^{-\frac{t_{mk}}{\sqrt{2\sigma}}-i\sqrt{2\sigma}\omega_{nl}}\mathbf{U}^{\frac{t_{mk}}{\sqrt{2\sigma}}-i\sqrt{2\sigma}\omega_{nl}}\mathbf{c}_{k,l}} \tag{5.149}$$

5.4.7. Spectral Overlap Integral

The spectral HG representation and its subsequent spectral overlap matrix is given by,

$$\tilde{\beta}_{m,n}(\omega) = e^{-it_m(\omega-\omega_n)}\tilde{\mathbf{\Phi}}^{\dagger}(\omega-\omega_n)\mathbf{c}_{m,n} \qquad \text{where} \quad \mathbf{c}_{m,n} \in \mathbb{C}^K. \tag{5.150}$$

Of course, the Hermitian conjugate is then given by, $\tilde{\beta}^{\dagger}_{m,n}(\omega) = \mathbf{c}^{\dagger}_{m,n}e^{it_m(\omega-\omega_n)}\tilde{\mathbf{\Phi}}^{\dagger}(\omega-\omega_n)$, so that,

$$\mathbb{W}^{k,l}_{m,n} = \langle\tilde{\beta}_{m,n}(\omega)|\tilde{\beta}_{k,l}(\omega)\rangle = \int_{-\infty}^{\infty}\tilde{\beta}^{\dagger}_{m,n}(\omega)\tilde{\beta}_{k,l}(\omega)\,\mathrm{d}\omega. \tag{5.151}$$

We, firstly, note the Hermite polynomials are all angular frequency shifted,

$$\mathbb{W}_{(m,n),(k,l)} = \mathbf{c}_{m,n}^{\dagger} \left(\int_{-\infty}^{\infty} e^{it_m(\omega-\omega_n)} \tilde{\boldsymbol{\Phi}}(\omega-\omega_n)\, e^{-it_k(\omega-\omega_l)} \tilde{\boldsymbol{\Phi}}^{\dagger}(\omega-\omega_l)\, \mathrm{d}\omega \right) \mathbf{c}_{k,l}. \tag{5.152}$$

In exactly an equivalent fashion, as the previous the spectral overlap integral is derived (cf. Appendix Appendix B), the spectral overlap matrix is given by,

$$\mathbb{W}_{m,n}^{k,l} = \mathbf{c}_{m,n}^{\dagger} e^{-\frac{1}{4}t_{mk}^2 - \frac{1}{4}\omega_{ln}^2 - \frac{1}{2}i\omega_{ln}(t_m+t_k)} \left[\mathbf{L}^{-\omega_{ln}-it_{mk}}\right] \left[\mathbf{U}^{\omega_{ln}-it_{mk}}\right] \mathbf{c}_{k,l}. \tag{5.153}$$

With the correct scaling we have,

$$\boxed{\mathbb{W}_{m,n}^{k,l} = \mathbf{c}_{m,n}^{\dagger} e^{-\frac{1}{8\sigma}t_{mk}^2 - \frac{\sigma}{2}\omega_{ln}^2 - \frac{1}{2}i\omega_{ln}(t_m+t_k)} \mathbf{L}^{-\sqrt{2\sigma}\omega_{ln} - i\frac{t_{mk}}{\sqrt{2\sigma}}} \mathbf{U}^{\sqrt{2\sigma}\omega_{ln} - i\frac{t_{mk}}{\sqrt{2\sigma}}} \mathbf{c}_{k,l}} \tag{5.154}$$

Although one would expect that the temporal and spectral overlap matrices to be equal we note subtle differences in the exponents of the **L** and **U** matrices. This will be addressed in the next Subsection 5.4.8.

5.4.8. Validity of the Overlap Integral

With the choice of, $\mathbf{c}_{m,n}^{T} = \begin{bmatrix} 1 & 0 & 0 & \cdots & 0 \end{bmatrix}, \forall m, n$, a simple validity check is to compare, $\mathbb{T}_{m,n}^{k,l}$, with the corresponding von Neumann overlap matrix Eq. (3.90),

$$\mathbb{S}_{m,n}^{k,l} = e^{-\frac{\sigma}{2}(\omega_n-\omega_l)^2 - \frac{1}{2}i(t_m+t_k)(\omega_n-\omega_l) - \frac{1}{8\sigma}(t_m-t_k)^2}.$$

Considering the basis vectors of the FHG TFR as lattice cube this corresponds to a slice of the cube in a plane section of the front portion. This proves then that, $\mathbb{T}_{m,n}^{k,l} = \mathbb{S}_{m,n}^{k,l}$, at least for the von Neumann TFR. The true test is accomplished by the evaluation of the corresponding, $\mathbb{W}_{m,n}^{k,l} = \left\langle \tilde{\beta}_{m,n}(\omega) | \tilde{\beta}_{k,l}(\omega) \right\rangle = \int_{-\infty}^{\infty} \tilde{\beta}_{m,n}^{*}(\omega) \tilde{\beta}_{k,l}(\omega)\, \mathrm{d}\omega$ and $\mathbb{T}_{m,n}^{k,l}$. It can be shown that,

$$\boxed{\mathbb{W}_{m,n}^{k,l} = \mathbf{c}_{m,n}^{\dagger} e^{-\frac{1}{8\sigma}t_{mk}^2 - \frac{\sigma}{2}\omega_{nl}^2 - \frac{1}{2}i\omega_{nl}(t_m+t_k)} \mathbf{L}^{\sqrt{2\sigma}\omega_{nl} + i\frac{t_{mk}}{\sqrt{2\sigma}}} \mathbf{U}^{-\sqrt{2\sigma}\omega_{nl} + i\frac{t_{mk}}{\sqrt{2\sigma}}} \mathbf{c}_{k,l}} \tag{5.155}$$

For the purpose of this exercise, great simplification can be obtained if we use **unscaled units**, i.e., allow $\sigma = \frac{1}{2}$, then the overlap integrals can be simplified to,

$$\mathbb{T}_{m,n}^{k,l} = \mathbf{c}_{m,n}^{\dagger} e^{-\frac{1}{4}t_{mk}^2 - \frac{1}{4}\omega_{ln}^2 - \frac{1}{2}i\omega_{nl}(t_m+t_k)} \mathbf{L}^{-t_{mk}-i\omega_{nl}} \mathbf{U}^{t_{mk}-i\omega_{nl}} \mathbf{c}_{k,l} \tag{5.156}$$

and

$$\mathbb{W}^{k,l}_{m,n} = \mathbf{c}^{\dagger}_{m,n} e^{-\frac{1}{4}t^2_{mk} - \frac{1}{4}\omega^2_{nl} - \frac{1}{2}i\omega_{nl}(t_m + t_k)} \mathbf{L}^{\omega_{nl}+it_{mk}} \mathbf{U}^{-\omega_{nl}+it_{mk}} \mathbf{c}_{k,l}. \tag{5.157}$$

For the general complete FHG TFR lattice cube the overlap matrices we have select $\mathbf{c}_{i,j} = \hat{\mathbf{e}}_k$ and $\mathbf{c}_{l,m} = \hat{\mathbf{e}}_n$, so that $\mathbb{W}^{k,l}_{m,n}$ can be written as

$$\mathbb{W}^{i,j,k}_{l,m,n} = \hat{\mathbf{e}}^T_n e^{-\frac{1}{4}t^2_{li} - \frac{1}{4}\omega^2_{mj} - \frac{1}{2}i\omega_{mj}(t_l + t_i)} \mathbf{L}^{\omega_{mj}+it_{li}} \mathbf{U}^{-\omega_{mj}+it_{li}} \hat{\mathbf{e}}_k \tag{5.158}$$

Unfortunately equality cannot be proved, but it can only be hoped that the matrices may be similar[1]. To prove that, $\mathbb{W}^{k,l}_{m,n} \simeq \mathbb{T}^{k,l}_{m,n}$, explicit use is made of Corollary 5.4.8 and the following theorem from linear algebra. The Lemmas and the two Corollaries and resulting Theorem 5.4.9 are specific to this FHG TFR and therefore novel to this thesis. In the following corollaries we use the following definitions (we list all the relations for convenience)

$$z = \omega_{nl} + it_{mk} \tag{5.159}$$

$$-iz = t_{mk} - i\omega_{nl} \tag{5.160}$$

$$iz = -t_{mk} + i\omega_{nl} \tag{5.161}$$

$$z^* = \omega_{nl} - it_{mk} \tag{5.162}$$

$$-z^* = -\omega_{nl} + it_{mk} \tag{5.163}$$

$$-iz^* = -t_{mk} - i\omega_{nl} \tag{5.164}$$

Substituting Eq. (5.159) and Eq. (5.163) into Eq. (5.157), we have,

$$\mathbf{L}^{\omega_{nl}+it_{mk}} \mathbf{U}^{-\omega_{nl}+it_{mk}} = \mathbf{L}^z \mathbf{U}^{-z^*}. \tag{5.165}$$

From Eq. (5.156), and substituting Eq. (5.164) and Eq. (5.160), we have,

$$\mathbf{L}^{-t_{mk}-i\omega_{nl}} \mathbf{U}^{t_{mk}-i\omega_{nl}} = \mathbf{L}^{-iz^*} \mathbf{U}^{-iz}. \tag{5.166}$$

---

[1] Similarity between two matrices is equivalent to a bases transformation

Another important property is that for all, $z \in \mathbb{C}$,

$$\boxed{(\mathbf{L}^{z})^{\dagger} = \mathbf{U}^{z^*}} \tag{5.167}$$

In terms of this notation Eq. (5.157) becomes,

$$\boxed{\left[\mathbb{W}^{k,l}_{\ \ m,n}\right] = e^{-\frac{1}{4}t_{mk}^{2}-\frac{1}{4}\omega_{nl}^{2}-\frac{1}{2}i\omega_{nl}(t_m+t_k)}\mathbf{L}^{z}\mathbf{U}^{-z^*}} \tag{5.168}$$

and Eq. (5.156),

$$\boxed{\left[\mathbb{T}^{k,l}_{\ \ m,n}\right] = e^{-\frac{1}{4}t_{mk}^{2}-\frac{1}{4}\omega_{ln}^{2}-\frac{1}{2}i\omega_{nl}(t_m+t_k)}\mathbf{L}^{-iz^*}\mathbf{U}^{-iz}} \tag{5.169}$$

We specifically add the square parentheses in Eq. (5.168) and Eq. (5.169) to indicate that, without the selection vectors $\mathbf{c}_{k,l}$, that they no longer are matrix elements, but have become matrices in their own right. We now define a few theorems, definitions, lemmas to try and find a possible relationship between the two overlap matrices in $\left[\mathbb{W}^{k,l}_{\ \ m,n}\right]$and $\left[\mathbb{T}^{k,l}_{\ \ m,n}\right]$.

Theorem 5.4.1. *Given any matrix,* $\mathbf{A} \in \mathbb{C}^{n\times n}$, *the associated eigenvalues, trace, determinant and abstract inner product are all invariant under a similarity transformation.*

Definition 5.4.2. Two matrices, $\mathbf{A}, \mathbf{B} \in \mathbb{C}^{n\times n}$ are similar, $\mathbf{A} \simeq \mathbf{B}$, if there exist a, $\mathbf{C} \in GL(n, \mathbb{C})$, $\det \mathbf{C} \neq 0$ and $\mathbf{A} = \mathbf{C}\mathbf{B}\mathbf{C}^{-1}$, i.e., are equal by means of a similarity transformation.

Lemma 5.4.3. *Given any,* $\mathbf{A}, \mathbf{B}, \mathbf{C}, \mathbf{D} \in \mathbb{C}^{n\times n}$ *none of them equal to each other, then if,* $\mathbf{A} \simeq \mathbf{B}$ *and* $\mathbf{C} \simeq \mathbf{D}$, *then the matrix product,* $\mathbf{AC} \simeq \mathbf{BD}$, *if and only if they are similar by means of the same,* $\mathbf{E} \in GL(n, \mathbb{C})$, $\det \mathbf{E} \neq 0$ *and* $\mathbf{A} = \mathbf{E}\mathbf{B}\mathbf{E}^{-1}$.

Proof. Since, $\mathbf{A} \simeq \mathbf{B}$, there exists, $\mathbf{M} \in GL(n, \mathbb{C})$, $\det \mathbf{M} \neq 0$ and $\mathbf{A} = \mathbf{M}\mathbf{B}\mathbf{M}^{-1}$. Similarly, since, $\mathbf{C} \simeq \mathbf{D}$ there exists a $\mathbf{N} \in GL(n, \mathbb{C})$, $\det \mathbf{N} \neq 0$ and $\mathbf{C} = \mathbf{N}\mathbf{D}\mathbf{N}^{-1}$. Now the matrix product is given by,

$$\mathbf{AC} = \left(\mathbf{M}\mathbf{B}\mathbf{M}^{-1}\right)\left(\mathbf{N}\mathbf{D}\mathbf{N}^{-1}\right) = \mathbf{M}\mathbf{B}\left(\mathbf{M}^{-1}\mathbf{N}\right)\mathbf{D}\mathbf{N}^{-1}.$$

Now this will be similar to $\mathbf{BD}$, if and only if, $\mathbf{M}^{-1}\mathbf{N} = \mathbf{I}$, which implies by the uniqueness of matrix inverses that,$\mathbf{N} = \mathbf{M}$.

□

As simple as the above Lemma 5.4.3 may appear, it is crucial to adhere to it in the product of similar matrices. It is extremely easy to fall into a trap by using similar matrices and then assuming they are similar by similarity, even though they are similar by different matrices and therefore not similar.

It is important to note that the matrix action of a similarity transformation inherently has a *direction*, i.e.,

$$\mathbf{A} = \mathbf{M}\mathbf{B}\mathbf{M}^{-1},$$

and the inverse,

$$\mathbf{B} = \mathbf{M}^{-1}\mathbf{A}\mathbf{M}.$$

Lemma 5.4.4. *For all $z \in \mathbb{C}$ and $\mathbf{L}$, ($\mathbf{U}$) the lower (upper) triangular Pascal matrix, then, $\mathbf{L}^z \simeq \mathbf{L}^{iz}$, ($\mathbf{U}^z \simeq \mathbf{U}^{-iz}$), with identical similarity transformations, $\mathbf{F}$, which is an unitary matrix, i.e., $\mathbf{F}\mathbf{F}^\dagger = \mathbf{F}^\dagger\mathbf{F} = \mathbf{I}$.*

Proof. Construct,

$$\mathbf{F} = \begin{bmatrix} 1 & 0 & 0 & 0 & \cdots & 0 \\ 0 & i & 0 & 0 & \cdots & 0 \\ 0 & 0 & -1 & 0 & \cdots & 0 \\ 0 & 0 & 0 & -i & \vdots & \vdots \\ \vdots & \vdots & \vdots & \ddots & \ddots & \end{bmatrix} = \text{diag}(i^k)_{k=0}^{N-1}, \tag{5.170}$$

and, $\mathbf{F}^\dagger = \text{diag}((-i)^k)_{k=0}^{N-1}$. Then, $\mathbf{F}\mathbf{F}^\dagger = \mathbf{F}^\dagger\mathbf{F} = \mathbf{I}$. Then,

$$\mathbf{L}^z \simeq \mathbf{F}\mathbf{L}^z\mathbf{F}^\dagger = \mathbf{L}^{iz},$$

$$\mathbf{U}^z \simeq \mathbf{F}\mathbf{U}^z\mathbf{F}^\dagger = \mathbf{U}^{-iz}.$$

□

Lemma 5.4.4 shows that the forward similarity action of the matrix, $\mathbf{F}$, is, $\mathbf{L}^z \to \mathbf{L}^{iz}$, i.e., to multiply the exponent with the imaginary number, i, and that its action on, $\mathbf{U}^z \to \mathbf{U}^{-iz}$, i.e., to multiply the exponent with, $-i$.

Lemma 5.4.5. *For all, $x \in \mathbb{R}$ and $\mathbf{L}$, ($\mathbf{U}$) the lower (upper) triangular Pascal matrix then, $\mathbf{L}^{-x} \simeq \mathbf{L}^x$, ($\mathbf{U}^{-x} \simeq \mathbf{U}^x$), with the similarity transformation satisfying, $\mathbf{G}^2 = \mathbf{I}$. Furthermore for, $z \in \mathbb{C}$, then, $\mathbf{L}^z \simeq \mathbf{L}^{-z}$ and $\mathbf{L}^{z^*} \simeq \mathbf{L}^{-z^*}$. ($\mathbf{U}^z \simeq \mathbf{U}^{-z}$ and $\mathbf{U}^{z^*} \simeq \mathbf{U}^{-z^*}$).*

Proof. Here $\mathbf{G} = \text{diag}((-1)^k)_{k=0}^{k=N-1}$. □

The above Lemma 5.4.5 shows that the similarity action of the matrix, $\mathbf{G}$, is $\mathbf{L}^z \to \mathbf{L}^{-z}$ ($\mathbf{U}^z \simeq \mathbf{U}^{-z}$), i.e., to multiply the exponent with -1.

Lemma 5.4.6. *The following relationships hold between the* $\mathbf{F}$ *and* $\mathbf{G}$*:*

1. $\mathbf{G}^2 = \mathbf{I}$
2. $\mathbf{F}\mathbf{F}^\dagger = \mathbf{F}^\dagger\mathbf{F} = \mathbf{I}$
3. $\mathbf{G}\mathbf{F}\mathbf{G} = \mathbf{F}$
4. $\mathbf{G}\mathbf{F}^\dagger\mathbf{G} = \mathbf{F}^\dagger$
5. $\mathbf{F}^\dagger\mathbf{G}\mathbf{F}^\dagger = \mathbf{F}\mathbf{G}\mathbf{F} = \mathbf{I}$
6. $\mathbf{F}^2 = (\mathbf{F}^\dagger)^2 = \mathbf{G}$
7. $[\mathbf{F}, \mathbf{G}] = \left[\mathbf{F}^\dagger, \mathbf{G}\right] = \mathbf{0}$
8. $\mathbf{F}^* = \mathbf{F}^\dagger$

The proof of this Lemma 5.4.6 is a simple exercise in matrix multiplication. These three Lemmas, however, imply the following Corollary 5.4.7.

Corollary 5.4.7. *For all* $z \in \mathbb{C}$ *and* $\mathbf{L}$*, (*$\mathbf{U}$*) the lower (upper) triangular Pascal matrix, then with the forward similarity action of* $\mathbf{F}$*, i.e.,* $\mathbf{F}\mathbf{L}^z\mathbf{F}^\dagger = \mathbf{L}^{iz}$*, we have,* $\mathbf{L}^z \simeq \mathbf{L}^{iz}$*,* $\mathbf{L}^{-z} \simeq \mathbf{L}^{-iz}$ *and* $\mathbf{L}^{z^*} \simeq \mathbf{L}^{iz^*}$*,* $\mathbf{L}^{-z^*} \simeq \mathbf{L}^{-iz^*}$*. With the additional action of* $\mathbf{G}$*, (which is direction independent due property 6), the two sets become individually similar. For the upper triangular Pascal matrix with forward action of* $\mathbf{F}$*, we have* $\mathbf{U}^z \simeq \mathbf{U}^{-iz}$*,* $\mathbf{U}^{-z} \simeq \mathbf{U}^{iz}$ *and* $\mathbf{U}^{z^*} \simeq \mathbf{U}^{-iz^*}$*,* $\mathbf{U}^{-z^*} \simeq \mathbf{U}^{iz^*}$*. With the additional action of* $\mathbf{G}$*, the two sets become individually similar.*

Proof. The similarities are easy enough to proof, but due to commutativity of the lower triangular Pascal matrix,

$$\mathbf{L}^z = \mathbf{L}^{x+iy} = \mathbf{L}^x\mathbf{L}^{iy}. \tag{5.171}$$

Furthermore if, $\mathbf{A} \simeq \mathbf{B}$, then $\exists \mathbf{C} \in GL(n, \mathbb{C})$, such that, $\mathbf{A} = \mathbf{C}\mathbf{B}\mathbf{C}^{-1}$, then for any, $\mathbf{D} \in GL(n, \mathbb{C})$, we have, $\mathbf{D}\mathbf{A} = \mathbf{D}\mathbf{C}\mathbf{B}\mathbf{C}^{-1}$. This shows as that,

$$\mathbf{L}^{z^*} = \mathbf{L}^{x-iy} = \mathbf{L}^x\mathbf{G}\mathbf{L}^{iy}\mathbf{G}.$$

By Lemma 5.4.3 this not similar to $\mathbf{L}^z$, i.e.,

$$\mathbf{L}^z \not\simeq \mathbf{L}^{z^*},$$

and a similar result for the upper triangular Pascal matrices.

□

The above Corollary 5.4.7 shows that complex conjugation splits the Pascal matrices into two groups.

Corollary 5.4.8. *For all, $z \in \mathbb{C}$ and $\mathbf{L}$, ($\mathbf{U}$) the lower (upper) triangular Pascal matrix then, $\mathbf{L}^z\mathbf{U}^{-z^*} \simeq \mathbf{L}^{iz}\mathbf{U}^{iz^*}$.*

Proof. Note that in the matrix products,

$$\mathbf{L}^z\mathbf{U}^{-z^*},$$

and fall into each of the different categories,

$$\mathbf{L}^{-iz^*}\mathbf{U}^{-iz}.$$

This can easily be remedied by taking the complex conjugate of the second equation,

$$\left(\mathbf{L}^{-iz^*}\mathbf{U}^{-iz}\right)^* = \mathbf{L}^{iz}\mathbf{U}^{iz^*}.$$

A direct consequence of the previous Corollary 5. 4. 7 is that by the forward action of $\mathbf{F}$ that

$$\mathbf{L}^z\mathbf{U}^{-z^*} \simeq \mathbf{L}^{iz}\mathbf{U}^{iz^*} = \left(\mathbf{L}^{-iz^*}\mathbf{U}^{-iz}\right)^*.$$

□

Now we see by Corollary 5.4.8 that by the inclusion of the exponential factor in Eq. (5.168) and Eq. (5.169) that

Theorem 5.4.9. *The spectral and temporal overlap matrices are related by the forward action of $\mathbf{F}$ by,*

$$\left[\mathbb{W}^{k,l}_{m,n}\right] \simeq \left[\mathbb{T}^{k,l}_{m,n}\right]^*. \tag{5.172}$$

for all m, n and k, l.

Proof. Direct consequence of Corollary 5.4.8 and the previous Lemmas.

□

This is a rather a reverse way to prove our final Theorem 5.4.9, but the various Lemmas and Corollaries are all necessary for the proof, so that the proof leads to the Theorem 5.4.9. Apparently this roundabout way is how most mathematical theorems are established. Now, this relationship gives us an indication how to actually choose our selection coefficients, $\mathbf{c}^\dagger_{m,n}$.

5.5. Introduction to Frame Theory

The HG basis vectors have essentially this additional freedom of the choice of the basis coefficient vectors, $\mathbf{c}_{m,n}$, which might be very useful. The only prerequisite is that the selected basis coefficient matrix, $\mathbf{C} = \left[\mathbf{c}^T_{m,n}\right]$, with $\dim \mathbf{C} = \sqrt{N} \times \sqrt{N}$, must ensure that the overlap matrix, $\mathbb{T}$, is invertible. The fact that only one column in the $\mathbf{C}$ matrix is non-zero for the Neumann TFR, given that if it were possible to factorize the constant coefficients and Pascal matrices in two, is probably the origin of the ill-conditioning of the von Neumann overlap matrix. This allows for great analytical latitude of this TFR and the authors, as yet, have not utilized to its full potential. A diagonal plane slice of the HG basis resulting in a diagonal plane section will definitely exploit the orthonormality of the HG polynomials. A generalization of the idea of a basis to sets which may be linearly dependent is known as a frame of a vector space V with an inner product. Since the HG basis is an overcomplete basis the theory of frames is the natural setting for any further study [34, 123]. Figure 5.3 represents the HG basis as a cube. In Figure 5.3(a) taking the front face of the cube would retrieve the von Neumann basis, whereas Figure 5.3(b) and Figure 5.3(c) would represent a spectral and temporal diagonal frame dissection, respectively, and, when projected to the front surface, then represents the TFR. This projection naturally occurs through the use of the overlap integrals (matrices), Eq. (5.149) and Eq. (5.154). The TFR are then given by Eq. (5.107),

$$\boldsymbol{\mathcal{A}}_{m,s} = \sum_{k,l} \left[\mathbb{T}^{k,l}_{m,s}\right]^{-1} \int_{-\infty}^{\infty} \beta^*_{k,l}(t)\varepsilon(t)\, dt$$

, and Eq. (5.108)

$$\boldsymbol{\mathcal{A}}_{m,s} = \sum_{k,l} \left[\mathbb{W}^{k,l}_{m,s}\right]^{-1} \int_{-\infty}^{\infty} \tilde{\beta}^*_{k,l}(\omega)\tilde{\varepsilon}(\omega)\, d\omega.$$

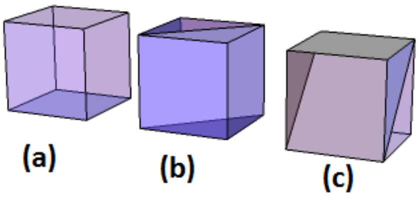

Figure 5.3.: (a) Front face of cube von Neumann and FHG basis (b) Vertical diagonal slice of cube FHG basis (c) Horizontal diagonal slice of cube FHG basis

For example, if we choose our frame to correspond with Figure 5.3(c) a horizontal diagonal slice of the FHG basis, then the basis coefficient matrix, $\mathbf{C} = \left[\mathbf{c}^T_{m,n}\right]$. has the following form for the temporal FHG basis,

$$\mathbf{c}^T_{m,n} = \hat{\mathbf{e}}^T_n,\ \forall m. \tag{5.173}$$

From the temporal FHG basis Eq. (5.100),

$$\begin{aligned}
\beta_{m,n}(t) &= \mathbf{c}^T_{m,n} e^{it\omega_n} e^{-\frac{t_m^2}{4\sigma}+\frac{t_m t}{2\sigma}} \mathbf{L}^{-2t_m/\sqrt{2\sigma}} \mathbf{\Phi}(\frac{t}{\sqrt{2\sigma}}) \\
&= \hat{\mathbf{e}}^T_n e^{it\omega_n} e^{-\frac{t_m^2}{4\sigma}+\frac{t_m t}{2\sigma}} \mathbf{L}^{-2t_m/\sqrt{2\sigma}} \mathbf{\Phi}(\frac{t}{\sqrt{2\sigma}}) \\
&= e^{it\omega_n} e^{-\frac{t_m^2}{4\sigma}+\frac{t_m t}{2\sigma}} \mathbf{L}^{-2t_m/\sqrt{2\sigma}} e^{-\frac{t^2}{4\sigma}} C_n H_n(\frac{t}{\sqrt{2\sigma}}),
\end{aligned} \tag{5.174}$$

where we have made use of the definition of $\mathbf{\Phi}(t)$, in Eq. (5.45) and Eq. (5.46). The effect of this choice of frame on the overlap matrix Eq. (5.149) is,

$$\mathbb{T}^{k,l}_{m,n} = e^{-\frac{1}{8\sigma}t^2_{mk}-\frac{\sigma}{2}\omega^2_{ln}-\frac{1}{2}i\omega_{nl}(t_m+t_k)} \left(\hat{\mathbf{e}}^T_n \mathbf{L}^{-\frac{t_{mk}}{\sqrt{2\sigma}}-i\sqrt{2\sigma}\omega_{nl}} \mathbf{U}^{\frac{t_{mk}}{\sqrt{2\sigma}}-i\sqrt{2\sigma}\omega_{nl}} \hat{\mathbf{e}}_l \right). \tag{5.175}$$

It is important to note that the unit basis vectors, $\hat{\mathbf{e}}_n$ and $\hat{\mathbf{e}}_l$, is indexed on the spectral indices, n and l. The effect of premultiplying the overlap matrix is in effect selecting the n, l, component of the matrix. The premultiplied transposed unit vector selects the row and the post multiplied vector select the column component. The temporal overlap matrix then becomes,

$$\mathbb{T}^{k,l}_{m,n} = e^{-\frac{1}{8\sigma}t^2_{mk}-\frac{\sigma}{2}\omega^2_{ln}-\frac{1}{2}i\omega_{nl}(t_m+t_k)} \left(\mathbf{L}^{-\frac{t_{mk}}{\sqrt{2\sigma}}-i\sqrt{2\sigma}\omega_{nl}} \mathbf{U}^{\frac{t_{mk}}{\sqrt{2\sigma}}-i\sqrt{2\sigma}\omega_{nl}} \right)_{n,l}. \tag{5.176}$$

A note of caution must be highlighted here. In defining the Hermite-Gauss polynomial in Eq. (5.45) and Eq. (5.46) we explicitly defined that the dimension of the Hermite polynomials start at 0 and step through $\sqrt{N}-1$ dimension. The time indices and inherited from the von Neumann basis Eq. (3.65),

$$t_m = -T/2 + (m - \frac{1}{2})\Delta t \quad m = 1, \cdots, K = \sqrt{N}.$$

The same applies to the spectral indices obtained from Eq. (3.66), (See also Eq. (5.97) and the discussion given there),

$$\omega_n = \omega_{min} + (n - \frac{1}{2})\Delta\omega \quad n = 1, \cdots, K = \sqrt{N}.$$

For the frame that corresponds with Figure 5.3(b), the use of the spectral FHG basis is more appropriate. Using Eq. (5.100),

$$\tilde{\beta}_{m,n}(\omega) = \mathbf{c}^T_{m,n} e^{-it_m(\omega-\omega_n)} e^{-\sigma\omega^2_{no}+2\sigma(\omega-\omega_o)\omega_{no}} \mathbf{L}^{-2\sqrt{2\sigma}\omega_{no}} \tilde{\mathbf{\Phi}}[\sqrt{2\sigma}(\omega-\omega_o)],$$

and choosing the basis coefficient frame,

$$\mathbf{c}^T_{m,n} = \hat{\mathbf{e}}^T_m,\ \forall n, \tag{5.177}$$

we obtain,

$$\begin{aligned}\tilde{\beta}_{m,n}(\omega) &= \mathbf{c}^T_{m,n} e^{-it_m(\omega-\omega_n)} e^{-\sigma\omega^2_{no}+2\sigma(\omega-\omega_o)\omega_{no}} \mathbf{L}^{-2\sqrt{2\sigma}\omega_{no}} \tilde{\mathbf{\Phi}}[\sqrt{2\sigma}(\omega-\omega_o)] \\ &= \hat{\mathbf{e}}^T_m e^{-it_m(\omega-\omega_n)} e^{-\sigma\omega^2_{no}+2\sigma(\omega-\omega_o)\omega_{no}} \mathbf{L}^{-2\sqrt{2\sigma}\omega_{no}} \tilde{\mathbf{\Phi}}[\sqrt{2\sigma}(\omega-\omega_o)] \\ &= e^{-it_m(\omega-\omega_n)} e^{-\sigma\omega^2_{no}+2\sigma(\omega-\omega_o)\omega_{no}} \mathbf{L}^{-2\sqrt{2\sigma}\omega_{no}} e^{-\sigma(\omega-\omega_o)^{2-}} C_m H_m[\sqrt{2\sigma}(\omega-\omega_o)],\end{aligned} \tag{5.178}$$

and using Eq. (5.178) the resulting effect on the spectral overlap matrix Eq. (5.154) is,

$$\mathbb{W}^{k,l}_{m,n} = e^{-\frac{1}{8\sigma}t^2_{mk}-\frac{\sigma}{2}\omega^2_{ln}-\frac{1}{2}i\omega_{ln}(t_m+t_k)} \left(\mathbf{L}^{-\sqrt{2\sigma}\omega_{ln}-i\frac{t_{mk}}{\sqrt{2\sigma}}} \mathbf{U}^{\sqrt{2\sigma}\omega_{ln}-i\frac{t_{mk}}{\sqrt{2\sigma}}}\right)_{m,k}. \tag{5.179}$$

Note that here the indexing is over the temporal indices, m and k. With the correct scaling we find that (See Eq. (6.2))

$$\sqrt{2\sigma}\omega_{ln} = \frac{t_{ln}}{\sqrt{2\sigma}}. \tag{5.180}$$

5.6. Application Results

Since the advent of laser in the 1960's the selective control of molecular bonds were realized with various complications (please also refer to Eq. (Chapter 4) were this also discussed). The importance of ultra-short laser pulses was soon recognized. Two main mechanisms for molecular control were developed, namely the pump-dump scheme of Tannor and Rice [47, 48] and the optical quantum interference of Brumer and Shapiro [44, 45] (cf. Eq. (Section 1.2)). One of the pioneer's of the field of femtochemistry is A. H. Zewail [132, 133, 134] An extensive overview of quantum control techniques is given in [1]. A simulation program of an open-loop quantum coherent control of an octahedral molecule's interaction with IR ultra-short laser pulse were developed in [55, 39, 135]. The simulation involves a femtosecond

Gaussian IR laser pulse passing through a 4f-SLM (Spatial Light Modulator) pulse shaper [136] to coherently shape the pulse to produce the maximum statistical population of a selected rovibrational level of the von Neumann density matrix $\rho(t)$ of the octahedral molecule under consideration.

A 640 pixel f4-SLM was simulated and therefore a corresponding $625 = 25 \times 25$ von Neumann lattice was chosen. The IR active ν_3-rovibrational mode frequency levels of the octahedral molecule and there IR dipole symmetry forbidden transitions (dotted lines) are shown in Figure 5.4(a). Due to laser frequency offset, all other IR rovibrational interactions can be ignored. Including the quasi-continuum (QC) this results in 17 different energy levels and therefore a IR dipole interaction Hamiltonian of 17×17. The rovibrational levels are grouped together into $0, 1, 2, 3, 4$, QC population levels. Initially it is assumed that the molecule is in canonical Boltzmann quantum statistical distribution. A genetic algorithm optimization program is used to selectively maximize the second population level of the octahedral molecule by solving the time evolution Liouville-von Neumann equation in the Dirac-interaction picture,

$$i\hbar\frac{d}{dt}\rho_I(t) = \left[H_{ID}(t), \rho_I(t)\right], \tag{5.181}$$

where, $H_{ID}(t) = \exp\left(\frac{i}{\hbar}H_m t\right) H_I(t) \exp\left(-\frac{i}{\hbar}H_m t\right)$, and H_m, is the unperturbed molecular Hamiltonian and $H_I(t) = \chi\Re[\varepsilon_{slm}(t)]$, is the dipole interaction Hamiltonian matrix, $\varepsilon_{slm}(t)$, is the modulated electric field of the laser pulse after the SLM and, $\chi = \int \psi_a^* \mathbf{D} \cdot \hat{\epsilon}\psi_b \, d\tau$, is the interaction dipole matrix of the molecule (this corresponds to the long wavelength or dipole approximation and the rotating wave approximation). $\mathbf{D} = \sum_j q_j \mathbf{r}_j$, is the sum of the position vectors and charges of the nuclei of the molecule. The time evolution of the various ν_3-rovibrational population levels with the optimized electric field is shown in Figure 5.4(b). This is a typical result obtained from the optimal genetic algorithm control of the selective excitation of rovibrational levels, here the second rovibrational is selectively excited to about 87%, and is used to compare the various TFRs.

One of the effects of the SLM is to temporally broaden the initial Gaussian pulse from a 150 fs Full-Width-Half-Maximum (FWHM) to approximately 1.5 ps as can be seen in Figure 5.5(a). Concurrently, the SLM spectrally shapes the electric field. Figure 5.5(b) shows the re-sampled spectral field, required for the von Neumann and FHG bases, as well as indicating the transitions frequencies of the XY_6, ν_3-rovibrational levels in blue circles. The broad shape over the transition frequencies is indicative of the underlying coherent correlation excitation process.

Originally, Wigner [63] developed his transform in the quantum mechanics (QM) qp-space and is an invaluable transform for representing QM wave functions, cf.

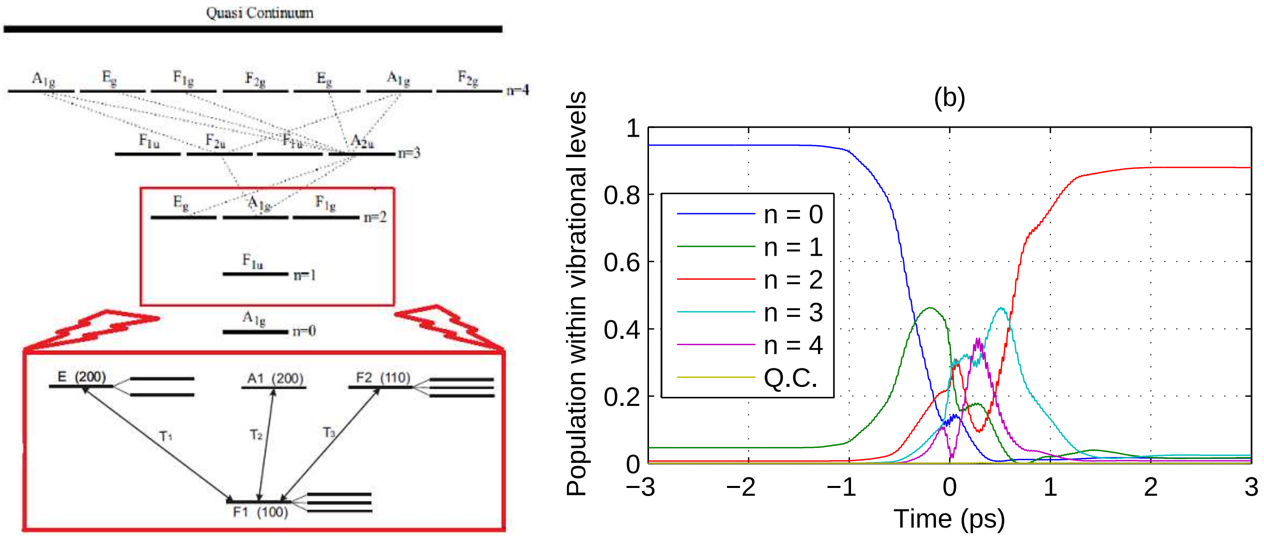

Figure 5.4.: XF_6 rovibrational energy levels with forbidden transitions shown in dashed lines. (b) Selective excitation of the XY_6 second ν_3-rovibrational population level.

Schleich [35] and Tannor [8]. Given a time signal, $\varepsilon(t)$, the *Wigner-Ville TFR* [65, 33] is defined as,

$$\boxed{\mathcal{W}_s(t,\nu) = \int_{-\infty}^{\infty} \varepsilon^*(t-\frac{\tau}{2})\varepsilon(t+\frac{\tau}{2})e^{-2\pi i\nu\tau}\,d\tau} \tag{5.182}$$

and the *Husimi TFR* [90] (originally, also in QM *qp*-space, see Schleich [35]), is the double convolution of the Wigner-Ville TFR with a Gaussian pulse,

$$\boxed{H_s(t,\nu;\alpha,\gamma) = \int_{-\infty}^{\infty}\int_{-\infty}^{\infty} G_{\alpha\gamma}(u-t,\theta-\nu))\mathcal{W}_s(u,\theta)\,du d\theta} \tag{5.183}$$

where,

$$F(t,\nu) = G_{\alpha\gamma}(t,\nu) = \frac{4}{\alpha}\exp\left[-\frac{1}{\alpha}\left(\frac{\nu^2}{\gamma^2}+4\gamma^2t^2\right)\right]. \tag{5.184}$$

Figure 5.6(a) depicts the Wigner-Ville TFR Eq. (5.182) of our representative signal. Clearly, the artifacts of the Wigner-Ville TFR can be seen here as negative values in a bilinear representation, appropriately earning it the name of a quasi-probability distribution. In Figure 5.6(b) the Husimi TFR Eq. (5.183) gets rid of the unwanted "negative" interference terms at the cost of smearing the signal somewhat.

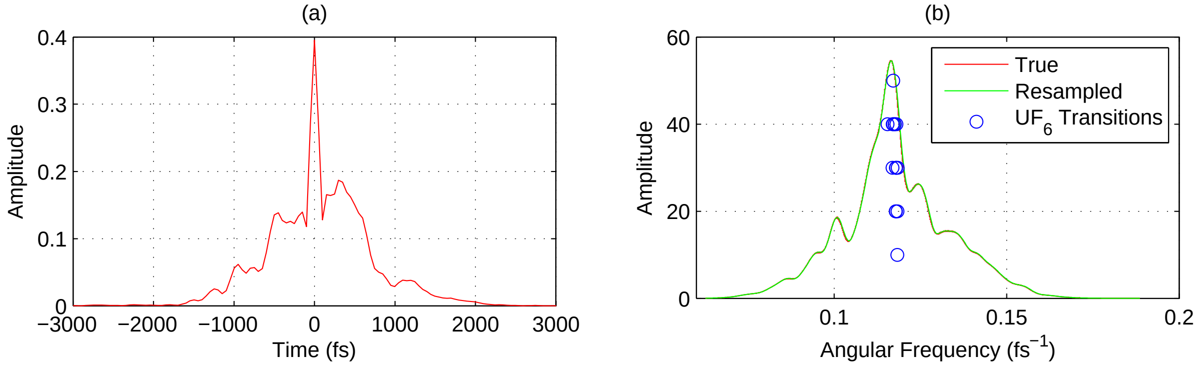

Figure 5.5.: (a) Temporal electric field (b) Spectral electric field showing the transitions frequencies the XY_6 ν_3-rovibrational levels in circles

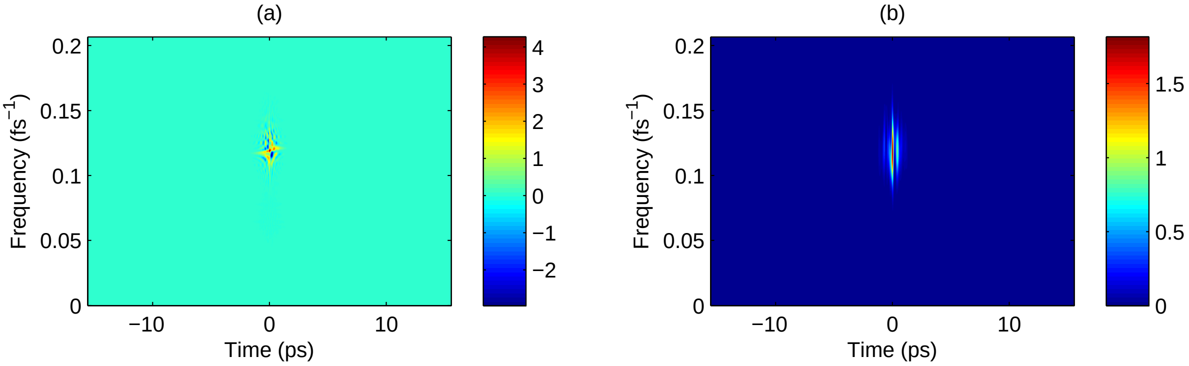

Figure 5.6.: (a) The Wigner-Ville TFR (b) The Husimi TFR

The von Neumann TFR Eq. (3.100) is shown in Figure 5.7(a) on a somewhat discrete 25x25 von Neumann lattice. The reconstructed spectral electric field Eq. (3.103) from the von Neumann TFR is given in Figure 5.7(b). The reconstruction was performed without using spectral periodic boundary conditions therefore one finds small recurring misfits to the true signal. In Dimler et al. [137], they have shown that the reconstruction is drastically improved by employing periodic boundary conditions.

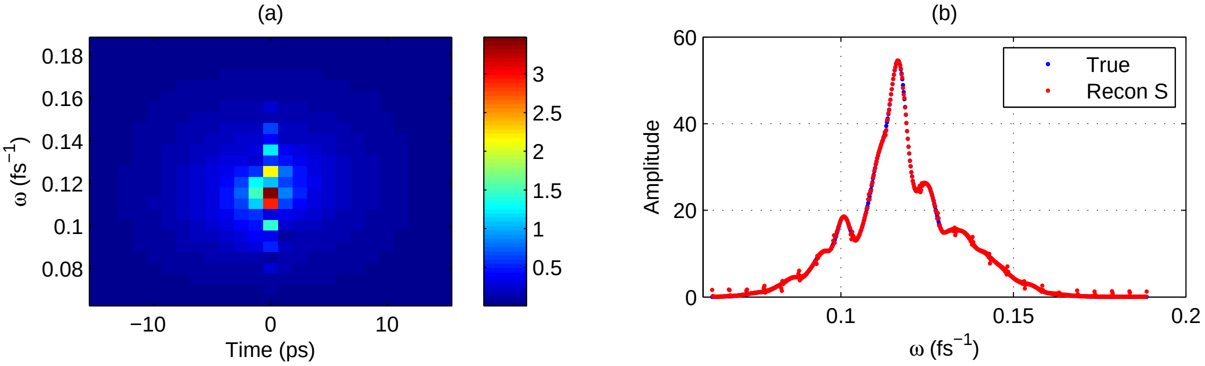

Figure 5.7.: (a) The von Neumann TFR (b) von Neumann spectral reconstruction of the electric field

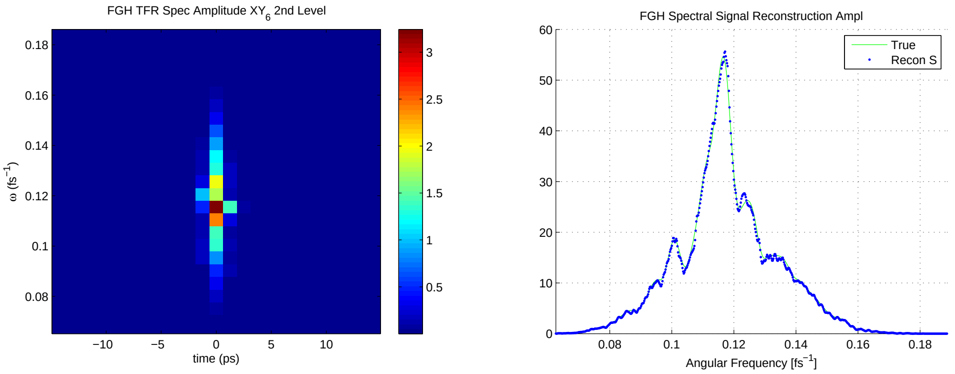

Figure 5.8.: (a) FHG TFR Amplitude (b) FHG spectral reconstruction of the electric field

The corresponding Fourier-Hermite-Gauss TFR is shown in Figure 5.8(a). Being an overcomplete basis one can conceive that the reconstruction of the spectral electric field be of a higher quality, which is shown in Figure 5.8(b) using Eq. (5.126). Although one could go on tirelessly showing all forms temporal and spectral amplitudes and phase plots of this TFR and compare it with various other TFRs, it is only the intention of the authors to show the operational applicability and to represent the mathematical detail of the FHG TFR.

Figure 5.9(a) shows the first 7 HG planes summed together and Figure 5.9(b) the spectral phase reconstruction. Figure 5.10(a) demonstrates the Fourier-Hermite-Gauss temporal reconstruction and Figure 5.10(b) Hermite-Gauss temporal phase reconstruction. Figure 5.11 and Figure 5.12 are included here for reference purposes and comparison with Figure 5.8, Figure 5.9 and Figure 5.10 as another example.

Firstly, they represent a different electric field signal, with virtually the same results as the electric field signal used in the previous figures. This illustrates the sensitivity of the process to amplitude and phase. Furthermore, they are all constructed from a spectral and temporal electric field signals of 625 data points. In the next Chapter 6, this electric field signal is used throughout as a reference signal.

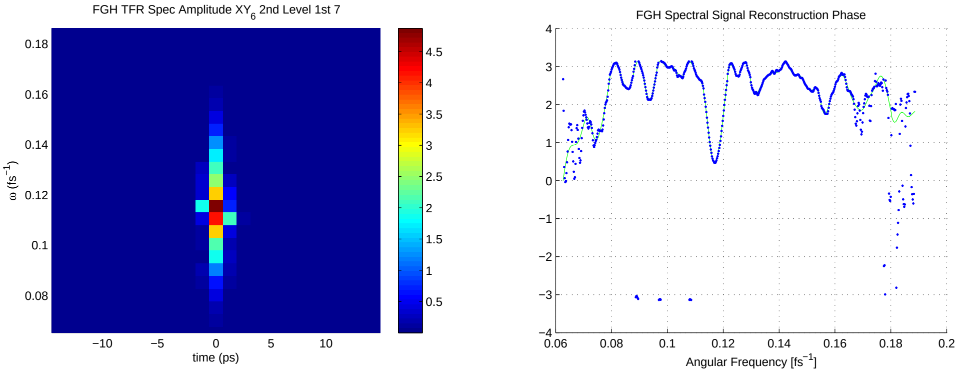

Figure 5.9.: (a) FHG TFR Amplitude First 7 (b) FHG spectral phase reconstruction

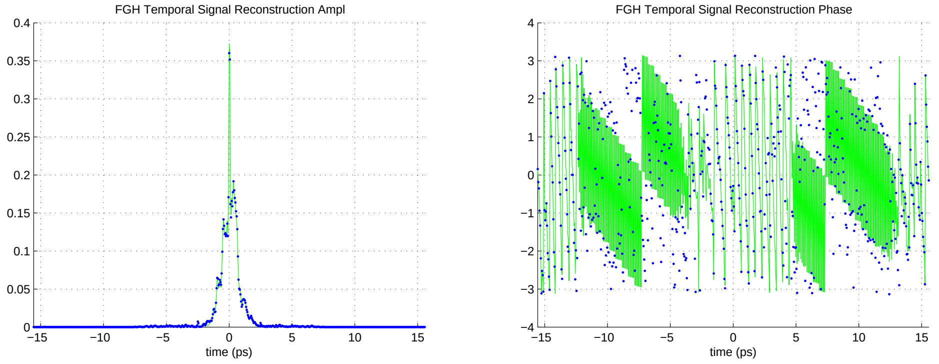

Figure 5.10.: (a) FHG temporal reconstruction (b) FHG temporal phase reconstruction

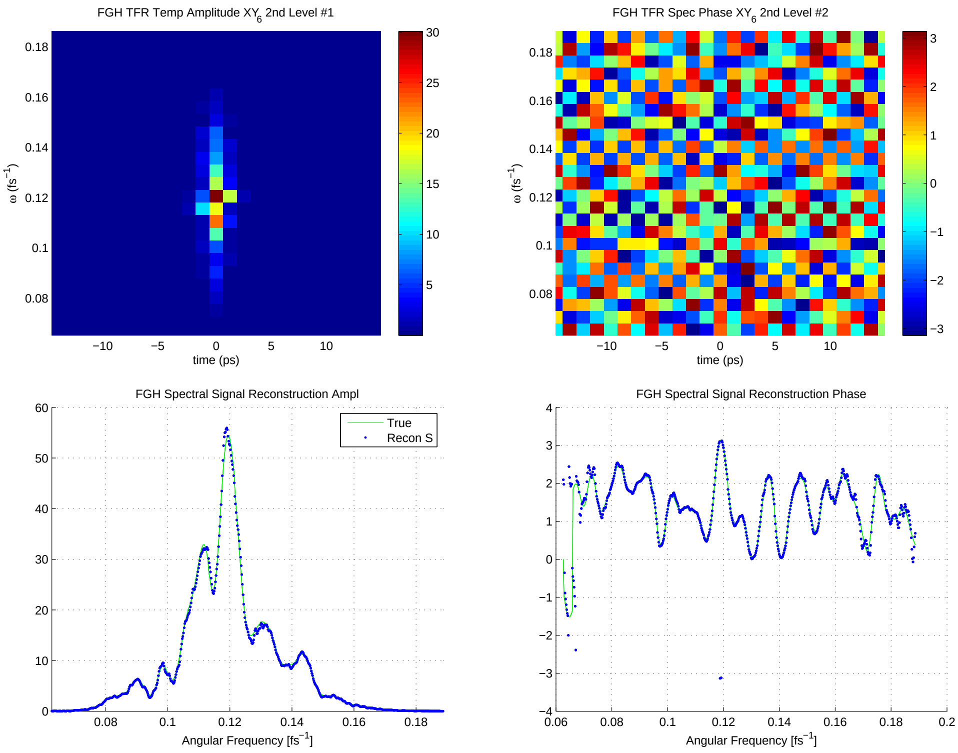

Figure 5.11.: (a) FHG TFR Amplitude (b) FHG TFR Phase (c) FHG Spectral Amplitude Reconstruction (d) FHG Spectral Phase Reconstruction

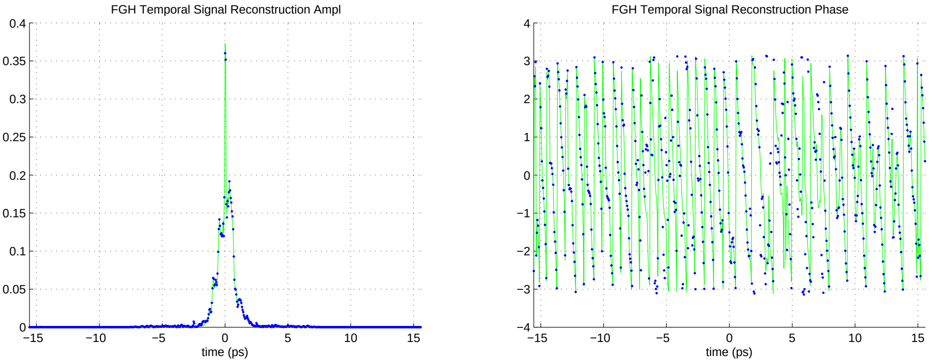

Figure 5.12.: (a) FHG Temporal Amplitude Reconstruction (b) FHG Temporal Phase Reconstruction

6. The Complete FHG TFR

6.1. Introduction

This Chapter originated as an outflow and extension to the previous Chapter 5, after trying to select a frame basis by the methods outlined in Section 5.5. While, using the full FHG basis allowed for faithful signal reconstruction, as illustrated in Figure 5.8(b), Figure 5.9(b), Figure 5.10(a), Figure 5.10(b), Figure 5.11(c), Figure 5.11(d), Figure 5.12(a) and Figure 5.12(b), to my shock and horror the frame methods worked awfully, for both the temporal and spectral frame choices. The results are shown in Section 6.2. By contrast, the simple addition of the spectral signal correlation cube of the first few HG planes, worked wonderfully as depicted in Figure 5.9.

This necessitated the calculation of the overlap matrices. The lower and upper triangular Pascal matrices, which proved so useful analytically, are unfortunately highly numerically unstable. They suffer from finite digit representation and as the dimension grows the elements explode. A major catastrophe. The calculation of the overlap matrices by means of FFTs where then accomplished, but at a numerical cost. In this method it was discovered that to actually determine the overlap matrices, it is necessary to double the bandwidths, which is described in Section 6.3 on periodicity and scaling. Without this doubling of the bandwidths, serious overlapping of the FHG bases occur at the edges of the von Neumann grid and just gets worse as the order of the HG increase. This is natural, since the support of the HG polynomials increase with their order.

Since the temporal and spectral signal reconstruction are magnificently performed by the methods given in Section 6.7, without even calculating an overlap matrix, it indicated that the complete FHG TFR lattice cube already contained all the necessary information. It was then deemed necessary to make a thorough investigation of the complete FHG TFR lattice cube, Section 6.4. One of the major advantages of introducing the Pascal matrices was, the then perceived numerical advantage of not having to calculate all the numerical intensive HG polynomials. As the temporal and spectral FHG bases are all just temporally and spectrally shifted, it was then recognized that only the central HG polynomial needs to be calculated and that the other HG polynomials can be generated by simply digitally shifting the polynomials as required. A further great numerical advantage and perception was achieved by unscaling FHG bases and signals, thereby placing the temporal and spectral bases on level playing fields. Applying Fourier properties, it was seen that we are actually calculating correlations. The background to the unscaled FHG signal correlation is given in Section 6.5. New functions were discovered to aid in the calculation of the correlations. This was conceptually seen so important that an alternative derivation of the unscaled signals is given in Subsection 6.5.1.

A thorough study is then performed of the complete FHG overlap matrices in Section 6.6. Thereafter numerical studies are done in Subsection 6.6.1 of the complete FHG bases correlation cube to effectively gain insight. A lot of interesting new results are revealed there.

The method employed here to reconstruct the temporal and spectral signals directly from the temporal and spectral FHG correlation lattice cubes is given in Section 6.7.

The rest of the chapter, in Section 6.8, is dedicated to the construction of a FHG TFR from the complete spectral and temporal FHG TFR lattice cubes. In developing this Chapter, the extent was totally underestimated. It cost an enormous great effort and so many new programs were written to test the theory. Too late the use of functional operators, as defined in Eq. (6.67), was discovered. This really highlights the essence of the techniques and would have greatly reduced the writing up. The reward of the insight and really starting to understand the techniques was maybe worth the effort.

6.2. TFR Frames

In Section 5.5 an outline of a method to select the basis selection vectors $\mathbf{c}_{m,n}$, defined in Eq. (5.59) and Eq. (5.62). In Figure 5.3 three cubes are shown representing the FHG lattice cubes. It is assumed that a simple reduction of the lattice cube, by a frame slice or sheet is necessary to reproduce the TFR of the FHG basis, accompanied with its much simplified overlap matrix, with the equivalent dimension of the von Neumann TFR. This was attempted and performed.

Figure 5.3(b) shows a vertical diagonal slice of the lattice cube FHG basis along the spectral vertical axis and stepping temporally. The correspond FHG selection vectors $\mathbf{c}_{m,n}$ are given in Eq. (5.177). Figure 6.1 represents the results of this spectral frame selection. They are atrocious. Firstly, one notes that the spectral and temporal TFRs do not resemble the spectral and temporal signals at all. Interestingly, with the inclusion of the overlap matrices, they once again have the same patterns. Strangely, the spectral and temporal reconstruction of the signals can still be performed, but extremely noisy. The spectral and temporal phase reconstructions are way off.

Figure 5.3(c) shows a horizontal diagonal slice of the lattice cube FHG basis and stepping spectrally from low frequencies to high. The corresponding FHG selection vectors are given in Eq. (5.173). This is what we call the bottom to top temporal frame. Figure 6.2 shows the results. It seems like some poor rotation has happened to the TFRs, relative to the spectral frame selection. The spectral and temporal signal reconstructions are just as noisy. The spectral phase reconstruction is better, but still poor.

It was then decided to check a horizontal diagonal slice of the lattice cube FHG basis and stepping spectrally from high frequencies to low. This is what we call the top to bottom temporal frame. Here the logic proceeded as follows. Since the zeroth order FHG is the just a Gaussian signal, it is best to take it is with the highest angular frequency. As one progresses into the HG planes, the HG polynomials each time comes with additional nodes, so that it is best to associate the lowest frequency with the highest order HG polynomial. Figure 6.3 depicts the various results. The TFRs improved so-so little, but is better than Figure 6.1 and Figure 6.2, if you use your imagination.

The conclusion is that the spectral and temporal TFRs of the various frames, utilizing the overlap matrices, are virtually the same, although deplorable. The signal amplitude reconstructions are very noisy, and the signal phase reconstructions are just not right. This warranted further research and investigation into the complete FHG TFR lattice cube.

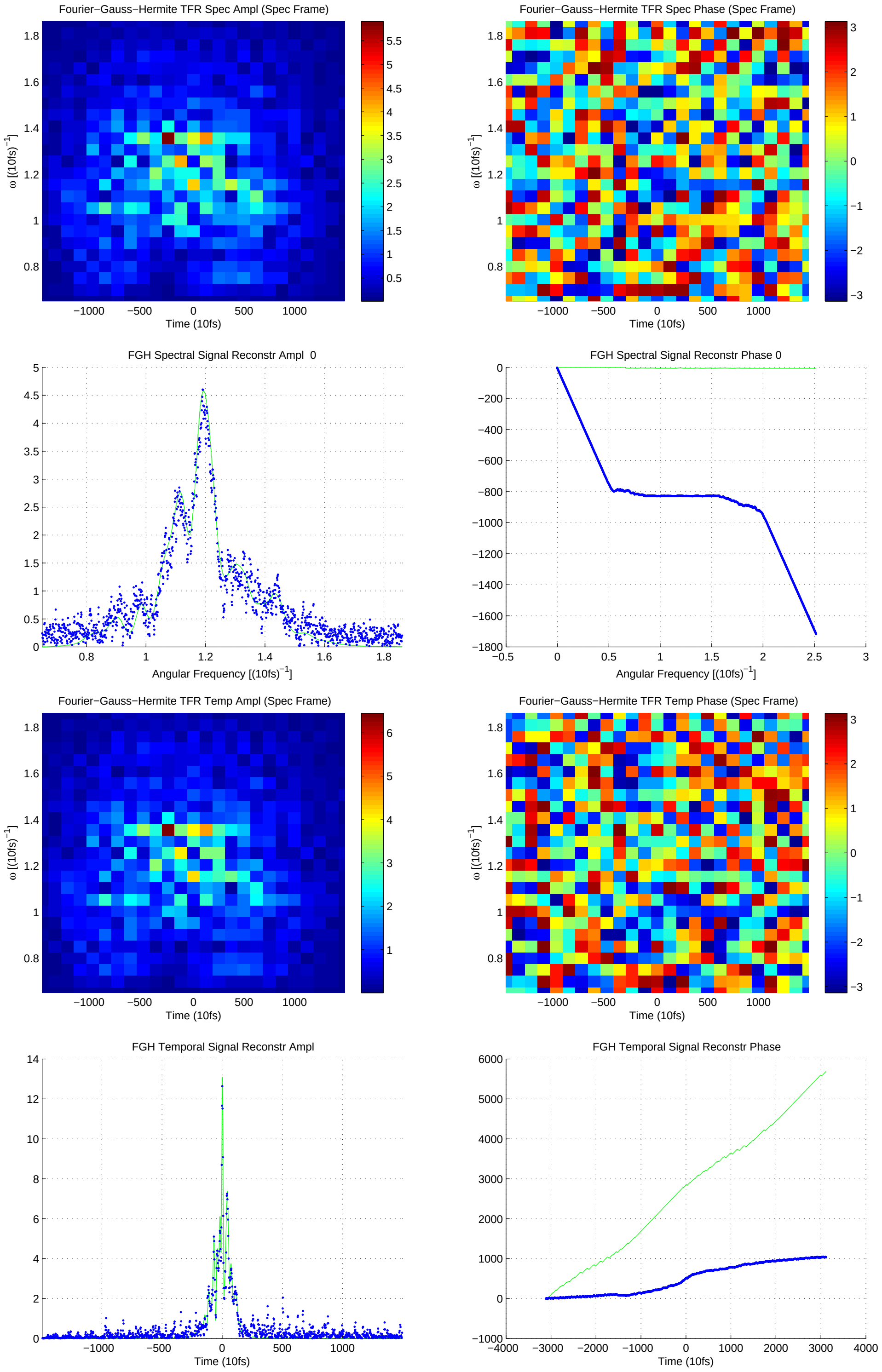

Figure 6.1.: FHG TFR of the Spectral Frame

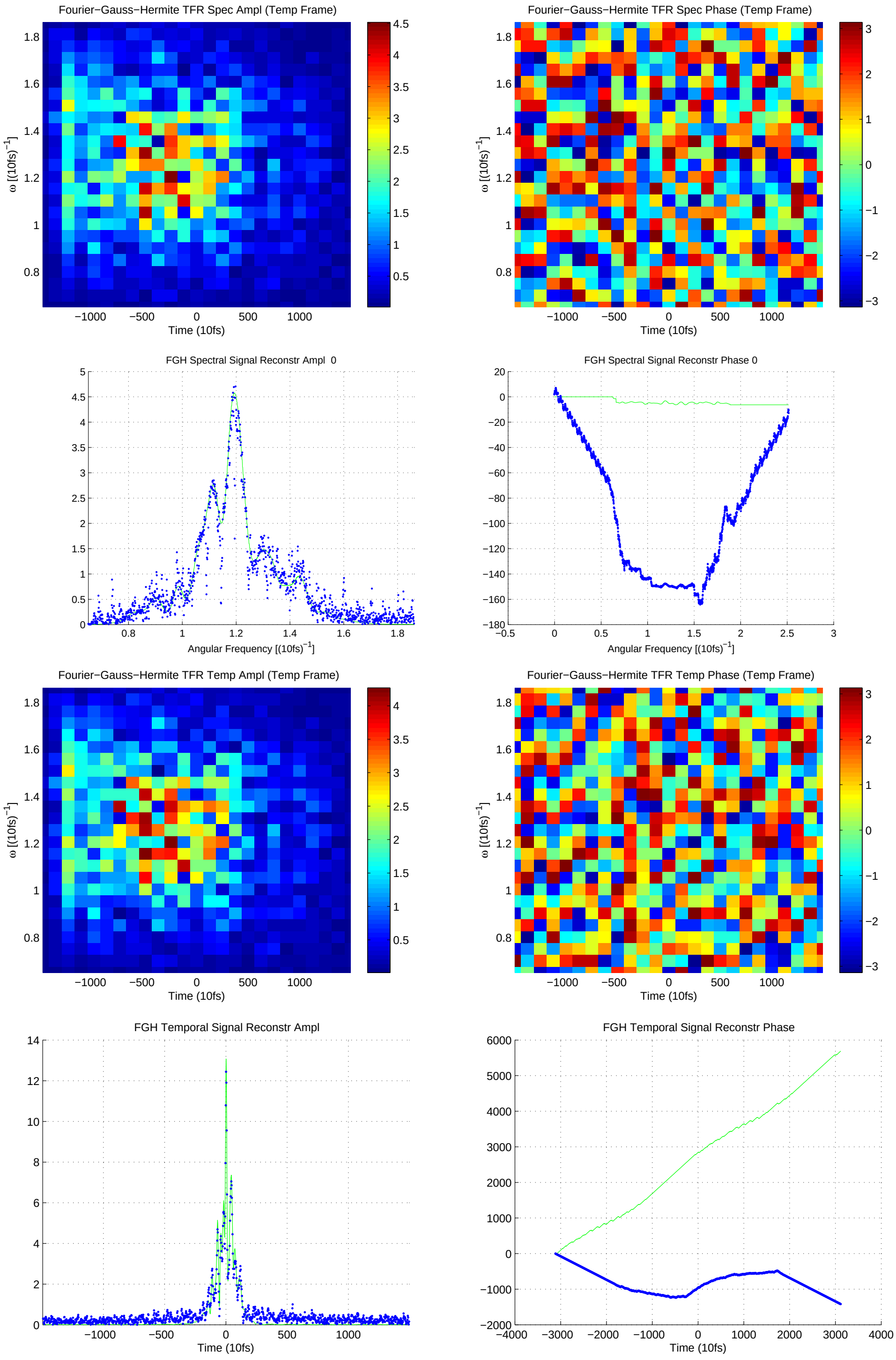

Figure 6.2.: FHG TFR of the Temporal Frame (Bottom to Top)

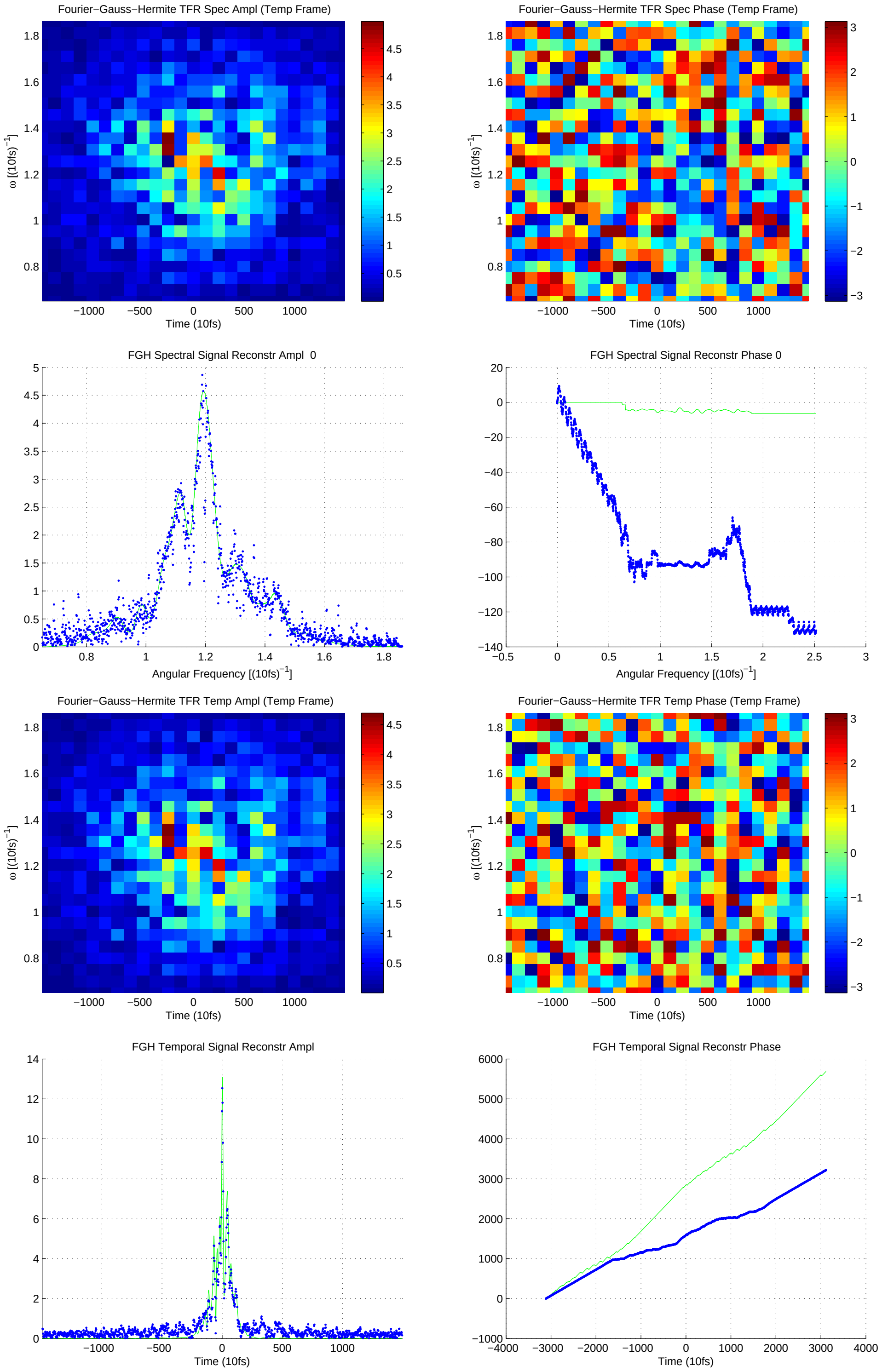

Figure 6.3.: FHG TFR of the Temporal Frame (Top to Bottom)

6.3. Periodicity and Scaling

Any real TFR application must necessary live in the confines of a discrete (digital) numerical algorithm. Traditionally, the Discrete Fourier Transform (DFT) is utilized to approximate a FT. A prerequisite for Fourier series analysis is that the signal, $f(t)$, must be periodic with period, T, i.e., $f(t+T) = f(t)$. The finiteness of the DFT inherently requires this condition on the sampled, $\hat{f}(t)$, but automatically by the inverse FT this periodicity is also imposed onto, $\hat{F}(\omega)$. Essentially a FFT transform produces a pair of periodic digital functions $\hat{f}(t) = \hat{f}(t+T)$ and $\hat{F}(\omega) = F(\omega + \Omega)$. The Nyquist-Shannon sampling theorem determines the maximum bandwidth, $\Omega = 2\pi/\delta t$, (support$[-\frac{\Omega}{2}, \frac{\Omega}{2}\ ]$). The reciprocal (inverse) Nyquist-Shannon determines the timespan, $T = 2\pi/\delta\omega$, (support$[-\frac{T}{2}, \frac{T}{2}]$) of the signal where, $\delta\omega$, is the angular frequency sampling rate. For a signal, $\hat{f}(t_i) = f[i]$, digitally sampled at, δt, with timespan, $T = N\delta t$, we have the corresponding DFT, $\hat{F}(\omega_i)$, with angular frequency bandwidth, $\Omega = N\delta\omega$. Shannon showed, Section A.10, that sampling signals that do not have baseband components, e.g., a laser pulse with bandpass, involves the width of the non-zero frequency interval, i.e., the bandpass width, as opposed to its highest frequency component, exactly as is done herein. The scaling parameter is defined by,

$$\sigma = \frac{T}{2\Omega} = \frac{\delta t}{2\delta\omega}. \tag{6.1}$$

The total phase space is given by, $\Omega \times T = 2\pi N$. On the von Neumann lattice we have, $K = \Omega/\Delta\omega = T/\Delta t$, and $K^2 = N$, i.e., $\Delta t \Delta\omega = 2\pi$, and $\sigma = \frac{\Delta t}{2\Delta\omega}$, therefore,

$$\Delta t/\sqrt{2\sigma} = \sqrt{2\pi} = \sqrt{2\sigma}\Delta\omega. \tag{6.2}$$

The maximum steplength is then, $\frac{K-1}{2}\sqrt{2\pi}$. To obtain a normalized scaled problem the time and angular frequency must be scaled in such a fashion, say, κ_t[fs] and κ_ω[fs^{-1}], $T = \kappa_t T_s$ and $\Omega = \kappa_\omega \Omega_s$, to ensure that the σ parameter is scale independent. This insures that the all problems can in essence be compared on the same footing.

For the von Neumann TFR, [98, 78] has shown that superior signal reconstruction is achieved by imposing periodic constraints on the representation basis functions, i.e., $\alpha_{m,n}(t) = \alpha_{m,n}(t+T)$ and $\tilde{\alpha}_{m,n}(\omega) = \tilde{\alpha}_{m,n}(\omega+\Omega)$. Similar periodic constraints can also be imposed on the HG TFR basis vectors, i.e., $\beta_{m,n}(t) = \beta_{m,n}(t+T)$ and $\tilde{\beta}_{m,n}(\omega) = \tilde{\beta}_{m,n}(\omega+\Omega)$.

The Nyquist-Shannon sampling theorem, Section A.10, only gives a minimum sampling rate to represent a signal with the maximum frequency bandwidth. It is general practice in DSP to actually oversample and to double (sometimes the higher the better, but often unnecessary) the sampling frequency. To comply with requirements of Eq. (6.1) and Eq. (6.2) this also means that the sampling time T must be doubled.

In fact all of this is motivated by the following digital facts. One of the greatest problems of representing the HG basis functions is at the boundaries of the von Neumann grid. In the von Neumann TFR, the Gaussian functions are still represented quite well at the edges of the grid. For the HG functions, on the other hand, as the Hermite polynomial's order increases, the HG function effectively broaden and unfortunately starts to extend increasingly beyond the boundaries of the discrete grid.

Therefore, to represent the FHG basis properly, this implies that we, for instance in the time domain, the time signal, not the grid, has to be extended. In accordance to the *ad hoc* rules of DSP we extend it to $2T$. Thus the time signal can be split over the grid shoulders as $T/2$ on the one side, T over the grid and $T/2$ on the other shoulder.

In the calculation of the of the overlap matrices on the von Neumann grid we require, $\omega_{nl} = \omega_n - \omega_l$. At the minimum and maximum indices, n and l are reversed in sign. This implies that we actually need two times the bandwidth Ω to cover the whole spectrum for the proper calculation of the overlap matrices, i.e.,

$$\omega_{nl} \in [-\Omega, \Omega] \qquad \forall n, l.$$

That means that the bandwidth we require for the signals is 2Ω. The requirement also arises in the time domain, i.e., $t_{mk} \in [-T, T]$, for all, m and k. Thus, $2T$. To comply to all these requirements, and still have the same, σ, we must have,

$$\delta t \rightarrow \frac{\delta t}{2}, \quad \text{and} \quad \delta\omega \rightarrow \frac{\delta\omega}{2},$$

so that, T, goes to, $2T$, and, Ω, goes to, 2Ω. Thus, to represent the TF von Neumann grid actually correctly, we must sample, $2T = (4N)\frac{\delta t}{2}$, i.e., increase the electric field digital representation to, $4N$, samples at double the sampling frequency. For our grid, $25 \times 25 = 625 = N$, that means, $4N = 2500$, sampling points. The von Neumann grid, remains untouched in its original form. The requirements are only on the signal it must represent and to actually calculated the overlap matrix correctly.

For periodic digital functions, $\hat{f}(t) = \hat{f}(t + 2T)$ and $\hat{F}(\omega) = F(\omega + 2\Omega)$. The maximum bandwidth, $2\Omega = 4\pi/\delta t$, (support$[-\Omega, \Omega\ ]$). The reciprocal (inverse) timespan, $2T = 4\pi/\delta\omega$, (support$[-T, T]$) of the signal where, $\frac{\delta\omega}{2}$, is the angular frequency sampling rate, corresponding to, $\frac{\delta t}{2}$. The doubling of the time and frequency bandwidths is demonstrated in Figure 6.4. Dimler et al. [96] also spend some time discussing issue of enlarging the bandwidths, but by simple zero padding the signals.

This also addresses the very important issue of aliasing. In DSP one of the design criteria is to sample at such and such a sampling frequency, $f_s = \frac{1}{\delta t}$ and timespan $T = N\delta t$, so as to ensure **anti-aliasing**. This is why they usually oversample. What is aliasing? Digitally, $\hat{f}(t) = \hat{f}(t+T)$ and $\hat{F}(\omega) = F(\omega + \Omega)$, we have only periodic signals. If the original signal, $f(t)$, extends beyond the digital support $[-\frac{T}{2}, \frac{T}{2}]$, then the digital signal, $\hat{f}(t)$, actually cuts off portions of the true signal at the wings. This means that the true signal actually overlaps at its periodic digital boundary, $\hat{f}(t+T)$. Naturally, this also occurs in the frequency domain if the spectrum, $F(\omega)$, of the original signal contains higher frequencies than our cut-off bandwidth limit. This overlapping at the wings of the periodic DFT is referred to as aliasing. The methods employed to counteract it, as anti-aliasing. Basically, anti-aliasing is then just extending the support of the signal, usually in the spectral domain. The *ad hoc* engineering approach is to sample at least at, $1\frac{1}{4}$, the required bandwidth, say, Ω. It is well known that the FFT with its radix algorithm is designed on the fact the signal should be multiple of 2. That is, $N = 2^m$, for some $m \in \mathbb{N}$.

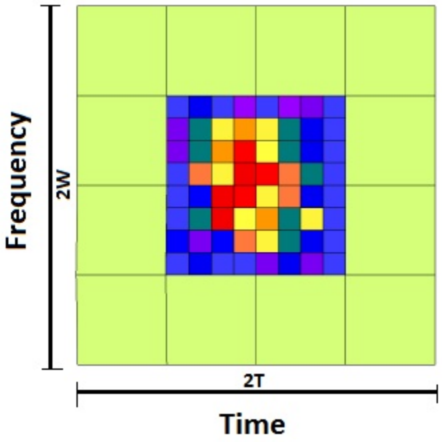

Figure 6.4.: Time-Frequency Doubling

In our application we're using a spatial light modulator (SLM) of 640 pixels. At first this seemed a funny number. This resulted in the choice of our grid of, $625 = 25 \times 25$, to fit in properly into the 640. To illustrate the issue of aliasing, we demonstrate the judicious choice of 640 pixels. Taking into consideration of the fact that FFT works in powers of 2, we have, $640 = 512 + 128 = 2^9 + 2^7 = 1\frac{1}{4} \times 512$.

The aliasing was directly considered!

6.4. The Complete FHG TFR Cube

In the course of developing this theory and FHG TFR, we assumed that it is necessary to define the FHG basis functions in terms of a frame, defined by the selection of a certain set of vectors, $\mathbf{c}^T_{m,n} \in \mathbb{C}^K$, to a define a frame as an intersection of the FHG TFR lattice cube, as in the temporal basis set in Eq. (5.99),

$$\beta_{m,n}(t) = \mathbf{c}^T_{m,n} e^{it\omega_n} \mathbf{\Phi}(t - t_m) \qquad \text{where} \quad \mathbf{c}^T_{m,n} \in \mathbb{C}^K,$$

and spectral basis set,

$$\tilde{\beta}_{m,n}(\omega) = \mathbf{c}^T_{m,n} e^{-it_m(\omega-\omega_n)} \tilde{\mathbf{\Phi}}(\omega - \omega_n) \qquad \text{where} \quad \mathbf{c}^T_{m,n} \in \mathbb{C}^K.$$

In this Section, rather than using the vector-matrix notation, we are going to define the full FHG temporal basis sets in terms of their indices on the von Neumann basis, (m, n), as,

$$f_{m,n,k}(t) = e^{it\omega_n} \phi_k(\frac{t - t_m}{\sqrt{2\sigma}}), \tag{6.3}$$

where, ϕ_k, refers to Hermite-Gauss polynomial of order, actually $(k - 1)$, see Eq. (5.38), since they are normally indexed from 0. The, $\frac{t-t_m}{\sqrt{2\sigma}}$, provides the correct scaling. As was shown in Section 5.3 and Eq. (5.40), Eq. (5.41) and Eq. (5.44), they form Fourier transform pairs, i.e.,

$$\boldsymbol{\mathcal{F}}\{f_{m,n,k}(t)\} = F_{m,n,k}(\omega),$$

where the Fourier transform is given by,

$$F_{m,n,k}(\omega) = e^{-it_m(\omega-\omega_n)} \phi_k[\sqrt{2\sigma}(\omega - \omega_n)]. \tag{6.4}$$

One further manipulation is required. In terms of **unscaled time and angular frequency units**, we can define, $f_{m,n,k}(t)$ and $F_{m,n,k}(\omega)$, as follows,

$$\hat{f}_{m,n,k}(t) = e^{it\omega_n} \phi_k(t - t_m), \tag{6.5}$$

and

$$\hat{F}_{m,n,k}(\omega) = e^{-it_m(\omega-\omega_n)} \phi_k(\omega - \omega_n), \tag{6.6}$$

where we have used the hat $\hat{}$ to indicate that the functions are unscaled and, of course, they will still remain Fourier transform pairs,

$$\boldsymbol{\mathcal{F}}\left\{\hat{f}_{m,n,k}(t)\right\} = \hat{F}_{m,n,k}(\omega), \tag{6.7}$$

In the course of the definition of the previous FHG TFR in Subsection 5.4.4, we see that it is necessary to take the integral inner product of the bases functions and the signal, $\varepsilon(t)$, Eq. (5.107)

$$\int_{-\infty}^{\infty} \beta^*_{k,l}(t)\varepsilon(t)\,dt$$

,

and its Fourier transform $\tilde{\varepsilon}(\omega)$, i.e.,

$$\int_{-\infty}^{\infty} \tilde{\beta}^*_{k,l}(\omega)\tilde{\varepsilon}(\omega)\,d\omega.$$

In terms of the new two functions Eq. (6.4) and Eq. (6.3) these integrals become,

$$\int_{-\infty}^{\infty} f^*_{m,n,k}(t)\varepsilon(t)\,dt = \int_{-\infty}^{\infty} e^{-it\omega_n}\phi_k(\frac{t-t_m}{\sqrt{2\sigma}})\varepsilon(t)\,dt, \tag{6.8}$$

and

$$\int_{-\infty}^{\infty} F^*_{m,n,k}(\omega)\tilde{\varepsilon}(\omega)\,d\omega = \int_{-\infty}^{\infty} e^{it_m(\omega-\omega_n)}\phi_k[\sqrt{2\sigma}(\omega-\omega_n)]\tilde{\varepsilon}(\omega)\,d\omega, \tag{6.9}$$

respectively. If we scale the incoming signal $\varepsilon(t)$, in accordance with the scaling used for the unscaled bases functions, $\hat{f}_{m,n,k}(t)$, i.e., $t = \sqrt{2\sigma}t'$, and using the Fourier transform scaling property Eq. (A.20), we obtain,

$$\boldsymbol{\mathcal{F}}\{\varepsilon(\sqrt{2\sigma}t)\} = \frac{1}{\sqrt{2\sigma}}\tilde{\varepsilon}(\frac{\omega}{\sqrt{2\sigma}}). \tag{6.10}$$

After this action has been performed to the electric signal Fourier transform pair, $\hat{\varepsilon}(t) \overset{\mathcal{F}}{\Longleftrightarrow} \hat{\tilde{\varepsilon}}(\omega)$, they are also in terms of unscaled units, and they can be directly implemented with the unscaled FHG TFR bases functions, $\hat{f}_{m,n,k}(t)$ and $\hat{F}_{m,n,k}(\omega)$. In the next Section 6.5, $\hat{\varepsilon}(t)$ and $\hat{\tilde{\varepsilon}}(\omega)$, are defined by Eq. (6.12) and Eq. (6.13), respectively.

6.5. Unscaled FHG Signal Correlation

If we scale the time as, $t = \sqrt{2\sigma}t'$, and the angular frequency, $\omega = \frac{\omega'}{\sqrt{2\sigma}}$, and the electric signals, Eq. (6.10), the basis functions become scale invariant, a very desirable property. In the rest of this section we assume this has been done and for notational convenience we indicate the unscaled electric field signal as, $\hat{\varepsilon}(t)$ and $\hat{\tilde{\varepsilon}}(\omega)$, or at times as, $\hat{s}(t)$ and $\hat{S}(\omega)$. The unscaled electric fields transform as follows. From Eq. (6.8) we have with, $t = \sqrt{2\sigma}t'$, and the angular frequency, $\omega = \frac{\omega'}{\sqrt{2\sigma}}$,

$$\int_{-\infty}^{\infty} f^{*}_{m,n,k}(t)\varepsilon(t)\,dt = \int_{-\infty}^{\infty} e^{-it'\omega'_n}\sqrt{2\sigma}\phi_k(t'-t'_m)\varepsilon(\sqrt{2\sigma}t')\,dt', \tag{6.11}$$

and from the definition of the HG polynomial, Eq. (5.38),

$$\phi_k(x) = 2^{-\frac{p}{2}}(k!)^{-\frac{1}{2}}\pi^{-\frac{1}{4}}e^{-\frac{x^2}{2}}H_k(x),$$

and the scaled normalized HG polynomial, Eq. (5.42),

$$\phi_k[(t-t_m)/\sqrt{2\sigma}] = (2\sigma)^{-\frac{1}{4}}\,2^{-\frac{k}{2}}(k!)^{-\frac{1}{2}}\pi^{-\frac{1}{4}}e^{-\frac{(t-t_m)^2}{4\sigma}}H_k[(t-t_m)/\sqrt{2\sigma}],$$

the integral, 6.11, transforms to,

$$\begin{aligned}\int_{-\infty}^{\infty} f^{*}_{m,n,k}(t)\varepsilon(t)\,dt &= \int_{-\infty}^{\infty} e^{-it'\omega'_n}\phi_k(t'-t'_m)\left[(2\sigma)^{\frac{1}{4}}\,\varepsilon(\sqrt{2\sigma}t')\right]\,dt' \\ &= \int_{-\infty}^{\infty} \hat{f}^{*}_{m,n,k}(t)\hat{\varepsilon}(t)\,dt.\end{aligned}$$

Thus the **unscaled temporal electric field signal** $\hat{\varepsilon}(t)$ is defined by,

$$\boxed{\hat{\varepsilon}(t) = (2\sigma)^{\frac{1}{4}}\,\varepsilon(\sqrt{2\sigma}t) = \hat{s}(t)} \tag{6.12}$$

Similarly, from Eq. (6.9), we have the angular frequency, $\omega = \frac{\omega'}{\sqrt{2\sigma}}$, transform and from the definition of the HG polynomial, Eq. (5.38) and the scaled normalized HG polynomial, Eq. (5.43), the integral transforms to

$$\begin{aligned}\int_{-\infty}^{\infty} F^{*}_{m,n,k}(\omega)\tilde{\varepsilon}(\omega)\,d\omega &= \int_{-\infty}^{\infty} e^{it'_m(\omega'-\omega'_n)}\phi_k(\omega'-\omega'_n)\left[(2\sigma)^{-\frac{1}{4}}\,\tilde{\varepsilon}(\frac{\omega'}{\sqrt{2\sigma}})\right]\,d\omega' \\ &= \int_{-\infty}^{\infty} \hat{F}^{*}_{m,n,k}(\omega)\hat{\tilde{\varepsilon}}(\omega)\,d\omega.\end{aligned}$$

Thus, the **unscaled spectral electric field signal**,$\hat{\tilde{\varepsilon}}(\omega)$, is defined by,

$$\boxed{\hat{\tilde{\varepsilon}}(\omega) = (2\sigma)^{-\frac{1}{4}}\,\tilde{\varepsilon}(\frac{\omega}{\sqrt{2\sigma}}) = \hat{S}(\omega)} \tag{6.13}$$

If we define the **unscaled temporal FHG basis** as, Eq. (6.5),

$$\boxed{\hat{f}_{m,n,k}(t) = e^{it\omega_n}\phi_k(t - t_m)} \tag{6.14}$$

and the **unscaled spectral FHG basis** as, Eq. (6.6),

$$\boxed{\hat{F}_{m,n,k}(\omega) = e^{-it_m(\omega-\omega_n)}\phi_k(\omega - \omega_n)} \tag{6.15}$$

where we have used the hat $\hat{}$ to indicate that the functions are unscaled. In both the above functions the Hermite-Gauss functions, $\phi_k(x)$, are the same functions as defined in Eq. (5.38), i.e., time, t, and angular frequency, ω, are in the same units, so that we can compare apples with apples and oranges with oranges. The playing fields have been leveled.

In terms of **unscaled time and angular frequency units** these two above integrals become,

$$\int_{-\infty}^{\infty} \hat{f}^*_{m,n,k}(t)\hat{\varepsilon}(t)\,dt = \int_{-\infty}^{\infty} e^{-it\omega_n}\phi_k(t - t_m)\hat{\varepsilon}(t)\,dt, \tag{6.16}$$

and

$$\int_{-\infty}^{\infty} \hat{F}^*_{m,n,k}(\omega)\hat{\tilde{\varepsilon}}(\omega)\,d\omega = \int_{-\infty}^{\infty} e^{it_m(\omega-\omega_n)}\phi_k(\omega - \omega_n)\hat{\tilde{\varepsilon}}(\omega)\,d\omega. \tag{6.17}$$

Now working in the **frequency domain** with the second integral, Eq. (6.17), the definition of convolution Eq. (A.41), shows that just by using, $f \to H^*(-\xi)$ and $g \to S = \tilde{\varepsilon}(\omega)$, and a change of the dummy integration variable, $\tau \to \omega$, and the convolution variable, $t \to \xi$, we have,

$$\begin{aligned} C(\xi) = H^*(-\xi) * S(\xi) &= \int_{-\infty}^{\infty} H^*[-(\xi - \omega)]S(\omega)\,d\omega \\ &= \int_{-\infty}^{\infty} H^*(\omega - \xi)S(\omega)\,d\omega. \end{aligned}$$

Using this definition, we are now going to show that the integration of the multiplication of a spectral FHG basis function with the spectral signal, is actually a convolution, and in this form, actually a correlation. Now let us define the, $H(\xi)$, function to be the following function, with, $\xi = x$,

$$\boxed{H_{m,k}(x) = e^{-it_m x}\phi_k(x)} \tag{6.18}$$

Using Eq. (5.39) and the reality of the Hermite-Gauss polynomials we have,

$$H^*_{m,k}(-\xi) = e^{it_m\xi}\phi_k(-\xi) = (-1)^{(k-1)}e^{it_m\xi}\phi_k(\xi) = (-1)^{(k-1)}H^*_{m,k}(\xi). \tag{6.19}$$

Thus with,

$$C_{m,k}(\xi) = H^*_{m,k}(-\xi) * \hat{S}(\xi) = \int_{-\infty}^{\infty} H^*_{m,k}(\omega - \xi)\hat{S}(\omega)\,d\omega.$$

According to Eq. (A.59) and the alternative form of a correlation, Eq. (A.52), this is just a correlation,

$$C_{m,k}(\xi) = \left(H_{m,k} \star \hat{S}\right)(\xi), \tag{6.20}$$

and, with, $\xi = \omega_n$, we have,

$$C_{m,k}(\omega_n) = \left(H_{m,k} \star \hat{S}\right)(\omega_n) = \int_{-\infty}^{\infty} H^*_{m,k}(\omega - \omega_n)\hat{S}(\omega)\,d\omega, \tag{6.21}$$

But,

$$\boxed{H^*_{m,k}(\omega - \omega_n) = e^{it_m(\omega-\omega_n)}\phi_k(\omega - \omega_n) = \hat{F}^*_{m,n,k}(\omega)} \tag{6.22}$$

This can be written more compactly by using the translation operator Eq. (A.102), $\mathcal{T}_{\omega_n}$, and removing the complex conjugation as,

$$\mathcal{T}_{\omega_n} H_{m,k}(\omega) = \hat{F}_{m,n,k}(\omega). \tag{6.23}$$

Now letting, $\hat{S}(\omega) = \hat{\varepsilon}(\omega)$, we find,

$$C_{m,k}(\omega_n) = \left(H_{m,k} \star \hat{S}\right)(\omega_n) = \int_{-\infty}^{\infty} \hat{F}^*_{m,n,k}(\omega)\hat{\hat{\varepsilon}}(\omega)\,d\omega.$$

Thus

$$\boxed{C_{m,k}(\omega_n) = \left(H_{m,k} \star \hat{S}\right)(\omega_n)} \tag{6.24}$$

Similarly, working in the **time domain** with the first integral Eq. (6.16),

$$\begin{aligned} X_{m,n,k}(t_m) = \int_{-\infty}^{\infty} \hat{f}^*_{m,n,k}(t)\hat{\varepsilon}(t)\,dt = \int_{-\infty}^{\infty} e^{-it\omega_n}\phi_k(t - t_m)\hat{\varepsilon}(t)\,dt \\ = e^{-it_m\omega_n}\int_{-\infty}^{\infty} e^{-i\omega_n(t-t_m)}\phi_k(t - t_m)\hat{\varepsilon}(t)\,dt. \end{aligned} \tag{6.25}$$

If we now allow the electric field, $\hat{\varepsilon}(t) = \hat{s}(t)$, so that, $\boldsymbol{\mathcal{F}}\{\hat{s}(t)\} = \hat{S}(\omega)$, we can compare the two methods on the same type of footing. Let us now define the functions,

$$\boxed{K_{m,n,k}(x) = e^{i\omega_n(x+t_m)}\phi_k(x)} \tag{6.26}$$

Thus

$$\boxed{K^*_{m,n,k}(t-t_m) = e^{-it\omega_n}\phi_k(t-t_m) = \hat{f}^*_{m,n,k}(t)} \tag{6.27}$$

or applying the translation operator Eq. (A.102) as,

$$\mathcal{T}_{t_m}K_{m,n,k}(t) = \hat{f}_{m,n,k}(t). \tag{6.28}$$

Lastly, we once again see that the integral Eq. (6.25) corresponds to a correlation with the time signal

$$\boxed{X_{m,n,k}(t_m) = \left(K_{m,n,k} \star \hat{s}\right)(t_m)} \tag{6.29}$$

Using the Fourier property of correlation Eq. (A.53),

$$\boldsymbol{\mathcal{F}}\{f(t) \star g(t)\} = F^*(\omega)G(\omega),$$

a obvious modification of Eq. (6.29) to a continuous correlation variable can be written as,

$$\boldsymbol{\mathcal{F}}\{K_{m,n,k} \star \hat{s}(t)\} = \left[\boldsymbol{\mathcal{F}}\{K_{m,n,k}(t)\}\right]^* S(\omega).$$

Using the definition Eq. (6.26),

$$\boldsymbol{\mathcal{F}}\{K_{m,n,k} \star \hat{s}(t)\} = \left[\boldsymbol{\mathcal{F}}\{e^{i\omega_n(t+t_m)}\phi_k(t)\}\right]^* S(\omega).$$

But,

$$\boldsymbol{\mathcal{F}}\{e^{i\omega_n(t+t_m)}\phi_k(t)\} = e^{i\omega_n t_m}\phi_k(\omega-\omega_n),$$

and from Eq. (6.15) we find,

$$\boldsymbol{\mathcal{F}}\{e^{i\omega_n(t+t_m)}\phi_k(t)\} = e^{i\omega t_m}\hat{F}_{m,n,k}(\omega)$$

.Thus

$$\boldsymbol{\mathcal{F}}\{K_{m,n,k} \star \hat{s}(t)\} = e^{-i\omega t_m}\hat{F}^*_{m,n,k}(\omega)S(\omega). \tag{6.30}$$

This is just a nifty alternative method to write the correlation as a product of its Fourier transform. Here its just conjugate multiplication with a phase with the spectral signal. To find the true correlation the inverse must still be taken and then the specific time, $t_{m.}$.

Summary

- The ***Unscaled Spectral FHG TFR Lattice Cube*** is defined in Eq. (6.17)

$$C_{m,k}(\omega_n) = \int_{-\infty}^{\infty} \hat{F}^*_{m,n,k}(\omega)\hat{\hat{\varepsilon}}(\omega)\, d\omega$$

This can be written as a correlation, Eq. (6.24), (spectral signal $\hat{\hat{\varepsilon}}(\omega) = \hat{S}(\omega)$)

$$\boxed{C_{m,k}(\omega_n) = \left(H_{m,k} \star \hat{S}\right)(\omega_n)}$$

where the $H_{m,k}$ is defined by Eq. (6.18)

$$\boxed{H_{m,k}(x) = e^{-it_m x}\phi_k(x)}$$

- The ***Unscaled Temporal FHG TFR Lattice Cube*** is defined in

$$X_{m,n,k}(t_m) = \int_{-\infty}^{\infty} \hat{f}^*_{m,n,k}(t)\hat{\varepsilon}(t)\, dt$$

This can be written as a correlation, Eq. (6.29), (temporal signal $\hat{\varepsilon}(t) = \hat{s}(t)$)

$$\boxed{X_{m,n,k}(t_m) = \left(K_{m,n,k} \star \hat{s}\right)(t_m)}$$

where the $K_{m,n,k}$ is defined by Eq. (6.26)

$$\boxed{K_{m,n,k}(x) = e^{i\omega_n(x+t_m)}\phi_k(x)}$$

6.5.1. Alternative Derivation of the Unscaled Signals

As can be seen, to place the time and angular frequency on the same footing, it is necessary to define the unscaled electric field signals, $\hat{\varepsilon}(t)$ and $\hat{\hat{\varepsilon}}(\omega)$, as was done in Eq. (6.12) and Eq. (6.13). Unfortunately, in a simulation we are forced to use digital Fourier transform algorithms, such as the FFT. In a digitized form the signal, $s[n]$, and Fourier transform, $S[n]$, are just sampling sequences, totally oblivious of the actual time and angular frequency, that has to be supplied by the user in accordance with the requirement that, $t \cdot \omega = 2\pi$. This can create scaling confusion. Now with,

$$s(t) \overset{\mathcal{F}}{\Longleftrightarrow} S(\omega).$$

We can, of course, use the scaling properties of Fourier transforms Eq. (A.20),

$$\boldsymbol{\mathcal{F}}\{s(at)\} = \frac{1}{|a|}S(\frac{\omega}{a}),$$

and Eq. (A.21),

$$\boldsymbol{\mathcal{F}}^{-1}\{S(a\omega\} = \frac{1}{|a|}s(\frac{t}{a}),$$

and immediately we see that the, $\frac{1}{|a|}$ factor often causes confusion. Substituting, $t = \sqrt{2\sigma}t'$, and the angular frequency, $\omega = \frac{\omega'}{\sqrt{2\sigma}}$, we also note that, $t \cdot \omega = t' \cdot \omega'$ in Eq. (A.71),

$$\int_{-\infty}^{\infty} s^*(\sqrt{2\sigma}t')s(\sqrt{2\sigma}t')\,dt' = \int_{-\infty}^{\infty} \left[\frac{1}{\sqrt{2\sigma}}S^*(\frac{\omega'}{\sqrt{2\sigma}})\right]\left[\frac{1}{\sqrt{2\sigma}}S(\frac{\omega'}{\sqrt{2\sigma}})\right]\,d\omega',$$

and with the scaling properties of Fourier transforms Eq. (A.20),

$$\boldsymbol{\mathcal{F}}\{s(\sqrt{2\sigma}t)\} = \frac{1}{\sqrt{2\sigma}}S(\frac{\omega}{\sqrt{2\sigma}}),$$

the result remains valid. In the definitions of the unscaled signals, Eq. (6.12) and Eq. (6.13) we actually have,

$$\hat{s}(t) = (2\sigma)^{\frac{1}{4}}\,s(\sqrt{2\sigma}t),$$

$$\hat{S}(\omega) = (2\sigma)^{-\frac{1}{4}}\,S(\frac{\omega}{\sqrt{2\sigma}}).$$

By the linearity property of Fourier transforms Eq. (A.15) we see that,

$$\boldsymbol{\mathcal{F}}\{\hat{s}(t)\} = \boldsymbol{\mathcal{F}}\{(2\sigma)^{\frac{1}{4}}\,s(\sqrt{2\sigma}t)\} = (2\sigma)^{-\frac{1}{4}}\,S(\frac{\omega}{\sqrt{2\sigma}}) = \hat{S}(\omega).$$

A simple method to detour this problem is to use the energy theorem (Parseval-Plancherel), Subsection A.3.10, and to replace, $f(t) = g(t) = s(t)$ and $F(\omega) = G(\omega) = S(\omega)$, in Eq. (A.71),

$$\int_{-\infty}^{\infty} s^*(t)s(t)\,dt = \int_{-\infty}^{\infty} S^*(\omega)S(\omega)\,d\omega,$$

which changes Eq. (A.72), the energy of the signal, to,

$$E^2 = \int_{-\infty}^{\infty} |s(t)|^2\,dt = \int_{-\infty}^{\infty} |S(\omega)|^2\,d\omega.$$

To insure digitally we are scaled correctly, and that t and ω have the same scale, we define,

$$E_s^2 = \int_{-\infty}^{\infty} |s(t)|^2 \, dt,$$

and

$$E_S^2 = \int_{-\infty}^{\infty} |S(\omega)|^2 \, d\omega.$$

If $E_s^2 \neq E_S^2$ then we just define the normalized signals as,

$$\hat{s}(t) = E \cdot \frac{s(t)}{E_s} \quad \text{and} \quad \hat{S}(\omega) = E \cdot \frac{S(\omega)}{E_S},$$

where, E, is an arbitrary energy attached to the signal and we still have,

$$\hat{s}(t) \overset{\mathcal{F}}{\Longleftrightarrow} \hat{S}(\omega).$$

6.6. The Complete FHG Overlap Matrices

According to the von Neumann TFR bases, the overlap matrix is defined as in Eq. (3.83) and Eq. (3.84) for the frequency and time, respectively. Basically it boils down to forming a matrix in which each basis vector is multiplied with each other in the two dual spaces. In the same manner we can construct an overlap matrix for the new unscaled FHG basis. Here each index in order, as in, (i, j, k) and (l, m, n), refers to the time, angular frequency and HG polynomial of the FHG basis, respectively. Let us also reformulate these in terms of the correlations along the lines of Section 6.5.

Thus, for the time we have the **temporal FHG overlap matrix**,

$$\mathbb{T}_{i,j,k}^{l,m,n} = \langle \hat{f}_{i,j,k}^{*}(t) | \hat{f}_{l,m,n}(t) \rangle = \int_{-\infty}^{\infty} \hat{f}_{i,j,k}^{*}(t) \, \hat{f}_{l,m,n}(t) \, \mathrm{d}t, \tag{6.31}$$

and the **spectral FHG overlap matrix**,

$$\mathbb{S}_{i,j,k}^{l,m,n} = \langle \hat{F}_{i,j,k}^{*}(\omega) | \hat{F}_{l,m,n}(\omega) \rangle = \int_{-\infty}^{\infty} \hat{F}_{i,j,k}^{*}(\omega) \, \hat{F}_{l,m,n}(\omega) \, \mathrm{d}\omega. \tag{6.32}$$

We define both because for the unscaled temporal FHG basis, Eq. (6.14), the Hermite-Gauss polynomials indexed with time, m, and for the unscaled spectral

FHG basis, Eq. (6.15), the Hermite-Gauss polynomials indexed with angular frequency, n. Thus,

$$\mathbb{T}^{l,m,n}_{i,j,k} = \int_{-\infty}^{\infty} e^{it(\omega_m - \omega_j)} \phi_k(t - t_i)\phi_n(t - t_l)\, dt, \tag{6.33}$$

and

$$\mathbb{S}^{l,m,n}_{i,j,k} = \int_{-\infty}^{\infty} e^{it_i(\omega-\omega_j) - it_l(\omega-\omega_m)} \phi_k(\omega - \omega_j)\phi_n(\omega - \omega_m)\, d\omega, \tag{6.34}$$

$$\mathbb{S}^{l,m,n}_{i,j,k} = \int_{-\infty}^{\infty} e^{it_i(\omega-\omega_j) - it_l(\omega-\omega_m)} \phi_k(\omega')\phi_n(\omega - \omega_m)\, d\omega.$$

We now only work with the ***spectral FHG overlap matrix***. This shows, using the dummy variable, $\omega' = \omega - \omega_j$ and $\omega_{jm} = \omega_j - \omega_m$, that Eq. (6.34) transforms to,

$$\mathbb{S}^{l,m,n}_{i,j,k} = \int_{-\infty}^{\infty} \left[e^{it_i\omega'}\phi_k(\omega')\right] \cdot \left[e^{-it_l(\omega'+\omega_{jm})}\phi_n(\omega' + \omega_{jm})\right] d\omega'. \tag{6.35}$$

Inserting our defined functions, $H_{l,n}(\omega)$, Eq. (6.18), and comparing with the definition of a correlation Eq. (A.51), Eq. (6.35) can be written succinctly as,

$$C^{l,n}_{i,k}(\omega) = \left(H_{i,k} \star H_{l,n}\right)(\omega), \tag{6.36}$$

so that with, $\omega = \omega_{jm}$, we have,

$$\boxed{\mathbb{S}^{l,m,n}_{i,j,k} = C^{l,n}_{i,k}(\omega_{jm}) = \left(H_{i,k} \star H_{l,n}\right)(\omega_{jm})} \tag{6.37}$$

Proposition 6.6.1. The functions, $H_{l,n}(\omega)$, are Hermitian, denoted by †, if $n = 0, 1, 2, \ldots$, are even and anti-Hermitian, denoted by ×, if n is odd. (See Subsection A.3.7 for the definition of Hermitian), i.e.,

$$H_{l,n}(\omega) = \begin{cases} H^{\dagger}_{l,n}(\omega) & \text{if } n \text{ is even} \\ H^{\times}_{l,n}(\omega) & \text{if } n \text{ is odd} \end{cases}$$

Proof. The Hermite-Gauss functions, $\phi_n(\omega)$, are even functions if, $n = 0, 1, 2, \ldots$, are even and odd functions if n is odd. Using Euler's formula we have,

$$\begin{aligned} H_{l,n}(\omega) &= e^{-it_l\omega}\phi_n(\omega) \\ &= \cos(t_l\omega)\phi_n(\omega) - i\sin(t_l\omega)\phi_n(\omega). \end{aligned}$$

Using the properties of even and odd functions in Subsection A.3.7, and knowing that, $\cos(x)$ and $\sin(x)$, are even and odd functions respectively, we see that if, $\phi_n(\omega)$, are even functions if $n = 0, 1, 2, \ldots$, then, $\cos(t_l\omega)\phi_n(\omega)$, is an even function and, $\sin(t_l\omega)\phi_n(\omega)$, is an odd function. Therefore, $H_{l,n}(\omega)$, is Hermitian. The anti-Hermitian condition is similarly proofed.

□

Let us define the following notation,

$$k = \begin{cases} k^+ & \text{if } k \text{ is even} \\ k^- & \text{if } k \text{ is odd} \end{cases} \tag{6.38}$$

Then, $H_{m,k^+} = H^{\dagger}_{m,k^+}$ and $H_{m,k^-} = H^{\times}_{m,k^-}$.

This proposition shows that if k and n are both even, then we have a cross-correlation of two Hermitian functions which according to property 1 of Subsection A.3.9.2 commute, i.e.,

$$\begin{aligned}
\mathbb{S}^{l,m,n^+}_{i,j,k^+} &= C^{l,n^+}_{i,k^+}(\omega_{jm}) \\
&= \left(H_{i,k^+} \star H_{l,n^+}\right)(\omega_{jm}) \\
&= \left(H_{l,n^+} \star H_{i,k^+}\right)(\omega_{jm}) \\
&= C^{i,k^+}_{l,n^+}(\omega_{jm}) \\
&= \mathbb{S}^{i,m,k^+}_{l,j,n^+}.
\end{aligned}$$

That is,

$$\boxed{\mathbb{S}^{l,m,n^+}_{i,j,k^+} = \mathbb{S}^{i,m,k^+}_{l,j,n^+}} \tag{6.39}$$

If k and n are both odd, the same relation holds, i.e.,

$$\boxed{\mathbb{S}^{l,m,n^-}_{i,j,k^-} = \mathbb{S}^{i,m,k^-}_{l,j,n^-}} \tag{6.40}$$

Using the translation operator (cf. Subsection A.4.8 for the definition), we see that,

$$\boxed{\mathcal{T}_{\omega_m} H_{l,n}(\omega) = e^{-it_l(\omega-\omega_m)}\phi_n(\omega-\omega_m) = \hat{F}_{l.m.n}(\omega)} \tag{6.41}$$

Applying the translational invariance of correlations, property 4 of Subsection A.3.9.2, we obtain,

$$\left[\mathcal{T}_{\omega_m} C^{l,n}_{i,k}\right](\omega) = H_{i,k} \star (\mathcal{T}_{\omega_m} H_{l,n}). \tag{6.42}$$

Thus from Eq. (6.41) we have,

$$\boxed{\left[\mathcal{T}_{\omega_m} C_{i,k}^{l,n}\right](\omega) = \left(H_{i,k} \star \hat{F}_{l.m.n}\right)(\omega)} \tag{6.43}$$

The Hermite-Gauss polynomials are orthogonal, i.e.,

$$\int_{-\infty}^{\infty} \phi_n(x)\, \phi_k(x)\, \mathrm{d}x = \delta_{nk}, \tag{6.44}$$

where we have used Kronecker delta function, δ_{nk}, defined in Eq. (A.84). Applying this we get the following simplification. If, $(i,j) = (l,m)$, then,

$$\boxed{\mathbb{S}_{i,j,k}^{i,j,n} = \delta_{nk}} \tag{6.45}$$

We note that the overlap matrix is the cross-correlation cube of the FHG basis polynomials, i.e., $\hat{S}(\omega) = \hat{F}_{l,m,n}(\omega)$, in Eq. (6.24) with the subscripts changed to, (i,j,k),

$$C_{i,k}(\omega_j) = \left(H_{i,k} \star \hat{F}_{l,m,n}\right)(\omega_j). \tag{6.46}$$

To fix the notation we will denote it with,

$$C_{i,k}(\omega_j) = C_{i,k}^{l,m,n}(\omega_j). \tag{6.47}$$

Translation invariance of the cross-correlation operation shows that with, $\mathcal{T}_{\omega_m}$,

$$\begin{aligned}
\mathcal{T}_{\omega_m} C_{i,k}^{l,m,n}(\omega_j) &= C_{i,k}^{l,m,n}(\omega_{jm}) \\
&= \left(H_{i,k} \star \hat{F}_{l,m,n}\right)(\omega_{jm}) \\
&= C_{i,k}^{l,n}(\omega_{jm}) \\
&= \mathbb{S}_{i,j,k}^{l,m,n}.
\end{aligned} \tag{6.48}$$

The last step of this operation is obtained from Eq. (6.37). For a specific, $\hat{F}_{l,m,n}(\omega)$, FHG basis function if we fix the Hermite-Gauss plane with, $k = n$, i.e., the time-frequency plane, we note that the cross-correlation functions with the other FHG basis functions, $\hat{F}_{i,j,n}$, form a specific overlap pattern about the center of, $\hat{F}_{l,m,n}$, i.e., $(i,j) = (l,m)$. If we translate the basis function in this plane with, (l,m), i.e., the time-frequency plane, say to, (p,q), then this FHG basis correlation pattern remains invariant, except for phase, but centered about, $(p,q) = (l,m)$. This suggests that,

$$C_{i,k}^{l,m,n}(\omega_j) = \left(H_{i,k} \star \hat{F}_{l,m,n}\right)(\omega_j) = e^{-it_i\omega_{jm}} \int_{-\infty}^{\infty} \phi_k(\omega) e^{-it_{li}(\omega+\omega_{jm})} \phi_n(\omega+\omega_{jm})\, d\omega, \tag{6.49}$$

Similarly,

$$C_{r,k}^{p,q,n}(\omega_s) = \left(H_{r,k} \star \hat{F}_{p,q,n}\right)(\omega_s) = e^{-it_r\omega_{sq}} \int_{-\infty}^{\infty} \phi_k(\omega) e^{-it_{pr}(\omega+\omega_{sq})} \phi_n(\omega+\omega_{sq})\, d\omega. \tag{6.50}$$

The integrals in Eq. (6.49) and Eq. (6.50) will be equal if, $t_{li} = t_{pr}$ and $\omega_{jm} = \omega_{sq}$. Thus, we have actually proven that the correlation patterns are translation invariant in the time-frequency planes, except for an addition of a phase that depends on the times, t_i and t_r, for, $n = k$, and even more, that this remains true for any two time-frequency planes, i.e., $n \neq k$,

$$\boxed{e^{it_i\omega_{jm}} C_{i,k}^{l,m,n}(\omega_j) = e^{it_r\omega_{sq}} C_{r,n}^{p,q,k}(\omega_s) \qquad \text{if } t_{li} = t_{pr} \quad \text{and} \quad \omega_{jm} = \omega_{sq}} \tag{6.51}$$

with both differences still in the bounds of the time-frequency plane. If furthermore, $t_i = t_r$, the phases are equal and the correlations are equal under the same conditions. Now we also know that Eq. (6.36),

$$C_{i,k}^{l,n}(\omega) = \left(H_{i,k} \star H_{l,n}\right)(\omega),$$

and, $H_{l,n^+} = H_{l,n^+}^{\dagger}$ and $H_{l,n^-} = H_{l,n^-}^{\times}$, as well as, $H_{i,k^+} = H_{i,k^+}^{\dagger}$ and $H_{i,k^-} = H_{i,k^-}^{\times}$. According to Subsection A.3.9.2, the cross-correlation operator commutes if the functions are both Hermitian or anti-Hermitian that is,

$$C_{l,n^+}^{i,j,k^+}(\omega_m) = C_{l,k^+}^{i,j,n^+}(\omega_m), \tag{6.52}$$

and

$$C_{l,n^-}^{i,j,k^-}(\omega_m) = C_{l,k^-}^{i,j,n^-}(\omega_m). \tag{6.53}$$

This creates even further structure in the correlation patterns. We also know that the addition of Hermitian or anti-Hermitian functions remain Hermitian of anti-Hermitian, according to Subsection A.3.9.2.

Similar relations hold for the ***temporal FHG overlap matrix***. We only summarize the main results.

Replacing, (m, n, k) with (i, j, k), and, (m, n, k), with, (l, m, n), in Eq. (6.26) we obtain,

$$K_{i,j,k}(t) = e^{i\omega_j(t+t_i)}\phi_k(t), \tag{6.54}$$

$$K_{l,m,n}(t) = e^{i\omega_m(t+t_l)}\phi_n(t), \tag{6.55}$$

respectively. We also have,

$$\begin{aligned}\mathcal{T}_{t_l}K_{l,m,n}(t) &= K_{l,m,n}(t-t_l),\\ &= e^{i\omega_m t}\phi_n(t-t_l) = \hat{f}_{l,m,n}(t).\end{aligned} \tag{6.56}$$

Similar to Eq. (6.36) we can define a cross-correlation function,

$$\boxed{X^{l,m,n}_{i,j,k}(t) = \left(K_{i,j,k} \star K_{l,m,n}\right)(t)} \tag{6.57}$$

From equation Eq. (6.29) replacing, (m,n,k) with (i,j,k), we find.

$$X_{i,j,k}(t_i) = \left(K_{i,j,k} \star \hat{s}\right)(t_i). \tag{6.58}$$

Now substituting the signal, $\hat{s}(t)$, with the FHG basis time function, $\hat{f}_{l,m,n}(t)$, the above equation transforms to,

$$X^{l,m,n}_{i.j,k}(t_i) = \left(K_{i,j,k} \star \hat{f}_{l,m,n}\right)(t_i). \tag{6.59}$$

From the definition of the temporal FHG overlap matrix, Eq. (6.31), and Eq. (6.57) we find,

$$\mathbb{T}^{l,m,n}_{i,j,k} = \left(K_{i,j,k} \star K_{l,m,n}\right)(t_{il}). \tag{6.60}$$

Using Eq. (6.59) the Eq. (6.60) transforms to,

$$\boxed{\mathbb{T}^{l,m,n}_{i,j,k} = X^{l,m,n}_{i,j,k}(t_{il})} \tag{6.61}$$

Proposition 6.6.2. The functions, $\hat{f}_{l,m,n}(t)$, are Hermitian, denoted by †, if, $n = 0, 1, 2, \ldots$, are even and anti-Hermitian, denoted by ×, if n is odd. (See Subsection A.3.7 for the definition of Hermitian), i.e.,

$$\hat{f}_{l,m,n}(t) = \begin{cases} \hat{f}^{\dagger}_{l,m,n}(t) & \text{if } n \text{ is even} \\ \hat{f}^{\times}_{l,m,n}(t) & \text{if } n \text{ is odd} \end{cases}$$

that is, $\hat{f}_{l,m,n^+}(t) = \hat{f}^{\dagger}_{l,m,n^+}(t)$ and $\hat{f}_{l,m,n^-}(t) = \hat{f}^{\times}_{l,m,n^-}(t)$.

Corollary 6.6.3. *From the property, $\mathcal{T}_{t_l} K_{l,m,n}(t) = \hat{f}_{l,m,n}(t)$, the functions, $K_{l,m,n}(t)$, do not possess this Hermitian and anti-Hermitian property, only the translated functions, $\mathcal{T}_{t_l} K_{l,m,n}(t)$.*

Translation invariance of the cross-correlation operation on the second function shows that with, $\mathcal{T}_{t_l}$,

$$\begin{aligned} \mathcal{T}_{t_l} X^{l,m,n}_{i.j,k}(t_i) &= X^{l,m,n}_{i.j,k}(t_{il}) \\ &= \left(K_{i,j,k} \star \hat{f}_{l,m,n}\right)(t_{il}) \\ &= \mathbb{T}^{l,m,n}_{i,j,k}. \end{aligned} \tag{6.62}$$

The orthogonality of the Hermite-Gauss polynomials once again imply,

$$\boxed{\mathbb{T}^{i,j,n}_{i,j,k} = \delta_{nk}} \tag{6.63}$$

We can also write,

$$X^{l,m,n}_{i.j,k}(t_i) = \left(K_{i,j,k} \star \hat{f}_{l,m,n}\right)(t_i) = e^{it_l\omega_{mj}} \int_{-\infty}^{\infty} \phi_k(t) e^{i\omega_{mj}(t+t_{il})} \phi_n(t+t_{il})\, dt. \tag{6.64}$$

Similarly,

$$X^{p,q,n}_{r,s,k}(t_r) = \left(K_{r,s,k} \star \hat{f}_{l,m,n}\right)(t_r) = e^{it_p\omega_{qs}} \int_{-\infty}^{\infty} \phi_k(t) e^{i\omega_{qs}(t+t_{rp})} \phi_n(t+t_{rp})\, dt. \tag{6.65}$$

The integrals in Eq. (6.64) and Eq. (6.65) will be equal if, $t_{il} = t_{rp}$ and $\omega_{mj} = \omega_{qs}$. Thus we have actually proofed that the correlation patterns are translation invariant in the time-frequency planes, except for an addition of a phase that depends on the times, t_l and t_p, for, $n = k$, and even more, that this remains true for any two time-frequency planes, i.e., $n \neq k$,

$$\boxed{e^{-it_l\omega_{mj}} X^{l,m,n}_{i.j,k}(t_i) = e^{-it_p\omega_{qs}} X^{p,q,n}_{r,s,k}(t_r) \qquad \text{if } t_{il} = t_{rp} \quad \text{and} \quad \omega_{mj} = \omega_{qs}} \tag{6.66}$$

with both differences still in the bounds of the time-frequency plane. If furthermore, $t_l = t_p$, the phases are equal and the correlations are equal under the same conditions.

Eq. (6.60) can be compared with Eq. (6.37),

$$\mathbb{T}^{l,m,n}_{i,j,k} = \left(K_{i,j,k} \star K_{l,m,n}\right)(t_{il}),$$

$$\mathbb{S}^{l,m,n}_{i,j,k} = \left(H_{i,k} \star H_{l,n}\right)(\omega_{jm}).$$

This exemplifies the differences between the two overlap matrices. Excluding the fact that the roles of time, t_{il}, and angular frequency, ω_{jm}, have been swopped they represent the cross-correlation of two different basis functions, namely the, $K_{i,j,k}$, and the, $H_{i,k}$, which exhibit different properties. This can more easily be seen from Eq. (6.56) and Eq. (6.41) which results in the following Fourier transform pair,

$$\mathcal{F}\left\{\mathcal{T}_{t_l} K_{l,m,n}(t)\right\} = \mathcal{T}_{\omega_m} H_{l,n}(\omega). \tag{6.67}$$

Summary

- The ***Spectral FHG Overlap Matrix*** is defined in, Eq. (6.32)

  $$\mathbb{S}^{l,m,n}_{i,j,k} = \langle \hat{F}^*_{i,j,k}(\omega) | \hat{F}_{l,m,n}(\omega) \rangle = \int_{-\infty}^{\infty} \hat{F}^*_{i,j,k}(\omega)\, \hat{F}_{l,m,n}(\omega)\, \mathrm{d}\omega.$$

  In terms of correlations this is defined as, Eq. (6.37)

  $$\boxed{\mathbb{S}^{l,m,n}_{i,j,k} = C^{l,n}_{i,k}(\omega_{jm}) = \left(H_{i,k} \star H_{l,n}\right)(\omega_{jm})}$$

If in Eq. (6.46) we substitute the spectral signal, $\hat{\hat{\varepsilon}}(\omega) = \hat{S}(\omega)$, with a spectral FHG basis function, $\hat{S}(\omega) = \hat{F}_{l,m,n}(\omega)$, we find, Eq. (6.47),

$$C^{l,m,n}_{i,k}(\omega_j) = C_{i,k}(\omega_j) = \left(H_{i,k} \star \hat{F}_{l,m,n}\right)(\omega_j).$$

- The ***Temporal FHG Overlap Matrix*** is defined in, Eq. (6.31)

  $$\mathbb{T}^{l,m,n}_{i,j,k} = \langle \hat{f}^*_{i,j,k}(t) | \hat{f}_{l,m,n}(t) \rangle = \int_{-\infty}^{\infty} \hat{f}^*_{i,j,k}(t)\, \hat{f}_{l,m,n}(t)\, \mathrm{d}t.$$

In terms of correlations this is defined as, Eq. (6.61),

$$\boxed{\mathbb{T}^{l,m,n}_{i,j,k} = X^{l,m,n}_{i,j,k}(t_{il}) = \left(K_{i,j,k} \star K_{l,m,n}\right)(t_{il})}$$

If in Eq. (6.29) we substitute the temporal signal, $\hat{\varepsilon}(t) = \hat{s}(t)$, with a spectral FHG basis function, $\hat{s}(t) = \hat{f}_{l,m,n}(t)$, we find, Eq. (6.57),

$$\boxed{X^{l,m,n}_{i,j,k}(t_m) = \left(K_{i,j,k} \star K_{l,m,n}\right)(t_m)}$$

6.6.1. Numerical Reconstruction of the Complete FHG Basis

The spectral cross-correlations of a spectral FHG basis is given by Eq. (6.46) and using the notation of Eq. (6.47) we have,

$$C^{l,m,n}_{i,k}(\omega_j) = \left(H_{i,k} \star \hat{F}_{l,m,n}\right)(\omega_j).$$

Similarly, the temporal cross-correlations of a temporal FHG basis is given by Eq. (6.59),

$$X^{l,m,n}_{i.j,k}(t_i) = \left(K_{i,j,k} \star \hat{f}_{l,m,n}\right)(t_i).$$

With a specific fixed basis in mind, (l, m, n). both, $C^{l,m,n}_{i,k}(\omega_j)$ and $X^{l,m,n}_{i.j,k}(t_i)$, form a discrete cube or lattice in three dimensional space, (x, y, z), corresponding to cross-correlation, as depicted graphically in Figure 5.2.

As a result of Eq. (6.51) the spectral cross-correlations, $C^{l,m,n}_{i,k}(\omega_j)$, form mosaic patterns on the various z-axis planes, the HG part of the basis, centered about the, (l, m), represented temporal FHG basis. Because of all the various symmetries, we find that these patterns remain translation invariant in the time-frequency, i.e., moving, $(l.m)$ to (p, q), results in the same patterns about, (p, q, n), and the patterns occurring in the various k-planes, although different in each k-plane centered about, (p, q).

Similar results due to Eq. (6.66) apply to the temporal cross-correlations, $X^{l,m,n}_{i.j,k}(t_i)$. Each forms mosaic patterns on the various z-axis planes, the HG part of the basis, centered about the, (l, m), represented temporal FHG basis, that remain translationally invariant in the time-frequency, (l, m), on a specific z-plane, and these various patterns remain invariant on the various k-planes.

To avoid the phases, we represent the planes only in absolute value, to demonstrate the effects of the previous two paragraphs. To conform, we numerically calculate the FHG TFR bases, for all (l, m, n) and (i, j, k) up to $(25, 25, 25)$, for the spectral and temporal bases. One of the consequences of unscaling the spectral and temporal FHG bases is that their amplitudes in the two representation are the same. This can easily be seen by comparing Figure 6.7 and Figure 6.10.

In Figure 6.5 and Figure 6.6, we show the absolute spectral FHG basis $(l, m, n) = (10, 16, 6)$ and the patterns formed on all $(i, j, k) = (i, j, 6)$ and the translated translated time-frequency $(l, m, n) = (15, 8, 6)$ and all $(i, j, k) = (i, j, 6)$, $(l, m, n) = (10, 16, 6)$ as well as and the patterns $(i, j, k) = (i, j, 14)$, i.e., still centered at the 6th HG at $(l, m, n) = (10, 16, 6)$, but what is the pattern on the 14th HG plane, and $(l, m, n) = (15, 8, 6)$ with all $(i, j, k) = (i, j, 14)$, respectively. In both figures the amplitudes are depicted with their accompanying phases patterns directly below.

In both these figures, it is obvious that the phase patterns also translate, but that the phase patterns are very complex. As an aside, one can say that these figures are mathematical rendering of beautiful mosaic artwork. To appreciate the mosaic phase patterns one must be aware that, standing in a forest that one does not see the leaves for the trees. As a consequence of Eq. (6.44) we see that in Figure 6.5 the center tiles are equal to one and in Figure 6.6 they are zero.

In Figure 6.7, we demonstrate the spectral reconstruction of the 6th FHG basis, dotted in blue compared to the true spectral basis in green. To paraphrase, in Figure 6.7, we treat one of the FHG basis, specifically the FHG basis $(l, m, n) = (10, 16, 6)$, as the signal, and reconstruct the spectral basis signal in Figure 6.7(a), and the temporal basis signal, Figure 6.7(b), using Eq. (6.76) and Eq. (6.74), respectively. Because we are using FHG bases, we must also replace $C_{m,k}(\omega_n)$ with $C_{i,k}^{l,m,n}(\omega_j)$ and $X_{m,n,k}(t_m)$ with $X_{i.j,k}^{l,m,n}(t_i)$, respectively. The unwrapped spectral phase reconstructions are shown directly below each amplitude reconstruction. The translated TF version is shown next to the first set.

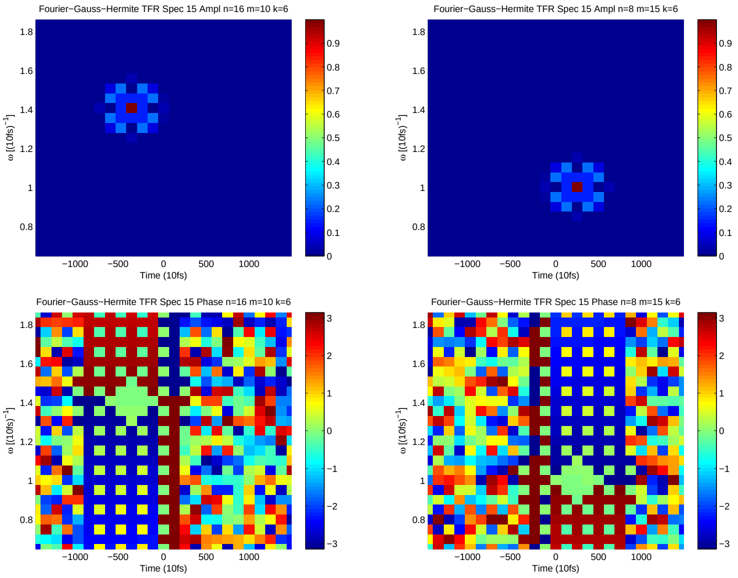

Figure 6.5.: FHG TFR Spectral 6th FHG basis and TF translation 6th HG

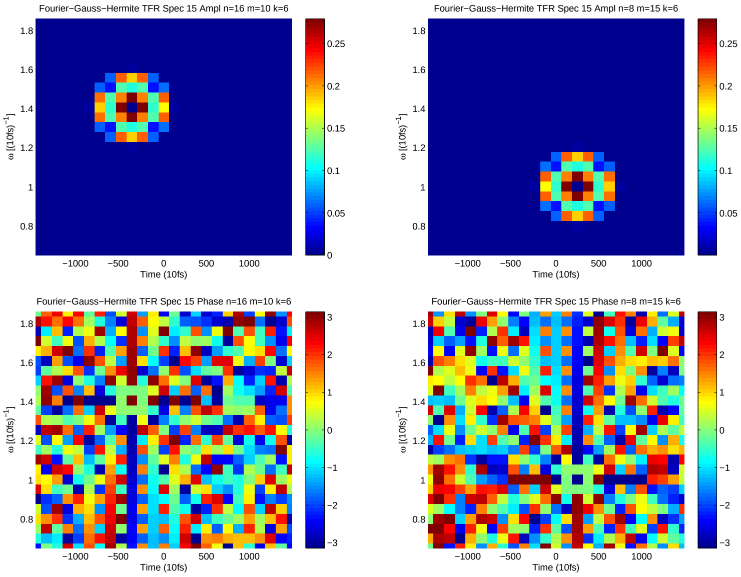

Figure 6.6.: FHG TFR Spectral 6th FHG basis and TF translation 14th HG

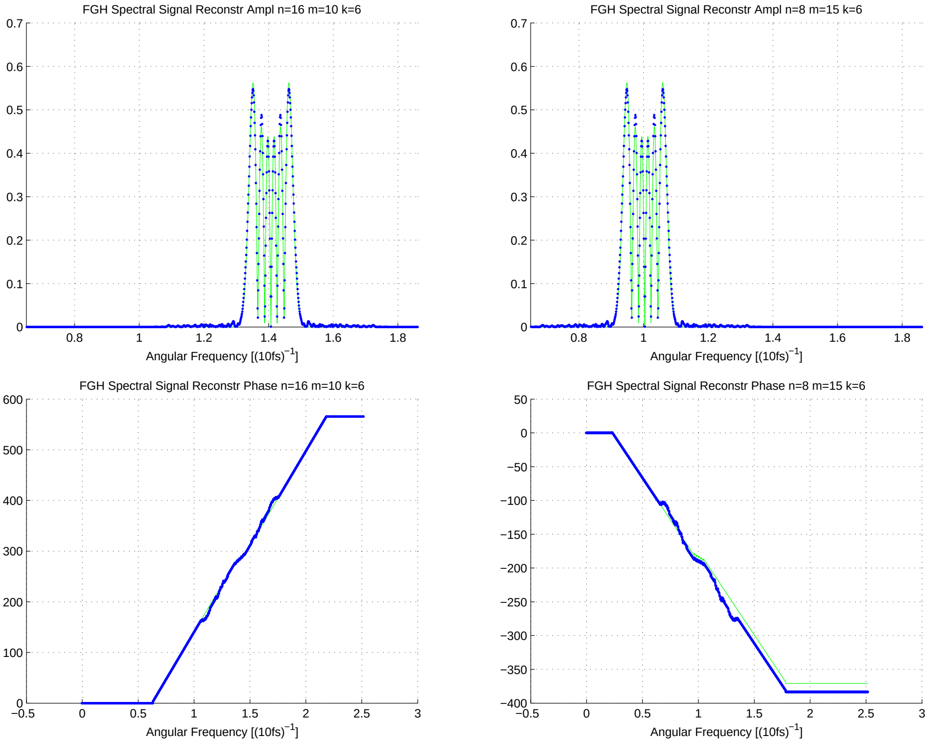

Figure 6.7.: FHG TFR Spectral 6th FHG basis reconstruction & TF translation

Similarly, for Figure 6.8 and Figure 6.9, we depict the absolute temporal FHG bases, exactly the same as in the previous figures. In Figure 6.8 and Figure 6.9, we show the absolute temporal FHG basis $(l, m, n) = (10, 16, 6)$ and the patterns formed on all $(i, j, k) = (i, j, 6)$ and the translated time-frequency (TF) $(l, m, n) = (15, 8, 6)$ and all $(i, j, k) = (i, j, 6)$, $(l, m, n) = (10, 16, 6)$, as well as the patterns $(i, j, k) = (i, j, 14)$ and $(l, m, n) = (15, 8, 6)$ with all $(i, j, k) = (i, j, 14)$, respectively. Once again, we see that that the accompanying phase also translate in the TF plane. This proves our analytic results numerically at least for the absolute (amplitude) values. As a consequence of Eq. (6.63) we see that in Figure 6.8 the center tiles are equal to one and in Figure 6.9 they are zero.

In Figure 6.10, we demonstrate the temporal reconstruction of the 6th FHG basis, dotted in blue compared to the true spectral basis in green. The unwrapped spectral phase reconstructions are shown directly below each amplitude reconstruction. The translated TF version is shown next to the first set.

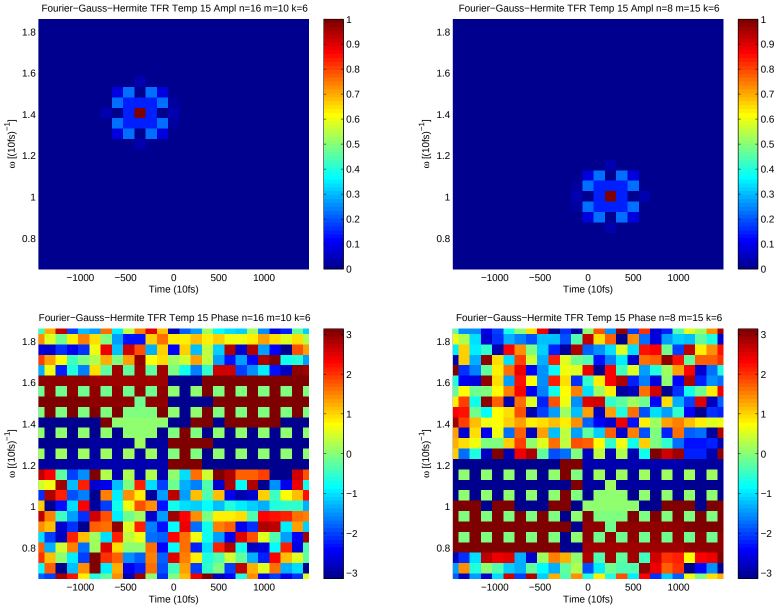

Figure 6.8.: FHG TFR Temporal 6th FHG basis and TF translation 6th HG

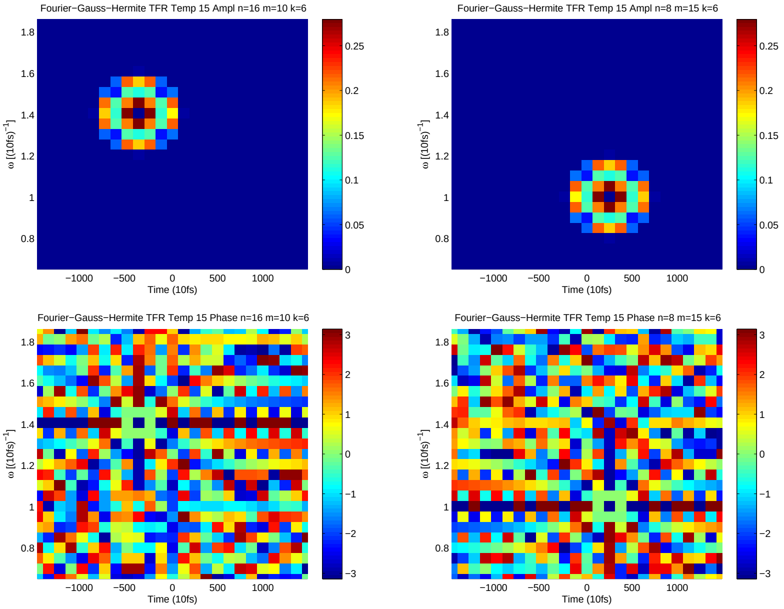

Figure 6.9.: FHG TFR Temporal 6th FHG basis and TF translation 14th HG

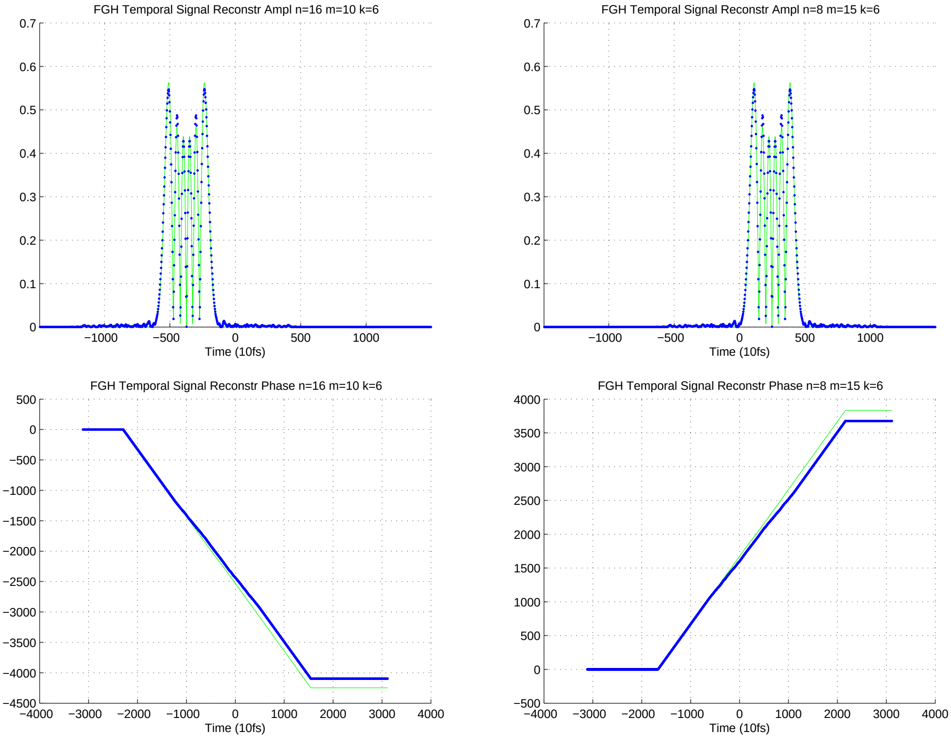

Figure 6.10.: FHG TFR Temporal 6th FHG basis reconstruction & TF translation

The amazing signal reconstruction of the temporal and spectral signals, see Section 6.7, and Figure 6.7 and Figure 6.10, reconstructed just with the temporal and spectral cross correlation lattice cube, shows, that somehow the temporal and spectral cross correlation lattice cubes contain the complete information of the TFR of the FHG. An ideal testing ground is to see how a TFR can be constructed given that the signal is precisely a FHG temporal or spectral FHG basis function.

The first thing that we notice, is the complex phase patterns that result. To remove the phase of each TF from the various HG correlations, we simply take the complex inner product of the of the FHG TFR correlation lattice cube of each of the spectral and temporal lattice cubes, Eq. (6.68) and Eq. (6.69), respectively. This then projects or collapses the lattice cube to just a time-frequency plane, i.e., a true TFR for the spectral and temporal bases functions.

In Figure 6.11, we plot the individual complex inner products of Eq. (6.68) of the spectral FHG lattice cube correlation of the spectral FHG basis $\hat{F}_{m.n,k}(\omega)$ centered on the center of the TF plane, i.e., $(m, n, k) = (13, 13, k)$ and $k = 1, \ldots, 24$. (We should have gone to $k = 25$, but this does not fit on a page). The complex inner product of course destroys the phase, and we have already shown the TF translation invariance. This means that the mosaic pattern shifts around without change in the TF plane, i.e., for any (m, n). Thus, although Figure 6.11 depicts the complex inner product spectral FHG lattice cube correlation of the spectral FHG basis, the *temporal* complex inner product FHG lattice cube correlation, have exactly the same patterns. Using Eq. (6.46) the complex inner product is just taken as,

$$\mathcal{C}_{i,j}^{m,n,k} = \sum_{l=1}^{25} C_{i,l}^{m,n,k}(\omega_j) \cdot \left[C_{i,l}^{m,n,k}(\omega_j) \right]^*, \tag{6.68}$$

where the TFR is taken over all $(i, j) = (t_i, \omega_j)$. If this same procedure is applied to the temporal FHG basis, $\hat{f}_{m.n,k}(t)$, centered on the center of the TF plane, i.e., $(m, n, k) = (13, 13, k)$ and $k = 1, \ldots, 24$. With the use of Eq. (6.59) we define,

$$\mathcal{X}_{i,j}^{m,n,k} = \sum_{l=1}^{25} X_{i.j,l}^{m,n,k}(t_i) \cdot \left[X_{i.j,l}^{m,n,k}(t_i) \right]^*. \tag{6.69}$$

Temporally, exactly the same mosaic patterns appear, i.e.,

$$\boxed{\mathcal{C}_{i,j}^{m,n,k} = \mathcal{X}_{i,j}^{m,n,k}} \tag{6.70}$$

We now define two **normal inner products** (in these definitions we retain the phase of the TFRs) as,

$$\mathcal{S}_{i,j}^{m,n,k} = \sqrt{\sum_{l=1}^{25} C_{i,l}^{m,n,k}(\omega_j) \cdot C_{i,l}^{m,n,k}(\omega_j)}, \tag{6.71}$$

and

$$\mathcal{T}_{i,j}^{m,n,k} = \sqrt{\sum_{l=1}^{25} X_{i.j,l}^{m,n,k}(t_i) \cdot X_{i.j,l}^{m,n,k}(t_i)}, \tag{6.72}$$

for the spectral and temporal TFRs respectively. In these inner products the phase is not destroyed and to avoid doubling the phase we take the square roots of the products. Figure 6.12 and Figure 6.13, show the amplitudes and their accompanying phases directly below each amplitude, of the various terms of Eq. (6.71), and Figure 6.14 and Figure 6.15 show the amplitudes and their accompanying phases directly below, of the various temporal FHG bases, i.e., Eq. (6.72).

We specifically decentered these graphs within the TF plane with $(m, n) = (10, 16)$, to show the main result of comparing Figure 6.12 and Figure 6.13 with Figure 6.14 and Figure 6.14, that the mosaic patterns are rotated by 90^0 about the center points in both amplitude and phase.

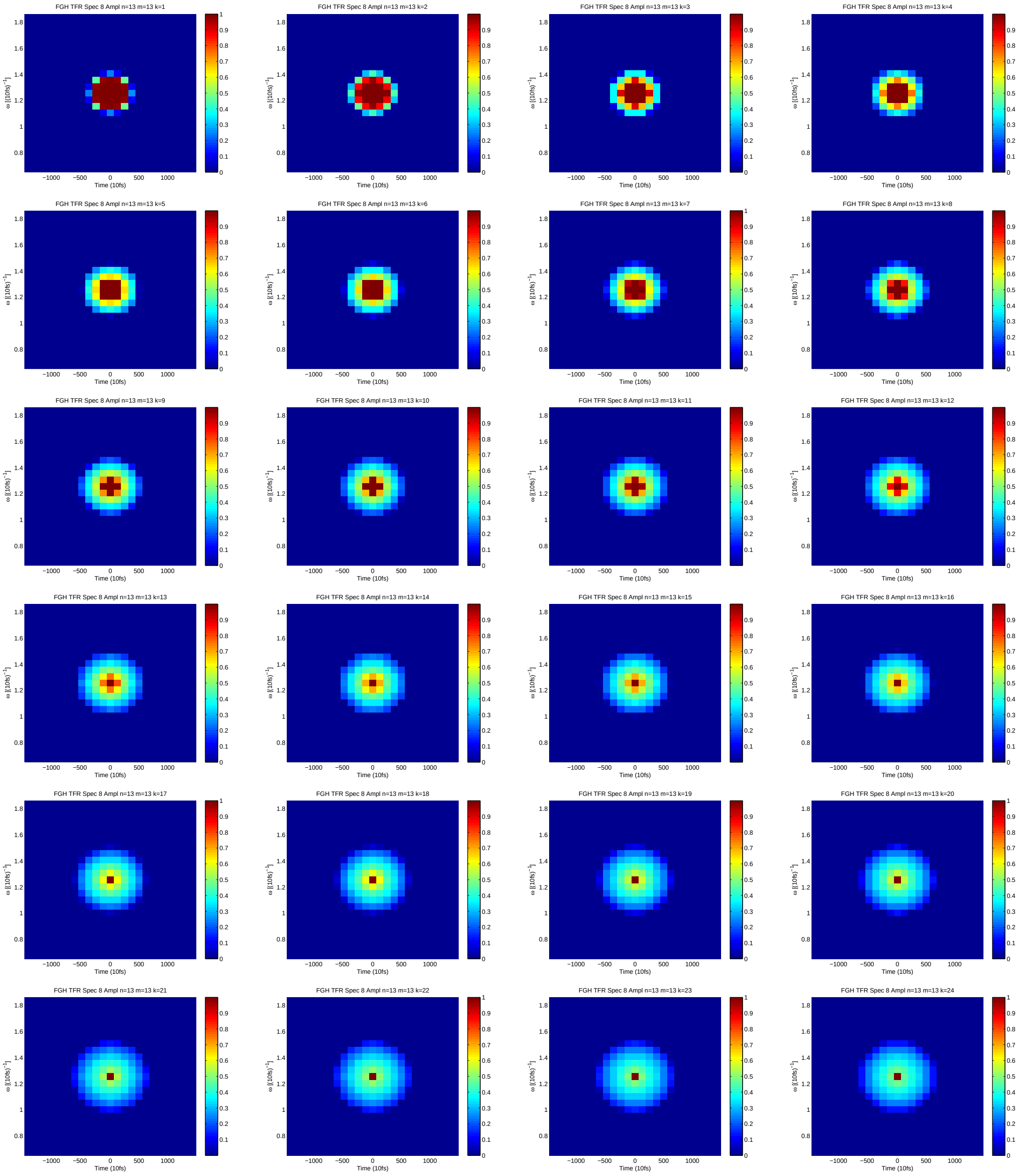

Figure 6.11.: FHG TFR Spectral HG complex inner product (All FHG Spectral bases)

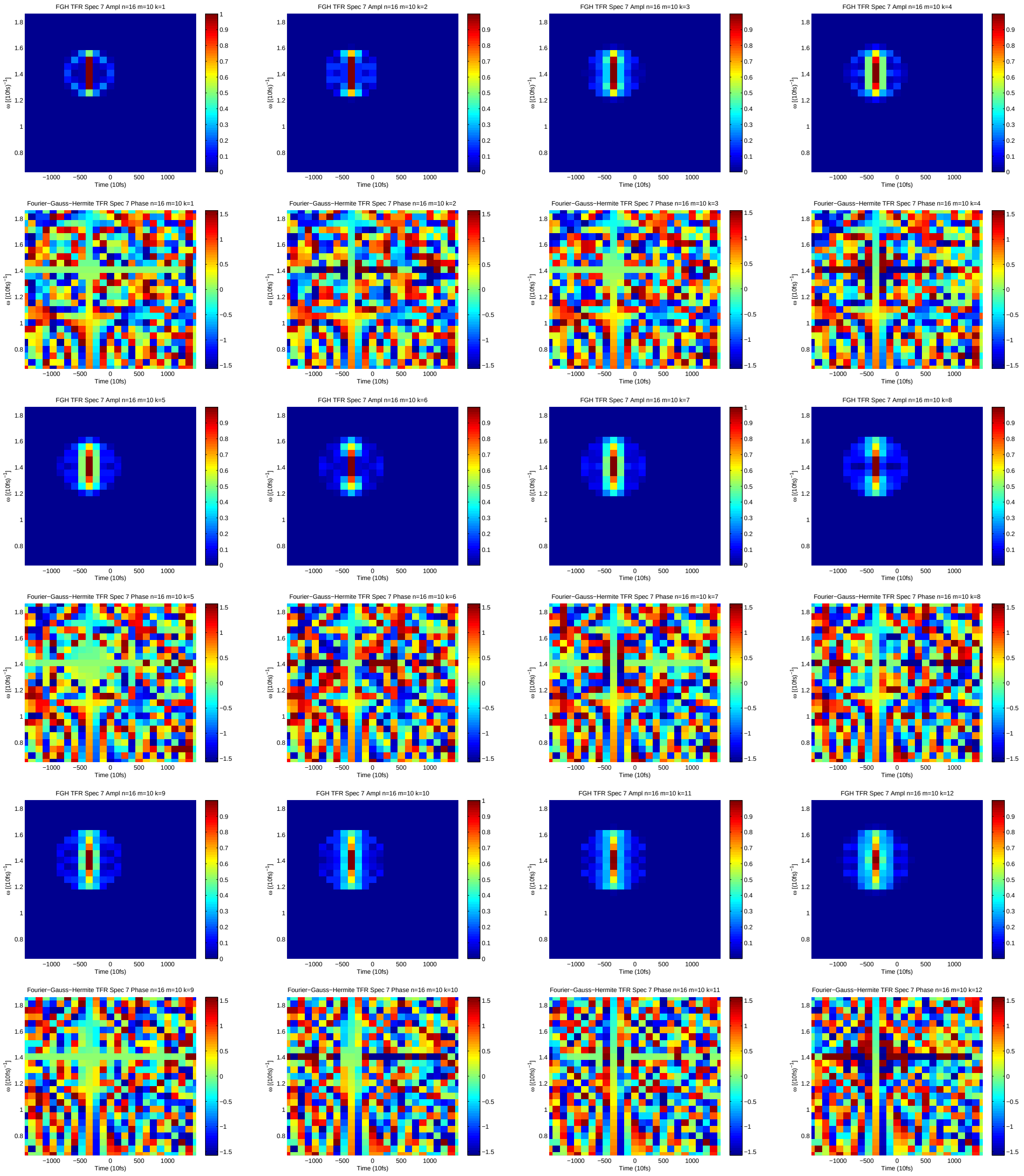

Figure 6.12.: FHG TFR Spectral HG inner product (1-12 FHG Spectral bases)

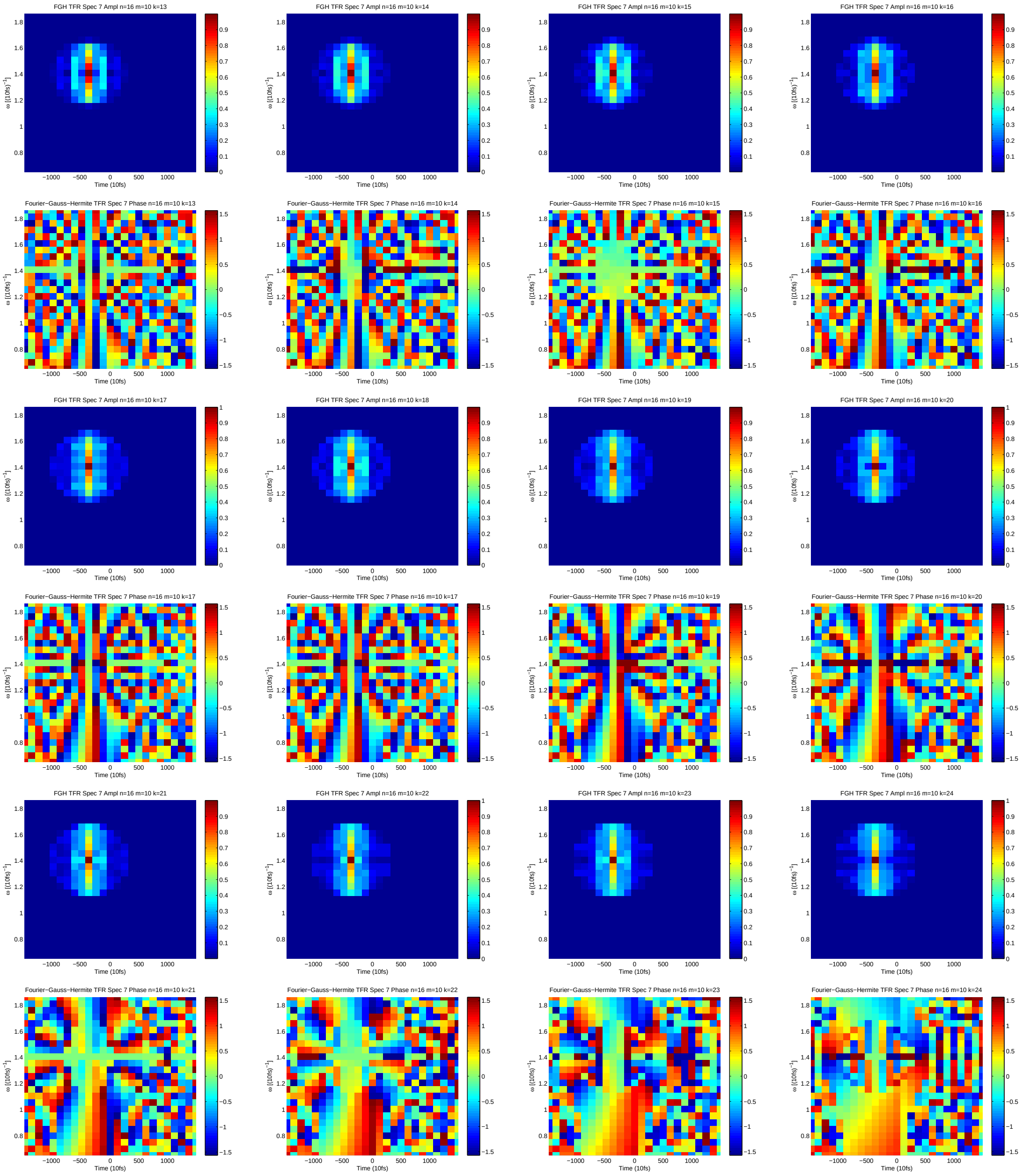

Figure 6.13.: FHG TFR Spectral HG inner product (13-24 FHG Spectral bases)

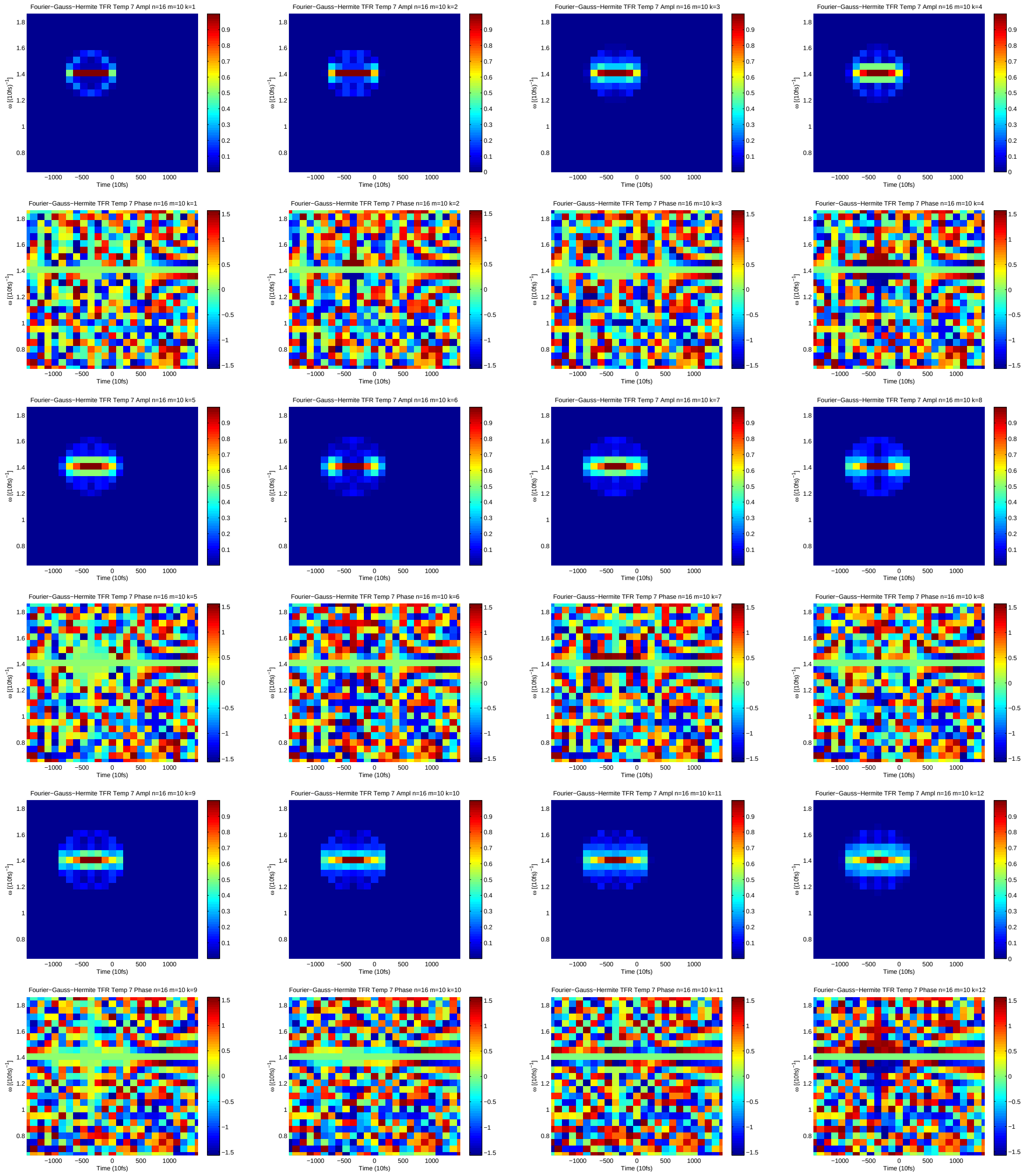

Figure 6.14.: FHG TFR Temporal HG inner product (1-12 FHG Temporal bases)

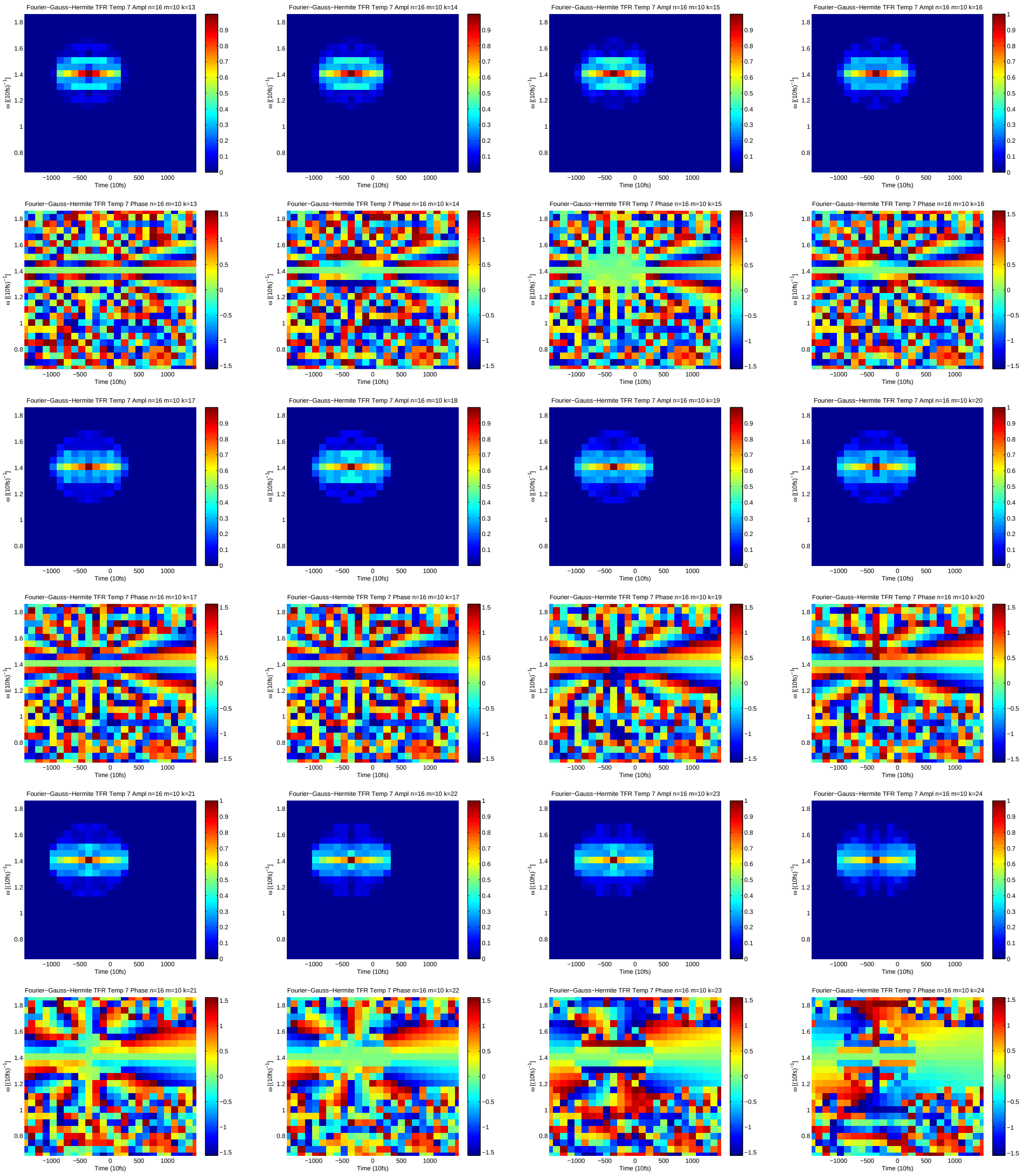

Figure 6.15.: FHG TFR Temporal HG inner product (13-24 FHG Temporal bases)

6.7. Signal Reconstruction with the Complete FHG TFR

The Hermite-Gauss polynomials are orthogonal. It is extremely desirable to exploit this fact to our benefit. For our FHG bases, the orthogonality can only be achieved at the same time and frequency, i.e., (t_m, ω_n). Because the integrals, in Section 6.5, were shown to be correlations with the signal, by taking the inner product with the reconstruction FHG basis vectors over the Hermite-Gauss polynomials, we effectively reconstruct a portion of the signal that correlates best with the specific chosen (t_m, ω_n). In fact we are collapsing the cube to form a FHG TFR. Every (t_m, ω_n) corresponds to the best signal correlation over time, see Eq. (6.29), i.e.,

$$\boxed{T_{m,n}(t) = \sum_k X_{m,n,k}(t_m) \cdot \hat{f}_{m,n,k}(t)} \tag{6.73}$$

The **temporal signal reconstruction** is then simply performed by summing over the (m, n), i.e.,

$$\boxed{s(t) = \sum_{m,n} T_{m,n}(t)} \tag{6.74}$$

Similarly, for the angular frequency, see Eq. (6.24), we define,

$$\boxed{W_{m,n}(\omega) = \sum_k C_{m,k}(\omega_n) \cdot \hat{F}_{m,n,k}(\omega)} \tag{6.75}$$

The **spectral signal reconstruction** of the angular frequency is given by,

$$\boxed{S(\omega) = \sum_{m,n} W_{m,n}(\omega)} \tag{6.76}$$

These reconstructions work amazingly well, in both amplitude and phase.

6.8. The Complete FHG TFR

However, $T_{m,n}(t)$ and $W_{m,n}(\omega)$, still do not represent TFRs. They definitely, however, contain all the signal information. One potential way to construct the TFRs representation, is by simply taking the **mean** over each (t_m, ω_n). This then contains the amplitude and phase information of the best reconstructed correlations for each (t_m, ω_n).

$$\boldsymbol{\mathcal{T}}_{m,n} = \mathrm{mean}_t\{T_{m,n}(t)\}, \tag{6.77}$$

and

$$\boldsymbol{\mathcal{W}}_{m,n} = \text{mean}_\omega\{W_{m,n}(\omega)\}. \tag{6.78}$$

A special word of warning is in order here. In the construction of the signal correlations, $X_{n,k}(t_m)$ and $C_{m,k}(\omega_n)$, special care must be taken for the signals, $s(t)$ and $S(\omega)$, so that their phases are masked to match the FHG basis functions phases. This improves the results. What really happens with the mean operation is that the phases tend to go out of phase and that the mean does not then represent the true TFR. Unfortunately, this does not give very good TFRs. In Figure 6.16 and Figure 6.17, the spectral and temporal FHG TFRs are shown respectively. Below each amplitude and phase TFR the spectral and temporal amplitude and phase signal reconstructions are also given. The reconstructions are remarkably good. All the signal reconstructions are done in the same manner and therefore in the following representations they are not shown. The problem remains to obtain an acceptable FHG TFR in amplitude and in phase. This is what we now concentrate on. Continuing in the vein of attempting to develop a normal inner product (without destroying the phase, Eq. (6.71) and Eq. (6.72)) of the spectral and temporal signal reconstructions. This is shown in Figure 6.18 and once again we see that the spectral and temporal FHG TFRs have no match. Thus we leave the attempts to construct TFRs from their individual signal reconstructions and move on to the two correlation lattice cubes, $X_{m,n,k}(t_m)$ and $C_{m,k}(\omega_n)$.

The two correlation lattice cubes $X_{m,n,k}(t_m)$ and $C_{m,k}(\omega_n)$ for the temporal and spectral signal correlation respectively, contain all the information of the TFRs and the signal reconstructions do not require the construction of an overlap matrix and, what a relief, its pseudo-inverse. As a first attempt we simply try FHG TFR (case 7)[1] spectral and temporal HG cube inner product, but this also gives rotten results, as depicted in Figure 6.19. It seems the two representations are orthogonally related with a similarity transformation of the conjugate as proven in Theorem 5.4.9.

In investigating and researching the spectral FHG TFRs we found that the TFRs of the FHG spectral and temporal representations, Eq. (6.71) and Eq. (6.72), respectively is rotated by 90^0 in the TF plane. One would expect the TFRs of both the temporal and spectral FHG bases to be symmetrical in a TFR since they are all just HG polynomials of various orders. We now define a average sum of two normal inner products as,

$$\boldsymbol{\mathcal{G}}_{i,j}^{m,n,k} = \left(\mathcal{S}_{i,j}^{m,n,k} + \mathcal{T}_{i,j}^{m,n,k}\right)/2. \tag{6.79}$$

---

[1] The cases are as they are numbered in the Matlab© program and do not appear here in sequence.

This immediately makes the representation of the FHG TFR bases symmetrical. Figure 6.20 and Figure 6.21 display the beautiful symmetrical mosaic Maltese crosses that result from Eq. (6.79), for all $(i, j) = (t_i, \omega_j)$ in TF plane and the FHG bases $(m, n, k) = (10, 16, k), \ \forall\, k$. What is also obvious in these TFRs, is that due to, most probably, phase dematching that the side mosaic patterns contribute mush less and that the TFRs are more centralized than the individual contributions of the spectral, Figure 6.12 and Figure 6.13, and temporal, Figure 6.14 and Figure 6.15, which is most desirable.

This suggests that for any signal, $s(t) \overset{\mathcal{F}}{\Longleftrightarrow} S(\omega)$, that we can define a spectral FHG TFR with the aid of Eq. (6.24),

$$\mathcal{S}_{i,j} = \sqrt{\sum_{k=1}^{25} C_{i,k}(\omega_j) \cdot C_{i,k}(\omega_j)}, \tag{6.80}$$

and a spectral FHG TFR with Eq. (6.29),

$$\mathcal{T}_{i,j} = \sqrt{\sum_{k=1}^{25} X_{i.j,k}(t_i) \cdot X_{i.j,k}(t_i)}, \tag{6.81}$$

and then a general TFRs of the signal just as in Eq. (6.79) as average of the Eq. (6.80) and Eq. (6.81),

$$\boxed{\boldsymbol{\mathcal{A}}_{m,s} = \left(\mathcal{S}_{m,s} + \mathcal{T}_{m,s}\right)/2} \tag{6.82}$$

Once again the TFR doesn't measure up to the expected standard. This is shown in Figure 6.22. It is definitely better, but doesn't come close to our originally summation of the first seven of the spectral lattice as shown in Figure 5.9.

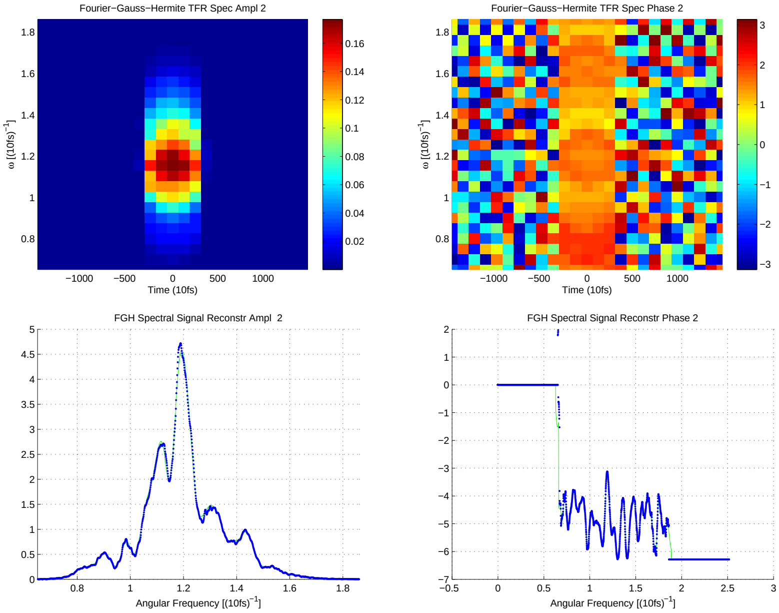

Figure 6.16.: FHG TFR case 2 Mean Spectral Signal with Spectral Amplitude and Phase Reconstruction

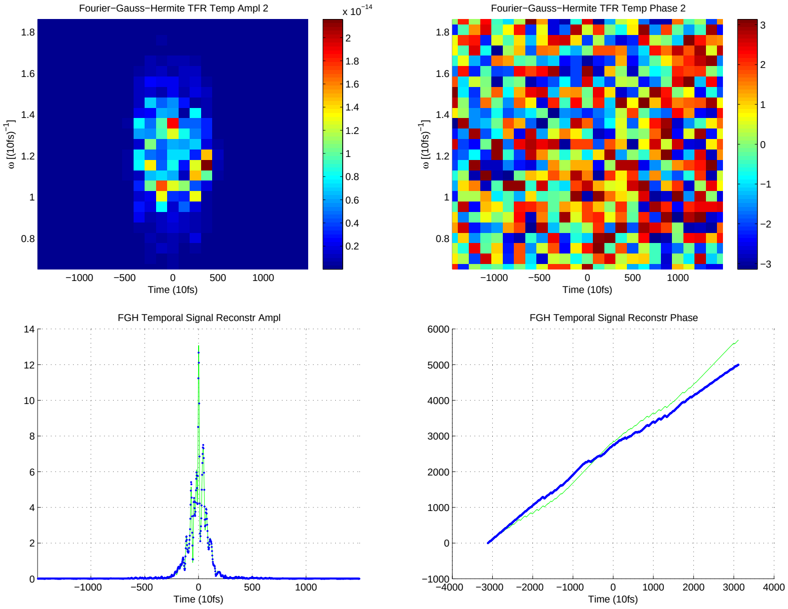

Figure 6.17.: FHG TFR case 2 Mean Temporal Signal with Temporal Amplitude and Phase Reconstruction

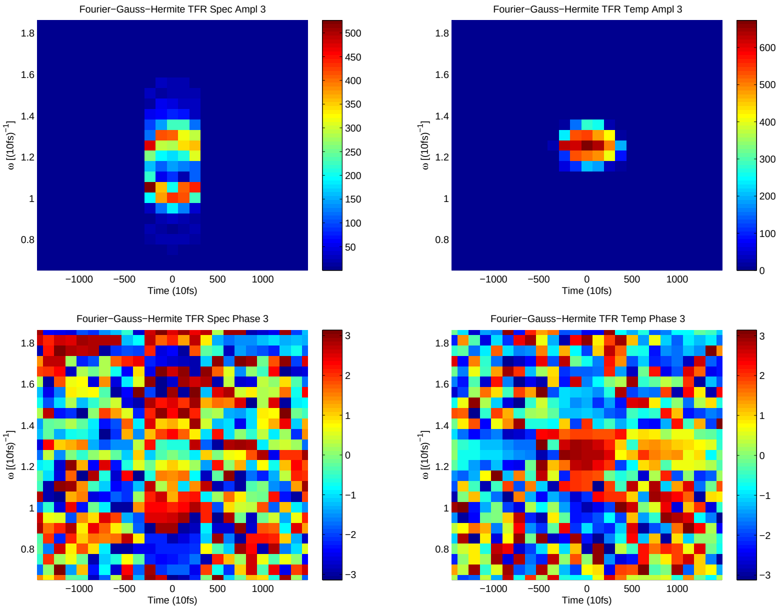

Figure 6.18.: FHG TFR case 3 Spectral and Temporal Signal Inner Product

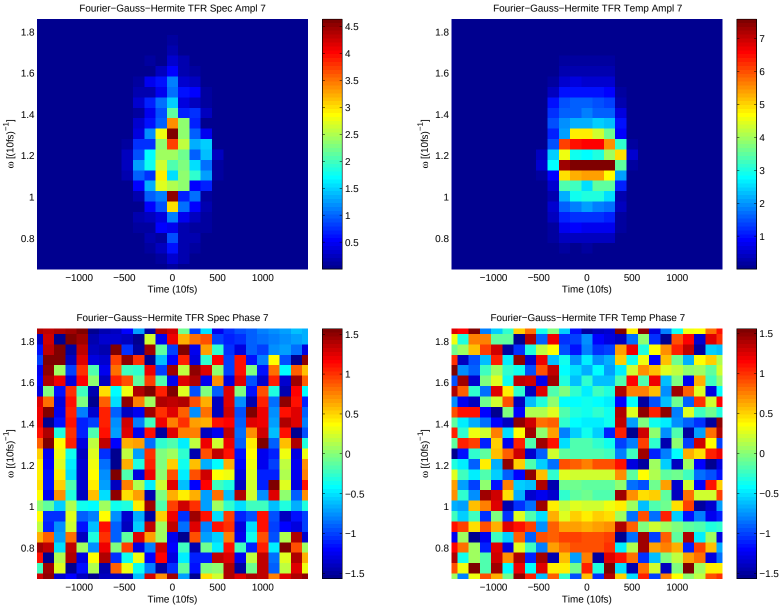

Figure 6.19.: FHG TFR case 7 Spectral and Temporal HG Cube Inner Product

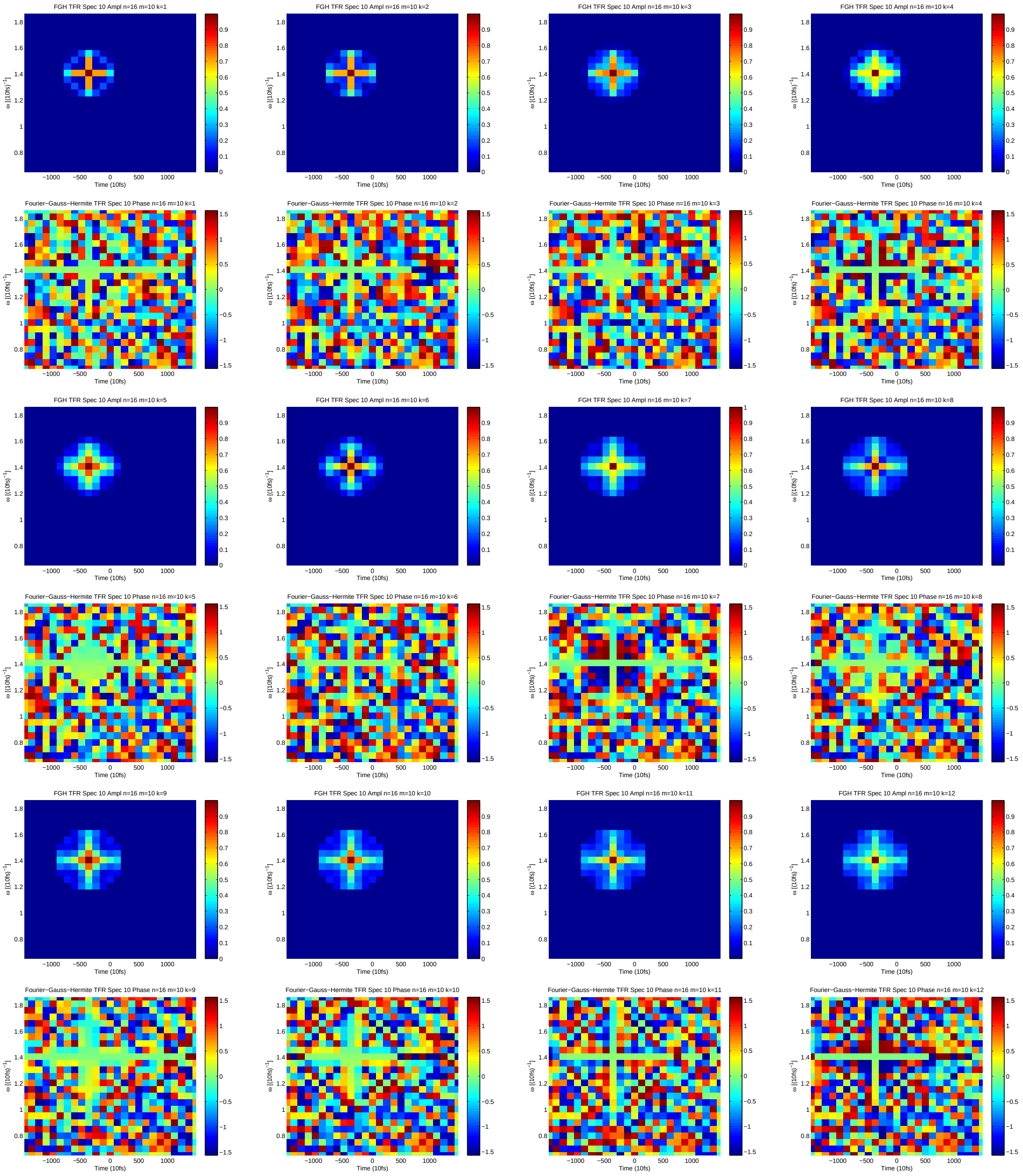

FGH TFR Spec 10 Ampl n=16 m=10 k=1
FGH TFR Spec 10 Ampl n=16 m=10 k=2
FGH TFR Spec 10 Ampl n=16 m=10 k=3
FGH TFR Spec 10 Ampl n=16 m=10 k=4
Fourier−Gauss−Hermite TFR Spec 10 Phase n=16 m=10 k=1
Fourier−Gauss−Hermite TFR Spec 10 Phase n=16 m=10 k=2
Fourier−Gauss−Hermite TFR Spec 10 Phase n=16 m=10 k=3
Fourier−Gauss−Hermite TFR Spec 10 Phase n=16 m=10 k=4
FGH TFR Spec 10 Ampl n=16 m=10 k=5
FGH TFR Spec 10 Ampl n=16 m=10 k=6
FGH TFR Spec 10 Ampl n=16 m=10 k=7
FGH TFR Spec 10 Ampl n=16 m=10 k=8
Fourier−Gauss−Hermite TFR Spec 10 Phase n=16 m=10 k=5
Fourier−Gauss−Hermite TFR Spec 10 Phase n=16 m=10 k=6
Fourier−Gauss−Hermite TFR Spec 10 Phase n=16 m=10 k=7
Fourier−Gauss−Hermite TFR Spec 10 Phase n=16 m=10 k=8
FGH TFR Spec 10 Ampl n=16 m=10 k=9
FGH TFR Spec 10 Ampl n=16 m=10 k=10
FGH TFR Spec 10 Ampl n=16 m=10 k=11
FGH TFR Spec 10 Ampl n=16 m=10 k=12
Fourier−Gauss−Hermite TFR Spec 10 Phase n=16 m=10 k=9
Fourier−Gauss−Hermite TFR Spec 10 Phase n=16 m=10 k=10
Fourier−Gauss−Hermite TFR Spec 10 Phase n=16 m=10 k=11
Fourier−Gauss−Hermite TFR Spec 10 Phase n=16 m=10 k=12

Figure 6.20.: FHG TFR symmetrical HG inner product (1-12 FHG bases)

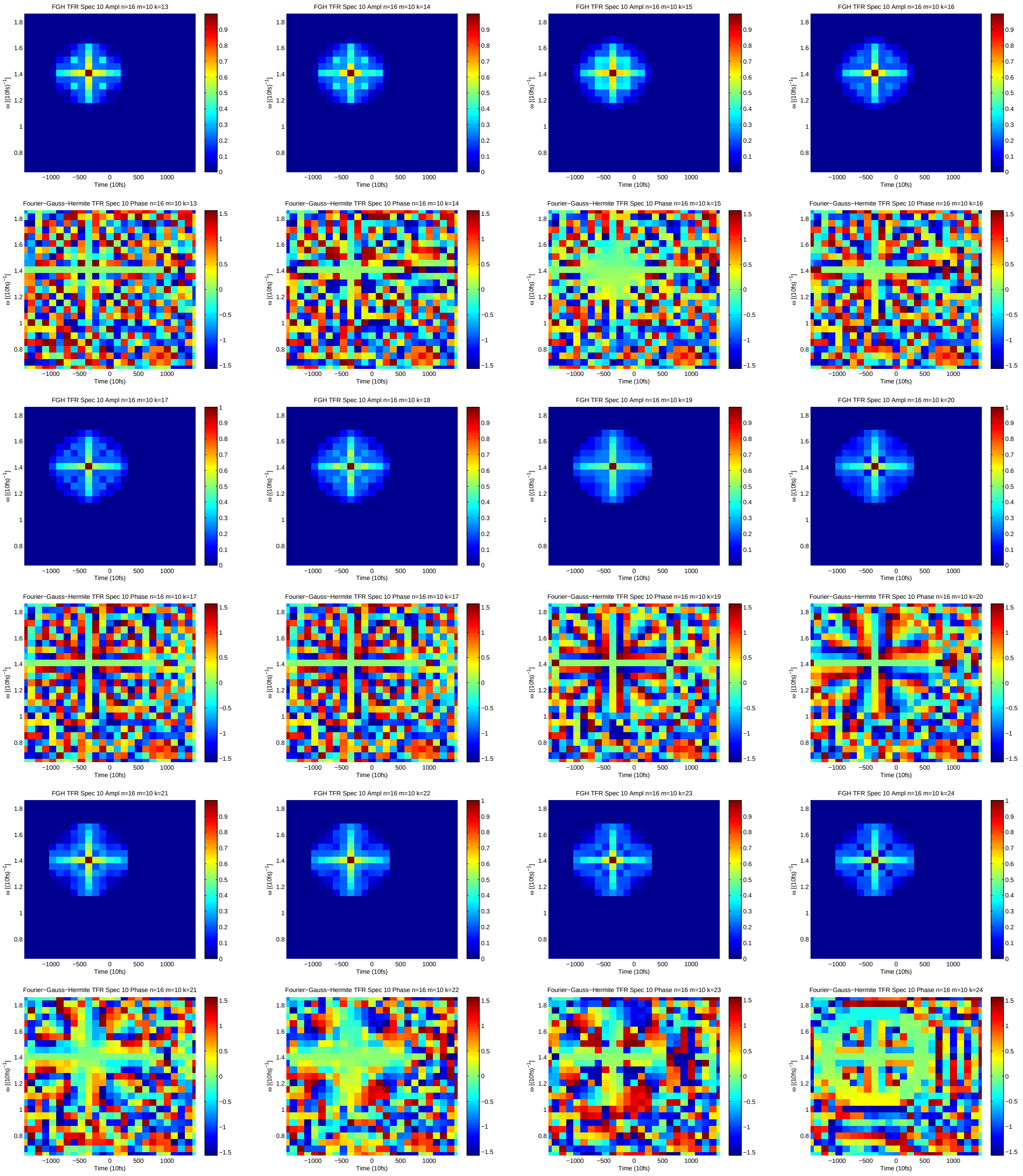

Figure 6.21.: FHG TFR symmetrical HG inner product (13-24 FHG bases)

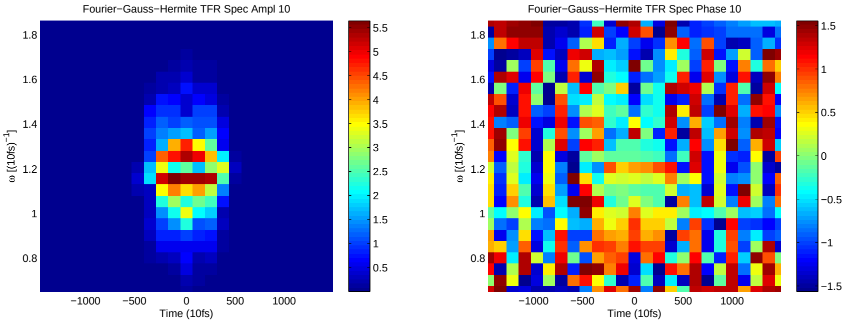

Figure 6.22.: FHG TFR symmetrical HG inner product

The next great question is, because HG frames are orthogonal to each other, spectrally and temporally, can one construct an overlap matrix for each HG TF frame, that can also be applied to both the spectral and temporal representations, as is so nicely performed on the first level, which just happens to be the von Neumann TFR. So let us calculate the overlap matrices for each HG TF frame, spectrally and temporally. In other words, each HG TF plane, as we move into the third dimension of our FHG TFR lattice cube, has a corresponding overlap matrix, that each time coincides with a specific HG order, k. In terms of the general complete overlap matrix, $\mathbb{W}^{i,j,k}_{l,m,n}$, this corresponds with Eq. (5.158), but with the modification, $k = n$, in the HG planes

$$\left[\mathbb{W}^{i,j}_{l,m}\right]_n = \mathbb{W}^{i,j,n}_{l,m,n}.$$

The absolute spectral overlap matrices (625x625) for the HG planes 1-24 are shown in Figure 6.25 (Specifically illustrated in black and white to retain contrast). Similar results are obtained for the absolute temporal overlap matrices. As one obviously notices, as one steps into the HG planes, the overlap matrices obtain extra bands. This is due to the increase of the nodes of the HG polynomials with increasing order. We start with three bands as in the von Neumann representation. As the order of the HG polynomials increase the bands become more prominent and reproduce extra bands up to 11 for our maximum order of 25.

For FHG spectral and temporal bases $(m, n, k) = (10, 16, 6)$, corresponding to Figure 6.24 and Figure 6.25, respectively, the various HG planes $(1 - 24)$ are each multiplied with the inverse of their own overlap matrices. Here we definitely see a direct similarity between the corresponding spectral and temporal patterns of Figure 6.24 and Figure 6.25, respectively. On the sixth pattern there is one prominent correlation, as expected since $(m, n, k) = (10, 16, 6)$, with all its overlapping normalized and wiped out. Compare Figure 6.5 with the overlapping. On the second HG plane we get a little yellow Maltese. On the eighth a diffraction pattern.

The tenth and fifteenth are similar. The third has something with two eyes and the rest resemble some nebulae and or ghostly images. Use your own imagination. But they are similar at least in amplitude.

In Figure 6.26 and Figure 6.27 the amplitude and phase TFRs of this representation is given respectively. At least now the amplitudes resemble each other approximately. The phases look like some abstract paintings I wouldn't mind owning. The usual almost random patterns are deformed into much more smoother patterns. The spectral and temporal amplitude and phases signal reconstructions are also shown. They are definitely are much noisier, than the amazing normal reconstruction. This shows that we are on the right track, but we have still not found the jewel of the Nile.

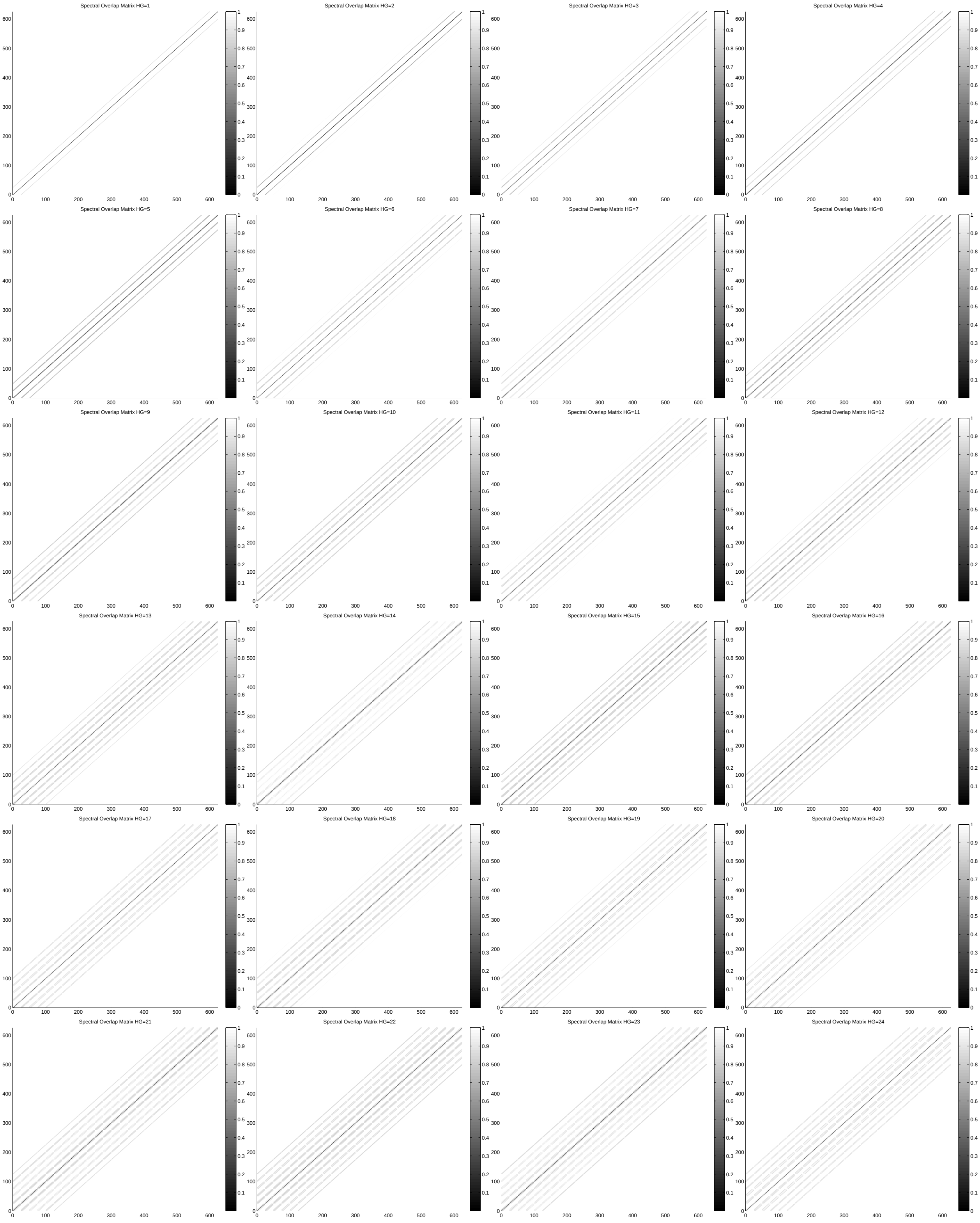

Figure 6.23.: The Spectral Overlap Matrices of the HG Planes

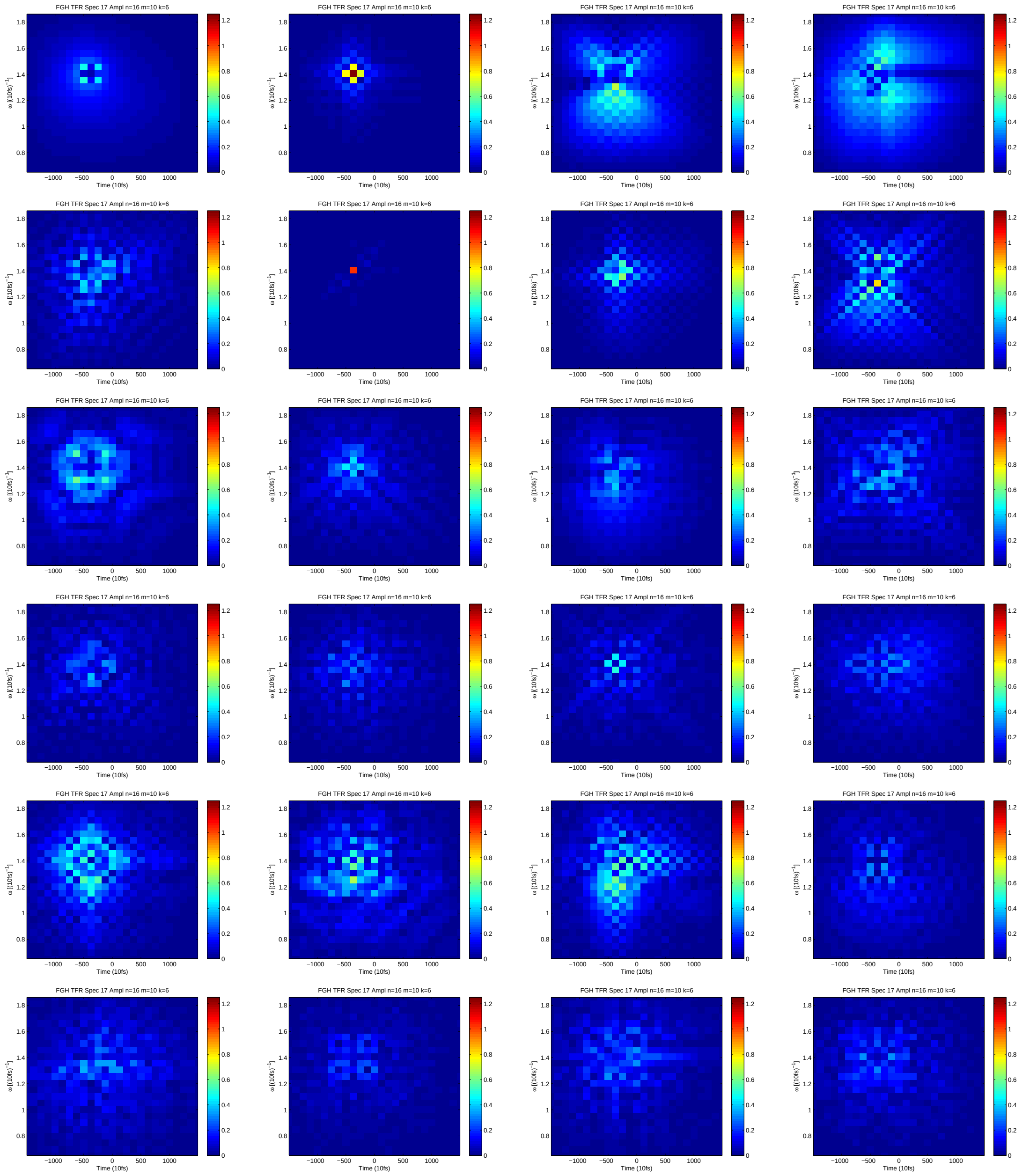

Figure 6.24.: FHG TFR Spectral HG Planes multiplied by their Overlap Matrices

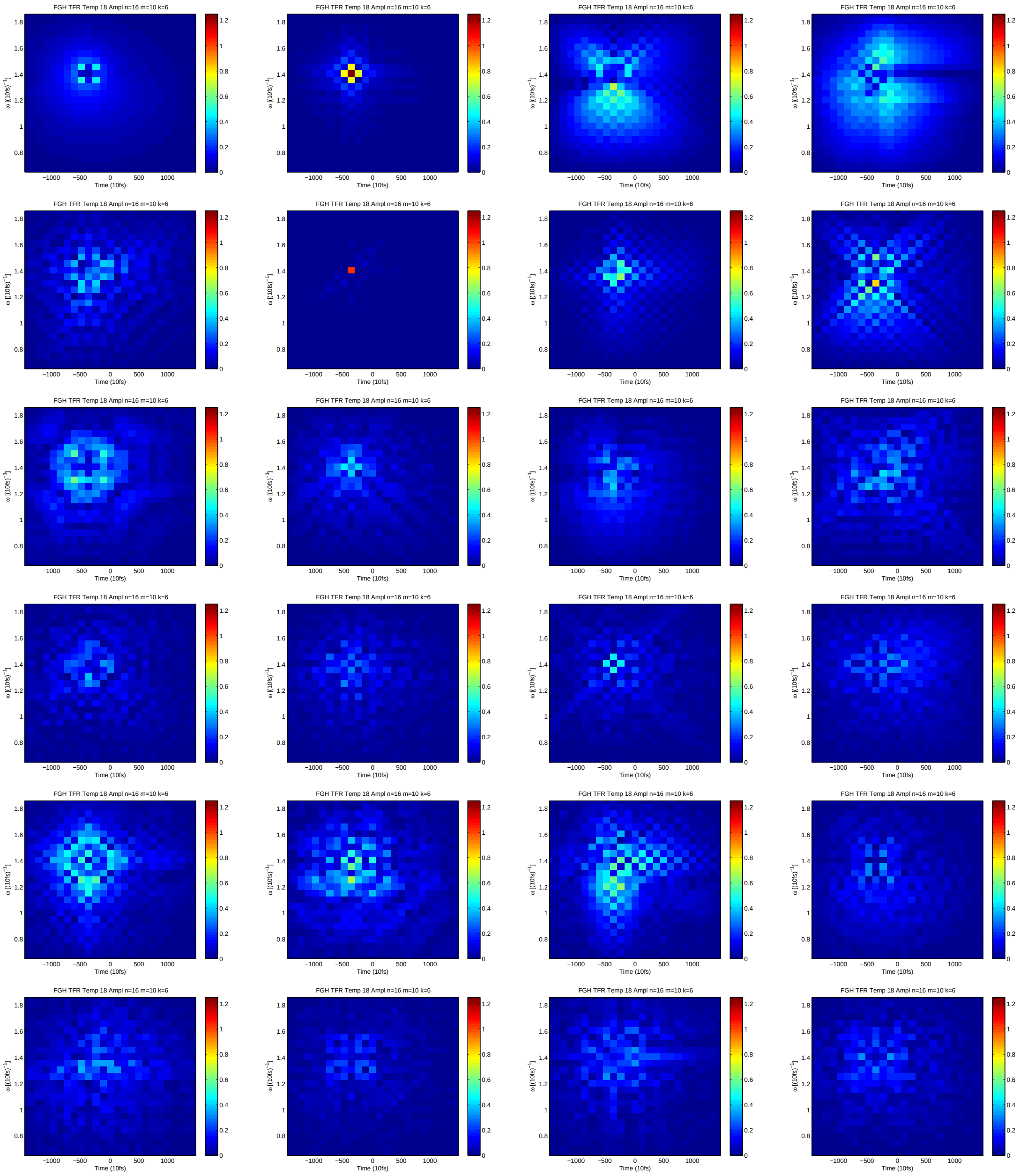

Figure 6.25.: FHG TFR Temporal HG Planes multiplied by their Overlap Matrices

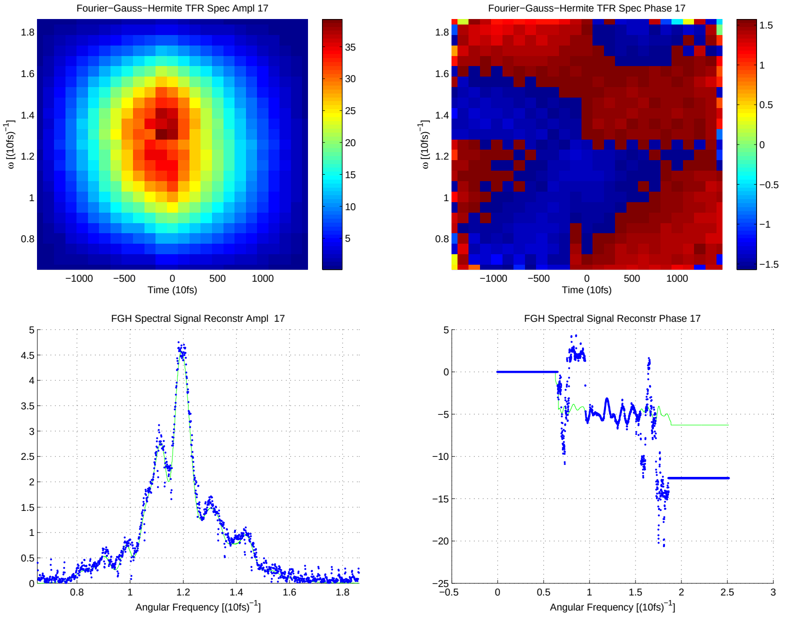

Figure 6.26.: FHG TFR Spectral HG Planes x Overlap Matrices

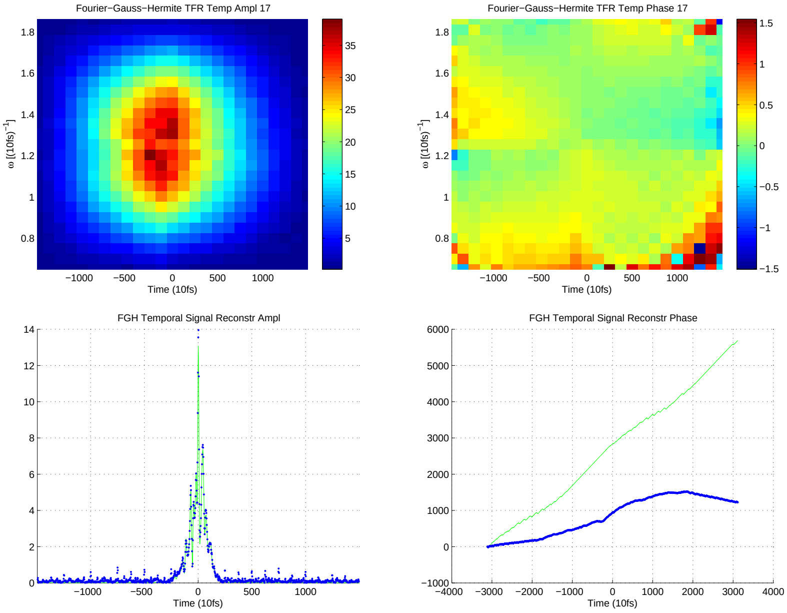

Figure 6.27.: FHG TFR Temporal HG Planes x Overlap Matrices

7. Coherent State FHG TFR Analogy

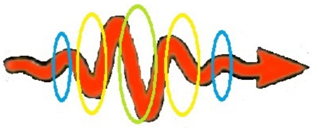

Figure 7.1.: Roy Glauber and E. C. George Sudarshan

7.1. Introduction

This Chapter 7, consist of various subsections that eventually discuss the novel FHG coherent state analogy. We begin with Section 7.2 which sets the background. Here we introduce some quantum field theory of QM Harmonic oscillator creation and annihilation operators and their statistical connection that leads to the Pauli-exclusion principle [138]. We then have a short discussion in Subsection 7.2.1 about Gaussian laser beams, circular, and the the higher order modes, namely the Hermite-Gaussian modes, Laguerre-Gaussian modes, and the encompassing Ince-Gaussian modes. This Subsection 7.2.1 then actually shows, that laser beams actually occur in Hermite-Gaussian multimodes and that the coherent states should also exhibit these properties.

A short introduction to optical phase space is given in Subsection 7.2.2. This commences with the standard quantization of free EM radiation, in the footsteps of the original derivation of Dirac [139]. The polarization of the quantum harmonic oscillators is reviewed. Unfortunately, this method is not relativistic invariant and underwent in few short years, quite a few revisions in search of the correct Lagrangian. It then discusses the consequences of the manifestly relativistic covariant Lagrangian of Fermi, especially that four quantum harmonic oscillators are required to describe the EM field. This is essential for our later classical correspondence analogy. Finally, the various relevant important Lagrangians are presented, culminating in the complete Dirac-Maxwell Lagrangian (including local gauge invariance), which clearly demonstrates the interrelationship of the source, charges, and the free EM radiation field. A further rather important observation is that each EM radiation field is quantized as a summation $\sum_{\mathbf{k}}$ (which in the limit of field in the continuum is an integral, Eq. (7.88), which describes a multimode EM radiation creation operator and in analogy a EM vector potential) as in Eq. (7.27) to Eq. (7.30).

An all to brief discussion of coherent states is presented in Section 7.3. Some definitions and properties are shown and the solution of the coherent states in terms of the overcomplete quantum harmonic states is given. Their interconnection with quantum harmonic oscillators of quantum field theory of EM radiation is re-established, with a generalized multimode superposition of coherent state representation, however, how the polarization enters is unclear.

From the previous Section 7.3, we proceed carefully into Section 7.4, concerning the new FHG TFR coherent state analogy. Actually it is double multimode superposition of "classical" coherent states correspondence analogy. Here we show that a optimal correlation function can be derived between the multimode superposition of "classical" coherent states and the FHG TFR temporal bases. A cost function is defined and optimized that eventually results in, what can we say, a type of optimized correlation correspondence analogy. In the end some results for our representative electric signals are given for the "classical" coherent state optimized correlation analogy.

In this Chapter 7 we raise a few questions and probably a few eyebrows. Here, we do not wish to demonstrate the exact equivalence, but only the plausibility of a very good analogy. *Fools rush in where angels fear to tread.* We now proceed cautiously.

7.2. A Brief Summary of Modern Light

The modern theory of light, started with the inability of the classical theory to explain

- black body radiation.
- Fraunhofer and Kirchhoff spectrum lines, and
- the photovoltaic effect of Hertz (Photoelectric effect).

Second quantization was introduced by Jordan and Wigner, in an article on Pauli's exclusion principle [140], now known as quantum field theory, without ever believing that it would have physical consequences. These two experiments and then theoretically Enrico Fermi (1934) published his theory of β decay (Eng. trans. [141]), placed the physics community on its head, totally baffled. P.A.M Dirac also developed quantum field theory [142, 143, 144]. Therein he proves that general field particles, that are identical particles, only come in terms of two varieties or categories (see Merzbacher [6]). This was established by means of their creation and annihilation quantum field operators, $\hat{\mathbf{a}}^\dagger$ and $\hat{\mathbf{a}}$, respectively, namely for identical particles i and j

$$\left[\hat{\mathbf{a}}_i^\dagger, \hat{\mathbf{a}}_j^\dagger\right] = \hat{\mathbf{a}}_i^\dagger \hat{\mathbf{a}}_j^\dagger - \hat{\mathbf{a}}_j^\dagger \hat{\mathbf{a}}_i^\dagger = 0, \tag{7.1}$$

or

$$\left\{\hat{\mathbf{a}}_i^\dagger, \hat{\mathbf{a}}_j^\dagger\right\} = \hat{\mathbf{a}}_i^\dagger \hat{\mathbf{a}}_j^\dagger + \hat{\mathbf{a}}_j^\dagger \hat{\mathbf{a}}_i^\dagger = 0, \tag{7.2}$$

and by their Hermitian adjoints, similar equations for the annihilation field operators, $\hat{\mathbf{a}}$. This was established to be a fundamental principle of quantum particles and related to the intrinsic spin of the particles, or their spin statistics, Pauli [138]. In quantum statistical mechanics, we have two types of particles, adhering to the following:

Bose-Einstein Statistics (*Bosons*). All particles with integral intrinsic spin, $s \in \mathbb{Z}$,

$$\begin{aligned} \left[\hat{\mathbf{a}}_k^\dagger, \hat{\mathbf{a}}_l^\dagger\right] &= 0 \\ \left[\hat{\mathbf{a}}_k, \hat{\mathbf{a}}_l\right] &= 0 \\ \left[\hat{\mathbf{a}}_k, \hat{\mathbf{a}}_l^\dagger\right] &= \delta_{kl} I \end{aligned} \tag{7.3}$$

Fermi-Dirac Statistics (*Fermions*). All particles with half-integral intrinsic spin, $s = \pm\frac{1}{2}, \pm\frac{3}{2}, \pm\frac{5}{2}, \ldots,$

$$\begin{aligned} \left\{\hat{\mathbf{a}}_k^\dagger, \hat{\mathbf{a}}_l^\dagger\right\} &= 0 \\ \left\{\hat{\mathbf{a}}_k, \hat{\mathbf{a}}_l\right\} &= 0 \\ \left\{\hat{\mathbf{a}}_k, \hat{\mathbf{a}}_l^\dagger\right\} &= \delta_{kl} I \end{aligned} \tag{7.4}$$

Normal matter is constituted by Fermi-Dirac particles (electrons orbiting a nucleus, consisting of protons and neutrons). Thus, deep within the categorization of Fermi-Dirac Statistics lies the reason of the Pauli-exclusion principle [138]. No two identical fermionic particles, with the same quantum numbers, may occupy the same space, since, $\hat{\mathbf{a}}_k^\dagger \hat{\mathbf{a}}_k^\dagger = 0$.

In Quantum Field Theory (QFT) [145, 146, 147] it is customary to describe a quantum particle in terms of its characteristic or intrinsic quantum numbers. At present we know that:

- The fundamental particle of light is called a photon.
- The photon is a transversal EM wave.
- The energy of a photon is $E = h\nu$.
- The speed of a photon *in vacuo* is $v = c$. In media $v < c$. (Ewald-Oseen extinction theorem [19]).
- The rest mass of the photon is $m_0 = 0$. Prescribed by Einstein ($E^2 = m_0^2 c^4 + p^2 c^2$).
- The linear momentum of the photon is $p = \frac{E}{c} = \hbar k$, consequence of $E = h\nu$ and $m_0 = 0$, i.e., massless.
- The photon has an intrinsic spin, $s = \pm 1$. This is circular polarization, right and left, in the direction of the momentum, known as *helicity*. The chirality or handedness property. (Total spin $s = 1$, in quantum mechanics requires three spin states, $s = -1, 0, +1$. The $s = 0$ is assumed not to exist and neglected, since $m_0 = 0$).
- The photon is a boson, the intrinsic spin is integral Eq. (7.3).
- A collection of photons, as in light, can have orbital angular momentum.

7.2.1. Gaussian Laser Beams

I once had the opportunity to read a translated version of C.F. Gauss' original paper, in which he derives his famous Gaussian function. The original Gaussian function was derived as an error function. Unlike Gauss this was done with slightly circular reasoning. The central-limit theorem of probability theory (Papoulis [70]) shows that the addition of continuous random variables, with any type of probability density, under certain limiting conditions, that the mean and variance remain finite, will approximate a Gaussian probability density function and as $n \to \infty$, the variance $\sum_{i=1}^{n} \sigma_i^2 \to \infty$, the approximation becomes an equality. Papoulis [70] shows that adding the simplest random variables, namely an uniformly distributed random variable, the addition of only three already resembles a Gaussian probability density. In probability theory, the probability density of the addition of random variables is a convolution operation. As a consequence random noise is often represented as a Gaussian probability density.

Wigner-Weisskopf theory (see Steck [23]) shows that the natural lineshape of a quantum transition, e.g., of a gas, has a Lorentzian distribution. Collision broadening (sometimes referred to as pressure broadening of a gas or fluid) also has a Lorentzian lineshape (Loudon [148]). Doppler broadening on the other has a Gaussian lineshape. At any rate, due to the central limit theorem, after the addition of many error sources, implies that the most natural lineshape of a laser will be Gaussian. Here we only give a brief definition of Gaussian beams, without defining the various parameters in detail, as these can be found in many references. We do give the mathematical definitions of Hermite-Gaussian modes, Laguerre-Gaussian modes and Ince-Gaussian modes. We say nothing about Bessel beams, because they are not relevant to our discussion.

The most general laser beam modes are the Hypergeometric-Gaussian modes (not represented here).

7.2.1.1. Circular Gaussian Beams

A circular Gaussian laser beam propagating in the z direction (beam axis) is described by

$$E(r,z) = E_0 \frac{w_0}{w(z)} \exp\left[-\frac{r^2}{w^2(z)} - ikz - ik\frac{r^2}{2R(z)} + iG(z) \right], \qquad (7.5)$$

where,

w_0 = $w(0)$ is the narrowest waist of the beam.
r = Radial distance from beam's axis
z = Axial distance from w_0.
k = The wave number.
E_0 = Electric field amplitude.
$w(z)$ = Where the waist is equal to $\frac{1}{e}$ and $\frac{1}{e^2}$ of the field amplitude and intensity of its axial value respectively.
$R(z)$ = Beam's radius of curvature.
$G(z)$ = Gouy phase shift. $\left[= \arctan\left(\frac{z}{z_R}\right)\right]$

7.2.1.2. Hermite-Gaussian modes

One-dimensional Cartesian coordinates

$$u_n(x,z) = \left(\frac{2}{\pi}\right)^{\frac{1}{4}} \left(\frac{1}{2^n n! w_0}\right)^{\frac{1}{2}} \left(\frac{\chi_0}{\chi(z)}\right)^{\frac{1}{2}} \left[\frac{\chi_0 \chi^*(z)}{\chi_0^* \chi(z)}\right]^{\frac{n}{2}} \times$$
$$H_n\left(\frac{\sqrt{2}x}{w(z)}\right) \exp\left[-i\frac{kx^2}{2\chi(z)}\right] \tag{7.6}$$

where,

$H_n(x)$ = Physicist's Hermite polynomial of order n. (cf. Subsection 5.2.1).
w_0 = $w(0)$ is the narrowest waist of the laser beam.
x = Horizontal Cartesian axis.
z = Axial distance from w_0.
k = The wave number.
E_0 = Electric field amplitude.
$w(z)$ = Where the waist is equal to $\frac{1}{e}$ and $\frac{1}{e^2}$ of the field amplitude and intensity of its axial value.
$\chi(z)$ = $z + \chi_0 = z + iz_R$, Complex beam parameter

Two-dimensional Cartesian modes

$$u_{nm}(x,y,z) = u_n(x,z)u_m(y,z), \tag{7.7}$$

and, $u_m(y,z)$, has exactly the same mathematical form as, $u_n(x,z)$. These give rise to the familiar Transverse-Electro-Magnetic modes of a laser, TEM$_{mn}$. Of course the TEM$_{00}$ is just the Gaussian beam mode defined in Eq. (7.6).

7.2.1.3. Laguerre-Gaussian modes

(In terms of cylindrical coordinates (r,θ,z)) (For the definition of, $L_n^{|m|}$, see Section C.2),

$$u(r,\theta,z) = c_{mn}\frac{1}{w(z)}\left[\frac{r\sqrt{2}}{w(z)}\right] \exp\left[-\frac{r^2}{w^2(z)}\right] L_n^{|m|}\left[\frac{2r^2}{w^2(z)}\right] \times$$
$$\exp\left[ik\frac{r^2}{2R(z)}\right] \exp(im\theta) \exp\left[i(2n+|m|+1)G(z)\right] \tag{7.8}$$

where,

$L_n^{|m|}(x)$ = Associated Laguerre polynomials, $n \geq 0$ is the radial index and m the azimuthal index. (cf. Section C.2).

c_{mn} = Normalization constant.

w_0 = $w(0)$ is the narrowest waist of the laser beam.

r = Radial distance from the laser beam's axis

θ = Azimuthal angle measured from laser beam axis.

z = Axial distance from w_0.

k = The wave number.

E_0 = Electric field amplitude.

$w(z)$ = Where the waist is equal to $\frac{1}{e}$ and $\frac{1}{e^2}$ of the field amplitude and intensity of its axial value.

$R(z)$ = Laser beam's radius of curvature.

$G(z)$ = Gouy phase shift $\left[= \arctan\left(\frac{z}{z_R}\right)\right]$

The laser beams can generally be categorized in terms of Ince-Gaussian modes and Hypergeometric-Gaussian modes. The above definitions are sufficient for our purposes.

7.2.1.4. Ince-Gaussian modes

(Elliptic coordinates) The even and odd functions are defined as (derived in Bandres and Vega [149])

$$u_\epsilon(\xi, \eta, z) = \frac{w_0}{w(z)} C_n^m(i\xi, \epsilon) C_n^m(\eta, \epsilon) \exp\left[-ik\frac{r^2}{2\chi(z)} - (n+1)G(z)\right], \tag{7.9}$$

where,

$C_n^m(\eta, \epsilon)$ = Even Ince polynomials, order n and degree m.
ϵ = Ellipticity parameter.
ξ = Radial elliptic coordinate.
η = Angular elliptic coordinate.
x = $\sqrt{\epsilon/2w(z)} \cosh \xi \cos \eta$
y = $\sqrt{\epsilon/2w(z)} \sinh \xi \sin \eta$
r = Radial distance from the laser beam's axis.
z = Axial distance from w_0.
k = The wave number.
w_0 = $w(0)$ is the narrowest waist of the laser beam.
$w(z)$ = Where the waist is equal to $\frac{1}{e}$ and $\frac{1}{e^2}$ of the field amplitude and intensity of its axial value.
$R(z)$ = Laser beam's radius of curvature.
$G(z)$ = Gouy phase shift $\left[= \arctan\left(\frac{z}{z_R}\right)\right]$
$\chi(z)$ = $z + \chi_0 = z + iz_R$, Complex beam parameter

Special cases of the Ince-Gaussian modes are the Hermite-Gaussian and Laguerre-Gaussian modes for, $\epsilon = \infty$ and $\epsilon = 0$, respectively. For a thorough discussion refer to Bandres Vega [149].

7.2.2. Optical Phase Space

Many text books deal with the subject of Optical Phase Space and Quantum Optics. Notably Schleich [35], Scully and Zubairy [150], Klauder and Sudarshan [151], Gerry and Knight [24], and Loudon [148].

Here, we firstly develop the standard quantization of an electromagnetic wave, in the footsteps of Dirac's original 1927 article [139], in terms of quantum harmonic oscillators. We introduce different, at times rather confusing, notations for the transversal polarization vectors. This is purposely done to emphasize the importance of the oversight of the Coulomb gauge. Dirac here, like Maxwell, assumed the ***Coulomb gauge*** for the vector potential, $\mathbf{A}$, (cf. [152, 153, 154]),

$$\nabla \cdot \mathbf{A} = 0, \tag{7.10}$$

as opposed to the ***Lorenz-Lorentz gauge***

$$\nabla \cdot \mathbf{A} + \frac{1}{c^2}\frac{\partial \phi}{\partial t} = 0, \tag{7.11}$$

where, ϕ, is the scalar Coulomb potential. These are related to the electric field, $\mathbf{E}$, and magnetic (induction) field, $\mathbf{B}$, by $\mathbf{E} = -\nabla\phi - \frac{\partial \mathbf{A}}{\partial t}$ and $\mathbf{B} = \nabla \times \mathbf{A}$, respectively.

The free classical EM radiation field, $\mathbf{J} = \mathbf{0}$, the vector potential, $\mathbf{A}$, must satisfy the wave equation,

$$\nabla^2 \mathbf{A} - \frac{1}{c^2}\frac{\partial^2 \mathbf{A}}{\partial t^2} = \mathbf{0}. \tag{7.12}$$

The vector potential, $\mathbf{A}$, can be expanded in terms of a 3-dimensional Fourier series in a cubic cavity L^3 as (Loudon [22]),

$$\mathbf{A}(t, \mathbf{r}) = \sum_{\mathbf{k}} \left[\mathbf{A}_{\mathbf{k}}(t) \exp\left(i\mathbf{k}\cdot\mathbf{r}\right) + \mathbf{A}^*_{\mathbf{k}}(t) \exp\left(-i\mathbf{k}\cdot\mathbf{r}\right)\right], \tag{7.13}$$

where, the wave vector, $\mathbf{k} = [k_x, k_y, k_z] = [2\pi\nu_x/L, 2\pi\nu_y/L, 2\pi\nu_z/L]$, with $\nu_x, \nu_y, \nu_z \in \mathbb{Z}$. The Coulomb gauge is satisfied if, $\mathbf{k}\cdot\mathbf{A}_{\mathbf{k}}(t) = \mathbf{k}\cdot\mathbf{A}^*_{\mathbf{k}}(t) = 0$. Of course, if the wave vector, $\mathbf{k}$, is the direction of propagation of the wave, this shows the transversality of the EM wave and that there are two independent orthogonal amplitudes, $\mathbf{A}_{\mathbf{k}}(t)$ and $\mathbf{A}^*_{\mathbf{k}}(t)$, associated with each wave vector. These two components must both satisfy the wave equation, Eq. (7.12), and when inserting Eq. (7.13) into Eq. (7.12) we obtain the following imposed condition,

$$k^2 \mathbf{A}_{\mathbf{k}}(t) + \frac{1}{c^2}\frac{d^2 \mathbf{A}_{\mathbf{k}}(t)}{dt^2} = \mathbf{0}. \tag{7.14}$$

Defining an angular frequency, $\omega_{\mathbf{k}} = ck$, the above equation is a simple harmonic DE with solution given by

$$\mathbf{A}_{\mathbf{k}}(t) = \mathbf{A}_{\mathbf{k}} \exp(-i\omega_{\mathbf{k}} t). \tag{7.15}$$

In general there is a second solution of the form, $\mathbf{C}_{\mathbf{k}} \exp(i\omega_{\mathbf{k}} t)$, but for matters of convention this is usually attributed to the complex conjugate, $\mathbf{A}^*_{\mathbf{k}}(t) = \mathbf{A}^*_{\mathbf{k}}(t) \exp(i\omega_{\mathbf{k}} t)$. Inserting Eq. (7.15) and its conjugate into Eq. (7.13) the vector potential can be written as,

$$\mathbf{A}(t, \mathbf{r}) = \sum_{\mathbf{k}} \left[\mathbf{A}_{\mathbf{k}}(t) \exp\left(-i\omega_{\mathbf{k}} t + i\mathbf{k}\cdot\mathbf{r}\right) + \mathbf{A}^*_{\mathbf{k}}(t) \exp\left(i\omega_{\mathbf{k}} t - i\mathbf{k}\cdot\mathbf{r}\right)\right].$$

The electrical, $\mathbf{E}_{\mathbf{k}}$, and magnetic, $\mathbf{H}_{\mathbf{k}}$, fields, for a single propagation mode, $\mathbf{k}$, of the EM radiation field, can be derived as in Loudon [22], from Maxwell's equations in the ***Coulomb gauge***, in terms of the vector potential, $\mathbf{A}_{\mathbf{k}}$, as,

$$\mathbf{E}_{\mathbf{k}} = i\omega_{\mathbf{k}} \left[\mathbf{A}_{\mathbf{k}} \exp\left(-i\omega_{\mathbf{k}} t + i\mathbf{k}\cdot\mathbf{r}\right) - \mathbf{A}^*_{\mathbf{k}} \exp\left(i\omega_{\mathbf{k}} t - i\mathbf{k}\cdot\mathbf{r}\right)\right], \tag{7.16}$$

$$\mathbf{H}_{\mathbf{k}} = (i/\mu_0)\mathbf{k} \times \left[\mathbf{A}_{\mathbf{k}} \exp\left(-i\omega_{\mathbf{k}} t + i\mathbf{k}\cdot\mathbf{r}\right) - \mathbf{A}^*_{\mathbf{k}} \exp\left(i\omega_{\mathbf{k}} t - i\mathbf{k}\cdot\mathbf{r}\right)\right]. \tag{7.17}$$

We now introduce *generalized mode "position",* $\mathbf{q}_{\mathbf{k}}$*, and "momentum",* $\mathbf{p}_{\mathbf{k}}$*,* coordinates. Since these are field operators, we do not associate any "mass" to the reciprocal coordinates. It has caused so many discussions and speculations, that Cohen-Tannoudji et al. [155] calls it a *fictitious space.* This is generally known as the **optical phase space** and the coordinates are known as quadrature coordinates,

$$\begin{aligned}\mathbf{A}_{\mathbf{k}} &= \left(4\epsilon_o V\omega_{\mathbf{k}}^2\right)^{-\frac{1}{2}}\left[\omega_{\mathbf{k}}\mathbf{q}_{\mathbf{k}} + i\mathbf{p}_{\mathbf{k}}\right]\varepsilon_{\mathbf{k}}, \qquad (7.18)\\ \mathbf{A}^*_{\mathbf{k}} &= \left(4\epsilon_o V\omega_{\mathbf{k}}^2\right)^{-\frac{1}{2}}\left[\omega_{\mathbf{k}}\mathbf{q}_{\mathbf{k}} - i\mathbf{p}_{\mathbf{k}}\right]\varepsilon_{\mathbf{k}}, \qquad (7.19)\end{aligned}$$

where, we have separated the vectorial part of the vector potential by means of a polarization vector, $\varepsilon_{\mathbf{k}}$, so that, $\varepsilon_{\mathbf{k}}\cdot\mathbf{k} = 0$. A single mode energy would correspond to

$$\mathcal{E}_{\mathbf{k}} = 2\epsilon_o V\omega_{\mathbf{k}}^2\mathbf{A}_{\mathbf{k}}\cdot\mathbf{A}^*_{\mathbf{k}} = \frac{1}{2}\left[\omega_{\mathbf{k}}{\mathbf{q}_{\mathbf{k}}}^2 + {\mathbf{p}_{\mathbf{k}}}^2\right]. \tag{7.20}$$

The quantization of the radiation field is now accomplished by associating the QM harmonic oscillator with the vector potential, allowing for the eminent identification of the vector potential, $\mathbf{A}(\mathbf{r}, t)$, with the annihilation operator of a quantum harmonic oscillator, $\mathbf{a}_{\mathbf{k}}$, as follows,

$$\begin{aligned}\mathbf{A}_{\mathbf{k}} &= \left(4\epsilon_o V\omega_{\mathbf{k}}^2\right)^{-\frac{1}{2}}\left[\omega_{\mathbf{k}}\mathbf{q}_{\mathbf{k}} + i\mathbf{p}_{\mathbf{k}}\right]\varepsilon_{\mathbf{k}} \longrightarrow \left(\hbar/2\epsilon_o V\omega_{\mathbf{k}}\right)^{\frac{1}{2}}\mathbf{a}_{\mathbf{k}}\varepsilon_{\mathbf{k}}, \qquad (7.21)\\ \mathbf{A}^*_{\mathbf{k}} &= \left(4\epsilon_o V\omega_{\mathbf{k}}^2\right)^{-\frac{1}{2}}\left[\omega_{\mathbf{k}}\mathbf{q}_{\mathbf{k}} - i\mathbf{p}_{\mathbf{k}}\right]\varepsilon_{\mathbf{k}} \longrightarrow \left(\hbar/2\epsilon_o V\omega_{\mathbf{k}}\right)^{\frac{1}{2}}\mathbf{a}^{\dagger}_{\mathbf{k}}\varepsilon_{\mathbf{k}}, \qquad (7.22)\end{aligned}$$

so that,

$$\mathbf{A}(\mathbf{r}, t) = \sum_{\mathbf{k}}\left(\hbar/2\epsilon_o V\omega_{\mathbf{k}}\right)^{\frac{1}{2}}\varepsilon_{\mathbf{k}}\left[\mathbf{a}_{\mathbf{k}}e^{-i(\omega_{\mathbf{k}}t-\mathbf{k}\cdot\mathbf{r})} + \mathbf{a}^{\dagger}_{\mathbf{k}}e^{i(\omega_{\mathbf{k}}t-\mathbf{k}\cdot\mathbf{r})}\right]. \tag{7.23}$$

The electric field, $\mathbf{E}$, is the given by,

$$\mathbf{E} = \sum_{\mathbf{k}} i\left(\hbar\omega_{\mathbf{k}}/2\epsilon_o V\right)^{\frac{1}{2}}\varepsilon_{\mathbf{k}}\left[\mathbf{a}_{\mathbf{k}}e^{-i(\omega_{\mathbf{k}}t-\mathbf{k}\cdot\mathbf{r})} - \mathbf{a}^{\dagger}_{\mathbf{k}}e^{i(\omega_{\mathbf{k}}t-\mathbf{k}\cdot\mathbf{r})}\right]. \tag{7.24}$$

or at a specific position, as a function of time

$$\mathbf{E}^{+}(t) = \sum_{\mathbf{k}} i\left(\hbar\omega_{\mathbf{k}}/2\epsilon_o V\right)^{\frac{1}{2}}\varepsilon_{\mathbf{k}}\mathbf{a}_{\mathbf{k}}e^{-i\omega_{\mathbf{k}}t}. \tag{7.25}$$

In the above we have separated the polarization by means of the *linear polarization vector,* $\varepsilon_{\mathbf{k}}$.

What is actually often done in modern text books, Merzbacher [6], is to define the operators, $\hat{\mathbf{a}}^{\dagger}_{R}(\mathbf{k})$ and $\hat{\mathbf{a}}^{\dagger}_{L}(\mathbf{k})$, that correspond to the creation of a photon with linear momentum, $\mathbf{p} = \hbar\mathbf{k}$, and intrinsic spin angular momentum's, $\mathbf{J}\cdot\mathbf{k} = \pm\hbar$, respectively, for right and left *circularly polarized* photons. The commutation relationships are given by (compare Eq. (7.3)),

$$\left[\hat{\mathbf{a}}_R(\mathbf{k}), \hat{\mathbf{a}}_R^\dagger(\mathbf{k}')\right] = \left[\hat{\mathbf{a}}_L(\mathbf{k}), \hat{\mathbf{a}}_L^\dagger(\mathbf{k}')\right] = \delta_{\mathbf{k}\mathbf{k}'}. \tag{7.26}$$

Making them bosons operators, with spin 1. All other commutation relations are zero. We are then in a position to define the following quantities for the quantized EM boson field.

- Total energy (Hamiltonian)

$$\mathscr{H} = \sum_{\mathbf{k}} c\hbar k \left[\hat{\mathbf{a}}_R^\dagger(\mathbf{k})\hat{\mathbf{a}}_R(\mathbf{k}) + \hat{\mathbf{a}}_L^\dagger(\mathbf{k})\hat{\mathbf{a}}_L(\mathbf{k})\right] \tag{7.27}$$

- Total linear momentum

$$\mathbf{P} = \sum_{\mathbf{k}} \hbar\mathbf{k} \left[\hat{\mathbf{a}}_R^\dagger(\mathbf{k})\hat{\mathbf{a}}_R(\mathbf{k}) + \hat{\mathbf{a}}_L^\dagger(\mathbf{k})\hat{\mathbf{a}}_L(\mathbf{k})\right] \tag{7.28}$$

- Total number of photons

$$N = \sum_{\mathbf{k}} \left[\hat{\mathbf{a}}_R^\dagger(\mathbf{k})\hat{\mathbf{a}}_R(\mathbf{k}) + \hat{\mathbf{a}}_L^\dagger(\mathbf{k})\hat{\mathbf{a}}_L(\mathbf{k})\right] \tag{7.29}$$

- Total angular momentum with linear momentum **k**

$$\left[\mathscr{J}\cdot\hat{\mathbf{k}}, \hat{\mathbf{a}}_R^\dagger(\mathbf{k})\right]\hat{\mathbf{a}}_R(\mathbf{k}) + \left[\mathscr{J}\cdot\hat{\mathbf{k}}, \hat{\mathbf{a}}_L^\dagger(\mathbf{k})\right]\hat{\mathbf{a}}_L(\mathbf{k}) = \hbar\left[\hat{\mathbf{a}}_R^\dagger(\mathbf{k})\hat{\mathbf{a}}_R(\mathbf{k}) - \hat{\mathbf{a}}_L^\dagger(\mathbf{k})\hat{\mathbf{a}}_L(\mathbf{k})\right]. \tag{7.30}$$

The boson field creation operators, $\hat{\mathbf{a}}_R^\dagger(\mathbf{k})$ and $\hat{\mathbf{a}}_L^\dagger(\mathbf{k})$, transform like the components of an irreducible tensor of rank one, T_1^1 and T_1^{-1}. A transformation to

$$\hat{\mathbf{a}}_1^\dagger(\mathbf{k}) = \frac{1}{\sqrt{2}}\left[-\hat{\mathbf{a}}_R^\dagger(\mathbf{k}) + \hat{\mathbf{a}}_L^\dagger(\mathbf{k})\right], \tag{7.31}$$

$$\hat{\mathbf{a}}_2^\dagger(\mathbf{k}) = \frac{i}{\sqrt{2}}\left[\hat{\mathbf{a}}_R^\dagger(\mathbf{k}) + \hat{\mathbf{a}}_L^\dagger(\mathbf{k})\right], \tag{7.32}$$

transforms them to two operators that transform like normal vector components under rotation, i.e., linear transverse. Introducing two unit vectors, $\hat{\mathbf{e}}_{\mathbf{k}}^1$ and $\hat{\mathbf{e}}_{\mathbf{k}}^2$, orthogonal (transverse) to the direction of propagation, $\hat{\mathbf{k}}$, so that, $\hat{\mathbf{e}}_{\mathbf{k}}^1\cdot\hat{\mathbf{e}}_{\mathbf{k}}^2 = 0$, $\hat{\mathbf{e}}_{\mathbf{k}}^1\cdot\hat{\mathbf{k}} = 0$, $\hat{\mathbf{e}}_{\mathbf{k}}^2\cdot\hat{\mathbf{k}} = 0$, $\hat{\mathbf{e}}_{\mathbf{k}}^1\times\hat{\mathbf{e}}_{\mathbf{k}}^2 = \hat{\mathbf{k}}$, $\hat{\mathbf{k}}\times\hat{\mathbf{e}}_{\mathbf{k}}^1 = \hat{\mathbf{e}}_{\mathbf{k}}^2$ and $\hat{\mathbf{e}}_{\mathbf{k}}^2\times\hat{\mathbf{k}} = \hat{\mathbf{e}}_{\mathbf{k}}^1$ form a mutually orthogonal triad, then,

$$\hat{\mathbf{a}}_1^\dagger(\mathbf{k})\hat{\mathbf{e}}_{\mathbf{k}}^1 + \hat{\mathbf{a}}_2^\dagger(\mathbf{k})\hat{\mathbf{e}}_{\mathbf{k}}^2 = \frac{1}{\sqrt{2}}\left[\hat{\mathbf{a}}_R^\dagger(\mathbf{k})\left(-\hat{\mathbf{e}}_{\mathbf{k}}^1 + i\hat{\mathbf{e}}_{\mathbf{k}}^2\right) + \hat{\mathbf{a}}_L^\dagger(\mathbf{k})\left(\hat{\mathbf{e}}_{\mathbf{k}}^1 + i\hat{\mathbf{e}}_{\mathbf{k}}^2\right)\right], \tag{7.33}$$

and its Hermitian conjugate operator,

$$\hat{\mathbf{a}}_1(\mathbf{k})\hat{\mathbf{e}}^1_{\mathbf{k}} + \hat{\mathbf{a}}_2(\mathbf{k})\hat{\mathbf{e}}^2_{\mathbf{k}} = \frac{1}{\sqrt{2}}\left[-\hat{\mathbf{a}}_R(\mathbf{k})\left(\hat{\mathbf{e}}^1_{\mathbf{k}} + i\hat{\mathbf{e}}^2_{\mathbf{k}}\right) + \hat{\mathbf{a}}_L(\mathbf{k})\left(\hat{\mathbf{e}}^1_{\mathbf{k}} - i\hat{\mathbf{e}}^2_{\mathbf{k}}\right)\right]. \tag{7.34}$$

This then reconnects the operators defined in Eq. (7.21) and Eq. (7.22).

In **relativity theory** great use is made of the tensorial notation. Given that the metric tensor, $g_{\mu\nu}$, is diagonal, i.e., $g_{00} = +1$, $g_{11} = g_{22} = g_{33} = -1$, (at least in special relativity theory, but also in electrodynamics [152],[154] and quantum mechanics [7],[146]), we have,

$$A_\mu = \sum_\nu g_{\mu\nu} A^\nu, \tag{7.35}$$

where the vector 4-potential defined as (in SI units),

$$A^\mu = [\frac{\phi}{c}, A_x, A_y, A_z]^T,$$

where, ϕ and $\mathbf{A}$, is the electromagnetic scalar and vector potentials. In this covariant notation the ***Lorentz-Lorentz gauge*** condition, Eq. (7.11), is simply written as (Einstein convention - there is an implicit sum over all values for pairs of equal upper/lower indices),

$$\partial_\mu A^\mu = 0. \tag{7.36}$$

Usually the non relativistic quantum wave equations are described in terms of a Hamiltonian. For quantum field theory it is more convenient to work with a Lagrangian formalism.

The **standard Lagrangian of a free EM field** is given by Cohen-Tannoudji et al. [155]

$$\mathscr{L}^{st}_R = -\frac{\varepsilon_0 c^2}{2}\sum_{\mu,\nu} F_{\mu\nu}F^{\mu\nu} \tag{7.37}$$

where, $F^{\mu\nu}$, is the EM field tensor, sometimes called the Faraday tensor by Misner et al. [156], and is defined by

$$F_{\mu\nu} = \partial_\mu A_\nu - \partial_\nu A_\mu. \tag{7.38}$$

In SI units $F^{\mu\nu}$ is given by an anti-symmetric tensor, the Faraday tensor,

$$F^{\mu\nu} = \begin{bmatrix} 0 & -\frac{E_x}{c} & -\frac{E_y}{c} & -\frac{E_z}{c} \\ \frac{E_x}{c} & 0 & -B_z & B_y \\ \frac{E_y}{c} & B_z & 0 & -B_x \\ \frac{E_z}{c} & -B_y & B_x & 0 \end{bmatrix}$$

The **interaction Lagrangian** must be included with the standard Lagrangian to allow for interaction with external charged particles. This is given by, ($j^\mu = [c\rho, \mathbf{j}]$, the current density (in SI units)),

$$\mathscr{L}_I = -\sum_\mu j_\mu A^\mu = \mathbf{j} \cdot \mathbf{A} - \rho\phi. \tag{7.39}$$

The addition of Eq. (7.37) and Eq. (7.39) gives us the **standard Lagrangian of an EM field**, that is,

$$\mathscr{L}_{em}^{st} = \mathscr{L}_R^{st} + \mathscr{L}_I. \tag{7.40}$$

In Einstein's notation this becomes

$$\mathscr{L}_{em}^{st} = -\frac{\varepsilon_0 c^2}{2} F^{\mu\nu} F_{\mu\nu} - j^\mu A_\mu. \tag{7.41}$$

Unfortunately, this formalism is still not truly relativistically covariant, see Cohen-Tannoudji et al. [155] and the following **relativistic Lagrangian for the free EM field** was proposed,

$$\mathscr{L}_R = -\frac{\varepsilon_0 c^2}{2} \sum_{\mu,\nu} (\partial_\mu A^\mu)(\partial^\nu A_\nu). \tag{7.42}$$

In 1932, Fermi [157], proposed the following manifestly relativistic **covariant Fermi Lagrangian for the free EM field**

$$\mathscr{L}_R^F = -\varepsilon_0 c^2 \left[\sum_{\mu,\nu} F_{\mu\nu} F^{\mu\nu} + \frac{1}{2} \sum_{\mu,\nu} (\partial_\mu A^\mu)^2 \right]. \tag{7.43}$$

This is all done in Cohen-Tannoudji et al. [155]. In the normal reciprocal Fourier space, $\mathbf{k}$, in the covariant formalism, the scalar and vector potential A^μ are considered independent dynamical variables. This implies that at *each point,* $\mathbf{k}$*, there are four independent degrees of freedom.* The four vector is given by,

$$k^\mu = [\frac{\omega}{c}, \mathbf{k}] = [k^0, k^1, k^2, k^3]. \tag{7.44}$$

We also have the wave relationship, that is $\omega = ck$, where $k = |\mathbf{k}| = k^0$. Thus this satisfies,

$$k^\mu k_\mu = 0. \tag{7.45}$$

For the propagation direction, $\mathbf{k}$, we can define a unit vector $\hat{\mathbf{k}} = \mathbf{k}/k$. We still have the two transverse polarization vectors, $\varepsilon_\mathbf{k}$ and $\varepsilon'_\mathbf{k}$, so that $\varepsilon_\mathbf{k} \cdot \mathbf{k} = \varepsilon'_\mathbf{k} \cdot \hat{\mathbf{k}} = 0$. The additional degrees of freedom imply that for each $\mathbf{k}$, there are now *four normal* *modes of vibration! Two transverse, one longitudinal and one scalar!* In the notation of Cohen-Tannoudji et al. [155], the quantum harmonic oscillator field operators, $\mathbf{a}_{\mathbf{k}}$, are written in covariant form as

$$[\alpha_\varepsilon, \alpha_{\varepsilon'}, \alpha_l, \alpha_s] \tag{7.46}$$

where $\alpha_\varepsilon, \alpha_{\varepsilon'}$ corresponds to normal transverse components and, α_l, to the new additional longitudinal harmonic oscillator and, α_s, to the scalar component. This implies

$$\alpha_\mu(\mathbf{k}) = \alpha_\varepsilon(\mathbf{k})\varepsilon_\mu + \alpha_{\varepsilon'}(\mathbf{k})\varepsilon'_\mu + \alpha_l(\mathbf{k})\kappa_\mu + \alpha_s(\mathbf{k})\eta_\mu. \tag{7.47}$$

The various four vectors are defined by

$$\begin{aligned} \varepsilon^\mu &= [0, \varepsilon_{\mathbf{k}}] \\ \varepsilon'^\mu &= [0, \varepsilon'_{\mathbf{k}}] \\ \kappa^\mu &= [0, \hat{\mathbf{k}}] \\ \eta^\mu &= [1, \mathbf{0}]. \end{aligned} \tag{7.48}$$

Up to this point the variables are considered independent, but the Lorenz-Lorentz gauge Eq. (7.11) imposes an additional constraint. Cohen-Tannoudji et al. [155] then shows that, for a free field, this leads to the following constraint,

$$\alpha_l(\mathbf{k}) - \alpha_s(\mathbf{k}) = 0, \qquad \forall \mathbf{k}. \tag{7.49}$$

From this condition, he then introduces two new variables simply as combinations,

$$\alpha_d = \frac{i}{\sqrt{2}} \left(\alpha_l - \alpha_s\right), \tag{7.50}$$

$$\alpha_g = \frac{1}{\sqrt{2}} \left(\alpha_l + \alpha_s\right). \tag{7.51}$$

The constraint is then simply, $\alpha_d = 0$. He then studies the effects of the gauge arbitrariness and shows a gauge transformation only effects, α_g. Then also,

$$\alpha_l(\mathbf{k})\kappa_\mu + \alpha_s(\mathbf{k})\eta_\mu = \frac{1}{\sqrt{2}} \left[i\alpha_d(\mathbf{k}) \left(\eta_\mu - \kappa_\mu\right) + \alpha_g(\mathbf{k}) \left(\kappa_\mu + \eta_\mu\right)\right]. \tag{7.52}$$

Then, finally this results in a separation of the four vector potential into

$$A_\mu = A^t_\mu + A^g_\mu + A^d_\mu, \tag{7.53}$$

where, A^t_μ, is the contribution from the transverse spatial components, α_ε and $\alpha_{\varepsilon'}$, and A^g_μ and A^d_μ, are the contributions from α_g and α_d, respectively. Finally, since $\alpha_d = 0$, for a physical field, we have, $A^d_\mu = 0$, and in the tensor, $F_{\mu\nu}$, the gauge portion, A^g_μ, also doesn't contribute, so that,

$$F_{\mu\nu} = \partial_\mu A^t_\nu - \partial_\nu A^t_\mu = F^t_{\mu\nu}. \tag{7.54}$$

Therefore the free-field EM fields are purely transversal in nature.

In Gaussian units, the Faraday tensor is given by,

$$F^{\mu\nu} = \begin{bmatrix} 0 & -E_x & -E_y & -E_z \\ E_x & 0 & -B_z & B_y \\ E_y & B_z & 0 & -B_x \\ E_z & -B_y & B_x & 0 \end{bmatrix}$$

. Physics can also be derived from a Lagrangian or as such a Hamiltonian. The action principle is, however, best stated in terms of a Lagrangian, so (cf. Griffiths [158], in Gaussian units)

- **The Dirac Lagrangian (Spin-$\frac{1}{2}$) Spinor Field**.

  $$\mathscr{L}_D = i(\hbar c)\bar{\psi}\gamma^\mu\partial_\mu\psi - (mc^2)\bar{\psi}\psi, \tag{7.55}$$

  where, $\bar{\psi}$, is the adjoint spinor and is considered as an independent solution to ψ.

- **The Maxwell Lagrangian** (**Spin**-1, $m_0 = 0$) **Vector Field with source** J^μ.

  $$\mathscr{L}_M = -\frac{1}{16\pi}F^{\mu\nu}F_{\mu\nu} - \frac{1}{c}J^\mu A_\mu. \tag{7.56}$$

  The Euler-Lagrange equation gives the Maxwell equation as,

  $$\partial_\mu F^{\mu\nu} = \frac{4\pi}{c}J^\nu, \tag{7.57}$$

  with the immediate consequence of charge conservation on the source, $\partial_\nu J^\nu = 0$.

- **The Complete Dirac-Maxwell Lagrangian** (including local gauge invariance)

  $$\mathscr{L}_{DM} = \left[+i(\hbar c)\bar{\psi}\gamma^\mu\partial_\mu\psi - (mc^2)\bar{\psi}\psi\right] + \left[-\frac{1}{16\pi}F^{\mu\nu}F_{\mu\nu}\right] - \left[\left(e\bar{\psi}\gamma^\mu\psi\right)A_\mu\right], \tag{7.58}$$

  with current density,

  $$J^\mu = c\left(e\bar{\psi}\gamma^\mu\psi\right). \tag{7.59}$$

This last Lagrangian shows that by simply imposing local gauge invariance (paramount to charge conservation) on the Dirac Lagrangian, forces the introduction of a massless vector field, A^{μ}, i.e., the EM field. This then demonstrates the inseparable intertwined relationship between fermionic charge and bosonic photon fields. $\mathscr{L}_M$, Eq. (7.56) can be compared with, $\mathscr{L}_{em}^{st}$,Eq. (7.41). They are the same except for the coefficients, $\frac{1}{16\pi}$ and $\frac{\varepsilon_0 c^2}{2}$, and the additional, $\frac{1}{c}$. This is attributable to the different EM units that are employed in the two books, Gaussian units vs SI units[1]. It is unfortunate, and there are very valid reasons, that different physics fields employ different units. So it is best to adapt quickly or die.

7.3. Coherent States

After the discovery of Hanbury-Brown and Twiss, in 1957, of the interferometric fluctuations of light [159] and the subsequent papers of Mandel and Wolf, [160], and to put the cherry on top, the invention of lasers (Section 7.2), an omission in the description of the quantum of light as bosons was evident.

In 1963, E. C. G. Sudarshan and R. Glauber independently introduced quantum coherent states specifically for light, as those states that are most closely related to classical states. When Glauber[2] discovered the states, he initially saw them as a mathematical curiosity. According to history, they were in communication with each other, and Sudarshan [161] sent a preliminary copy of his article to Glauber, only requiring that Glauber should acknowledge him. Unfortunately, Glauber [162, 163, 164] ignored the request. One of the great controversies of the Nobel prize is that the 1973 Nobel prize was solely awarded to Glauber, without recognition of Sudarshan's contribution. In the physics literature there is an attempt to correct this oversight by referring to them as **Sudarshan-Glauber coherent states**. They essential describe the quantum state of a laser. Where normally we talk about the number of quanta in a harmonic oscillator, here we should replace it with the number of photons in the laser mode. At present many text books discuss this topic, Klauder and Sudarshan [151], Perelomov [165], Rousseau and Blaise [166], Gazeau [167], Combescure and Robert [168] with mathematical applications, and in the selected works of Glauber [169]. Concurrently, Mandel and Wolf [170, 38]

Given a quantum harmonic oscillator with the Hamiltonian,

$$\hat{\mathbf{H}} = \frac{1}{2}(\hat{\mathbf{p}}^2 + \omega^2 \hat{\mathbf{q}}^2), \tag{7.60}$$

---

[1] There is a third set of units used, namely Heaviside-Lorentz units, cf. Jackson [152].

[2] Another child prodigy, as was Gauss, Hamilton, Schwinger and Mozart to name a few.

with the usual, $[\hat{\mathbf{q}}, \hat{\mathbf{p}}] = i\hbar$, we define non-Hermitian **annihilation** and **creation operators** (with "unit mass", but essentially with no mass, i.e., zero mass, only field energy) in optical phase space or quadrature space,

$$\hat{\mathbf{a}} = (2\omega\hbar)^{-\frac{1}{2}}(\omega\hat{\mathbf{q}} + i\hat{\mathbf{p}}), \tag{7.61}$$

$$\hat{\mathbf{a}}^\dagger = (2\omega\hbar)^{-\frac{1}{2}}(\omega\hat{\mathbf{q}} - i\hat{\mathbf{p}}). \tag{7.62}$$

The associated quantum mechanical harmonic oscillator Hamiltonian is given by,

$$\hat{\mathbf{H}} = \hbar\omega\left(\hat{\mathbf{a}}^\dagger\hat{\mathbf{a}} + \frac{1}{2}\right), \tag{7.63}$$

where, the vacuum zero-point energy, $E_o = \hbar\omega/2$, arises as a direct consequence of Heisenberg's uncertainty principle, and therefore also places an uncertainty on energy. The **number operator** is given by,

$$\hat{\mathbf{n}} = \hat{\mathbf{a}}^\dagger\hat{\mathbf{a}}. \tag{7.64}$$

This number operator is directly related to the amplitude of the coherent state, $|\alpha\rangle$. A **coherent quantum state** is usually defined as the eigenvalue problem of the annihilation operator $\hat{\mathbf{a}}$ of a quantum harmonic oscillator,

$$\hat{\mathbf{a}}\,|\alpha\rangle = \alpha\,|\alpha\rangle\,, \tag{7.65}$$

where the eigenvalue, $\alpha \in \mathbb{C}$. The Hermitian conjugate of the above is given by,

$$\langle\alpha|\,\hat{\mathbf{a}}^\dagger = \langle\alpha|\,\alpha^*, \tag{7.66}$$

and with the aid of the commutator relationship of a harmonic oscillator,

$$\left[\hat{\mathbf{a}}, \hat{\mathbf{a}}^\dagger\right] = \mathbf{1}, \tag{7.67}$$

we can expand the coherent state, $|\alpha\rangle$, in terms of number of occupation states, $|n\rangle$, of the harmonic oscillator and obtain

$$|\alpha\rangle = e^{-|\alpha|^2/2}\sum_{n=0}^{\infty}\frac{\alpha^n}{\sqrt{n!}}\,|n\rangle\,. \tag{7.68}$$

The inner product of two coherent states, $|\alpha\rangle$ and $|\beta\rangle$, is given by,

$$\begin{aligned}\langle\alpha|\beta\rangle &= e^{-\frac{|\alpha|^2+|\beta|^2}{2}}\sum_{m,n=0}^{\infty}\frac{\alpha^{*m}\beta^n}{\sqrt{m!}\sqrt{n!}}\,\langle m|n\rangle \\ &= e^{-\frac{|\alpha|^2+|\beta|^2}{2}}\sum_{n=0}^{\infty}\frac{(\alpha^*\beta)^n}{n!} \\ &= e^{-\frac{|\alpha|^2+|\beta|^2}{2}+\alpha^*\beta},\end{aligned} \tag{7.69}$$

which proves that two coherent states are not orthogonal. Furthermore, we have, $|\langle\alpha|\beta\rangle|^2 = e^{-|\alpha-\beta|^2}$. The position, $\hat{\mathbf{q}}$, and momentum, $\hat{\mathbf{p}}$, operator i.t.o., $\hat{\mathbf{a}}$ and $\hat{\mathbf{a}}^\dagger$, are given by,

$$\hat{\mathbf{q}} = \sqrt{\frac{\hbar}{2\omega}} \left(\hat{\mathbf{a}} + \hat{\mathbf{a}}^\dagger\right), \tag{7.70}$$

$$\hat{\mathbf{p}} = i\sqrt{2\omega\hbar} \left(\hat{\mathbf{a}}^\dagger - \hat{\mathbf{a}}\right), \tag{7.71}$$

respectively. The coherent state wave packet is then given by,

$$\psi_\alpha(q) = \langle q|\alpha\rangle, \tag{7.72}$$

and the position expectation is given by,

$$\langle\hat{\mathbf{q}}\rangle = \int_{-\infty}^{\infty} \psi_\alpha^*(x) x \psi_\alpha(x)\, dx. \tag{7.73}$$

Rather than doing this integral we use the operator technique directly,

$$\begin{aligned}\langle\hat{\mathbf{q}}\rangle &= \langle\alpha|\sqrt{\frac{\hbar}{2\omega}} \left(\hat{\mathbf{a}} + \hat{\mathbf{a}}^\dagger\right)|\alpha\rangle \\ &= \sqrt{\frac{\hbar}{2\omega}}(\alpha^* + \alpha) = 2\sqrt{\frac{\hbar}{2\omega}}\Re\{\alpha\}.\end{aligned} \tag{7.74}$$

The variance of the position operator is given by,

$$\triangle\hat{\mathbf{q}} = \sqrt{\langle\hat{\mathbf{q}}^2\rangle - \langle\hat{\mathbf{q}}\rangle^2}. \tag{7.75}$$

Similarly, the expectation value of the momentum and its variance can be calculated as,

$$\langle\hat{\mathbf{p}}\rangle = \langle\alpha|i\sqrt{2\omega\hbar}\left(\hat{\mathbf{a}}^\dagger - \hat{\mathbf{a}}\right)|\alpha\rangle = 2\sqrt{2\omega\hbar}\Im\{\alpha\}. \tag{7.76}$$

The coherent state complex eigenvalue can then be written as,

$$\alpha = \frac{1}{2}\left((\frac{\hbar}{2\omega})^{-\frac{1}{2}} \langle\hat{\mathbf{q}}\rangle + i(2\omega\hbar)^{-\frac{1}{2}} \langle\hat{\mathbf{p}}\rangle \right). \tag{7.77}$$

As was previously stated the number operator, $\hat{\mathbf{n}}$, Eq. (7.64), is directly related to the amplitude of the coherent state, $|\alpha\rangle$. Using both Eq. (7.65) and Eq. (7.66), the probability of the number of states, is given by,

$$\begin{aligned}\langle\alpha|\,\hat{\mathbf{n}}\,|\alpha\rangle &= \langle\alpha|\,\hat{\mathbf{a}}^\dagger\hat{\mathbf{a}}\,|\alpha\rangle \\ &= \langle\alpha|\,\alpha^*\alpha\,|\alpha\rangle \\ &= \|\alpha\|^2\,\langle\alpha|\alpha\rangle,\end{aligned} \tag{7.78}$$

and from Eq. (7.69), with $\alpha = \beta$, we have $\langle\alpha|\alpha\rangle = 1$. Thus, the probability of the number state, $\hat{\mathbf{n}}$, is given by,

$$\langle\alpha|\,\hat{\mathbf{n}}\,|\alpha\rangle = \|\alpha\|^2 . \tag{7.79}$$

Thus the complex eigenvalue, α, of Eq. (7.65), is related to the number state or amplitude of the coherent state $|\alpha\rangle$, by $\alpha^*\alpha = \|\alpha\|^2$.

The **displacement operator, $\hat{\mathbf{D}}(\alpha)$,** for quantum coherent states [150, 35, 24, 167, 166] also displays some kind of an analogy with Hermite and Fourier translation properties. For a single quantum mode, the displacement operator,

$$\hat{\mathbf{D}}(\alpha) = \exp\left(\alpha\hat{\mathbf{a}}^\dagger - \alpha^*\hat{\mathbf{a}}\right), \tag{7.80}$$

where, α, corresponds to the displacement in optical phase space and, $\hat{\mathbf{a}}^\dagger$, is the creation operator. When acting on the vacuum state, $|0\rangle$, the state is displaced into a coherent state, i.e.,

$$\hat{\mathbf{D}}(\alpha)\,|0\rangle = |\alpha\rangle\,.$$

Milonni has a whole textbook on "The Quantum Vacuum" [37]. The displacement of the vacuum state is shown in Figure 7.2. The displacement operator is an unitary operator, and by using the Baker-Campbell-Hausdorff formula, the product of two displacement operators is just another displacement operator with an added phase,

$$\hat{\mathbf{D}}(\alpha)\hat{\mathbf{D}}(\beta) = e^{(\alpha\beta^*-\alpha^*\beta)/2}\hat{\mathbf{D}}(\alpha+\beta). \tag{7.81}$$

The **phase shifting operator** rotates the coherent state by an angle, θ, in the phase space, $(\hat{\mathbf{q}},\hat{\mathbf{p}})$ or $(\theta,\hat{\mathbf{n}})$,

$$\hat{\mathbf{U}}(\theta) = e^{-i\theta\hat{\mathbf{n}}}. \tag{7.82}$$

From this definition it is easy to see that $[\hat{\mathbf{n}},\hat{\mathbf{U}}] = 0$. Taking the phase angle, θ, derivative of the unitary transformation by the phase shifting operator, $\hat{\mathbf{U}}$, of the annihilation operator $\hat{\mathbf{a}}$, then gives

$$\frac{d}{d\theta}\left(\hat{\mathbf{U}}^\dagger\hat{\mathbf{a}}\hat{\mathbf{U}}\right) = i\hat{\mathbf{U}}^\dagger[\hat{\mathbf{n}},\hat{\mathbf{a}}]\hat{\mathbf{U}}. \tag{7.83}$$

Using the operator algebra, we find $[\hat{\mathbf{n}},\hat{\mathbf{a}}] = -\hat{\mathbf{a}}$, resulting in the following differential equation,

$$\frac{d}{d\theta}\left(\hat{\mathbf{U}}^\dagger\hat{\mathbf{a}}\hat{\mathbf{U}}\right) = -i\left(\hat{\mathbf{U}}^\dagger\hat{\mathbf{a}}\hat{\mathbf{U}}\right), \tag{7.84}$$

with solution (given that the initial condition is $\theta = 0$),

$$\hat{\mathbf{U}}^\dagger\hat{\mathbf{a}}\hat{\mathbf{U}} = \hat{\mathbf{a}}e^{-i\theta}. \tag{7.85}$$

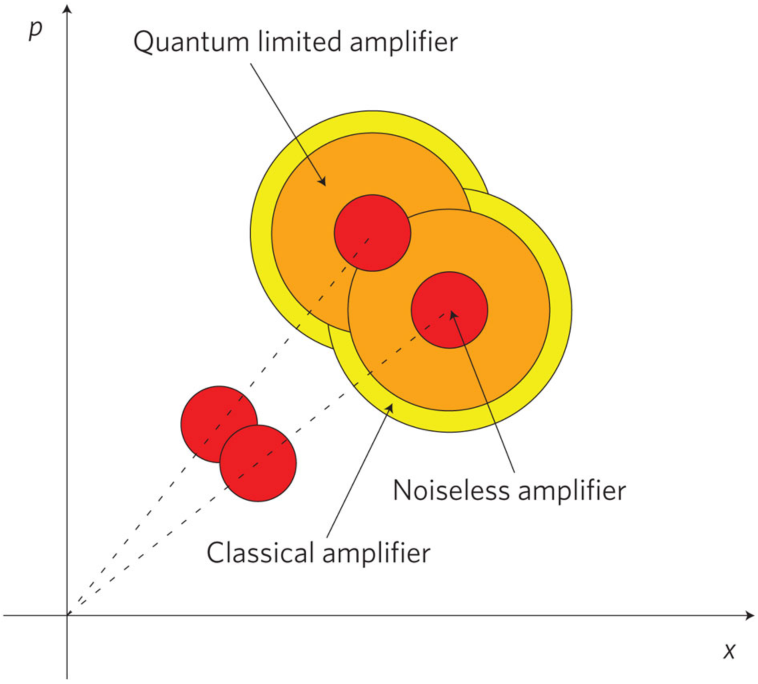

Figure 7.2.: Phase Space Uncertainties

The phase of a spatial temporal mode of a laser,

$$\hat{\mathbf{E}} = u^*(x,t)\hat{\mathbf{a}} + u(x,t)\hat{\mathbf{a}}^\dagger, \tag{7.86}$$

can now be changed by an observer by the unitary transformation of the phase shifting operator, $\hat{\mathbf{U}}(\theta)$, to

$$\hat{\mathbf{E}}' = u^*(x,t)e^{-i\theta}\hat{\mathbf{a}} + u(x,t)e^{i\theta}\hat{\mathbf{a}}^\dagger. \tag{7.87}$$

A multimode creation operator (3-dimensional) can be defined as,

$$\hat{\mathbf{A}}_\psi^\dagger = \int d\mathbf{k}\psi(\mathbf{k})\hat{\mathbf{a}}^\dagger(\mathbf{k}), \tag{7.88}$$

where, $\mathbf{k}$, is the wave vector with, $\|\mathbf{k}\| = \omega_\mathbf{k}/c$, and then associate a multimode displacement operator, $\hat{\mathbf{D}}_\psi(\alpha) = \exp\left(\alpha\hat{\mathbf{A}}_\psi^\dagger - \alpha^*\hat{\mathbf{A}}_\psi\right)$, and subsequently, define a multimode Glauber-Sudarshan state as,

$$|\alpha_\psi\rangle = \hat{\mathbf{D}}_\psi(\alpha)\,|0\rangle\,. \tag{7.89}$$

The electromagnetic field is then quantized by associating with each mode, $\mathbf{k}$, of the EM radiation field, the occupation number, $n_{\mathbf{k}}$, of a quantum harmonic oscillator, with photon energy $\hbar\omega_{\mathbf{k}}$. Generally the EM field is written in terms of the Fock space as,

$$|n_{\mathbf{k}_1}, n_{\mathbf{k}_2}, n_{\mathbf{k}_3}, \ldots\rangle = |n_{\mathbf{k}_1}\rangle\, |n_{\mathbf{k}_2}\rangle\, |n_{\mathbf{k}_3}\rangle \cdots = |\{n_{\mathbf{k}}\}\rangle\,. \tag{7.90}$$

In the Fock space, $\{n_{\mathbf{k}}\}$, the electromagnetic field can be considered as a collection of coherent states, $|\alpha_k\rangle$, each corresponding to a specific $\mathbf{k}$-mode of the number states $|n_{\mathbf{k}}\rangle = |n_k\rangle$, i.e.,

$$|\alpha_k\rangle = e^{-|\alpha_k|^2/2} \sum_{n_k=0}^{\infty} \frac{\alpha^{n_k}}{\sqrt{n_k!}}\, |n_k\rangle\,. \tag{7.91}$$

The time, $e^{i\omega_k t}$, and an amplitude, $a_k = \|\alpha_k\|^2$, Eq. (7.79), which is already indirectly included in the coherent state, can also be introduced, as is done in the quantization of the EM radiation field, Eq. (7.23), then ignoring the polarization, by assuming all modes are plane polarized as in laser light, we may write a general *multimode superposition of coherent state* as,

$$\boxed{||\alpha_\varepsilon; t\rangle\rangle = \sum_k e^{i\omega_k t} e^{-|\alpha_k|^2/2} \sum_{n_k=0}^{\infty} \frac{\alpha^{n_k}}{\sqrt{n_k!}}\, |n_k\rangle} \tag{7.92}$$

Including polarization, we write, $\varepsilon_{\mathbf{k}} \cdot \hat{\mathbf{k}} = 0$,

$$||\alpha_\varepsilon; t\rangle\rangle = \sum_k e^{-|\alpha_k|^2/2} \varepsilon_{\mathbf{k}} \sum_{n_k=0}^{\infty} \frac{\alpha^{n_k}}{\sqrt{n_k!}}\, |n_k\rangle\,. \tag{7.93}$$

How one should include the second polarization is still unclear to the author. If we assume that each coherent state for a specific, $\mathbf{k}$, manifests itself in two varieties, as in Eq. (7.26), i.e., $\hat{\mathbf{a}}_R(\mathbf{k})$ and $\hat{\mathbf{a}}_L(\mathbf{k})$, with associated transversal vectors, $\varepsilon_{\mathbf{k}}$ and $\varepsilon'_{\mathbf{k}}$, this can be accomplished (see the discussion in Subsection 7.2.2). This would then generally imply something like, and we would only hope that it is additive from the superposition principle, that we have two coherent state expansion for every, k,

$$\begin{aligned} ||\alpha_\varepsilon; t\rangle\rangle = \sum_k \Bigg\{ & e^{-|\alpha_k|^2/2} \varepsilon_{\mathbf{k}} \sum_{n_k=0}^{\infty} \frac{\alpha^{n_k}}{\sqrt{n_k!}}\, |n_k\rangle + \\ & e^{-|\alpha'_k|^2/2} \varepsilon'_{\mathbf{k}} \sum_{n'_k=0}^{\infty} \frac{\alpha'^{n'_k}}{\sqrt{n'_k!}}\, |n'_k\rangle \Bigg\}\,. \end{aligned} \tag{7.94}$$

7.4. FHG Coherent State Analogy

In the Fock space, $\{n_{\mathbf{k}}\}$, the electromagnetic field (strictly speaking the electric field is an operator in optical phase space, but its representation i.t.o. of state vectors clarifies the situation), $\varepsilon(t)$, can then be considered as a collection of Glauber-Sudarshan coherent states, $|\alpha_k\rangle$, each corresponding to a specific $\mathbf{k}$-mode of the number states $|n_{\mathbf{k}}\rangle = |n_k\rangle$, i.e., including time dependence, but ignoring the polarization, by assuming all modes are plane polarized 7.92

$$||\alpha_\varepsilon; t\rangle\rangle = \sum_k \sum_{n_k=0}^{\infty} e^{i\omega_k t} e^{-|\alpha_k|^2/2} \frac{\alpha_k^{n_k}}{\sqrt{n_k!}} |n_k\rangle \,, \tag{7.95}$$

where, $|n_k\rangle$, are the number states of the electromagnetic quantum harmonic oscillator and, $\alpha_k \in \mathbb{C}$. Excluding the dependence on the wavenumber, k, i.e., $n_k \to n$, the functional form of the q-representation of the orthonormal number states, $|n\rangle$, of the harmonic oscillator, i.e., $\langle q|n\rangle$, are exactly our HG basis functions, $\phi_n(x)$, (cf. Merzbacher [6]). In fact in quantum wave mechanics, the functional forms of the q-representation and p-representation are related to each other by a Fourier transform. This is the essence of quantum wave mechanics. Originally, Schrödinger used the Copenhagen correspondence from classical to quantum mechanics to “derive” his equation,[3] with the specific requirement that it had to only contain the first partial derivative of time, to correspond with the canonical classical mechanic equations of Hamilton. The manifestly relativistic covariance of space-time and energy-momentum with their Heisenberg uncertainties, $\triangle q \triangle p \geq \frac{\hbar}{2}$ and $\triangle t \triangle E \geq \frac{\hbar}{2}$, results in the Heisenberg-Gabor uncertainty, $\triangle t \triangle \omega \geq \frac{1}{2}$, showing that they are also reciprocal variables (The name originates from Cohen [33], see Section 2.3). Ever since Heisenberg’s formulation, the time-energy uncertainty relation (The non-relativistic QM derivation in Messiah [7] emphasizes the problems) is still subject to an ongoing debate cf. Busch [171], "The Time-Energy Uncertainty Relation", 2007.

The celebrated relativistic energy equation of Einstein i.t.o the rest mass m_0 of a particle,

$$E^2 = m_0^2 c^4 + p^2 c^2.$$

For a photon moving necessarily at the speed of light, we must have, $m_0 = 0$, and therefore,

$$E = pc, \tag{7.96}$$

$$p = \frac{E}{c}. \tag{7.97}$$

---

[3] The non-relativistic PDE of Schrödinger cannot be “derived” from first principles. It can only be seen as a plausible correspondence with the wave-particle duality equation of de Broglie.

In the manifestly relativistic formulation we have the covariant position 4-vector representation,

$$\begin{bmatrix} ct & q_1 & q_2 & q_3 \end{bmatrix}, \tag{7.98}$$

and similarly, the momentum,

$$\begin{bmatrix} \frac{E}{c} & p_1 & p_2 & p_3 \end{bmatrix}. \tag{7.99}$$

Now according to Planck's formula (1901),

$$E = h\nu = \hbar\omega. \tag{7.100}$$

or more generally as,

$$E_n = n\hbar\omega \qquad \text{with} \quad n = 1, 2, \ldots, \tag{7.101}$$

where, ν and ω, is the frequency an angular frequency of a photon, respectively and, h, is of course Planck's constant. Furthermore, from the de Broglie equation, rearranged to, $p = \hbar k$ and $k = \frac{\omega}{c}$, we also obtain from Eq. (7.99) (Compare Eq. (7.44), without the $\hbar$),

$$\hbar \begin{bmatrix} \frac{\omega}{c} & k_1 & k_2 & k_3 \end{bmatrix}. \tag{7.102}$$

Thus we notice that,

$$\begin{bmatrix} ct & q_1 & q_2 & q_3 \end{bmatrix} \tag{7.103}$$

$$\downarrow \; \downarrow \; \downarrow \; \downarrow$$

$$\begin{bmatrix} \frac{h\nu}{c} & p_1 & p_2 & p_3 \end{bmatrix} \tag{7.104}$$

$$\downarrow \; \downarrow \; \downarrow \; \downarrow$$

$$\begin{bmatrix} \frac{\omega}{c} & k_1 & k_2 & k_3 \end{bmatrix} \tag{7.105}$$

and that in quantum mechanics, $\mathbf{q}$ and $\mathbf{p}$, are considered canonical reciprocal variables, it is only natural by analogy to consider, ct and $\frac{h\nu}{c}$, $\frac{\omega}{c}$, as canonical reciprocal variables. Notice the direct correspondence of Eq. (7.105) with the manifestly relativistic covariant derivation of the quantum EM radiation field and its wavenumber, $k^\mu = [\frac{\omega}{c}, \mathbf{k}]$, Eq. (7.44). The Heisenberg uncertainty principle states that for quantum states, (q, p),

$$\triangle q \triangle p \geq \frac{\hbar}{2}, \tag{7.106}$$

and its associated commutator relationship,

$$[q, p] = i\hbar, \tag{7.107}$$

must therefore also be extended in this covariant formulation to (recall the vacuum zero-point energy, $E_o = \hbar\omega/2$, which implies that the energy can only be known to some uncertainty),

$$\triangle\, t \triangle\, E \geq \frac{\hbar}{2}. \tag{7.108}$$

Associated with $\triangle t \triangle\, E \geq \frac{\hbar}{2}$, we have a time and frequency or angular frequency (related to the Heisenberg-Gabor inequality, Eq. (2.8)) inequality,

$$\triangle\, t \triangle\, \omega \geq \frac{1}{2}, \tag{7.109}$$

and its associated commutator relationship,

$$[t, \omega] = 1. \tag{7.110}$$

Going from Eq. (7.106) to Eq. (7.108) to Eq. (7.109), we are actually performing the Wigner-Ville correspondence, cf. Section 2.8. Ignoring the polarization, by assuming all modes are plane polarized, the total field (a multimode superposition of coherent states 7.92) can then be written as, in the q_k-representation, where (q_k, p_k), is the corresponding optical phase space of the k-mode,

$$\langle\langle \mathbf{q}|\alpha_\varepsilon; t\rangle\rangle = \sum_k \sum_{n_k=0}^{\infty} e^{i\omega_k t} e^{-|\alpha_k|^2/2} \frac{\alpha_k^{n_k}}{\sqrt{n_k!}} \langle q_k|n_k\rangle\,, \tag{7.111}$$

where, $|n_k\rangle$, are the number states of the electromagnetic quantum harmonic oscillator and, $\alpha_k \in \mathbb{C}$. By declaring that the quantum canonical position-momentum states, (q, p), correspond to the classical variables, (t, ω), we have exactly the Ville correspondence. From the (q, p) quasi-probability distribution of Wigner, we move over to the "classical" Wigner-Ville TFR. This is in accord with the fundamental quantum mechanical principle of the quantum Copenhagen correspondence, but now in the opposite direction, to canonical quantization, and is also a requirement. From quantum to classical (this is analogous to the Wigner-Ville TFR and Feynman-Kac formula, see the footnote 4 of Section 2.8). Since, the q-representation of the orthonormal, $|n_k\rangle$, are exactly our HG, $\phi_{n_k}(t)$, states, (now with wavenumber k) and we know that in quantum mechanics all you need is, preferably, an orthonormal polynomial expansion,

$$\begin{aligned}
\langle n_k | n_l \rangle &= \delta_{kl} \\
\int_{-\infty}^{\infty} \langle n_k | q \rangle \langle q | n_l \rangle \, dq &= \delta_{kl} \\
\int_{-\infty}^{\infty} \phi_{n_k}(q) \phi_{n_k}(q) \, dq &= \delta_{kl} \\
\int_{-\infty}^{\infty} \phi_{n_k}(t) \phi_{n_k}(t) \, dt &= \delta_{kl} \\
\int_{-\infty}^{\infty} \phi_k(t) \phi_l(t) \, dt &= \delta_{kl}
\end{aligned}$$

We are aware that in non-relativistic quantum mechanics that time has some issues attached to it, but that it naturally enters in its manifestly relativistic covariant field theory formulation. We know, however, that for every m, n, in the FHG TFR, that,

$$\int_{-\infty}^{\infty} \phi_p(\frac{t - t_m}{\sqrt{2\sigma}}) \phi_k(\frac{t - t_m}{\sqrt{2\sigma}}) \, dt = \delta_{pk},$$

if the HG polynomials are properly scaled.

Considering this, we now actually make a bold step, by stating that, by **analogy,** that *a multimode superposition of coherent states* expansion Eq. (7.111),

$$\begin{aligned}
\langle\langle \mathbf{q} | \alpha_\varepsilon ; t \rangle\rangle &= \sum_k \sum_{n_k=0}^{\infty} e^{i\omega_k t} e^{-|\alpha_k|^2/2} \frac{\alpha_k^{n_k}}{\sqrt{n_k!}} \langle q_k | n_k \rangle \\
&\downarrow \downarrow \downarrow \downarrow \downarrow \\
\langle E; t \rangle &= \sum_{m,n=0}^{\infty} c_{m,n} \sum_{p=0}^{N} e^{i\omega_n t} e^{-|\alpha_{m,n}|^2/2} \frac{\alpha_{m,n}^p}{\sqrt{p!}} \phi_p(\frac{t - t_m}{\sqrt{2\sigma}}) \qquad (7.112)
\end{aligned}$$

to an analogous *"classical" multimode superposition of coherent state* expansion $\langle E; t \rangle$, i.e., the correspondence analogy, $\langle\langle \mathbf{q} | \alpha_\varepsilon ; t \rangle\rangle \longmapsto \langle E; t \rangle$, by the following variable correspondence[4]

$$\begin{aligned}
\langle q_k|n_k\rangle &\longmapsto \phi_p(\frac{t-t_m}{\sqrt{2\sigma}}) \\
n_k &\longmapsto p \\
k &\longmapsto m,n \\
\alpha_k &\longmapsto \alpha_{m,n} \\
\omega_k &\longmapsto \omega_n \\
\sum_k &\longmapsto \sum_{m,n=0} c_{m,n}
\end{aligned} \tag{7.113}$$

where, $c_{m,n} \in \mathbb{C}$, is an additional correlation expansion coefficient, corresponding to the amplitude α_k, that we assume is allowable because we are neglecting the specific polarization, given in Eq. (7.94). Eventually, $c_{m,n} \in \mathbb{C}$, becomes our **correlation coefficient** in this coherent state analogy. This is important, since in the whole process in modulating the laser beam, we are actually modifying the phase and amplitude. Exclusively for the temporal FHG basis (this is why it is only an analogy), we also have, for electric field representation of the coherent laser pulse $\varepsilon(t)$, the following correspondence $\langle E;t\rangle \longmapsto \varepsilon(t)$,

$$\langle E;t\rangle = \sum_{m,n=0}^{\infty} c_{m,n} \sum_{p=0}^{N} e^{i\omega_n t} e^{-|\alpha_{m,n}|^2/2} \frac{\alpha_{m,n}^p}{\sqrt{p!}} \phi_p(\frac{t-t_m}{\sqrt{2\sigma}}) \tag{7.114}$$

$$\downarrow \quad \downarrow \qquad \downarrow \quad \downarrow \quad \downarrow \quad \downarrow$$

$$\varepsilon(t) = \sum_{m,n=0}^{\infty} \sum_{p=0}^{N} e^{i\omega_n t} a_{m,n}^p \phi_p(\frac{t-t_m}{\sqrt{2\sigma}}), \tag{7.115}$$

where FHG coefficients are given by,

$$\mathbf{a}_{m,n}^T = [\; a_{m,n}^0 \quad a_{m,n}^1 \quad a_{m,n}^2 \quad \cdots \quad a_{m,n}^p \;]. \tag{7.116}$$

In Eq. (7.115) we make the following proportional **analogy**. Firstly, the coefficients of the FHG TFR are just proportional to "classical" multimode superposition of coherent state coefficients, i.e.,

$$\boxed{a_{m,n}^k \propto e^{-|\alpha_{m,n}|^2/2} \frac{\alpha_{m,n}^k}{\sqrt{k!}}} \tag{7.117}$$

Notice that in Eq. (7.114), we also have the expansion coefficient, $c_{m,n}$, available. By the inclusion of the so-called correlation coefficient, $c_{m,n}$, in Eq. (7.117) this can be made into an equality,

---

[4] We use the symbol $\longmapsto$ to denote a correspondence analogy

$$\boxed{a^k_{m,n} = c_{m,n} e^{-|\alpha_{m,n}|^2/2} \frac{\alpha^k_{m,n}}{\sqrt{k!}}} \tag{7.118}$$

Notice that from Eq. (7.111) to Eq. (7.112) to Eq. (7.115), we actually have two analogies, i.e.,

$$\langle\langle \mathbf{q} | \alpha_\varepsilon; t\rangle\rangle \longmapsto \langle E; t\rangle \longmapsto \varepsilon(t).$$

The bold step, then becomes a leap into an unexplored mine field, so we tread lightly. This is not an equivalence or an equality, but just a plausible correspondence analogy. In the old quantum mechanics even Einstein, 1917 [172], discovered the stimulated emission coefficient, by requiring detailed balancing with the black-body radiation formula of Planck.

To complete the correspondence of Eq. (7.118), we therefore, for each HG expansion, $\mathbf{a}_{m,n}$, frequency-translated by, $e^{it\omega_n}$, we set up the *corresponding optimization problem* to find the best, $\alpha_{m,n}, c_{m,n} \in \mathbb{C}$, that minimizes the following **cost function**

$$\mathbb{J}_{m,n} = \min_{\alpha_{m,n}, c_{m,n} \in \mathbb{C}} \|\mathbf{a}_{m,n} - \mathbf{b}(\alpha_{m,n}, c_{m,n})\|^2 \tag{7.119}$$

where,

$$\mathbf{b}(\alpha_{m,n}, c_{m,n}) = c_{m,n} e^{-|\alpha_{m,n}|^2/2} \begin{bmatrix} 1 & \alpha_{m,n} & \alpha^2_{m,n}/\sqrt{2!} & \cdots & \alpha^p_{m,n}/\sqrt{p!} \end{bmatrix}^T. \tag{7.120}$$

The cost function, $\mathbb{J}_{m,n}$, is then a measure of the correspondence of the FHG TFR coefficients with a analogous "classical" coherent state. A few explanatory notes relating to the cost function and the resulting "classical" coherent state analogy correlation matrix, $c_{m,n} \in \mathbb{C}$, are in order now. In the cost function, $\mathbb{J}_{m,n}$, Eq. (7.119), we are comparing, $\mathbf{a}_{m,n} - \mathbf{b}(\alpha_{m,n}, c_{m,n})$, by finding the optimal, $\alpha_{m,n}, c_{m,n}$, of the analogy vector $\mathbf{b}(\alpha_{m,n}, c_{m,n})$, Eq. (7.120). If in the optimization, which corresponds to the minimum of the cost function matrix $\mathbb{J}_{m,n}$, then if we have perfect minimization, i.e., $\mathbb{J}_{m,n} = 0$, it implies that we could find a, $\alpha_{m,n}, c_{m,n} \in \mathbb{C}$, that, $\|\mathbf{a}_{m,n} - \mathbf{b}(\alpha_{m,n}, c_{m,n})\| = 0$, i.e., $\mathbf{b}(\alpha_{m,n}, c_{m,n}) \sim \mathbf{a}_{m,n}$, at least in amplitude. This means, $\alpha_{m,n}, c_{m,n} \in \mathbb{C}$, i.e., the amplitude, $\alpha_{m,n}$, and correlation coefficient, $c_{m,n}$, have a direct match, $\mathbf{a}_{m,n}$ of the FHG TFR coefficient vector, Eq. (7.116), and Eq. (7.118) is true. This means that, $\|c_{m,n}\| = 1$, in Eq. (7.118), i.e., $c_{m,n}$, only contributes a phase, $e^{i\phi}$. When $\mathbb{J}_{m,n} \neq 0$, the correspondence between the coefficients are not exact, and immediately implies that the correlation coefficient $\|c_{m,n}\| \neq 1$. To take this into consideration, we define a normalized "classical" coherent state analogy correlation matrix $\mathscr{C}_{m,n}$, which is real-valued, be means of

$$\mathscr{C}_{m,n} = \mathbb{I} - \mathbb{J}_{m,n} / \max_m(\max_n(\|c_{m,n}\|)). \tag{7.121}$$

This normalized “classical” coherent state analogy correlation matrix can then also be plotted as a “classical” coherent state analogy TFR. Figure 7.3 and Figure 7.4 two “classical” coherent state analogy TFRs are presented for our first and second laser pulses respectively. For convenience the spectral graphs of the two laser pulses are given next to the coherent state TFR analogy. Since a coherent state is just a quantum displacement of the vacuum state, one would expect that there is a perfect correlation in areas of TFR where their is no signal. This is exactly what we observe in the two graphs, for our “classical” coherent state analogy TFR. In the presence of the laser pulses we see that the correlation between the “classical” coherent state analogy TFR deteriorates. This is also expected. We clearly see that there is greater correlation with respect to the second laser pulse Figure 7.4. Just off the wings of the laser pulse, in the time domain the correlation is very low in both cases.

This cannot be seen as a mathematical rigorous equivalence or equality. We believe, however, that we have shown the plausibility of a correlation analogy between FHG TFR temporal bases and some kind of Glauber-Sudarshan multimode superposition of “classical” coherent states. The proof of the pudding is in the eating. The fruits of our endeavor and the plausibility of our double correspondence analogy, can be witnessed in Figure 7.3 and Figure 7.4 and they clearly illustrate that the two “classical” coherent state analogy TFRs actually correspond to the electric signals magnificently well.

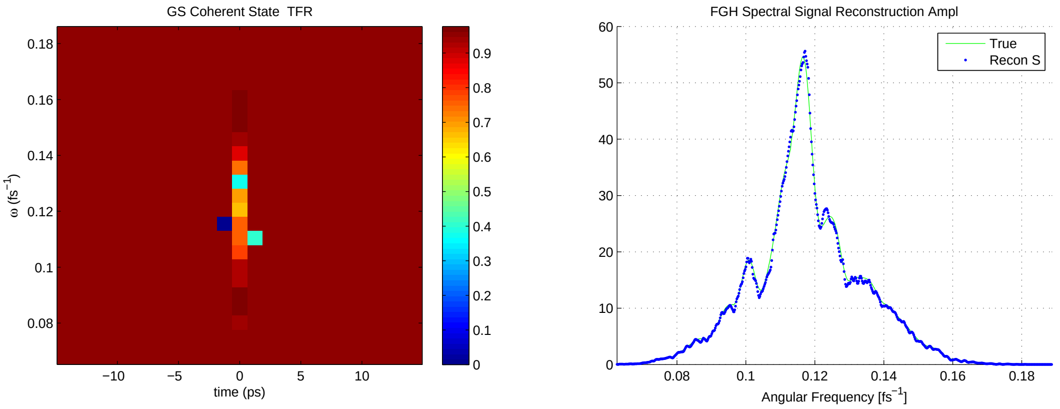

Figure 7.3.: Coherent State TFR Analogy (First Representative Laser Pulse)

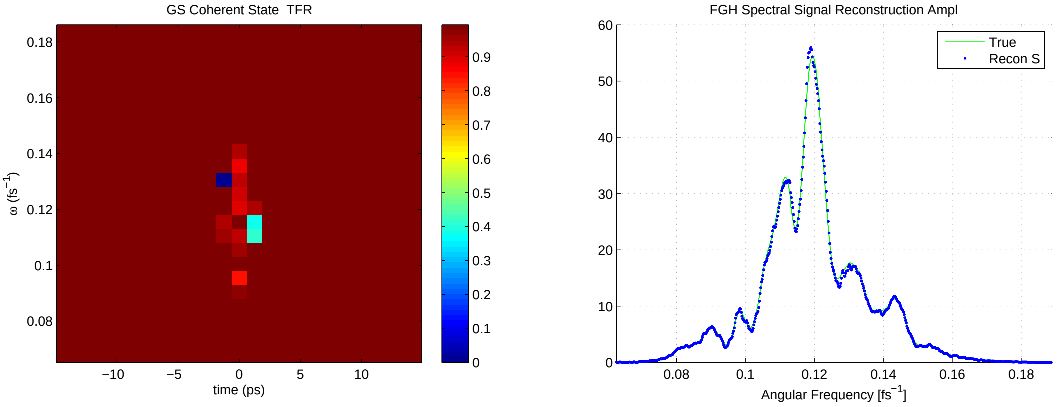

Figure 7.4.: Coherent State TFR Analogy (Second Representative Laser Pulse)

7.5. Conclusion

A concrete example of an orthogonal expansion of signals has been constructed with an additional benefit of analogy with Glauber-Sudarshan quantum coherent states and the generation of a “classical” coherent state correlation TFR. The analytical freedom offered by this new HG TFR must still be explored to its full potential. The discovery of the “classical” coherent state analogy definitely warrants further investigation and is under current research.

8. Conclusion

One can ask, what is your wish or desire? This can be an ultimate question. The question is so broad that one has to narrow it to more manageable terrains. The use of the word terrain is specifically chosen to denote a portion of the whole world. Zoom in to a specific question. Here we have explored the existence of different domains and fields, actually in digital information coding.

The true question in this field than becomes: What is the minimum coding requirement to represent a set of digital information? Ah, presuming that all information is of harmonic content (closest to binary). At least this is how we communicate with longitudinal sound waves. Light being an electromagnetic phenomenon is also governed by a transversal wave or harmonic principle. Thereby making wave phenomena the basic communication principle. Now... Even and odd, reality, imaginary, analyticity, Hermiticy vs anti-Hermiticy, orthogonality, and anti-aliasing, data, coding and information, all play a crucial role. All the properties are intertwined. All these questions must still be properly addressed. Somehow the **orthogonality of the Hermite-Gauss** functions are of immeasurable importance in the coding theory and the clue to unraveling the knot.

One great unaddressed question, is the relationship between precision and resolution of a signal. In representing a signal in terms of a finite polynomial bases, the precision of reconstruction and resolving the two bases polynomials have a reciprocal relationship. The finer the grid the better the precision of reconstruction, but the resolution of two neighbouring bases deteriorates. This is also related to correlation. For higher resolution two neighbouring bases polynomials must have lower correlation. This would also explain the small grid choice of 11×11 in (Tannor et al. [94]). This is to improve resolution.

To give us some flavour of some future work, let us investigate what a translation in the temporal and spectral domains actually causes. Let us assume that we can only create a real function in the temporal domain with modulation unscaled shifted in time with, t_l, i.e., totally real (modifying our basis),

$$\cos(\omega_m t) 2^{-\frac{n}{2}} (n!)^{-\frac{1}{2}} \pi^{-\frac{1}{4}} e^{-\frac{(t-t_l)^2}{2}} H_n(t-t_l).$$

Using Euler's formula this can be written as,

$$\frac{1}{2}\left(e^{i\omega_m t}+e^{-i\omega_m t}\right)2^{-\frac{n}{2}}\left(n!\right)^{-\frac{1}{2}}\pi^{-\frac{1}{4}}e^{-\frac{(t-t_l)^2}{2}}H_n(t-t_l),$$

which does not resemble our defined basis at all. Being odd and even, real and imaginary, as well as Hermitian and anti-Hermitian, and thrown into it all analyticity, we find, starting with a real function (presumably something we can create) that the Fourier transform will translate into two side-lobes in the frequency domain,

$$F(\omega)=\frac{1}{2}\cdot 2^{-\frac{n}{2}}\left(n!\right)^{-\frac{1}{2}}\pi^{-\frac{1}{4}}\left[e^{-i(\omega-\omega_m)t_l}e^{-\frac{(\omega-\omega_m)^2}{2}}H_n(\omega-\omega_m)+\right.$$
$$\left.e^{-i(\omega+\omega_m)t_l}e^{-\frac{(\omega+\omega_m)^2}{2}}H_n(\omega+\omega_m)\right].$$

According to Subsection A.3.7 the Fourier transform must be Hermitian, i.e., $F(-\omega)=F^*(\omega)$, which is not so evident from the above equation, but can quite easily be proven. The important fact to note is that real signals Fourier transform into two side-lobes, one at ω_m and one at $-\omega_m$, which is simply a well known property of modulation, i.e., the multiplication of, $e^{i\omega_m t}$. This is exactly the reason for the introduction of analytical functions to avoid negative frequencies. But with the disadvantage of being imaginary.

In the calculation of the of the overlap matrices on the von Neumann grid we found the requirement of **doubling the bandwidth** on the electric signal,

$$\omega_{nl}\in[-\Omega,\Omega]\qquad\forall n,l$$

.That means the bandwidth we require for the signals is 2Ω. The requirement also arises in the time domain, i.e., $t_{mk}\in[-T,T]$, for all m and k. Thus, $2T$. To comply to all these requirements, and still have the same σ, we must have,

$$\delta t\to\frac{\delta t}{2},\quad\text{and}\quad\delta\omega\to\frac{\delta\omega}{2},$$

so that, T, goes to, $2T$, and, Ω, goes to, 2Ω.

The judicious choice of a 640 pixel SLM was also shown, primarily to take into account **anti-aliasing**. The SLM therefore was only designed to function on the central 512 pixels, i.e., $640=64+512+64$. Once again this was only discovered after the fact. Thus, the correct choice is to narrow our bandwidth accordingly. Hand in hand the correct grid choice would have been $512\simeq 529=23\times 23$. So the suggestion for the grid is $\Omega\times T=2\pi N$ and then take $N=529$. At present we have it at $N = 625$. After this correction we should also narrow our bandwidth to correspond to the central 529 pixels of the SLM.

Also to late was the discovery of the **functional operator notation** that results in writing the FHG bases as Eq. (5.52),

$$\boxed{\mathcal{M}_{\omega_n}\mathcal{T}_{t_m}\mathbf{\Phi}(t) \overset{\mathcal{F}}{\Longleftrightarrow} \mathcal{T}_{\omega_n}\mathcal{M}_{-t_m}\mathbf{\Phi}(\omega)}$$

This would have greatly simplified this work. The definition of the spectral function Eq. (6.18),

$$\boxed{H_{m,k}(x) = e^{-it_m x}\phi_k(x)}$$

and the temporal function Eq. (6.26),

$$\boxed{K_{m,n,k}(x) = e^{i\omega_n(x+t_m)}\phi_k(x)}$$

to facilitate the correlation functions of the overlap matrices are also novel to this thesis.

In summary we have:

1. The application of the von Neumann TFR to enhance the numerical optimization of quantum control problems.
2. Adaptive quantum coherent control of a multilevel molecular system in the von Neumann time-frequency domain.
3. The discovery of the novel Fourier-Hermite-Gauss TFR as an expansion and generalization of the von Neumann TFR.
4. The FHG TFR overlap matrices are different for the temporal and spectral cases.
5. The requirement of doubling the bandwidths of the signal on a von Neumann grid and its anti-aliasing effects.
6. The discovery of the functional operator notation that so succinctly summarizes the FHG TFR.
7. The definition of two new functions for the use in the correlation function
8. The temporal and spectral FHG TFR correlation cubes contain all the information to reconstruct the temporal and spectral signals.
9. The discovery of the relationship Eq. (5.172) of Theorem 5.4.9

$$\left[\mathbb{W}^{k,l}_{m,n}\right] \simeq \left[\mathbb{T}^{k,l}_{m,n}\right]^{*}.$$

10. The discovery of the "classical" coherent State TFR correspondence analogy with the novel FHG TFR, which leads to a correlation TFR.

It has recently come to my attention that a good engineering friend of mine, that specializes in DSP, radar and sonar, that I gave a personal lecture on this work, has found it so fascinating enough to implement it on some of standard benchmark programs. What programs and have not yet had the opportunity to study, since I was finalizing this thesis. To his shock he reported back to me telephonically, that the implementation of these methods and his normal standard methods showed a signal to noise ratio (SNR) improvement from 28 dB to over 300 dB. This must still be confirmed, but this is absolutely amazing and will have enormous implication on some applications.

The question for almost all the financial backers is always: So its new and novel, but what is the possible applications? And how can it financially benefit my pocket? Well here is short list of possible applications:

1. Adaptive quantum coherent control for ultra-short laser pulses.
2. Digital communication.
3. Information theory.
4. Radar and Sonar.

As for future work in this field the first we chapters at least gives an outline. Of course the very next subject I will investigate is the DSP application. Before I was abruptly derailed and convinced to this current work, I was busy on quantum control of closed systems. At that time January 2012 I was busy with a new method to enhance our own optimization procedure for the interaction of IR femtosecond laser pulses with octahedral molecules. If funded I would still to complete this work with two article entitled:

1. Quantum Molecular Control with Ultra Short Laser Pulses using Levi Decomposition of the Lie Group Interaction Hamiltonian.
2. A Modified Hadamard Lemma for Phenomenological Quantum Decay

At that time I just about completed reading d'Alessandro [2] and good portions of Breuer and Petruccione, "The theory of open quantum systems" [173] and the work "Quantum Noise" [174]. The real love of my heart is to do what I originally signed up for, namely "Stochastic coherent control of quantum processes" or any open quantum system work. If it were up to me, given that I am doing research in this field, I would be in seventh heaven and health prevailing never cease.

One of the best quotes about light is to be found in (Hecht and Zajac, [18]) at the end of their Chapter 1, A Brief History:

“Profound insights are slow in coming. What few we have took over three thousand years to glean even though the pace is ever quickening. It is marvelous indeed to watch the answer subtly change while the question immutably remains – What Is Light?”

As I am getting on in life, I hope that there is still a little child in me, since

. . . for geometry, you know, is the gate of science, and the gate is so low and small that one can only enter it as a little child. William Kingdon Clifford (1845-1879)

Acknowledgments

Firstly and foremostly, I must thank my co-supervisor Dr. Lourens Rasmus Botha for being a colleague and a friend. He was such a great inspiration. His tragic unfortunate passing away from the Big C, the Heart, was emotionally shattering. It left me traumatically shipwrecked on a deserted island. Maybe one coconut tree to keep me alive.

It was under his encouragement that this work was done. For his assistance and for backing me, even with unfounded political resistance, and allowing me to attend the 2013 Femto14 Conference in Copenhagen on the centenary year of the great discovery in quantum physics of the Nobel prize winner Niels Bohr. I was so fortunate. At least I brought back the best poster award, to silence and shock a few. Lourens was so proud of me. His loss left an emotional hole in my heart.

I thank Dr. Hermann Uys, that was appointed as my new co-supervisor, that he came and rescued me from the one palm tree island. Prof. Dr. Thomas Konrad for allowing me to write the obituary of Lourens for Physics Comment. In this regard I must sincerely thank his widow Erna Botha for her assistance.

I extend my gratitude to Prof. David Tannor for the pleasant conversations, even of so short a nature, in Copenhagen, and a personal copy of the pre-published article [104], relating to the von Neumann TFR. For his inspirational articles. His book made me understand quantum mechanics, fundamentally being probabilistic, in the time domain.

Prof. Francesco Petruccione, for the financing of a colloquium of this work in Durban, UKZN. Of course his book [173] remains one of the the best on open quantum systems.

I would also like to acknowledge the financial assistance of the National Laser Center, CSIR and the National Research Foundation of South Africa (NRF) for the financial grant under which this work was performed. For all the co-workers at the CSIR that assisted me. Especially, my tennis and “singing” mates, Dr. Cingo and Dr. Paul. Something to recall with happiness.

I would like to thank my co-supervisor, Dr. H. Uys, for allowing me to do some experimental work in 2012, resulting in the acceptance of it RADIO 2014 conference in Mauritius for a full lecture. Unfortunately, due to the tragic demise of my

first co-supervisor, Dr. L. R. Botha, which was approved by him, and the ensuing financial constraints, I had to cancel my invitation.

Lastly, but not least, for my supervisor Prof. Dr. Erich Rohwer and the University of Stellenbosch, for his patience, and most of all his Secretary, Christine, for her understanding and assistance. Thank you. May God Bless you all.

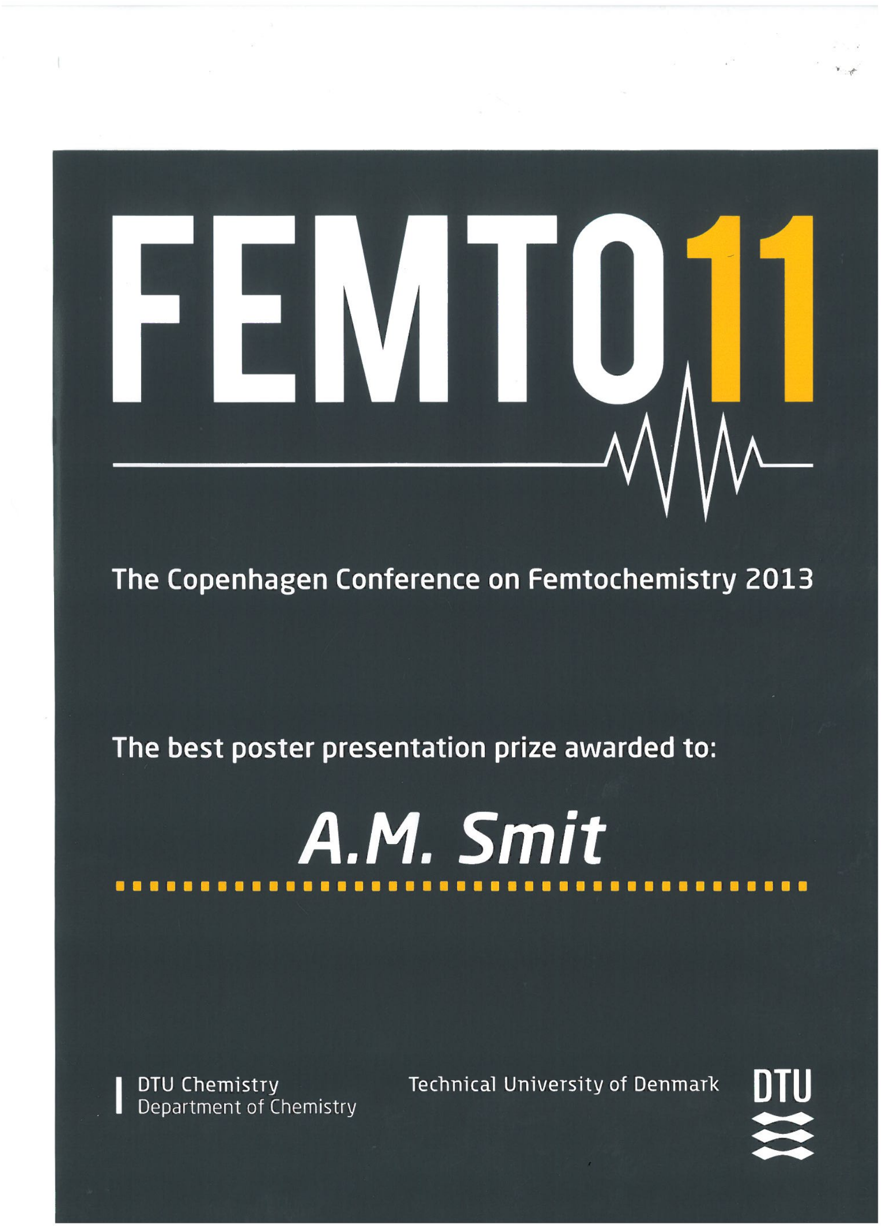

FEMTO11

The Copenhagen Conference on Femtochemistry 2013

The best poster presentation prize awarded to:

A.M. Smit

DTU Chemistry
Department of Chemistry

Technical University of Denmark

DTU

Verification of the Near Field EM Field for a Dipole Microwave Antenna derived from the Liénhard-Wiechert Potential

A.M. Smit[1], H.P. Kloppers[1] and H. Uys[1]

[1]National Laser Centre, CSIR, P O Box 395, Pretoria 0001, South Africa,

Generally most radio applications are interested in the far field effects of the EM field for communications purposes. In our quantum control experiment the requirement is to manipulate quantum dots (essentially atoms) by means of coherent microwaves in an extremely confined environment. This necessitated the investigation of the near field EM effects for microwaves in cavity. A short derivation of the EM fields and radiation patterns of a dipole antenna from first principles is given, using the Liénhard-Wiechert potentials [1], [2],

$$\mathbf{\Phi}(\mathbf{r},t)=\frac{1}{4\pi\varepsilon_o}\iiint_V \frac{\rho(\mathbf{r}',t_r)}{\mathfrak{r}}\,d\tau' \;; \qquad \mathbf{A}(\mathbf{r},t)=\frac{1}{4\pi\varepsilon_o}\iiint_V \frac{\mathbf{J}(\mathbf{r}',t_r)}{\mathfrak{r}}\,d\tau'$$

where the relative position vector is defined as $\boldsymbol{\mathfrak{r}}(t\,,t_r)=\mathbf{r}(t)-\mathbf{r}'(t,t_r)$ and t_r is the retarded time, $\rho(\mathbf{r}',t_r)$ and $\mathbf{J}(\mathbf{r}',t_r)$ are the charge and current densities respectively, and also employing Jefimenko's equations for the EM field [3], resulting in

$$\mathbf{E}=\frac{p_o k^2}{4\pi\varepsilon_o r}\exp j\omega\left(t-\frac{r}{c}\right)\left\{2\left(\frac{1}{k^2r^2}+j\frac{1}{kr}\right)\cos\theta\hat{\mathbf{r}}+\left(\frac{1}{k^2r^2}+j\frac{1}{kr}-1\right)\sin\theta\hat{\theta}\right\}$$

The experimental setup and measurements of the near field microwave dipole electric field will then be presented. The experimental results unequivocally demonstrate, see e.g. the excellent fit in Figure 1 below, the validity of the derived near field EM fields for a dipole antenna.

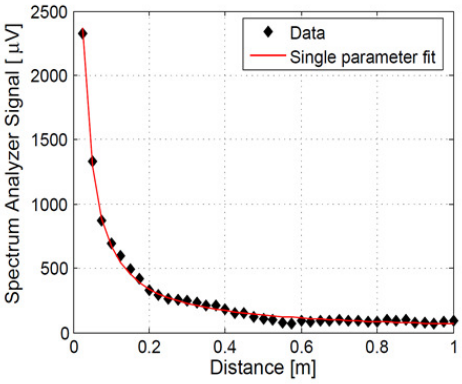

Figure 1: Nearfield Dipole Radiation Field

References

[1] P. Lorrain and D. Corson, *Electromagnetic Fields and Waves*, 2nd Ed, W.H. Freeman & Co., 1970.

[2] J.D. Jackson, *Classical Electrodynamics*, 2nd Ed, John Wiley & Sons, New York, 1975.

[3] D.J. Griffiths, *Introduction to Electrodynamics,* 3rd Ed, Pearson Education, Dorling Kindersley, 2007

A. The Fourier Series and Transform

A.1. Introduction

(Latin. alias—at another time)

1799 Energy theorem of Fourier Series

1807 Fourier Series

1822 Fourier Transform

Historically, Baron Jean Baptiste Joseph Fourier (1768-1830) invented the Fourier series technique to solve the partial differential equation for heat diffusion. Other great contemporary scientists were Count Joseph-Louis Lagrange (1736-1813), Pierre-Simon, Marquis de Laplace (1749-1827), Baron Simeon Denis Poisson (1781-1840), famous, amongst other things for his Poisson summation theorem used in DSP.

All these scientists/mathematicians lived through the French revolution that toppled the French nobility and the royalists. It is ironic that all their noble titles were subsequently bestowed on them by Napoleon who proclaimed himself as Emperor of France. Two other Frenchmen Marc-Antoine Parseval (1755-1836) and Adrien-Marie Legendre (1752-1833) (Legendre functions, 1783) probably were just not favoured. It is not clear when the continuous Fourier transform was developed from the Fourier series, but since the Laplace transform was already invented in 1785, we can only assume that this extension was made soon after the discovery of the Fourier series, by Laplace in 1809, since the Fourier transform is included in the Laplace transform with $s = \sigma + i\omega$ with $\sigma = 0$. The Laplace transform of a function $f(t)$ is defined as (cf. Beerends [175]),

$$F(s) = \int_{-\infty}^{\infty} f(t)\, e^{-st}\, \mathrm{d}t.$$

This Appendix gives a short summary of the relevant properties of the Fourier series and transform. The enormous literature on Fourier transforms and analysis clear shows the extreme importance as a mathematical tool in physics and engineering. Here is a brief list [124, 125, 126, 176, 175, 177, 20, 178, 67, 127]. There exists various definitions of the Fourier transform defined in Section A.2. In Section A.3 most of the properties of the Fourier transform are listed without proof. Some common functions that normally occur in Fourier transform analysis are defined in Section A.4 along with a special Subsection on the distribution function known as the Dirac-δ function and its properties, which is so prevalent in Fourier analysis.

Then, however, in Subsection A.4.7 the functional mirror image operator is introduced. This was actually conceived by the author at a late stage to help with the understanding of correlation. The conception thereof was actually learning about, Subsection A.4.8, the translation operator. The author did not attempt to search for a reference for the definition of modulation operator defined in Subsection A.4.9, but is sure it must be common knowledge in some circles. Rewriting certain formula in terms of these function operators greatly simplifies the understanding of the processes occurring. Unfortunately, this came to late.

A table of various Fourier transform pairs is presented in Section A.5. The Fourier transforms of even and odd functions are discussed in Section A.6.

The next few Sections are devoted to topics that occur in Digital Signal Processing (DSP), starting with sampling theory, properties of bandlimited signals, the Poisson summation theorem and lastly the Nyquist-Shannon sampling theorem. We didn't think it prudent to include the Discrete Fourier Transform and Fast Fourier Transform (FFT) as the last algorithm and its derivatives is probably the most widely used algorithm in digital sciences.

A.1.1. Fourier Series

Any periodic signal $f(t)$ with period T, i.e.,

$$f(t) = f(t + nT), \quad n \in \mathbb{Z},\ t \in \mathbb{R}, \tag{A.1}$$

can be written as a Fourier series as,

$$\boxed{f(t) = \sum_{n=-\infty}^{\infty} a_n e^{in\omega_o t} \quad, \omega_o = \frac{2\pi}{T}} \tag{A.2}$$

where,

$$\boxed{a_n = \frac{1}{T}\int_{-T/2}^{T/2} f(t)e^{-in\omega_o t}dt} \tag{A.3}$$

Definition A.1.1. (**Trigonometric polynomials**) A Fourier series with finitely many terms is known as a trigonometric polynomial,

$$y(t) = \sum_{n=-M}^{M} c_n e^{in\omega t}. \tag{A.4}$$

A.2. Various Definitions of the Fourier Transform

- The Fourier transform (Unitary, ordinary frequency) (Notice that there is no scaling constant)

$$\mathcal{F}\left\{f\left(t\right)\right\} = F\left(\nu\right) = \int_{-\infty}^{\infty} f\left(t\right) e^{-2\pi i\nu t}\,\mathrm{d}t \tag{A.5}$$

$$\mathcal{F}^{-1}\left\{F\left(\nu\right)\right\} = f\left(t\right) = \int_{-\infty}^{\infty} F\left(\nu\right) e^{2\pi i\nu t}\,\mathrm{d}\nu \tag{A.6}$$

- The Fourier transform and its inverse Fourier transform are only similar with the same normalization constant if the two variables are commensurate, that is if the units of the variables are each others inverses, e.g., $\nu = [1/t]$ where as for, $\omega = 2\pi\nu$, we obtain,

$$\mathcal{F}\left\{f\left(t\right)\right\} = F\left(\omega\right) = \int_{-\infty}^{\infty} f\left(t\right) e^{-i\omega t}\,\mathrm{d}t, \tag{A.7}$$

$$\mathcal{F}^{-1}\left\{F\left(\omega\right)\right\} = f\left(t\right) = \frac{1}{2\pi}\int_{-\infty}^{\infty} F\left(\omega\right) e^{i\omega t}\,\mathrm{d}\omega. \tag{A.8}$$

- The Fourier transform (Unitary, angular frequency, symmetric)

$$\mathcal{F}\left\{f\left(t\right)\right\} = F\left(\omega\right) = \frac{1}{\sqrt{2\pi}}\int_{-\infty}^{\infty} f\left(t\right) e^{-i\omega t}\,\mathrm{d}t \tag{A.9}$$

$$\boldsymbol{\mathcal{F}}^{-1}\left\{F\left(\omega\right)\right\} = f\left(t\right) = \frac{1}{\sqrt{2\pi}}\int_{-\infty}^{\infty} F\left(\omega\right)e^{i\omega t}\,\mathrm{d}\omega \tag{A.10}$$

- The Fourier transform (Non unitary)

$$\boldsymbol{\mathcal{F}}\left\{f\left(q\right)\right\} = F\left(p\right) = \int_{-\infty}^{\infty} f\left(t\right)e^{-ipq}\,\mathrm{d}q \tag{A.11}$$

$$\boldsymbol{\mathcal{F}}^{-1}\left\{F\left(p\right)\right\} = f\left(q\right) = \frac{1}{2\pi}\int_{-\infty}^{\infty} F\left(p\right)e^{ipqt}\,\mathrm{d}p \tag{A.12}$$

- To indicate that a pair of functions are Fourier transform pairs, we often also employ the following notation,

$$f(t) \overset{\mathcal{F}}{\Longleftrightarrow} F(\omega). \tag{A.13}$$

A.3. Properties

In the following let, $f(t)$, $g(t) \in L^2(\mathbb{R})$, be any two integrable functions on the real line with Fourier transforms, $F(\omega)$, $G(\omega)$, respectively and given $a, b \in \mathbb{C}$, and $h(t) = af(t) + bg(t)$, its corresponding Fourier transform, $H(\omega)$. In general, $f(t)$, $g(t)$ and $F(\omega)$, $G(\omega)$, may be complex valued functions, but that $t, \omega \in \mathbb{R}$. That is,

$$\begin{aligned} f(t) &= f_1(t) + if_2(t), \\ F(\omega) &= R(\omega) + iX(\omega). \end{aligned}$$

A.3.1. Linearity

$$\boldsymbol{\mathcal{F}}\{h(t)\} = \boldsymbol{\mathcal{F}}\{af(t) + bg(t)\} = a\boldsymbol{\mathcal{F}}\{f(t)\} + b\boldsymbol{\mathcal{F}}\{g(t)\} \tag{A.14}$$

$$\boxed{H(\omega) = aF(\omega) + bG(\omega)} \tag{A.15}$$

A.3.2. Duality (Symmetry)

If $\mathcal{F}\{f(t)\} = F(\omega)$ then,

$$\boxed{\mathcal{F}\{F(t)\} = f(-\omega)} \tag{A.16}$$

or,

$$\boxed{F(t) = \mathcal{F}^{-1}\{f(-\omega)\}} \tag{A.17}$$

Also,

$$F(-t) = \mathcal{F}^{-1}\{f(\omega)\}.$$

A.3.3. Complex Conjugation

If, $\mathcal{F}\{f(t)\} = F(\omega)$, then,

$$\boxed{F^*(t) = \mathcal{F}^{-1}\{f^*(\omega)\}} \tag{A.18}$$

$$\boxed{F^*(\omega) = \mathcal{F}\{f^*(-t)\}} \tag{A.19}$$

Also,

$$\begin{aligned} \mathcal{F}\left\{f^*\left(t\right)\right\} &= F^*(-\omega), \\ \left[\mathcal{F}\{F(t)\}\right]^* &= f^*(-\omega). \end{aligned}$$

A.3.4. Scaling (Reciprocity)

For any real, $a \neq 0$, then, $h(t) = f(at)$,

$$\boxed{H(\omega) = \mathcal{F}\{f(at)\} = \frac{1}{|a|}F(\frac{\omega}{a})} \tag{A.20}$$

Notice, the inverse (thus inverse scaling both ways),

$$\boxed{\mathcal{F}^{-1}\{F(a\omega\} = \frac{1}{|a|}f(\frac{t}{a})} \tag{A.21}$$

A.3.5. Shifting

- Temporal Shifting

Let, $h(t) = f(t - t_0)$, then

$$\boxed{H(\omega) = \boldsymbol{\mathcal{F}}\{f(t - t_0)\} = e^{-i\omega t_o} F(\omega)} \tag{A.22}$$

- Spectral Shifting

Let, $H(\omega) = F(\omega - \omega_o)$, then

$$\boxed{h(t) = \boldsymbol{\mathcal{F}}^{-1}\{F(\omega - \omega_o)\} = e^{i\omega_o t} f(t)} \tag{A.23}$$

- Modulation. $\boldsymbol{\mathcal{F}}\{h(t)\} = H(\omega)$,

$$\boxed{\boldsymbol{\mathcal{F}}\{e^{i\omega_o t} h(t)\} = H(\omega - \omega_o)} \tag{A.24}$$

- Combining Temporal shifting and Modulation, $g(t) = e^{i\omega_o t} h(t) = e^{i\omega_o t} f(t - t_0)$,

$$\boxed{\boldsymbol{\mathcal{F}}\{e^{i\omega_o t} f(t - t_0)\} = H(\omega - \omega_o) = e^{-it_o(\omega - \omega_0)} F(\omega - \omega_0)} \tag{A.25}$$

A.3.6. Differentiation

- Time derivatives

$$\boxed{\boldsymbol{\mathcal{F}}\{\frac{d^n}{dt^n} f(t)\} = (i\omega)^n F(\omega)} \tag{A.26}$$

- Frequency derivatives

$$\boxed{\boldsymbol{\mathcal{F}}^{-1}\{\frac{d^n}{d\omega^n} F(\omega)\} = (-it)^n f(t)} \tag{A.27}$$

A.3.7. Real and Hermitian Functions

Definition A.3.1. A function, $f(x)$, is **Hermitian** if,

$$f(-x) = f^*(x). \tag{A.28}$$

Then we have

- If $f(t)$ is real, i.e., $f(t) = \Re\{f(t)\}$, then its Fourier transform, $\boldsymbol{\mathcal{F}}\{f(t)\} = F(\omega)$ is Hermitian, i.e., $F(-\omega) = F^*(\omega)$.
- If $f(t)$ is Hermitian, i.e., $f(-t) = f^*(t)$, then its Fourier transform, $\boldsymbol{\mathcal{F}}\{f(t)\} = F(\omega)$ is real, i.e., $F(\omega) = \Re\{F(\omega)\}$.

In general, with g and h all real functions, we have,

$$f(t) = g(t) + ih(t). \tag{A.29}$$

Then, $f(t)$, will be Hermitian if, $f(-t) = f^*(t)$, i.e., if $g(t) = g(-t)$, is an **even function** and, $h(-t) = -h(t)$, is an **odd function**

$$f(-t) = g(-t) + ih(-t) = f^*(t) = g(t) - ih(t).$$

The same conditions are applicable for $f(t) = g(t) - ih(t)$.

Every function, $f(x)$, can be be written as the sum of even and odd functions, that is,

$$f(x) = f^+(x) + f^-(x), \tag{A.30}$$

where, $f^+(x)=\frac{1}{2}\left[f(x) + f(-x)\right]$, denotes the even function and $f^-(x) = \frac{1}{2}\left[f(x) - f(-x)\right]$, denotes the odd function.

For **even and odd functions** the following properties are valid:

1. The addition and subtraction of two even or two odd functions remain even and odd respectively.
2. The product of two even functions is an even function.
3. The product of two odd functions is an even function.
4. The product of an even function with an odd function is an odd function.

Definition A.3.2. A function, $f(x)$, is **anti-Hermitian** if,

$$-f(-x) = f^*(x). \tag{A.31}$$

Then we have:

- If $f(t)$ is imaginary, i.e., $f(t) = i\Im\{f(t)\}$, then its Fourier transform, $\boldsymbol{\mathcal{F}}\{f(t)\} = F(\omega)$ is anti-Hermitian, i.e., $-F(-\omega) = F^*(\omega)$.
- If $f(t)$ is anti-Hermitian, i.e., $f(-t) = f^*(t)$, then its Fourier transform, $\boldsymbol{\mathcal{F}}\{f(t)\} = F(\omega)$ is imaginary, i.e., $F(\omega) = i\Im\{F(\omega)\}$.

In general, with g and h, all real functions, we have,

$$f(t) = g(t) + ih(t)$$

Then, $f(t)$, will be anti-Hermitian if, $-f(-t) = f^*(t)$, i.e., if, $-g(t) = g(-t)$, is an **odd function** and, $h(-t) = h(t)$, is an **even function**,

$$f(-t) = g(-t) + ih(-t) = f^*(t) = g(t) - ih(t).$$

The same conditions are valid for $f(t) = g(t) - ih(t)$.

Proposition A.3.3. Every analytical function, $f(x)$, can be written as the sum of a Hermitian and anti-Hermitian functions, that is,

$$f(x) = f^{\dagger}(x) + f^{\times}(x), \tag{A.32}$$

where, $f^{\dagger}(x)$, denotes the Hermitian function and, $f^{\times}(x)$, denotes the anti-Hermitian function. If, $f(x) = g(x) + ih(x)$, then,

$$f^{\dagger}(x) = g^{+}(x) + ih^{-}(x), \tag{A.33}$$

$$f^{\times}(x) = g^{-}(x) + ih^{+}(x). \tag{A.34}$$

The following properties for **Hermitian and anti-Hermitian functions** are valid:

1. The addition and subtraction of two Hermitian or two anti-Hermitian functions remain Hermitian and anti-Hermitian respectively.
2. The product of two Hermitian functions is a Hermitian function.
3. The product of two anti-Hermitian functions is a Hermitian function.
4. The product of a Hermitian and an anti-Hermitian function is an anti-Hermitian function.

Note that Hermitian functions have similar properties to even functions and anti-Hermitian functions have similar properties to odd functions.

In summary, we have,

$$\Re\{f(t)\} \overset{\mathcal{F}}{\Longleftrightarrow} F^{\dagger}(\omega) \tag{A.35}$$

$$f^{\dagger}(t) \overset{\mathcal{F}}{\Longleftrightarrow} \Re\{F(\omega)\} \tag{A.36}$$

$$i\Im\{f(t)\} \overset{\mathcal{F}}{\Longleftrightarrow} F^{\times}(\omega) \tag{A.37}$$

$$f^{\times}(t) \overset{\mathcal{F}}{\Longleftrightarrow} i\Im\{F(\omega)\} \tag{A.38}$$

If, $f(t) = \Re\{f(t)\} = f^{+}(t) + f^{-}(t)$, then,

$$f^{+}(t) \overset{\mathcal{F}}{\Longleftrightarrow} \Re\{F(\omega)\} \tag{A.39}$$

$$f^{-}(t) \overset{\mathcal{F}}{\Longleftrightarrow} i\Im\{F(\omega)\} \tag{A.40}$$

A.3.8. Convolution

Let, $h(t) = f(t) * g(t)$, that is,

$$h(t) = (f * g)(t) = f(t) * g(t) = \int_{-\infty}^{\infty} f(t-\tau)g(\tau)\,d\tau \tag{A.41}$$

then,

$$\boxed{H(\omega) = \boldsymbol{\mathcal{F}}\{f(t) * g(t)\} = F(\omega)G(\omega)} \tag{A.42}$$

$$\int_{-\infty}^{\infty}\left[\int_{-\infty}^{\infty} f(t-\tau)g(\tau)\,d\tau\right] e^{-i\omega t}\,dt = \int_{-\infty}^{\infty}\int_{-\infty}^{\infty} f(t-\tau)\,e^{-i\omega(t-\tau)}\,dt\,g(\tau)e^{-i\omega\tau}\,d\tau \tag{A.43}$$

Change of variables, $\theta = t - \tau$, then,

$$\int_{-\infty}^{\infty} f(t-\tau)\,e^{-i\omega(t-\tau)}\,dt = \int_{-\infty}^{\infty} f(\theta)\,e^{-i\omega\theta}\,d\theta = \boldsymbol{\mathcal{F}}\{f(t)\}, \tag{A.44}$$

and the second integral is independent thus,

$$H(\omega) = \boldsymbol{\mathcal{F}}\{f(t) * g(t)\} = F(\omega)G(\omega). \tag{A.45}$$

It is also important to see what the convolution of the Fourier transforms represent, i.e., $F * G$. Using Eq. (A.42) and the duality property Eq. (A.16),

$$\boldsymbol{\mathcal{F}}\{F(t) * G(t)\} = f(-\omega)g(-\omega). \tag{A.46}$$

The convolution operation has the following **algebraic properties**:

1. **Commutative**

$$f * g = g * f \tag{A.47}$$

2. **Associative**

$$f * (g * h) = (f * g) * h \tag{A.48}$$

3. **Distributive**

$$f * (g + h) = f * g + f * h \tag{A.49}$$

4. **Translation invariance** (Commutes with the translation operator $\mathcal{T}_x$, cf. definition Eq. (A.102)),

$$\mathcal{T}_x(f * g) = (\mathcal{T}_x f) * g = f * (\mathcal{T}_x g) \tag{A.50}$$

$$\begin{aligned} \mathcal{T}_x(f * g)(t) &= (f * g)(t - x) \\ &= \int_{-\infty}^{\infty} f(t - x - \tau) g(\tau)\, d\tau \end{aligned}$$

$$\begin{aligned} \left[f * (\mathcal{T}_x g)\right](t) &= \int_{-\infty}^{\infty} f(t - \tau) g(\tau - x)\, d\tau \\ &= \int_{-\infty}^{\infty} f(t - x - \tau) g(\tau)\, d\tau \end{aligned}$$

$$\left[(\mathcal{T}_x f) * g\right](t) = \int_{-\infty}^{\infty} f(t - x - \tau) g(\tau - x)\, d\tau$$

A.3.9. Correlation

The cross correlation between two functions is defined as,

$$h(t) = (f \star g)(t) = \int_{-\infty}^{\infty} f^*(\tau) g(\tau + t)\, d\tau. \tag{A.51}$$

Substitute $\tau' = \tau + t$ then the correlation can be written in the alternative form,

$$h(t) = (f \star g)(t) = \int_{-\infty}^{\infty} f^*(\tau - t) g(\tau)\, d\tau, \tag{A.52}$$

then,

$$\boxed{H(\omega) = \boldsymbol{\mathcal{F}}\{f(t) \star g(t)\} = F^*(\omega)G(\omega)} \tag{A.53}$$

That is,

$$\int_{-\infty}^{\infty} \left[\int_{-\infty}^{\infty} f^*(\tau)g(\tau+t)\, d\tau \right] e^{-i\omega t}\, dt = \int_{-\infty}^{\infty} f^*(\tau)\, e^{i\omega\tau} \int_{-\infty}^{\infty} g(\tau+t)e^{-i\omega(\tau+t)}\, dt\, d\tau. \tag{A.54}$$

Substitute,$\eta = \tau + t$, then,

$$\int_{-\infty}^{\infty} g(\tau+t)e^{-i\omega(\tau+t)}\, dt = \int_{-\infty}^{\infty} g(\eta)\, e^{-i\omega\eta}\, d\eta = \boldsymbol{\mathcal{F}}\{g(t)\} = G(\omega), \tag{A.55}$$

and the remaining integral is equal to, $F^*(\omega)$, thus,

$$H(\omega) = \boldsymbol{\mathcal{F}}\{f(t) \star g(t)\} = F^*(\omega)G(\omega). \tag{A.56}$$

It is also important to see what the correlation of the Fourier transforms represent, i.e., $F \star G$. Using the Fourier transform property Eq. (A.53), duality Eq. (A.16) and its complex conjugate conjugation,

$$\begin{aligned} \boldsymbol{\mathcal{F}}\{F \star G\} &= [\boldsymbol{\mathcal{F}}\{F(t)\}]^* \boldsymbol{\mathcal{F}}\{G(t)\} \\ &= f^*(-\omega)g(-\omega) \end{aligned} \tag{A.57}$$

A.3.9.1. Convolution vs Correlation

There exist important relationships between convolution and correlation. Simply comparing Eq. (A.42) and Eq. (A.53) and using Eq. (A.19) we see that,

$$\boldsymbol{\mathcal{F}}\{f(t) * g(t)\} = F(\omega)G(\omega) = \boldsymbol{\mathcal{F}}\{f^*(-t) \star g(t)\},$$

so that,

$$\boxed{f(t) * g(t) = f^*(-t) \star g(t)} \tag{A.58}$$

Similarly, using the Fourier transform relation for correlation Eq. (A.53) and the relationship for complex conjugation Eq. (A.19) and then the Fourier transform relation for convolution Eq. (A.42),

$$\boldsymbol{\mathcal{F}}\{f(t) \star g(t)\} = F^*(\omega)G(\omega) = \boldsymbol{\mathcal{F}}\{f^*(-t)\}\boldsymbol{\mathcal{F}}\{g(t)\} = \boldsymbol{\mathcal{F}}\{f^*(-t) * g(t)\},$$

and

$$\boxed{f(t) \star g(t) = f^*(-t) * g(t)} \tag{A.59}$$

In Subsection A.4.10 mirror and conjugation operator is defined as, $\mathcal{I}_c$. Using this operator Eq. (A.58) and Eq. (A.59) can be compactly written as,

$$\begin{aligned} f * g &= (\mathcal{I}_c f) \star g \\ f \star g &= (\mathcal{I}_c f) * g \end{aligned}$$

A.3.9.2. Algebraic Properties of Correlation

The algebraic properties of correlation can all be derived from the algebraic properties of convolution, Eq. (A.47) to Eq. (A.50), and the relationship between convolution and correlation, Eq. (A.58) and Eq. (A.59).

1. **Non-Commutative**. In general,

$$f \star g \neq g \star f \tag{A.60}$$

If, however, $\mathcal{I}_c f = f$ and $\mathcal{I}_c g = g$, i.e., the functions are **Hermitian**, then the correlation operation is **commutative**,

$$f \star g = g \star f, \tag{A.61}$$

and

$$f \star g = f * g. \tag{A.62}$$

If, however, $\mathcal{I}_c f = -f$ and $\mathcal{I}_c g = -g$, i.e., the functions are **anti-Hermitian**, then the correlation operation is **commutative**,

$$f \star g = g \star f, \tag{A.63}$$

and

$$f \star g = -f * g. \tag{A.64}$$

2. **Non-Associative**. In general,

$$f \star (g \star h) \neq (f \star g) \star h. \tag{A.65}$$

If, however, $\mathcal{I}_c f = f$, $\mathcal{I}_c g = g$, and $\mathcal{I}_c h = h$, i.e., the functions are all **Hermitian**, then the correlation operation is **associative**,

$$f \star (g \star h) = (f \star g) \star h. \tag{A.66}$$

If, however, $\mathcal{I}_c f = -f$, $\mathcal{I}_c g = -g$, and $\mathcal{I}_c h = -h$, i.e., the functions are all **anti-Hermitian**, then the correlation operation is **associative**,

$$f \star (g \star h) = (f \star g) \star h \tag{A.67}$$

3. **Distributive.**

$$f \star (g + h) = f \star g + f \star h \tag{A.68}$$

4. **Translation invariance.** Only if the functions are both Hermitian or anti-Hermitian is the following valid,

$$\mathcal{T}_x(f \star g) = (\mathcal{T}_x f) \star g = f \star (\mathcal{T}_x g). \tag{A.69}$$

In general we have,

$$\boxed{\mathcal{T}_x(f \star g) = f \star (\mathcal{T}_x g) = \mathcal{T}_{2x}\left[(\mathcal{T}_x f) \star g\right]} \tag{A.70}$$

Since,

$$\begin{aligned}
\mathcal{T}_x(f \star g)(t) &= (f \star g)\,(t - x) \\
&= \int_{-\infty}^{\infty} f^*(\tau) g(\tau + t - x)\,d\tau \\
&= \int_{-\infty}^{\infty} f^*(\tau) \mathcal{T}_x g(\tau + t)\,d\tau \\
&= \left[f \star (\mathcal{T}_x g)\right](t).
\end{aligned}$$

Furthermore,

$$\left[(\mathcal{T}_x f) \star g\right](t) = \int_{-\infty}^{\infty} f^*(\tau - x) g(\tau + t)\,d\tau.$$

A change of dummy variable, $\tau' = \tau - x$,

$$\begin{aligned}
\left[(\mathcal{T}_x f) \star g\right](t) &= \int_{-\infty}^{\infty} f^*(\tau') g(\tau' + t + x)\,d\tau' \\
&= (f \star g)\,(t + x) \\
&= \mathcal{T}_{-x}(f \star g)(t).
\end{aligned}$$

A.3.10. Energy Theorem (Parseval-Plancherel)

This is accredit to Parseval (1799) for Fourier series, strangely before the advent of Fourier series, and was generalized for Fourier transforms by Plancherel (1910) so is often referred to as the Parseval-Plancherel theorem.

For all quadratically integrable functions

$$\boxed{\int_{-\infty}^{\infty} f^*(t)g(t)\,dt = \int_{-\infty}^{\infty} F^*(\omega)G(\omega)\,d\omega} \tag{A.71}$$

in particular, if $f(t) = g(t)$,

$$\boxed{\int_{-\infty}^{\infty} |f(t)|^2\ dt = \int_{-\infty}^{\infty} |F(\omega)|^2\ d\omega} \tag{A.72}$$

which can be considered as the total energy in a signal, $f(t)$.

A.4. Common Functions

A.4.1. Sign Function

$$\boxed{\operatorname{sgn}(x) = \begin{cases} +1 & x \geq 0 \\ -1 & x < 0 \end{cases}} \tag{A.73}$$

A.4.2. Step Function (Heaviside Function)

$$\boxed{u(x) = \eta(x) = h(x) = \begin{cases} 1 & x \geq 0 \\ 0 & x < 0 \end{cases}} \tag{A.74}$$

$$u(x) = \frac{1}{2}\left[\operatorname{sgn}(x) + 1\right] \tag{A.75}$$

A.4.3. Rectangular Function (Hat function)

Sometimes also referred as the hat function

$$\boxed{\pi(x) = \operatorname{rect}(x) = \begin{cases} 0 & |x| > \frac{1}{2} \\ \frac{1}{2} & |x| = \frac{1}{2} \\ 1 & |x| < \frac{1}{2} \end{cases}} \tag{A.76}$$

$$\pi(x) = \frac{1}{2}\left[\operatorname{sgn}(x+1) - \operatorname{sgn}(x-1)\right] \tag{A.77}$$

$$\pi\left(\frac{x}{a}\right) = u\left(x+\frac{a}{2}\right) - u\left(x-\frac{a}{2}\right) = \pi_a\left(x\right) \tag{A.78}$$

$$\pi\left(\frac{x-b}{a}\right) = u\left(x-b+\frac{a}{2}\right) - u\left(x-b-\frac{a}{2}\right) = \pi_a\left(x-b\right) \tag{A.79}$$

A.4.4. Triangular Function

$$\boxed{\Lambda\left(x\right) = \mathrm{tri}\left(x\right) = \begin{cases} 0 & \left|x\right| \geq 1 \\ 1-\left|x\right| & \left|x\right| < 1 \end{cases}} \tag{A.80}$$

$$\Lambda\left(x\right) = \pi_2\left(x\right)\cdot\left(1-x\cdot\mathrm{sgn}\left(x\right)\right) \tag{A.81}$$

A.4.5. Sinc Function

The unnormalized sinc function

$$\boxed{\mathrm{sinc}\left(x\right) = \frac{\sin\left(x\right)}{x}} \tag{A.82}$$

The normalized sinc function (an abbreviation of its Latin name *sinus cardinalis*)

$$\boxed{\mathrm{sinc}\left(x\right) = \frac{\sin\left(\pi x\right)}{\pi x}} \tag{A.83}$$

In this form, we have,

$$\mathrm{sinc}\left(0\right) = 1$$

$$\mathrm{sinc}\left(\pm n\right) = 0 \quad n \in \mathbb{N}$$

A.4.6. The Dirac-δ function

The *discrete Kronecker delta function* $\delta_{ij}$for discrete $i, j \in \mathbb{Z}$ is defined such that,

$$\boxed{\delta_{ij} = \begin{cases} 1 & i = j \\ 0 & i \neq j \end{cases}} \tag{A.84}$$

which is usually applied in a discrete sum operation for a discrete function, $f(k)$,

$$f(k) = \sum_{i=1}^{\infty} \delta_{ik} f(i) \tag{A.85}$$

can be "generalized", ignoring mathematical rigor, for a continuous well behaved function, $g : x \in \mathbb{R} \to g(x) \in \mathbb{R}$ using the heuristic analogy that, $\lim \sum \to \int \mathrm{d}x$, to

$$g(y) = \int_{-\infty}^{\infty} \delta(x, y) g(x) \, \mathrm{d}x \tag{A.86}$$

Since, x and y, are arbitrary the above shows that, $\delta(x, y)$ must somehow be equal to zero everywhere unless, $x = y$. From this we infer that the "function" has translational invariance since, $x + a = y + a$, for any, a, even, $a = -y$

$$g(y) = \int_{-\infty}^{\infty} \delta(x - y, 0) g(x) \, \mathrm{d}x \tag{A.87}$$

and with the additional symmetry condition, i.e., $\delta(x, y)$=$\delta(y, x)$ the function only depends on the difference,

$$g(y) = \int_{-\infty}^{\infty} \delta(x - y) g(x) \, \mathrm{d}x. \tag{A.88}$$

In particular, this defines the Dirac-δdistribution function, $\delta(x)$,

$$g(0) = \int_{-\infty}^{\infty} \delta(x) g(x) \, \mathrm{d}x \tag{A.89}$$

It is called a distribution function, for strictly speaking it is only to be used within a integral as defined above. If, $g(x)$, is an odd function, i.e., $g(0) = 0$ then, $\delta(x)$, must be an even function, i.e.,

$$\delta(x) = \delta(-x) \tag{A.90}$$

Let, $f\left(x\right)$, be any Fourier integral function with transform, $F\left(p\right)$, then from,

$$F\left(p\right)=\frac{1}{\sqrt{2\pi}}\int_{-\infty}^{\infty}f\left(x\right)e^{-ipx}\,\mathrm{d}x \tag{A.91}$$

$$f\left(x'\right)=\frac{1}{\sqrt{2\pi}}\int_{-\infty}^{\infty}F\left(p\right)e^{ipx'}\,\mathrm{d}p \tag{A.92}$$

$$f\left(x'\right)=\frac{1}{2\pi}\int_{-\infty}^{\infty}\int_{-\infty}^{\infty}f\left(x\right)e^{-ip(x-x')}\,\mathrm{d}x\,\mathrm{d}p \tag{A.93}$$

$$f\left(x'\right)=\int_{-\infty}^{\infty}f\left(x\right)\left[\frac{1}{2\pi}\int_{-\infty}^{\infty}e^{-ip(x-x')}\,\mathrm{d}p\right]\mathrm{d}x, \tag{A.94}$$

thus we make the connection,

$$\delta\left(x\right)=\frac{1}{2\pi}\int_{-\infty}^{\infty}e^{-ipx}\,\mathrm{d}p=\frac{1}{2\pi}\int_{-\infty}^{\infty}e^{ixp}\,\mathrm{d}p=\delta\left(-x\right). \tag{A.95}$$

This integral does not exist in any conventional definition of a integral, but is an extremely convenient way of interpreting the Dirac-δ distribution function and is often used in Fourier analysis without further ado. Continuing in this vein the following properties easily follow from similar properties of the Fourier transform

A.4.6.1. Scaling

$$\boxed{\delta\left(ax\right)=\frac{1}{\left|a\right|}\delta\left(x\right)} \tag{A.96}$$

A.4.6.2. Translation

$$\boxed{f\left(x\right)\delta\left(x-a\right)=f\left(a\right)\delta\left(x-a\right)} \tag{A.97}$$

A.4.6.3. Dirac-δ of a function

If, $g\left(x\right)$, is analytic near its zeros, $g\left(x_i\right)=0$ for $i=1,2,\ldots$ then using the first order Taylor approximation for, $g\left(x\right)\approx g'\left(x_i\right)\left(x-x_i\right)$, provided that, $g'\left(x_i\right)\neq 0$, we find,

$$\boxed{\delta\left(g\left(x\right)\right)=\sum_{i}\frac{1}{\left|g'\left(x_i\right)\right|}\delta\left(x-x_i\right)} \tag{A.98}$$

A.4.6.4. The unit step function (Heaviside function)

$$\boxed{u\left(x\right)=\int_{-\infty}^{x}\delta\left(p\right)\,\mathrm{d}p} \tag{A.99}$$

A.4.6.5. Dirac Comb

$$\boxed{\sum_{n=-\infty}^{\infty}\delta\left(x-nT\right)} \tag{A.100}$$

A.4.7. Mirror Image Operator

Given any function, $f\in\mathcal{L}^2(\mathbb{C})$, the mirror image operator, $\mathcal{I}:\mathcal{L}^2(\mathbb{C})\to\mathcal{L}^2(\mathbb{C})$, with $x\in\mathbb{R}$, is defined as,

$$\boxed{\mathcal{I}:[f(x)]=f(-x)} \tag{A.101}$$

To get a better understanding of functional operators on functions, probably the simplest examples are the complex conjugation operator, and functional multiplication and addition. We note that these operations have been used previously quite often in Section A.3. The condition $x\in\mathbb{R}$ is valid since in terms of Fourier transforms $t,\omega\in\mathbb{R}$. The mirror image operator $\mathcal{I}$ is idempotent, that is, $\mathcal{I}^2=\mathcal{I}\circ\mathcal{I}=e$, where, e, is the unit operator, i.e., $e(f)=f$.

A.4.8. Translation Operator

Given any function, $f\in\mathcal{L}^2(\mathbb{C})$, the translation operator is a functional operator, $\mathcal{T}_x:\mathcal{L}^2(\mathbb{C})\to\mathcal{L}^2(\mathbb{C})$, with $x\in\mathbb{C}$, and is defined as,

$$\boxed{\mathcal{T}_x[f(y)]=f(y-x)} \tag{A.102}$$

Translation operators commute, i.e.,

$$\mathcal{T}_x\mathcal{T}_y=\mathcal{T}_y\mathcal{T}_x=\mathcal{T}_{x+y}$$

A.4.9. Modulation Operator

Given any function, $f \in \mathcal{L}^2(\mathbb{C})$, the modulation operator is a functional operator, $\mathcal{M}_x : \mathcal{L}^2(\mathbb{C}) \to \mathcal{L}^2(\mathbb{C})$, with $x \in \mathbb{R}$, specifically used with Fourier transforms, defined for a temporal function, $f(t)$, as,

$$\mathcal{M}_{\omega_n} f(t) = e^{i\omega_n t} f(t), \tag{A.103}$$

and for a spectral function, $F(\omega)$, as

$$\mathcal{M}_{-t_l} F(\omega) = e^{-it_l \omega} F(\omega), \tag{A.104}$$

with the requirement that, $\omega t = 2\pi$, as usual. If, $f(t) \overset{\mathcal{F}}{\Longleftrightarrow} F(\omega)$, then with the translation, $\mathcal{T}$, and modulation, $\mathcal{M}$, operators we know that, from Eq. (A.22), temporal translation Fourier transforms to spectral modulation,

$$\boxed{\mathcal{T}_{t_0} f(t) \overset{\mathcal{F}}{\Longleftrightarrow} \mathcal{M}_{-t_0} F(\omega)} \tag{A.105}$$

From Eq. (A.67) we note the temporal modulation Fourier transforms to spectral translation,

$$\boxed{\mathcal{M}_{\omega_0} f(t) \overset{\mathcal{F}}{\Longleftrightarrow} \mathcal{T}_{\omega_0} F(\omega)} \tag{A.106}$$

Then Eq. (A.68) shows that the translation and modulation also Fourier transform transform in order,

$$\boxed{\mathcal{M}_{\omega_0} \mathcal{T}_{t_0} f(t) \overset{\mathcal{F}}{\Longleftrightarrow} \mathcal{T}_{\omega_0} \mathcal{M}_{-t_0} F(\omega)} \tag{A.107}$$

Thus, a natural consequence of Eq. (A.107) by simply taking into account Eq. (A.105) and Eq. (A.106) is

$$\boxed{\mathcal{T}_{t_0} \mathcal{M}_{\omega_0} f(t) \overset{\mathcal{F}}{\Longleftrightarrow} \mathcal{M}_{-t_0} \mathcal{T}_{\omega_0} F(\omega)} \tag{A.108}$$

But please remember that functional operators are position specific and that, $\mathcal{M}_{\omega_0} \mathcal{T}_{t_0} \neq \mathcal{T}_{t_0} \mathcal{M}_{\omega_0}$. This functional operator notation is an excellent method to exhibit the true behaviour of the Fourier transform.

A.4.10. Mirror Image and Complex Conjugation Commute

Given any function, $f \in \mathcal{L}^2(\mathbb{C})$, the complex conjugation functional operator, $\mathcal{C} : \mathcal{L}^2(\mathbb{C}) \to \mathcal{L}^2(\mathbb{C})$, then,

$$\mathcal{C} \circ \mathcal{I} = \mathcal{I} \circ \mathcal{C}.$$

The complex conjugation operator is also idempotent, i.e., $\mathcal{C}^2 = \mathcal{C} \circ \mathcal{C} = e$

Let us write, $f(t) \in \mathcal{L}^2(\mathbb{C})$ with, $t \in \mathbb{R}$ as, $f(t) = x(t) + iy(t)$, and $x(t), y(t) \in \mathcal{L}^2(\mathbb{R})$ then,

$$\begin{aligned}\mathcal{C} \circ \mathcal{I}(f) &= \mathcal{C}\{\mathcal{I}[f(t)]\}\\ &= \mathcal{C}\{f(-t)\} = \mathcal{C}\{x(-t) + iy(-t)\}\\ &= x(-t) - iy(-t)\\ &= \mathcal{I}\{\mathcal{C}[f(t)]\}.\end{aligned}$$

The combined operation we shall denote with, $\mathcal{I}_c$. The operator, $\mathcal{I}_c$, is idempotent, that is, $\mathcal{I}_c^2 = \mathcal{I}_c \circ \mathcal{I}_c = e$.

It is of real importance to establish when a function, $f(t)$, which in general can be written as,

$$f(t) = g(t) + ih(t)$$

, with g and h all real functions is invariant under the $\mathcal{I}_c$ operation, i.e., $\mathcal{I}_c f(t) = f(t)$, i.e.,

$$\begin{aligned}f(t) &= g(t) + ih(t)\\ \mathcal{I}_c f(t) &= g(-t) - ih(-t).\end{aligned}$$

This will only occur if, $g(t) = g(-t)$, is an **even function** and, $h(-t) = -h(t)$, is an **odd function**, but this is just the condition that the function, $f(t)$, is **Hermitian**. (See Subsection A.3.7 for the definition of a Hermitian function).

A.4.11. Translation and $\mathcal{I}_c$ Commute

The operator $\mathcal{T}_x\mathcal{I}_c$ commute, i.e.,

$$\mathcal{T}_x\mathcal{I}_c = \mathcal{I}_c\mathcal{T}_x.$$

Let, $h = \mathcal{I}_c f$, then,

$$(\mathcal{T}_x\mathcal{I}_c f)(t) = \mathcal{T}_x h = h(t - x) = (\mathcal{I}_c f)(t - x) = f^*(x - t),$$

but,

$$(\mathcal{I}_c\mathcal{T}_x f)(t) = \mathcal{I}_c f(t - x) = f^*(x - t).$$

A.5. Fourier Transforms

In Table A.1 a list common Fourier transforms are given for the ordinary frequency ν definitions, Eq. (A.5) and Eq. (A.6), and the symmetrical (unitary) angular frequency ω definitions, Eq. (A.9) and Eq. (A.10).

Function	**Frequency** ν	**Angular Frequency** ω
$\mathrm{rect}\left(at\right)$	$\frac{1}{\lvert a\rvert}\mathrm{sinc}\left(\frac{\nu}{a}\right)$	$\frac{1}{\sqrt{2\pi a^2}}\mathrm{sinc}\left(\frac{\omega}{2\pi a}\right)$
$\mathrm{sinc}\left(at\right)$	$\frac{1}{\lvert a\rvert}\mathrm{rect}\left(\frac{\nu}{a}\right)$	$\frac{1}{\sqrt{2\pi a^2}}\mathrm{rect}\left(\frac{\omega}{2\pi a}\right)$
$\mathrm{sinc}^2\left(at\right)$	$\frac{1}{\lvert a\rvert}\mathrm{tri}\left(\frac{\nu}{a}\right)$	$\frac{1}{\sqrt{2\pi a^2}}\mathrm{tri}\left(\frac{\omega}{2\pi a}\right)$
$\mathrm{tri}\left(at\right)$	$\frac{1}{\lvert a\rvert}\mathrm{sinc}^2\left(\frac{\nu}{a}\right)$	$\frac{1}{\sqrt{2\pi a^2}}\mathrm{sinc}^2\left(\frac{\omega}{2\pi a}\right)$
$e^{-at}u\left(t\right)$	$\frac{1}{a+2\pi i\nu}$	$\frac{1}{\sqrt{2\pi}(a+i\omega)}$
$e^{-\alpha t^2}$	$\sqrt{\frac{\pi}{\alpha}}e^{-\frac{(\pi\nu)^2}{\alpha}}$	$\frac{1}{\sqrt{2\alpha}}e^{-\frac{\omega^2}{4\alpha}}$
$e^{-a\lvert t\rvert}$	$\frac{2a}{a^2+4\pi^2\nu^2}$	$\sqrt{\frac{2}{\pi}}\frac{a}{a^2+\omega^2}$
$e^{-\frac{a^2t^2}{2}}H_n\left(at\right)$	$\frac{\sqrt{2\pi}(-i)^n}{a}e^{-\frac{2\pi^2\nu^2}{a^2}}H_n\left(\frac{2\pi\nu}{a}\right)$	$\frac{(-i)^n}{a}e^{-\frac{\omega^2}{2a^2}}H_n\left(\frac{\omega}{a}\right)$
1	$\delta\left(\nu\right)$	$\sqrt{2\pi}\delta\left(\omega\right)$
$\delta\left(t\right)$	1	$\frac{1}{\sqrt{2\pi}}$
e^{iat}	$\delta\left(\nu-\frac{a}{2\pi}\right)$	$\sqrt{2\pi}\delta\left(\omega-a\right)$
$\cos\left(at^2\right)$	$\sqrt{\frac{\pi}{a}}\cos\left(\frac{\pi^2\nu^2}{a}-\frac{\pi}{4}\right)$	$\frac{1}{\sqrt{2a}}\cos\left(\frac{\omega^2}{4a}-\frac{\pi}{4}\right)$
$\sin\left(at^2\right)$	$-\sqrt{\frac{\pi}{a}}\sin\left(\frac{\pi^2\nu^2}{a}-\frac{\pi}{4}\right)$	$-\frac{1}{\sqrt{2a}}\sin\left(\frac{\omega^2}{4a}-\frac{\pi}{4}\right)$
t^n	$\left(\frac{i}{2\pi}\right)^n\delta^{(n)}\left(\nu\right)$	$i^n\sqrt{2\pi}\delta^{(n)}\left(\omega\right)$
$\mathcal{P}\frac{1}{t}$	$-i\pi\mathrm{sgn}\left(\nu\right)$	$-i\sqrt{\frac{\pi}{2}}\mathrm{sgn}\left(\omega\right)$
$\mathrm{sgn}\left(t\right)$	$\frac{1}{i\pi}\mathcal{P}\frac{1}{\nu}$	$-i\sqrt{\frac{2}{\pi}}\mathcal{P}\frac{1}{\omega}$
$u\left(t\right)=\frac{1}{2}\left[\mathrm{sgn}\left(t\right)+1\right]$	$\frac{1}{2}\left(\frac{1}{i\pi}\mathcal{P}\frac{1}{\nu}+\delta\left(\nu\right)\right)$	$\sqrt{\frac{\pi}{2}}\left(\frac{1}{i\pi}\mathcal{P}\frac{1}{p}+\delta\left(\omega\right)\right)$
$\sum_{n=-\infty}^{\infty}\delta\left(t-nT\right)$	$\frac{1}{T}\sum_{k=-\infty}^{\infty}\delta\left(\nu-\frac{k}{T}\right)$	$\frac{\sqrt{2\pi}}{T}\sum_{k=-\infty}^{\infty}\delta\left(\omega-\frac{2\pi k}{T}\right)$

Table A.1.: Fourier Transform Pairs

A.6. Even and Odd Transforms

In general the functions, $f(t)$, and its transform, $F(\omega)$, are complex functions so that we may write (cf. [125, 69]),

$$\begin{aligned} f(t) &= f_1(t)+if_2(t), \\ F(\omega) &= R(\omega)+iX(\omega), \end{aligned}$$

and using Euler's formula, $e^{i\omega t} = \cos\omega t + i\sin\omega t$, the functions can be decomposed as,

$$\begin{aligned}
R(\omega) &= \frac{1}{\sqrt{2\pi}}\int_{-\infty}^{\infty}\left[f_1(t)\cos\omega t + f_2(t)\sin\omega t\right]\,\mathrm{d}t \\
X(\omega) &= \frac{1}{\sqrt{2\pi}}\int_{-\infty}^{\infty}\left[f_2(t)\cos\omega t - f_1(t)\sin\omega t\right]\,\mathrm{d}t \\
f_1(t) &= \frac{1}{\sqrt{2\pi}}\int_{-\infty}^{\infty}\left[R(\omega)\cos\omega t - X(\omega)\sin\omega t\right]\,\mathrm{d}\omega \\
f_2(t) &= \frac{1}{\sqrt{2\pi}}\int_{-\infty}^{\infty}\left[R(\omega)\sin\omega t + X(\omega)\cos\omega t\right]\,\mathrm{d}\omega
\end{aligned}$$

If we therefore have a **real signal**, $f(t) = f_1(t)$, then,

$$R(\omega) = \frac{1}{\sqrt{2\pi}}\int_{-\infty}^{\infty} f(t)\cos\omega t\,\mathrm{d}t \qquad X(\omega) = -\frac{1}{\sqrt{2\pi}}\int_{-\infty}^{\infty} f(t)\sin\omega t\,\mathrm{d}t, \tag{A.109}$$

then,

$$R(-\omega) = R(\omega) \qquad \text{and} \qquad X(-\omega) = -X(\omega). \tag{A.110}$$

This means that the real part of the Fourier transform of a real function is symmetrical (even) and the imaginary part is asymmetrical (odd), or

$$F(-\omega) = R(-\omega) + iX(-\omega) = R(\omega) - iX(\omega) = F^*(\omega). \tag{A.111}$$

The real signal thus implies that,

$$\boxed{f(t) = \Re e\{f(t)\} \qquad \Longleftrightarrow \qquad F(-\omega) = F^*(\omega)} \tag{A.112}$$

For a **real even function**, $f(t) = f(-t) = f^+(t) \Rightarrow X(\omega) = 0$,

$$F(\omega) = R(\omega) = 2\frac{1}{\sqrt{2\pi}}\int_0^{\infty} f(t)\cos\omega t\,\mathrm{d}t, \tag{A.113}$$

$$\boxed{f^+(t) \overset{\mathcal{F}}{\Longleftrightarrow} \Re e\{F(\omega)\} = R(\omega)} \tag{A.114}$$

For a **real odd function**, $f(-t) = -f(t) = f^-(t) \Rightarrow R(\omega) = 0$,

$$F(\omega) = iX(\omega) = -2i\frac{1}{\sqrt{2\pi}}\int_0^{\infty} f(t)\sin\omega t\,\mathrm{d}t, \tag{A.115}$$

$$\boxed{f^{-}(t) \overset{\mathcal{F}}{\Longleftrightarrow} i\Im\{F(\omega)\} = iX(\omega)} \tag{A.116}$$

Now, consider for example the real odd function, $f(t) = \frac{1}{t}$; applying the above Fourier transform formula we obtain,

$$F(\omega) = -i\frac{1}{\sqrt{2\pi}}\int_{-\infty}^{\infty}\frac{\sin\omega t}{t}\,\mathrm{d}t = \begin{cases} -i\sqrt{\frac{\pi}{2}} & \omega > 0 \\ +i\sqrt{\frac{\pi}{2}} & \omega < 0 \end{cases} = -i\sqrt{\tfrac{\pi}{2}}\,\mathrm{sgn}(\omega), \tag{A.117}$$

since,

$$\int_{-\infty}^{\infty}\frac{\sin\omega t}{t}\,\mathrm{d}t = \begin{cases} \pi & \omega > 0 \\ -\pi & \omega < 0 \end{cases} = \pi\,\mathrm{sgn}(\omega). \tag{A.118}$$

A.7. Sampling Theory

To represent a function, $f(t)$, in terms of its sampled values, $f(nT)$, as a sequence of equidistant points, $n \in \mathbb{Z}$, and T, the sampling period, we formally form the sum,

$$f_h(t) = \sum_{n=-\infty}^{\infty} T \cdot f(nT) \cdot h(t - nT), \tag{A.119}$$

where, $h(t)$, a given function (It can be considered as a type of impulse response function or a polynomial expansion function). Under the following conditions for the function $h(t)$, namely,

$$\begin{aligned} T \cdot h(0) &= 1 \\ h(nT) &= 0 \quad \text{for} \quad n \neq 0 \end{aligned}$$

then,

$$f_h(nT) = f(nT), \tag{A.120}$$

in other words, $f_h(t)$ **interpolates** $f(t)$. To study the properties of, $f_h(t)$, it is convenient to introduce the following function,

$$f_*(t) = \sum_{n=-\infty}^{\infty} T \cdot f(nT) \cdot \delta(t - nT). \tag{A.121}$$

If, $F_*(\omega)$, is the Fourier transform of, $f_*(t)$, then using the Poisson summation formula, we obtain,

$$F_*(\omega) = \sum_{n=-\infty}^{\infty} T \cdot f(nT)e^{-inT\omega} = \sum_{n=-\infty}^{\infty} F(\omega + 2n\sigma) \quad \sigma = \frac{\pi}{T}. \tag{A.122}$$

Clearly,

$$f_h(t) = f_*(t) * h(t). \tag{A.123}$$

Therefore $f_h(t)$ is the output of a system with input, $f(t)$, and impulse response, $h(t)$.

If, $H(\omega)$, is the Fourier transform of, $h(t)$, then we also have,

$$F_h(\omega) = F_*(\omega)H(\omega) = H(\omega) \sum_{n=-\infty}^{\infty} F(\omega + 2n\sigma). \tag{A.124}$$

A finite energy function, $f(t)$, is frequency bandlimited or simply ***bandlimited*** or σ-BL if,

$$F(\omega) = 0 \qquad |\omega| > \sigma \tag{A.125}$$

and the finite energy,

$$E = \frac{1}{\sqrt{2\pi}} \int_{-\infty}^{\infty} |f(t)|^2 \,\mathrm{d}t = \frac{1}{\sqrt{2\pi}} \int_{-\infty}^{\infty} |F(\omega)|^2 \,\mathrm{d}\omega = \frac{1}{\sqrt{2\pi}} \int_{-\sigma}^{\sigma} |F(\omega)|^2 \,\mathrm{d}\omega < \infty. \tag{A.126}$$

A finite energy function $f(t)$ is ***time-limited*** or τ-TL, if,

$$f(t) = 0 \quad \text{for} \quad |t| > \tau \quad \text{and} \quad E < \infty, \tag{A.127}$$

and then,

$$F(\omega) = F_*(\omega)\pi_\sigma(\omega) \quad \forall\omega. \tag{A.128}$$

Thus the output, $f_h(t)$, of the filter,

$$h(t) = \frac{\sin \sigma t}{\pi t} \overset{\mathcal{F}}{\Longleftrightarrow} \pi_\sigma(\omega) = H(\omega), \tag{A.129}$$

with the input, $f_*(t)$, equals, $f(t)$. This then leads to a fundamental result known as the **sampling theorem**,

$$\boxed{f(t) = \sum_{n=-\infty}^{\infty} f(nT) \cdot \frac{\sin \sigma(t - nT)}{\sigma(t - nT)} \qquad \sigma = \frac{\pi}{T}} \tag{A.130}$$

This is specifically valid for a σ-BL signal. Note that the whole function, $f(t)$, is described in terms of its sampled values, $f(nT)$, at a sequence of equidistant points, $t = nT$. The sampling rate or frequency is known as the **Nyquist rate**

$$\boxed{\nu = \frac{1}{T} = \frac{\sigma}{\pi}} \tag{A.131}$$

If the frequency of the signal contains frequencies higher than the σ-BL the most undesirable effect of **aliasing** occurs. This is when the periodic DFT starts overlapping with neighbouring repeated periods and starts corrupting the DFT with unreal frequency spectrums.

A.8. Properties of Bandlimited Functions

Let $f(t)$ be σ-bandlimited function, then,

$$f(t) = \frac{1}{\sqrt{2\pi}} \int_{-\sigma}^{\sigma} F(\omega) e^{i\omega t} \, \mathrm{d}\omega. \tag{A.132}$$

1. The Fourier transform, $F(\omega)$, of σ-BL function is absolutely integrable, i.e.,

$$\int_{-\sigma}^{\sigma} |F(\omega)| \, \mathrm{d}\omega < \infty. \tag{A.133}$$

2. For any t real or complex, $f(t)$, is of exponential type,

$$|f(t)| \leq \sqrt{\frac{\sigma E}{\pi}} e^{\sigma |t|}. \tag{A.134}$$

3. A σ-bandlimited function, $f(t)$, is an analytical (entire, holomorphic) function on the entire t-Wessel (Complex, Argand) plane. The time derivative is given by,

$$f^{'}(t) = \frac{1}{\sqrt{2\pi}} \int_{-\sigma}^{\sigma} i\omega F(\omega) e^{i\omega t} \, \mathrm{d}\omega. \tag{A.135}$$

4. **Paley-Wiener Theorem:** If a finite energy function, $f(t)$, is analytic and of exponential type then it is σ-BL.
5. A finite energy function, $f(t)$, is **periodic BL** if it a trigonometric polynomial,

$$f(t) = \sum_{k=-M}^{M} a_k e^{ik\omega t}, \tag{A.136}$$

   in the time interval $(0, T)$.
6. A periodic TL function cannot be a trigonometric polynomial.
7. **A function cannot be bandlimited and time-limited.**

A.9. Poisson Summation Formula

Consider the *Dirac comb* sampling function (an impulse sampling train),

$$d(t) = \sum_{n=-\infty}^{\infty} \delta\left(t + nT\right) = d(t + mT), \qquad m \in \mathbb{Z}, \tag{A.137}$$

and noting that it is a *periodic function* with Fourier series coefficients given by,

$$a_n = \frac{1}{T}\int_{-T/2}^{T/2} \delta(t) e^{-in\omega_o t}\,\mathrm{d}t = \frac{1}{T}, \tag{A.138}$$

therefore its Fourier series is given by,

$$\sum_{n=-\infty}^{\infty} \delta\left(t + nT\right) = \frac{1}{T}\sum_{n=-\infty}^{\infty} e^{in\omega_o t} \quad , \omega_o = \frac{2\pi}{T}. \tag{A.139}$$

Now given any function, $y(t)$, with Fourier transform (non unitary),

$$Y(\omega) = \int_{-\infty}^{\infty} y(t) e^{-i\omega t}\,\mathrm{d}t, \tag{A.140}$$

then the function, $x(t)$,

$$x(t) = \sum_{n=-\infty}^{\infty} y\left(t + nT\right), \tag{A.141}$$

is periodic with period, T, with Fourier series coefficients,

$$\begin{aligned} b_m &= \frac{1}{T}\int_{-T/2}^{T/2} x(t) e^{-im\omega_o t}\,\mathrm{d}t = \frac{1}{T}\sum_{k=-\infty}^{\infty}\int_{-T/2}^{T/2} y\left(t + kT\right) e^{-im\omega_o t}\,\mathrm{d}t \\ &= \frac{1}{T}\sum_{k=-\infty}^{\infty}\int_{-kT/2}^{(k+1)T/2} y\left(t\right) e^{-im\omega_o t}\,\mathrm{d}t, \end{aligned} \tag{A.142}$$

$$b_m = \frac{1}{T}\sum_{k=-\infty}^{\infty}\int_{-kT/2}^{(k+1)T/2} y\left(t\right) e^{-im\omega_o t}\,\mathrm{d}t = \frac{1}{T}\int_{-\infty}^{\infty} y(t) e^{-im\omega_o t}\,\mathrm{d}t = Y(m\omega_o)/T. \tag{A.143}$$

Thus we obtain the *Poisson summation formula*

$$\boxed{\bar{y}(t) = \sum_{n=-\infty}^{\infty} y\left(t + nT\right) = \frac{1}{T}\sum_{n=-\infty}^{\infty} Y(n\omega_o) e^{in\omega_o t} \quad \omega_o = \frac{2\pi}{T}} \tag{A.144}$$

A.10. Nyquist-Shannon Sampling Theorem

A function, $f(t)$, is band limited, if it has finite energy and

$$F(\nu) = 0 \qquad for \ |\nu| > B. \tag{A.145}$$

The inverse Fourier transform is given by

$$f(t) = \int_{-\infty}^{\infty} F(\nu) e^{2\pi i \nu t} \, d\nu = \int_{-B}^{B} F(\nu) e^{2\pi i \nu t} \, d\nu. \tag{A.146}$$

Now, for any $n \in \mathbb{Z}$, if we let,

$$t = nt_s = \frac{n}{2B}, \tag{A.147}$$

then,

$$f(nT_s) = \int_{-B}^{B} F(\nu) e^{2\pi i \nu \frac{n}{2B}} \, d\nu = \frac{1}{2\pi} \int_{-2\pi B}^{2\pi B} F(\omega) e^{int_s \omega} \, d\omega. \tag{A.148}$$

The term “looks” like a *inverse* Fourier series coefficient expansion of $F(\omega)$, with, $t_s = \frac{1}{2B}$, and sampling duration, 2π, except that it is not periodic,

$$A_n = \frac{1}{2\pi} \int_{-2\pi B}^{2\pi B} F(\omega) e^{int_s \omega} \, d\omega \quad , t_s = \frac{1}{2B} \quad \rightsquigarrow \quad a_n = \frac{1}{T} \int_{-T/2}^{T/2} f(t) e^{-in\omega_o t} dt \quad , \omega_o = \frac{2\pi}{T} \tag{A.149}$$

If, $f(t)$, is band limited then,

$$F(\nu) = F(\nu) \pi_{2B}(\nu). \tag{A.150}$$

From the Fourier transform pair, $(\pi\left(\frac{x}{a}\right) = \pi_a\left(x\right))$,

$$\operatorname{sinc}\left(2Bt\right) \overset{\mathcal{F}}{\Longleftrightarrow} \frac{1}{2B} \pi_{2B}\left(\nu\right). \tag{A.151}$$

Applying the convolution theorem and the Poisson sum formula, the signal can be reconstructed as (Whitaker-Shannon Interpolation Formula),

$$\boxed{f(t) = \sum_{n=-\infty}^{\infty} f\left(nt_s\right) \operatorname{sinc}[2B(t - nt_s)]} \tag{A.152}$$

where, T_s, is the digital sampling time (Nyquist-Shannon Sampling Theorem),

$$\boxed{2B = \frac{1}{t_s}} \tag{A.153}$$

is called the *Nyquist rate*. Notice the function must be sampled at *twice* the bandwidth frequency to represent the signal. In practice the sampling frequency is usually taken to at least, πB.

A.10.1. Inverse Nyquist-Shannon Sampling Theorem

From the duality of the Fourier transform,

$$\boxed{F(\nu) = \sum_{n=-\infty}^{\infty} F\left(n\nu_s\right) \mathrm{sinc}[2T_W(\nu - n\nu_s)]} \tag{A.154}$$

where, $2T_W$, is the time-bandwidth or time duration of the signal, $f(t)$ and ν_s, is the digital sampling frequency or frequency sampling resolution in the Fourier domain (Inverse Nyquist-Shannon Sampling Theorem),

$$\boxed{2T_W = \frac{1}{\nu_s}} \tag{A.155}$$

Thus, sampling, $f(t)$, every $t_s{=}\frac{1}{2B}$ seconds for a time period, $t \in [-T_W, T_W]$, will insure a frequency representation of frequency bandwidth B, $\nu \in [-B, B]$ with frequency sampling ν_s. Thus,

$$\boxed{t_s = \frac{1}{2B} \qquad \text{and} \qquad \nu_s = \frac{1}{2T_W}} \tag{A.156}$$

B. The FHG Spectral Overlap Matrix

For completeness, this is included in the appendices, only because the result is not equal to the temporal overlap matrix. It is also derived in three parts. The FHG spectral overlap matrix is given by Eq. (5.113),

$$\begin{aligned}\mathbb{W}^{k,l}_{m,n} &= \mathbf{c}^{\dagger}_{m,n}\left(\int_{-\infty}^{\infty} e^{it_m(\omega-\omega_n)}\tilde{\boldsymbol{\Phi}}(\omega-\omega_n)\, e^{-it_k(\omega-\omega_l)}\tilde{\boldsymbol{\Phi}}^T(\omega-\omega_l)\,\mathrm{d}\omega\right)\mathbf{c}_{k,l}\\ &= \mathbf{c}^{\dagger}_{m,n}e^{it_k\omega_l-it_m\omega_n}\left(\int_{-\infty}^{\infty}\tilde{\boldsymbol{\Phi}}(\omega-\omega_n)\,\tilde{\boldsymbol{\Phi}}^T(\omega-\omega_l)e^{it_{mk}\omega}\,\mathrm{d}\omega\right)\mathbf{c}_{k,l}\end{aligned} \tag{B.1}$$

where,

$$t_{mk} = t_m - t_k. \tag{B.2}$$

Part I

We are now in a position to evaluate the integral of the spectral overlap matrix,

$$\int_{-\infty}^{\infty}\tilde{\boldsymbol{\Psi}}^{*}_{m,n}(\omega)\tilde{\boldsymbol{\Psi}}^{T}_{k,l}(\omega)\,\mathrm{d}\omega = e^{it_k\omega_l-it_m\omega_n}\left(\int_{-\infty}^{\infty}\tilde{\boldsymbol{\Phi}}(\omega-\omega_n)\,\tilde{\boldsymbol{\Phi}}^T(\omega-\omega_l)e^{it_{mk}\omega}\,\mathrm{d}\omega\right), \tag{B.3}$$

with the integrand of Eq. (B.3) given by, (ignoring the HG normalization constants, $2^{-\frac{p}{2}}(p!)^{-\frac{1}{2}}\pi^{-\frac{1}{4}}$, which is p dependent and also neglecting the angular frequency scaling which we shall include at a later stage),

$$\boldsymbol{\Psi}^{*}_{m,n}(t)\boldsymbol{\Psi}^{T}_{k,l}(t) = e^{-\frac{1}{2}(\omega-\omega_n)^2-\frac{1}{2}(\omega-\omega_l)^2+it_{mk}\omega+it_k\omega_l-it_m\omega_n}\mathbf{h}(\omega-\omega_n)\mathbf{h}^T(\omega-\omega_l). \tag{B.4}$$

It was previously shown that it is possible to handle the two spectral translation,s ω_n and ω_l, for the Hermitian polynomial vectors, $\mathbf{h}$. Substitute,

$$\Omega = \omega - \frac{\omega_n+\omega_l}{2}, \tag{B.5}$$

so that,

$$\omega - \omega_n = \Omega - \frac{\omega_{nl}}{2} \text{ and } \omega - \omega_l = \Omega + \frac{\omega_{nl}}{2}. \tag{B.6}$$

Inserting Eq. (B.5) and Eq. (B.6) into the integrand of Eq. (B.4) the quadratic exponent then becomes,

$$\begin{aligned} -\frac{1}{2}\left(\Omega - \frac{\omega_{nl}}{2}\right)^2 - \frac{1}{2}\left(\Omega + \frac{\omega_{nl}}{2}\right)^2 + it_{mk}(\Omega + \frac{\omega_n + \omega_l}{2}) + it_k\omega_l - it_m\omega_n = \\ -\Omega^2 + it_{mk}\Omega - \left(\frac{\omega_{nl}}{2}\right)^2 - i\omega_{nl}\left(\frac{t_m + t_k}{2}\right). \end{aligned} \tag{B.7}$$

With the aid of Eq. (B.5), Eq. (B.6) and Eq. (B.7) the overlap matrix transforms to

$$\int_{-\infty}^{\infty} \tilde{\mathbf{\Psi}}^*_{m,n}(\omega)\tilde{\mathbf{\Psi}}^T_{k,l}(\omega)\,\mathrm{d}\omega = e^{-\left(\frac{\omega_{nl}}{2}\right)^2 - i\omega_{nl}\left(\frac{t_m+t_k}{2}\right)} \int_{-\infty}^{\infty} \mathbf{h}(\Omega - \frac{\omega_{nl}}{2})\mathbf{h}^T(\Omega + \frac{\omega_{nl}}{2})e^{-\Omega^2 + it_{mk}\Omega}\,\mathrm{d}\Omega, \tag{B.8}$$

Using the translation property of the Hermite polynomials Eq. (5.70), the above integral becomes,

$$\boxed{e^{-\left(\frac{\omega_{nl}}{2}\right)^2 - i\omega_{nl}\left(\frac{t_m+t_k}{2}\right)}\mathbf{L}^{-\omega_{nl}} \int_{-\infty}^{\infty} \mathbf{h}(\Omega)\mathbf{h}^T(\Omega)e^{-\Omega^2 + it_{mk}\Omega}\,\mathrm{d}\Omega\mathbf{U}^{\omega_{nl}}} \tag{B.9}$$

Part II

Now, secondly, let's just focus on the remaining integral of Eq. (B.9), namely,

$$\int_{-\infty}^{\infty} \left[e^{-\frac{\Omega^2}{2}}\mathbf{h}(\Omega)\right]\left[e^{-\frac{\Omega^2}{2}}\mathbf{h}^T(\Omega)\right]e^{+it_{mk}\Omega}\,\mathrm{d}\Omega. \tag{B.10}$$

Now,

$$\mathbf{h}(\Omega)\mathbf{h}^T(\Omega) = \begin{bmatrix} H_0(\Omega) \\ H_1(\Omega) \\ \vdots \\ H_N(\Omega) \end{bmatrix} \begin{bmatrix} H_0(\Omega) & H_1(\Omega) & \cdots & H_N(\Omega) \end{bmatrix}.$$

Here, we evaluate the inverse Fourier transform of the product of two quantum harmonic oscillator polynomials,

$$\mathbb{K}_{nm}(t) = \int_{-\infty}^{\infty} \left[e^{-\frac{\omega^2}{2}}H_n(\omega)\right]\left[e^{-\frac{\omega^2}{2}}H_m(\omega)\right]e^{it\omega}\,\mathrm{d}\omega. \tag{B.11}$$

The generating function of the Hermite polynomials is given by Eq. (5.28). Taking a second generating function with dummy variable, y, and multiplying the two, we obtain,

$$e^{2\omega(x+y)-\left(x^2+y^2\right)} = \sum_{n=0}^{\infty}\sum_{m=0}^{\infty} H_n(\omega)H_m(\omega)\frac{x^n y^m}{n!m!}. \tag{B.12}$$

Multiplying the Eq. (B.12) by, $e^{-\omega^2}$,

$$e^{-\omega^2+2\omega(x+y)-\left(x^2+y^2\right)} = \sum_{n=0}^{\infty}\sum_{m=0}^{\infty} \left[e^{-\frac{\omega^2}{2}}H_n(\omega)\right]\left[e^{-\frac{\omega^2}{2}}H_m(\omega)\right]\frac{x^n y^m}{n!m!}. \tag{B.13}$$

Now multiplying Eq. (B.13) by, $e^{i\omega t}$, and integrating with respect to, ω,

$$\begin{aligned}\int_{-\infty}^{\infty} \exp\left[-\omega^2+2\omega\left(x+y\right)-\left(x^2+y^2\right)\right]e^{i\omega t}\,\mathrm{d}\omega = \\ = \sum_{n=0}^{\infty}\sum_{n=0}^{\infty}\left\{\int_{-\infty}^{\infty}\left[e^{-\frac{\omega^2}{2}}H_n(\omega)\right]\left[e^{-\frac{\omega^2}{2}}H_m(\omega)\right]e^{i\omega t}\,\mathrm{d}\omega\right\}\frac{x^n y^m}{n!m!} \\ = \sum_{n=0}^{\infty}\sum_{m=0}^{\infty}\mathbb{K}_{nm}(t)\frac{x^n y^m}{n!m!}.\end{aligned} \tag{B.14}$$

Consider the left hand integral Eq. (B.14) and complete the square of the exponent of the exponential

$$-\omega^2+2\omega\left(x+y\right)-\left(x^2+y^2\right) = -\left[\omega-\left(x+y\right)\right]^2+2xy \tag{B.15}$$

and substitute, $\Omega = \omega-\left(x+y\right), \quad d\Omega = d\omega$, then the left-hand integral Eq. (B.14) transforms to

$$e^{it(x+y)+2xy}\int_{-\infty}^{\infty} e^{-\Omega^2+it\Omega}\,\mathrm{d}\Omega. \tag{B.16}$$

This integral in Eq. (B.15) is once again in the form of our standard Gaussian integral so that,

$$\boxed{\left[\sqrt{\pi}e^{-\frac{t^2}{4}}\right]e^{it(x+y)+2xy} = \sum_{n=0}^{\infty}\sum_{m=0}^{\infty}\mathbb{K}_{nm}(t)\frac{x^n y^m}{n!m!}} \tag{B.17}$$

Expanding the left hand exponentials of Eq. (B.17) in terms of a Taylor series,

$$e^{x(2y+it)}e^{ity} = \sum_{n=0}^{\infty}\frac{x^n(2y+it)^n}{n!}\sum_{q=0}^{\infty}\frac{y^q}{q!}(it)^q, \tag{B.18}$$

and using the binomial theorem for, $(2y+it)^n$,

$$e^{x(2y+it)}e^{ity} = \sum_{n=0}^{\infty}\frac{x^n}{n!}\sum_{q=0}^{\infty}\sum_{p=0}^{n}2^p\binom{n}{p}\frac{y^{p+q}}{(p+q)!}\frac{(p+q)!}{q!}(it)^{n+q-p}. \tag{B.19}$$

The binomial factorial becomes,

$$\binom{p+q}{p} = \frac{(p+q)!}{p!q!}. \tag{B.20}$$

thus substituting Eq. (B.20) into Eq. (B.19), we obtain,

$$e^{x(2y+it)}e^{ity} = \sum_{n=0}^{\infty}\frac{x^n}{n!}\sum_{q=0}^{\infty}\sum_{p=0}^{n}2^p p!\binom{n}{p}\binom{p+q}{p}\frac{y^{p+q}}{(p+q)!}(it)^{n+q-p}. \tag{B.21}$$

Now, substitute, $m=p+q$, into Eq. (B.21),

$$e^{x(2y+it)}e^{ity} = \sum_{n=0}^{\infty}\sum_{m=0}^{\infty}\left\{\sum_{p=0}^{\min(n,m)}2^p p!\binom{n}{p}\binom{m}{p}(it)^{n+m-2p}\right\}\frac{x^n}{n!}\frac{y^m}{m!}. \tag{B.22}$$

Comparing the coefficients Eq. (B.22) with Eq. (B.14), we obtain,

$$\boxed{\mathbb{K}_{nm}(t) = \sqrt{\pi}e^{-\frac{t^2}{4}}\sum_{p=0}^{\min(n,m)}2^p p!\binom{n}{p}\binom{m}{p}(it)^{n+m-2p}} \tag{B.23}$$

Thus Eq. (B.11),

$$\mathbb{K}_{nm}(t) = \int_{-\infty}^{\infty}\left[e^{-\frac{\omega^2}{2}}H_n(\omega)\right]\left[e^{-\frac{\omega^2}{2}}H_m(\omega)\right]e^{it\omega}\,\mathrm{d}\omega$$

$$\Downarrow$$

$$\boxed{\mathbb{K}_{nm}(t) = \sqrt{\pi}e^{-\frac{t^2}{4}}\sum_{p=0}^{\min(n,m)}2^p p!\binom{n}{p}\binom{m}{p}(it)^{n+m-2p}} \tag{B.24}$$

Recalling that, $\mathbb{K}_{nm}$, Eq. (B.24) (see Eq. (B.10)) is just an element of a matrix, the structure of this element with the presence with two binomial coefficients is reminiscent of the triangular Pascal matrix that we previously investigated in Eq. (5.141). Let us rewrite this element as

$$\mathbb{K}_{nm}(t) = e^{-\frac{t^2}{4}} \sum_{p=0}^{\min(n,m)} \left[\pi^{\frac{1}{4}} 2^{\frac{p}{2}} \sqrt{p!} \binom{n}{p} (it)^{n-p}\right] \left[\pi^{\frac{1}{4}} 2^{\frac{p}{2}} \sqrt{p!} \binom{m}{p} (it)^{m-p}\right] \tag{B.25}$$

This is just the product of two of Pascal's triangles except for the, $\pi^{\frac{1}{4}} 2^{\frac{p}{2}} \sqrt{p!}$, factor. It is still, however, possible to factorize this matrix as

$$\boxed{\int_{-\infty}^{\infty} \left[e^{-\frac{\omega^2}{2}} \mathbf{h}(\omega)\right] \left[e^{-\frac{\omega^2}{2}} \mathbf{h}^T(\omega)\right] e^{i\omega\tau} \, \mathrm{d}\omega = e^{-\frac{t^2}{4}} \mathbf{L}^{it} \mathbf{N}^{\frac{1}{2}} \mathbf{N}^{\frac{1}{2}} \left[\mathbf{L}^{it}\right]^T} \tag{B.26}$$

where, $\mathbf{N} = \operatorname{diag}\left(\sqrt{\pi} \begin{bmatrix} 2^0 0! & 2^1 \cdot 1! & 2^2 \cdot 2! & 2^3 \cdot 3! & 2^4 \cdot 4 & \cdots & 2^n \cdot n! \end{bmatrix}\right)$, or,

$$\mathbf{N} = \sqrt{\pi} \begin{bmatrix} 2^0 0! & 0 & 0 & 0 & 0 & \cdots & 0 \\ 0 & 2^1 \cdot 1! & 0 & 0 & 0 & \cdots & 0 \\ 0 & 0 & 2^2 \cdot 2! & 0 & 0 & \cdots & 0 \\ 0 & 0 & 0 & 2^3 \cdot 3! & 0 & \cdots & 0 \\ 0 & 0 & 0 & 0 & 2^4 \cdot 4! & \vdots & \vdots \\ 0 & 0 & 0 & 0 & 0 & \ddots & 0 \\ 0 & 0 & 0 & 0 & 0 & 0 & 2^n \cdot n! \end{bmatrix}. \tag{B.27}$$

The HG normalization constants must still be included as before, we obtain,

$$\boxed{\int_{-\infty}^{\infty} \Phi(\omega) \Phi^T(\omega) e^{i\omega\tau} \, \mathrm{d}\omega = e^{-\frac{t^2}{4}} \mathbf{L}^{it} \mathbf{U}^{it}} \tag{B.28}$$

Part III

The overlap matrix element Eq. (B.14) can thus be written as $(t = t_{mk})$,

$$\mathbb{W}^{k,l}_{m,n} = \mathbf{c}^{\dagger}_{m,n} e^{-\frac{1}{4} t_{mk}^2 - \frac{1}{4} \omega_{ln}^2 - \frac{1}{2} i\omega_{nl}(t_m + t_k)} \mathbf{L}^{-\omega_{nl} + it_{mk}} \mathbf{U}^{\omega_{nl} + it_{mk}} \mathbf{c}_{k,l}. \tag{B.29}$$

With the correct angular frequency scaling, we have,

$$\boxed{\mathbb{W}^{k,l}_{m,n} = \mathbf{c}^{\dagger}_{m,n} e^{-\frac{1}{8\sigma} t_{mk}^2 - \frac{\sigma}{2} \omega_{ln}^2 - \frac{1}{2} i\omega_{nl}(t_m + t_k)} \mathbf{L}^{-\sqrt{2\sigma}\omega_{nl} + i\frac{t_{mk}}{\sqrt{2\sigma}}} \mathbf{U}^{\sqrt{2\sigma}\omega_{nl} + i\frac{t_{mk}}{\sqrt{2\sigma}}} \mathbf{c}_{k,l}} \tag{B.30}$$

C. Other Orthogonal Polynomials

The other orthogonal polynomials are also defined in [130, 129].

C.1. Laguerre Polynomials

C.1.1. Differential equation

$$x\frac{d^2L_n}{dx^2} + (1-x)\frac{dL_n}{dx} + nL_n = 0$$

C.1.2. Rodrigues' formula

For, $n = 0, 1, \ldots$, then

$$L_n(x) = e^x \frac{d^n}{dx^n}\left(x^n e^{-x}\right)$$

C.1.3. Generating function

$$\frac{e^{-tx/(1-t)}}{1-t} = \sum_{n=0}^{\infty} L_n(x)\frac{t^n}{n!}$$

C.1.4. Orthogonality

$$\int_0^{\infty} e^{-x} L_n(x) L_m(x)\,\mathrm{d}x = \begin{cases} 0 & n \neq m \\ (n!)^2 & n = m \end{cases}$$

C.2. Associated Laguerre Polynomials

C.2.1. Differential equation

$$x\frac{d^2L_n^m}{dx^2}+(m+1-x)\frac{dL_n^m}{dx}+(n-m)L_n^m=0$$

C.2.2. Rodrigues' formula

For, $n, m = 0, 1, \ldots$, then

$$L_n^m(x)=\frac{d^m}{dx^m}L_n(x)$$

where, $L_n(x)$, are the Laguerre polynomials with,

$$L_n^0(x)=L_n(x)$$

$$L_n^m(x)=0 \quad \text{if} \quad m>n$$

C.2.3. Generating function

$$\frac{(-1)^m t^m}{(1-t)^{m+1}}e^{-tx/(1-t)}=\sum_{n=m}^{\infty}L_n^m(x)\frac{t^n}{n!}$$

C.2.4. Orthogonality

$$\int_0^\infty x^m e^{-x}L_n^m(x)L_p^m(x)\,\mathrm{d}x=\begin{cases}0 & n\neq p\\ \frac{(n!)^2}{(n-m)!} & n=p\end{cases}$$

C.3. Ince Polynomials

[?] does not have a definition of Ince polynomials, but the other two references do have, [130, 129]. *Hill's Differential Equation* with three terms (constants A, B, k and c)

$$w''+\left(A+B\cos(2x)-\frac{1}{2}(kc)^2\cos(4x)\right)w=0$$

However, when $k^2 < 0$, i.e., $k \in \mathbb{C}$,we substitute

$$\begin{aligned} \xi^2 &= -4k^2c^2 \\ A &= \eta - \frac{1}{8}\xi^2 \\ B &= -(n+1)\xi \\ w(x) &= C_n(x)\exp\left(-\frac{1}{4}\xi\cos(2x)\right) \end{aligned}$$

$$\frac{d^2C_n}{dx^2} + \xi\sin(2x)\frac{dC_n}{dx} + [\eta - n\xi\cos(2x)]C_n = 0, \qquad n \in \mathbb{N}.$$

D. Matlab Code

The author always enjoyed finding program code in books, documents and theses, to lighten the burden of reprogramming everything from the start. Obviously, this is actually propriety information, and the exclusion thereof can certainly be understood. Under the advice of my co-supervisor, I have been instructed to eliminate this from the thesis, mainly because he considered it unnecessary and that it enlarged the thesis considerably. This can be understood, since the software code is still under development and obviously not in a neat form to be published. Especially, considering the amount of revisions it has undergone. Reluctantly, I concurred. However, for the enjoyment, happiness and benefit of a few, I have considered it prudent to include the following software listing all written in Matlab©.

D.1. Main Molecule Function

```

function func = RunMoleculeAMSvN(x)
%{
%%%%%%%%%%%%%%%%%%%%%%%%%%%%%%%%%%%%%%%%%%%%%%%%%%%%%%%%%%%%%%%%%%%%%%%%%%%
FUNCTION :  RunMoleculeAMSv1(x)
—————————

DESCRIPTION : The main function of the Genetic Algorithm (GA) to ...
    simulate
————————————  the Optical Bloch equations(Louiville —von Neumann)
              commutator bracket of the von Neumann density ...
                 matrix of
              the UF6 molecules—laser interaction with a Gaussian ...
                 laser
              pulse that has been modulated by a 4f—Spatial Light
              Modulator (SLM).

              Originally all the subfunctions were incorporated ...
                 in this
              single main program. To enhance computation speed all
              unnecessary precalculatible program functions have been
              extracted and placed in external functions. The ...
                 required
              variables have been then saved in global ...
                 structures. There
              are three such functions:
              (1) Physical constants (PhysConst)
              (2) The laser pulse and SLM parameters (LaserPulses)
              (3) The UF6 Molecule parameters (UF_6Molecule)

              I. Amplitude and Phase for SLM
              II. Laser Pulse Temporal Window
              III. Louiville-von Neumann Density matrix Laser Pulse
              Interaction


INPUT :      x - The vector incorporating the SLM paramerers ...
   (Amplitude
------        and Phase) 1280 Dbl Real
              GLOBAL STURCTURES
              =================
             PC - Physical Constants Global Structure
             LPOut - Laser Pulse parameters Global Structure
             SLMOut - Spatial Light Modulator parameters Global ...
                Structure
             UF6_Molecule - Molecular Interaction Hamiltonian
             INTERNAL
               %OptFunc = 'Second'  MUST BE SET Choose ONE of the ...
                  CASES
              plotit = true or false          To plot level ...
                 populations


OUTPUT : func -  Minimization Vibrational Level
------   OptFunc = 'Second'  MUST BE SET Choose ONE of the CASES

AUTHOR : A M Smit (Version 1) smoothvectorLudwigSLM REMOVED ...
   dim(x)=1282
------

DATE : November 2011
-----
%%%%%%%%%%%%%%%%%%%%%%%%%%%%%%%%%%%%%%%%%%%%%%%%%%%%%%%%%%%%%%%%%%%%%%%%%%
%}

global PC LPOut SLMOut UF6;
%
% Flags and Settings
% %%%%%%%%%%%%%%%%%%
```

```
    plotit = true;                   % Plots Only Level Population
                                     % When optimizing set to false
%
    OptFunc = 'Second';              % % MUST BE SET  ...
       Optimization Maximum
              % 'First'
              % 'Third'
              % 'Fourth'
              % 'QC'

% Required for Ludwig's Smoother
x(1281)     = 80;
x(1282)     = 80;

%%
%%%%%%%%%%%%%%%%%%%%%%%%%%%%%%%%%%%%%
% I. Amplitude and Phase for SLM
%%%%%%%%%%%%%%%%%%%%%%%%%%%%%%%%%%%%%
am      = x(1:640);
ph      = x(641:1280);

%
% Smoothing Function (Required to remove discretization spikes)
% ------------------
% x = Is the input
% Frequency Domain Amplitude and Phase of SLM Laser Pulse
am      = smoothvectorLudwigSLM(am,x(1281));
ph      = pi*smoothvectorLudwigSLM(ph,x(1282));

%
% SLM Amplitude
% -------------
amplHbuild   = ones(SLMOut.NumberFreqnew,1)*am;
amplHbuild   = reshape(amplHbuild,SLMOut.delNRnew,1)';
%
% SLM Phase
% ---------
phasesHbuild = ones(SLMOut.NumberFreqnew,1)*ph;
phasesHbuild = reshape(phasesHbuild,SLMOut.delNRnew,1)';
phasesHbuild = mod(phasesHbuild,2*pi);

%
% SLM Mask
% --------
Mask1        = amplHbuild.*exp(1i*( phasesHbuild ));

%
% Zero Padding
% ------------
```

```
MASK     = horzcat(SLMOut.VecLeft,Mask1,SLMOut.VecRight);

%
% SLM of Laser Pulse (Frequency Domain)
% ------------------
EFF2            = (SLMOut.EFF1).*MASK;

%
% 4-f Confocal SLM Second Lens (Fourier Optics)
% Inverse Fast Fourier Transform (Effective time domain pulse)
EFoutMask     = ifft(EFF2);

% Renormalize Pulse
absEF2 = abs(EFF2)/max(abs(EFF2));
phase  = mod(unwrap(angle(EFF2)),pi);

% Normalize SLM Mask time domain pulse
EFoutMask     = EFoutMask/max(EFoutMask);

%%
%%%%%%%%%%%%%%%%%%%%%%%%%%%%%%%%%%%%%%%%%%%%%%%%%%%%%%%%%%%%%%%%%%%%%%%%%%
% I.1 von Neumann TFR Representation
%%%%%%%%%%%%%%%%%%%%%%%%%%%%%%%%%%%%%%%%%%%%%%%%%%%%%%%%%%%%%%%%%%%%%%%%%%
%
vNTFRPlots
%%
%%%%%%%%%%%%%%%%%%%%%%%%%%%%%%%%%%%%%%%%%%%%%%%%%%%%%%%%%%%%%%%%%%%%%%%%%%
% II. Laser Pulse Temporal Window
%%%%%%%%%%%%%%%%%%%%%%%%%%%%%%%%%%%%%%%%%%%%%%%%%%%%%%%%%%%%%%%%%%%%%%%%%%

% Windowed real Electric Field Laser Pulse Out
% --------------------------------------------
EF        = real(EFoutMask(LPOut.postl :LPOut.postr));

% Laser Pulse Out Intensity
% -------------------------
Intensity    = LPOut.I0*EF.*EF;

% Laser Pulse Out Energy
% ----------------------
area     = LPOut.delt*sum(Intensity); % Euler integration
%area     = LPOut.delt/2*sum(Intensity(1:N-1)+Intensity(2:N));% ...
    Trapezuim integration

% Laser Pulse Out Normalisation
% -----------------------------
E0            = sqrt(188*LPOut.I0*(LPOut.Fpulse/area));


```

```
%%%%%%%%%%%%%%%%%%%%%%%%%%%%%%%%%%%%%%%%%%%%%%%%%%%%%%%%%%%%%%%%%%%%%%%%%%
clear MASK Mask1 absEF2 phase amplHbuild phasesHbuild am ph area ...
   EFoutMask;
clear EFF2 Intensity;
%%%%%%%%%%%%%%%%%%%%%%%%%%%%%%%%%%%%%%%%%%%%%%%%%%%%%%%%%%%%%%%%%%%%%%%%%%

%%%%%%%%%%%%%%%%%%%%%%%%%%%%%%%%%%%%%%%%%%%%%%%%%%%%%%%%%%%%%%%%%%%%%%%%%%%
% III. Louiville-von Neumann Density matrix Laser Pulse
%               Interaction
%%%%%%%%%%%%%%%%%%%%%%%%%%%%%%%%%%%%%%%%%%%%%%%%%%%%%%%%%%%%%%%%%%%%%%%%%%%
%%
%simplification Physical laser Electric Field Amplitude
LPOA   = (PC.e*E0)/PC.hbar;

% --------------------------------------------------------------

Nm = UF6.Nm;
Decay = false;
UnitNm = eye(Nm);
LPO_EF = (-1i*LPOut.delt*LPOA)*EF;
nn = floor(LPOut.N/1000);
%
% Performs time integration of interaction Hamiltonian
H_matI = zeros(Nm,Nm);
    for r = 1: LPOut.N-1
      % Scale interaction Hamiltonian with laser
      H_matI         = H_matI + LPO_EF(r)*UF6.I_Hmlt(:,:,r);
%      Exp_H = UnitNm + H_matI + 0.5*H_matI*H_matI;
      if ( (mod(r,nn) == 0)|| (r == LPOut.N-1))
          Exp_H = expm(H_matI);
          UF6.rhoM(:,:,r+1) = Exp_H*UF6.rhoM(:,:,r)*Exp_H';
          H_matI = zeros(Nm,Nm);
      else
          UF6.rhoM(:,:,r+1) = UF6.rhoM(:,:,r);
      end
    end
%
% Now perform superoperator unitary transformation
%
%Exp_H = expm(H_matI);
%UF6.rhoM(:,:,LPOut.N) = Exp_H*UF6.rhoM(:,:,1)*Exp_H';
%%
%%
%%
% Minimization Vibrational Level;
    rhoMdiag = diag(UF6.rhoM(:,:,LPOut.N));

    switch OptFunc
        case 'First'                   % 2
```

```matlab
            func = (1.0 - (real(rhoMdiag(2))) );
        case 'Second'                  % 3,4,5
            func = (1.0 - (real(sum(rhoMdiag(3:5)))) );
        case 'Third'                   % 6,7,8,9
            func = (1.0 - (real(sum(rhoMdiag(6:9)))) );
        case 'Fourth'                  % 10,...,16
            func = (1.0 - (real(sum(rhoMdiag(10:16)))) );
        case 'QC'                      % 17
            func = (1.0 - (real(sum(rhoMdiag(17)))) );
        otherwise
            disp('Unknown Minimization Vibrational Level Condition')
    end

if (plotit)
figure(10)
LevPopl = zeros(6,LPOut.N);
LevPopl(1,:) = real(UF6.rhoM(1,1,:));
LevPopl(2,:) = real(UF6.rhoM(2,2,:));
LevPopl(3,:) = real(UF6.rhoM(3,3,:)+UF6.rhoM(4,4,:)+UF6.rhoM(5,5,:));
LevPopl(4,:) = ...
   real(UF6.rhoM(6,6,:)+UF6.rhoM(7,7,:)+UF6.rhoM(8,8,:)+UF6.rhoM(9,9,:));
LevPopl(5,:) = ...
   real(UF6.rhoM(10,10,:)+UF6.rhoM(11,11,:)+UF6.rhoM(12,12,:)...
    +UF6.rhoM(13,13,:)+UF6.rhoM(14,14,:)+UF6.rhoM(15,15,:)+UF6.rhoM(16,16,:));
LevPopl(6,:) = real(UF6.rhoM(17,17,:));
plot(LPOut.t/PC.fs,LevPopl(1,:),LPOut.t/PC.fs,LevPopl(2,:),...
     LPOut.t/PC.fs,LevPopl(3,:),...
     LPOut.t/PC.fs,LevPopl(4,:),...
     LPOut.t/PC.fs,LevPopl(5,:),...
     LPOut.t/PC.fs,LevPopl(6,:))
% title('The end population percentage as a function of FWHM ...
    (Transform-Limited)')
xlabel('Time (fs)');
ylabel('Population within vibrational levels')
title('UF_6 Population 2nd Level Excitation')
legend('n = 0','n = 1',...
       'n = 2','n = 3',...
       'n = 4','Q.C.')
% xlim([t0 tF]);
ylim([0 1])
grid on;
end
end
```

D.2. von Neumann TFR Functions

D.2.1. Spec2vNTFR.m

```
function vNTFR = Spec2vNTFR(EFw,wsmpl,vNOLM,vNSB,FlgInt)
%% Spectral Signal to von Neumann TFR
%{
%%%%%%%%%%%%%%%%%%%%%%%%%%%%%%%%%%%%%%%%%%%%%%%%%%%%%%%%%%%%%%%%%%%%%%%%%
FUNCTION : vNTFR = Spec2vNTFR(EFw,wsmpl,vNOLM,vNSB,FlgInt)
————————

DESCRIPTION : Given the Spectral Electric Field calculate
———————————   the von Neumann Time—Frequency Representation
              PREVIOUS CALLED FUNCTIONS:
              1. vNGrid
              2. vNOverlapAMS
              3. vNSpecB

INPUT :      EFw    — Spectral (Fourier Transform) Electric Field ...
   Angular
—————                 Frequency vector [dim=N^2]
             wsmpl  — Spectral angular frequency sampling vector ...
                [dim=N^2]
             vNOLM  — von Neumann Overlap Matrix [dim N2xN2]
             vNSB   — von Neumann Spectral Basis [dim N2xN2]
             FlgInt — Flag for integration

OUTPUT :     vNTFR  — von Neuman Time—Frequency Representation
——————                in unpacked matrix form

AUTHOR : A M Smit
——————

DATE : August 2012
————
%%%%%%%%%%%%%%%%%%%%%%%%%%%%%%%%%%%%%%%%%%%%%%%%%%%%%%%%%%%%%%%%%%%%%%%%%%
%}

%% Check row column vector
%
N2        = numel(wsmpl);
N         = sqrt(N2);
% EFSpec must be column vector
[r,c] = size(EFw);
if r < c
    EFc = EFw.';
else
    EFc = EFw;
end

%% 1. Spectral von Neumann TFR coefficients
%  ————————————————————————————————————————
%
```

```
SvNc  = zeros(N2,1);
%
% Delta Electric Field sampling frequency
%
deltW = wsmpl(2) - wsmpl(1);
if (FlgInt)
    % Euler Integration vector
    SvNc  = deltW*conj(vNSB)*EFc;
else
    % Trapezium Integration vector
    for ii=1:N2
        SvNc(ii)  = trapz(wsmpl,conj(vNSB(ii,:)).*EFc.');
    end
end

%% 2. The von Neumann Time Frequency Representation
%   ------------------------------------------------
%
% Multiply with the inverse overlap matrix
%
Qwt = vNOLM\SvNc;

%% 3. Unpack the von Neumann Representation
%  ----------------------------------------
%
vNTFR = reshape(Qwt,N,N);         % Matrix is time x freq
```

D.2.2. Temp2vNTFR.m

```
function vNTFR = Temp2vNTFR(EFt,tsmpl,vNOLM,vNTB,FlgInt)
%% Temporal Signal to von Neumann TFR
%{
%%%%%%%%%%%%%%%%%%%%%%%%%%%%%%%%%%%%%%%%%%%%%%%%%%%%%%%%%%%%%%%%%%%%%%%%%
FUNCTION : vNTFR = Temp2vNTFR(EFt,tsmpl,vNOLM,vNTB,FlgInt)
--------

DESCRIPTION : Given the Spectral Electric Field calculate
-----------   the von Neumann Time-Frequency Representation
              PREVIOUS CALLED FUNCTIONS:
              1. vNGrid
              2. vNOverlapAMS
              3. vNTempB

INPUT :      EFt    - Temporal Electric Field Time Series vector ...
    [dim=N^2]
-----        tsmpl  - temporal sampling vector [dim=N^2]
             vNOLM  - von Neumann Overlap Matrix [dim N2xN2]
             vNTB   - von Neumann Temporal Basis [dim N2xN2]
             FlgInt - Flag for integration (Euler 1 Trapezium 0)

OUTPUT :     vNTFR  - von Neuman Time-Frequency Representation
------                in unpacked matrix form

AUTHOR : A M Smit
------

DATE : August 2012
----
%%%%%%%%%%%%%%%%%%%%%%%%%%%%%%%%%%%%%%%%%%%%%%%%%%%%%%%%%%%%%%%%%%%%%%%%%%
%}

%% Initialize
%
N2       = numel(tsmpl);
N        = sqrt(N2);
% EFt must be column vector
[r,c] = size(EFt);
if r < c
    EFc = EFt.';
else
    EFc = EFt;
end

%%  1. Temporal von Neumann TFR coefficients
%   ----------------------------------------
%
TvNc = zeros(N2,1);
% Delta Electric Field sampling time
%
deltT = tsmpl(2) - tsmpl(1);
if FlgInt
    % Euler Integration vector
    TvNc  = deltT*conj(vNTB)*EFc;
else
    % Trapezium Integration vector
    for ii=1:N2
        TvNc(ii,:) = trapz(tsmpl,conj(vNTB(ii,:)).*EFc.');
    end
end

%% 2. The von Neumann Time Frequency Representation
%  ------------------------------------------------
%
% Multiply with the inverse overlap matrix
%
Qwt = vNOLM\TvNc;
```

```

%% 3. Unpack the von Neumann Representation
%  ————————————————————————————————————————
%
vNTFR = reshape(Qwt,N,N);         % Matrix is time x freq
```

D.2.3. vNGrid.m

```
function vN = vNGrid(MinW,MaxW,Nfourier,NvN)
%% Set up von Neumann latiice grid
%{
%%%%%%%%%%%%%%%%%%%%%%%%%%%%%%%%%%%%%%%%%%%%%%%%%%%%%%%%%%%%%%%%%%%%%%%%%
FUNCTION : vN = vNGrid(MinW,MaxW,Nfourier,NvN)
————————

DESCRIPTION : Calculates the various parameters of the von Neumann
———————————   representation. The von Neumann reticule ofr grid ...
    in the
              time—frequency domain and the associated von Neumann
              variance alpha.
              NB — The time and frequency vectors are slightly offset
              from the boundaries, effectively with half an increment

INPUT :  MinW     — Minimum Angular Frequency von Neumann Grid
—————    MaxW     — Maximum Angular Frequency von Neumann Grid
         TimeBW   — Time Bandwidth von Neumann Grid
         Nfourier — Fourier sampled Electric Field Dimension

OUTPUT : vN.alpha   — von Neumann Basis Alpha
——————   vN.N       — Grid Dimension
         vN.MaxW    — Maximum Angular frequency
         vN.MinW    — Minimum Angular frequency
         vN.TimeBW  — Time Bandwidth
         vN.FreqBW  — Frequency Bandwidth
         vN.delW    — Incremental ∆ frequency
         vN.delT    — Incremental ∆ time
         vN.time    — von Neumann Grid time discrete time vector
         vN.omega   — von Neumann Grid discrete angular frequency ...
            vector

AUTHOR : A M Smit
——————

DATE : December 2011
————
%%%%%%%%%%%%%%%%%%%%%%%%%%%%%%%%%%%%%%%%%%%%%%%%%%%%%%%%%%%%%%%%%%%%%%%%%%
%}
```

```
%% Dimension of Electric Field and time
%
if NvN == 0.0
NvN   = sqrt(Nfourier);          % largest von Neumann Basis ...
    Dimension;
end

%% Angular Frequency Bandwidth
%
FreqBW   = MaxW−MinW;

%% Fourier Angular Frequency Increment
%
dW = FreqBW/(Nfourier−1);

%% Total Time Bandwidth (range)
%
TimeBW = 2*pi/dW;
%
MaxT = TimeBW/2;
MinT = − TimeBW/2;

%% von Neumann Alpha
%
alpha    = TimeBW/(2*FreqBW);

%% von Neumann basis time and angular frequency increments
%
delW   = FreqBW/(NvN);
delT   = TimeBW/(NvN);

%% von Neumann Representation Structure
% ────────────────────────────────────
%
vN.alpha   = alpha;
vN.N       = NvN;
vN.MaxW    = MaxW;
vN.MinW    = MinW;
vN.MaxT    = MaxT;
vN.MinT    = MinT;
vN.TimeBW  = TimeBW;
vN.FreqBW  = FreqBW;
vN.delW    = delW;
vN.delT    = delT;

%% von Neumann Basis Representation Grid Vectors
% ─────────────────────────────────────────────
%
fct = (1−1/NvN);
```

```
vN.time  = linspace(MinT*fct,MaxT*fct,NvN);
vN.omega = linspace(MinW+0.5*delW,MaxW-0.5*delW,NvN);
```

D.2.4. vNOverlapAMS.m

```
function S = vNOverlapAMS(omega,time,alpha,N)
%% von Neumann Overlap Matrix
%{
%%%%%%%%%%%%%%%%%%%%%%%%%%%%%%%%%%%%%%%%%%%%%%%%%%%%%%%%%%%%%%%%%%%%%%%%%%
FUNCTION : S = vNOverlapAMS(omega,time,alpha,N)
--------

DESCRIPTION : Calculates the von Neumann overlap matrix given the von
-----------   Neumann spectral and temporal reticule with the ...
    associated
              von Neumann basis alpha parameter (variance). This
              calculates S using matrix techniques to speed up the
              process.
              Related is S = vNOverlapM(omega,time,alpha,N)

INPUT : omega - discrete von Neumann Grid frequency vector
-----   time  - discrete von Neumann Grid time vector
        alpha - von Neumann alpha parameter (variance)
        N     - von Neumann dimension (Sqrt dimension of Electric ...
            Field)

OUTPUT : S - von Neumann Overlap matrix
------

AUTHOR : A M Smit
------

DATE : December 2011
----
%%%%%%%%%%%%%%%%%%%%%%%%%%%%%%%%%%%%%%%%%%%%%%%%%%%%%%%%%%%%%%%%%%%%%%%%%%%
%}
%% Basis AMplitudes
%
% OLAmp    = sqrt(2*alpha/pi);       % This used in Tannor in error
OLw      = alpha/2;
OLt      = 1/(8*alpha);
%% Intermediate variables
%
N2       = N*N;
N2m1     = N2-N+1;
Nvec     = [1:N]-1;
Nones    = ones(1,N);
```

```
Omvec    = omega.'*Nones;
tmvec    = time.'*Nones;
Omvd     = Omvec - Omvec.';         % vNomega(n)-vNomega(i)
Omd2     = -OLw*(Omvd.^2);
tmvd     = tmvec - tmvec.';         % vNtime(m)-vNtime(j)
tmd2     = -OLt*(tmvd.^2);
tmpl     = 1i/2*(tmvec + tmvec.'); % vNtime(m)+vNtime(j)
%% von Neumann Overlap Matrix
%
S = zeros(N2,N2);
%
k = 0;
for ij = 1:N:N2m1       % step row    omega  (Sub-matrix time)
    k = k + 1;
    l = 0;
    for kl=1:N:N2m1     % step column omega  (Sub-matrix time)
        l = l + 1;
        S(ij+Nvec,kl+Nvec) = exp(Omd2(k,l)+tmd2+Omvd(l,k)*tmpl);
    end
end
```

D.2.5. vNSpecB.m

```
function vNSB = vNSpecB(EFw,alpha,omega,time)
%% von Neumann Spectral Basis Functions
%{
%%%%%%%%%%%%%%%%%%%%%%%%%%%%%%%%%%%%%%%%%%%%%%%%%%%%%%%%%%%%%%%%%%%%%%%%%
FUNCTION : vNSB = vNSpecB(EFw,alpha,omega,time)
--------

DESCRIPTION : Given the von Neumann Grid and Spectral Electric Field
-----------   sampling generates the Spectral von Neumann Basis

INPUT :      EFw    - Spectral (Fourier Transform) Electric Field ...
   Angular
-----                Frequency increment vector [dim(EFw)=N^2 ]
             alpha  - von Neumann Basis alpha
             omega  - von Neumann Grid Discrete angular frequency ...
                vector
             time   - von Neumann Grid Discrete time vector ...
                [dim(time)=N]

OUTPUT :     vNSB   - von Neuman Spectral Basis
------

AUTHOR : A M Smit
------

DATE : August 2012
----
%%%%%%%%%%%%%%%%%%%%%%%%%%%%%%%%%%%%%%%%%%%%%%%%%%%%%%%%%%%%%%%%%%%%%%%%%%
%}

%% Inialization
%
N        = numel(time);
No       = numel(omega);
EFN      = numel(EFw);
N2       = N*N;

%% The von Neumann Spectral Basis
%  ------------------------------
%
Aw = (2*alpha/pi)^.25;               % von Neumann Spectral Basis ...
   Amplitude
vNSB= zeros(N2,EFN);                 % von Neumann Spectral Basis
                                     % Row indices index basis wt
                                     % Column Frequency development
r_cnt = 0;
for nn = 1:N                         % Frequency
    EFwd = EFw-omega(nn);
    for mm = 1:N                     % Time
        r_cnt = r_cnt + 1;
        vNSB(r_cnt,:) = Aw*exp(-alpha*EFwd.^2-1i*time(mm)*EFwd);
    end
end
```

D.2.6. vNTempB.m

```
function vNTB = vNTempB(EFtime,alpha,omega,time)
%% von Neumann Temporal Basis Functions
%{
%%%%%%%%%%%%%%%%%%%%%%%%%%%%%%%%%%%%%%%%%%%%%%%%%%%%%%%%%%%%%%%%%%%%%%%%%
FUNCTION : vNTB = vNTempB(EFtime,alpha,omega,time)
--------

DESCRIPTION : Given the von Neumann Grid and Temporal Electric Field
-----------   sampling generates the Temporal von Neumann Basis

INPUT :      EFtime - Temporal Electric Field Time
-----                 increment vector [dim(EFw)=N^2 ]
             alpha  - von Neumann Basis alpha
             omega  - von Neumann Grid Discrete angular frequency ...
                vector
             time   - von Neumann Grid Discrete time vector ...
                 [dim(time)=N]



OUTPUT :     vNBT   - Temporal von Neumann Basis
------

AUTHOR : A M Smit
------

DATE : August 2012
----
%%%%%%%%%%%%%%%%%%%%%%%%%%%%%%%%%%%%%%%%%%%%%%%%%%%%%%%%%%%%%%%%%%%%%%%%%%%
%}

%% Initialization
%
N        = numel(time);             % von Neumann Grid Dimension
No       = numel(omega);            % von Neumann Grid Dimension
EFN      = numel(EFtime);           % Electric Field time ...
    increments N2
N2       = N*N;                     % N2 should equal EFN

%% The von Neumann Temporal Basis
%  -------------------------------
% NB NB Phase has been made Plus +++++
%
At = (1/(2*alpha*pi))^.25;         % von Neumann Basis Temporal ...
    Amplitude
sfct   = - 1/(4*alpha);
vNTB   = zeros(N2,EFN);            % von Neumann Temporal Basis
                                   % Row indices index basis wt
                                   % Column Time development
r_cnt = 0;
for nn = 1:N                       % Frequency
    for mm = 1:N                   % Time
        r_cnt = r_cnt + 1;
        vNTB(r_cnt,:)= ...
            At*exp(sfct*(EFtime-time(mm)).^2+1i*omega(nn)*EFtime);
    end
end
```

D.2.7. vNTFR2Spec.m

```
function EFvNSpec = vNTFR2Spec(Qwt,vNSB,N)
%% von Neumann TFR to Spectral Signal
```

```
%{
%%%%%%%%%%%%%%%%%%%%%%%%%%%%%%%%%%%%%%%%%%%%%%%%%%%%%%%%%%%%%%%%%%%%%%%%%
FUNCTION : EFvNSpec = vNTFR2Spec(Qwt,vNSB)
--------

DESCRIPTION : Given the von Neumann Representation Qwt of an Electric
-----------   Field, this function regenerates the spectral (Fourier
              Transform) Electric Field via the inverse von Neumann

INPUT :      Qwt    - von Neumann Representation Time-Frequency
-----                 Representation vector
             vNSB   - von Neumann Spectral basis
 NB NB       Requires that the von Neumann matrix be reshaped to ...
    a vector
                         Qwt = reshape(QvN,1,N2);

OUTPUT :     EFvN   - Spectral Electric Field Recreated
------

AUTHOR : A M Smit
------

DATE : August 2012
----
%%%%%%%%%%%%%%%%%%%%%%%%%%%%%%%%%%%%%%%%%%%%%%%%%%%%%%%%%%%%%%%%%%%%%%%%%%
%}

%% von Neumann Representation Frequency Inverse
% --------------------------------------------
%
EFvNSpec = zeros(1,N*N);
%
r_cnt = 0;
for nn=1:N                          % Frequency
    for mm=1:N                      % Time
        r_cnt = r_cnt + 1;
        EFvNSpec   = EFvNSpec+Qwt(r_cnt)*vNSB(r_cnt,:);   % vNSB is ...
           now a row vector
    end
end
```

D.2.8. vNTFR2Temp.m

```
function EFvNTemp = vNTFR2Temp(Qwt,vNTB,N)
%% von Neumann TFR to Temporal Signal
%{
%%%%%%%%%%%%%%%%%%%%%%%%%%%%%%%%%%%%%%%%%%%%%%%%%%%%%%%%%%%%%%%%%%%%%%%%%
FUNCTION : EFvNTemp = vNTFR2Temp(Qwt,vNTB,N)
--------

DESCRIPTION : Given the von Neumann Representation Qwt of an Electric
-----------   Field, this function regenerates the spectral (Fourier
              Transform) Electric Field via the inverse von Neumann

INPUT :      Qwt    - von Neumann Representation Time-Frequency
-----                 Representation vector
             vNSB   - von Neumann Temporal basis
 NB NB       Requires that the von Neumann matrix be reshaped to ...
    a vector
                        Qwt = reshape(vNTFR,1,N2);

OUTPUT :     EFvNTemp - Temporal Electric Field Recreated
------

AUTHOR : A M Smit
------

DATE : August 2012
----
%%%%%%%%%%%%%%%%%%%%%%%%%%%%%%%%%%%%%%%%%%%%%%%%%%%%%%%%%%%%%%%%%%%%%%%%%%%
%}

%%
% von Neumann Representation Temporal Inverse
% --------------------------------------------
%
EFvNTemp = zeros(1,N*N);                % Row vector
%
r_cnt = 0;
for nn=1:N                          % Frequency
    for mm=1:N                      % Time (Summation of row ...
       vectors N^2)
        r_cnt = r_cnt + 1;
        EFvNTemp = EFvNTemp+Qwt(r_cnt)*vNTB(r_cnt,:); % vNTB is ...
           now a row vector
    end
end
```

D.2.9. vNTFRPlots.m

```
%% Used in Main Genetic Algorithm to Convert to von Neumann
%{
%%%%%%%%%%%%%%%%%%%%%%%%%%%%%%%%%%%%%%%%%%%%%%%%%%%%%%%%%%%%%%%%%%%%%%%%%%
```

```
FUNCTION :     NOT A FUNCTION --- CALLED DIRECTLY FROM ...
   RunMoleculeAMSvN
--------

DESCRIPTION : Called by RunMoleculeAMSvN to generate the von Neumann
-----------   Time-Frequency-Rpresentation of the Spectral ...
   Electric Field
              after being masked by the Spatial Light Modulator (SLM)
              This is the input Electric Field

INPUT :      x - The vector incorporating the SLM paramerers ...
   (Amplitude
-----

OUTPUT : von Neumann Basis Plots
------

AUTHOR : A M Smit (Version 1)
------

DATE : August 2012
----
%%%%%%%%%%%%%%%%%%%%%%%%%%%%%%%%%%%%%%%%%%%%%%%%%%%%%%%%%%%%%%%%%%%%%%%%%%%
%}


%% I. von Neumann TFR Representation
%%%%%%%%%%%%%%%%%%%%%%%%%%%%%%%%%%%%%%%%%%%%%%%%%%%%%%%%%%%%%%%%%%%%%%%%%%%

%% Choose the von Neumann Grid dimension NvN
%
NvN = round(25);
NF  = NvN*NvN;

%% Resample the Electric Field Fourier Transform to Match
% Firstly only over the SLM
EFFstep = SLMOut.delNRnew/NF ;
nwl = numel(SLMOut.VecLeft);
nwr = numel(SLMOut.VecLeft)+SLMOut.delNRnew;
EFFM = EFF2(nwl+1:EFFstep:nwr);

%% Frequency Bandwidth Range
%
wmin = SLMOut.wl;
wmax = SLMOut.wr;

%
%% Frequency von Neumann Fourier Samples for Resampling
EFFsmpl= linspace(wmin,wmax,NF);
```

```

%
% Save the data for later processing
% save EFS_15_5_1_100 NvN NF EFFsmpl EFFM wmin wmax;
save EFS_26_11_300 NvN NF EFFsmpl EFFM wmin wmax;

%% von Neumann Grid Lattice
%
vN = vNGrid(wmin,wmax,NF,NvN);

%% Unpack the von Neumann Structure to program variables
%
to = vN.MinT;                    % Initial Time
tf = vN.MaxT;                    % Final Time
alpha = vN.alpha;                % von Neumann basis alpha
time  = vN.time;                 % von Neumann Grid time vector
omega = vN.omega;                % von Neumann Grid angular ...
    frequency vector
% wsmpl = linspace(wmin,wmax,NF);   % EF sampled angular ...
    frequency vector(EFFsmpl)
tsmpl = linspace(to,tf,NF);   % EF sampled time vector
%
inttt = 0;

%%  von Neumann Overlap matrix
%
vNOLM = vNOverlapAMS(omega,time,alpha,NvN);

%%  von Neumann Spectral representation
%
vNSB  = vNSpecB(EFFsmpl,alpha,omega,time);

%% von Neuman TFR
%
QvN1  = Spec2vNTFR(EFFM,EFFsmpl,vNOLM,vNSB,inttt);

%% Spectral representation
Qwt   = reshape(QvN1,1,NF);
EFvN1 = vNTFR2Spec(Qwt,vNSB,NvN);

%%  PLOTS
%
%Plots to Check Sampling
%
if (plotit)
    load ...
       C:\Users\asmit1\Documents\MATLAB\ASmit\LaserControl\UF_6\wnUF6.mat;
    wnl = ones(size(wn));
    Fgrn = 11;
```

```
figure(Fgrn)
EFFww = LPOut.w(SLMOut.posL:SLMOut.posR);
plot(EFFww*PC.fs,abs(EFF2(SLMOut.posL:SLMOut.posR)),'r');
hold on;
plot(EFFsmpl*PC.fs,abs(EFFM),'g');
plot(wn*PC.fs,wnl,'b*');
xlabel('Angular Frequency [fs^{-1}]');
grid;
hold off;


Fgrn = Fgrn +1;
figure(Fgrn)
plot(EFFsmpl*PC.fs,abs(EFFM));
title('Electric Field FT Amplitude UF_6 2nd Level');
%xlim([2.27  2.442])
xlabel('\omega [fs^{-1}]');
ylabel('Amplitude');
grid on;
hold on;
% plot(wsmpl*PC.fs,abs(EF),'g.');
plot(EFFsmpl*PC.fs,abs(EFvN1),'r.');
%plot(w*fs,abs(EFvNw1),'y.');

hold off;

Fgrn = Fgrn +1;
figure(Fgrn)
plot(EFFsmpl*PC.fs,angle(EFFM),'b.');
title('Electric Field FT Phase UF_6 2nd Level');
%xlim([2.27  2.442]);
xlabel('\omega [fs^{-1}]');
ylabel('Phase [rad]');
grid on;
hold on;
% plot(wsmpl*PC.fs,angle(EF),'g.');
plot(EFFsmpl*PC.fs,angle(EFvN1),'r.');
hold off;

Fgrn = Fgrn +1;
figure(Fgrn)
% imagesc(x,y,fct(x,y)) with QvN1 the y-axis points down
% therefore the flipud
%imagesc(omega*PC.fs,time/PC.fs,abs(flipud(QvN1)));
imagesc(time/PC.fs,omega*PC.fs,abs(QvN1.'));
%colormap(clrmp);
ylabel('\omega [fs^{-1}]');
xlabel('Time (fs)');
title('von Neumann TFR Amplitude UF_6 2nd Level');
```

```
colorbar;
% AXIS XY  puts MATLAB into its default "Cartesian" axes mode.  The
%         coordinate system origin is at the lower left corner.  ...
    The x
%         axis is horizontal and is numbered from left to right.  ...
    The y
%         axis is vertical and is numbered from bottom to top.
axis xy;

Fgrn = Fgrn +1;
figure(Fgrn)
% imagesc(x,y,fct(x,y)) with QvN1 the y-axis points down
% therefore the flipud
%imagesc(omega*PC.fs,time/PC.fs,angle(flipud(QvN1)));
imagesc(time/PC.fs,omega*PC.fs,angle(QvN1.'));
%colormap(clrmp);
ylabel('\omega [fs^{-1}]');
xlabel('Time (fs)');
title('von Neumann TFR Phase UF_6 2nd Level');
colorbar;
axis xy;
end
```

D.3. Coherent State Analogy Functions

```
function GSCohStTFR = FGH_T2GSCohSt(FGHTFR)
%%
%%%%%%%%%%%%%%%%%%%%%%%%%%%%%%%%%%%%%%%%%%%%%%%%%%%%%%%%%%%%%%%%%%%%%%%%%%%
% FUNCTION : GSCohSt = FGH_T2GSCohSt(FGHTFR)
% ----------
%
% DESCRIPTION : Given the Temporal the Fourier-Gauss-Hermite (FGH)TFR
% -------------   Determine the Glauber-Sudarshan Coherent State ...
    Complex
%                 coefficient (alpha)
%
%
% INPUT :       FGHTFR - FGH Time-Frequency Representation
% ------
%
% OUTPUT :      GSCohSt - NxN Frequency time
% -------
%
% AUTHOR : A M Smit
% -------
%
```

```
% DATE : June 2013
% -----
%%%%%%%%%%%%%%%%%%%%%%%%%%%%%%%%%%%%%%%%%%%%%%%%%%%%%%%%%%%%%%%%%%%%%%%%%%%
%%
%
[r,c,d] = size(FGHTFR);
N = r;
GSCohStTFR = zeros(N,N);
GSCohSt    = zeros(N,N);
CSalpha    = zeros(N,N);
CScmn2     = zeros(N,N);
II         = ones(N,N);
eps2       = 1.0e-16;
thres      = 1.0e-1;

for ll=1:N
    for mm=1:N
        start_point = [1.0 +1i*1.0e-17;1.0 +1i*1.0e-17];
        HGC = squeeze(FGHTFR(ll,mm,:));
        model = @(params)GSCohS(params,HGC);
        estimates = fminsearch(model, start_point);
%%
% ...
   %%%%%%%%%%%%%%%%%%%%%%%%%%%%%%%%%%%%%%%%%%%%%%%%%%%%%%%%%%%%%%%%%%%%%%%%%
% 2. The FGH Glauber-Sudarshan Coherent state TFR
% -----------------------------------------------
        [sse, GSC, cmn1] = GSCohS(estimates,HGC);
        CSalpha(ll,mm)  = estimates(1);
        cf2             = estimates(2)*estimates(2)';
        CScmn2(ll,mm)   = cf2;
        if cf2 > thres
            GSCohSt(ll,mm)  = sse/cf2;
        else
            GSCohSt(ll,mm)  = 1.0;
        end
    end
end
figure(5);
imagesc(CScmn2)
colorbar;
mGScmn  = max(max(abs(CScmn2)));
mGSS  = max(max(abs(GSCohSt)));
GSCohStTFR = II-GSCohSt/mGSS;

%
% Coherent State Function Glauber-Sudarshan
    function [sse, GScoef, cmn] = GSCohS(params,HGCc)
        alpha   = params(1);
        cmn     = params(2);
        GScoef = zeros(N,1);
        for kk=0:N−1
            if kk == 0
                nfct = 1;
                GScoef(kk+1) = 1;
            else
                nfct = nfct⋆kk;
                GScoef(kk+1) = alpha^kk/sqrt(nfct);
            end
        end
        ErrorVector = cmn⋆exp(−alpha⋆alpha'/2)⋆GScoef − HGCc;
        sse = ErrorVector'⋆ErrorVector;
    end
end
```

Bibliography

[1] Constantin Brif, Raj Chakrabarti, and Herschel Rabitz. Control of quantum phenomena: past, present and future. *New Journal of Physics*, 12(7):075008, 2010.

[2] Domenico d'Alessandro. *Introduction to quantum control and dynamics*. CRC press, 2007.

[3] S. A. Rice and M. Zhao. *Optical Control of Molecular Dynamics*. Wiley-InterscienceWiley-Interscience, New York, 2000.

[4] Paul Adrien Maurice Dirac. *The principles of quantum mechanics*. Cambridge, 1930.

[5] Stephen Gasiorowicz. *Quantum physics*. John Wiley & Sons, 2007.

[6] Eugen Merzbacher. *Quantum mechanics*. John Wiley & Sons, New York, 1970.

[7] Albert Messiah. *Quantum Mechanics*. Dover Publ., Trans., 2nd edition, 1958.

[8] D. J. Tannor. *Introduction to Quantum Mechanics: A Time-Dependent Perspective*. London: Palgrave Macmillan, 2007.

[9] Robert F. Stengel. *Optimal control and estimation*. Courier Dover Publications, 2012.

[10] Arthur Earl Bryson and Ho. *Applied optimal control: optimization, estimation and control*. CRC Press, 1975.

[11] Donald E. Kirk. *Optimal control theory: an introduction*. Courier Dover Publications, 2012.

[12] Huibert Kwakernaak and Raphael Sivan. *Linear optimal control systems*, volume 1. Wiley-interscience New York, 1972.

[13] John J. D'azzo and Constantine H. Houpis. *Feedback control system analysis and synthesis*. McGraw-Hill, 1966.

[14] Peter S. Maybeck. *Stochastic models, estimation, and control*, volume 1. Academic press, 1982.

[15] Peter S. Maybeck. *Stochastic models, estimation, and control*, volume 2. Academic press, 1982.

[16] Peter S. Maybeck. *Stochastic models, estimation, and control*, volume 3. Academic press, 1982.

[17] Jean-Jacques E. Slotine and Weiping Li. *Applied nonlinear control*, volume 199. Prentice-Hall Englewood Cliffs, NJ, 1991.

[18] Eugene Hecht and A. Zajac. *Optics*. Addison-Wesley, 1974.

[19] Max Born and Emil Wolf. *Principles of optics: electromagnetic theory of propagation, interference and diffraction of light*. CUP Archive, 1999.

[20] Joseph Goodman. *Introduction to Fourier optics*. McGraw-hill, second edition, 2008.

[21] Joseph W. Goodman. *Statistical optics*, volume 1. Wiley-Interscience, New York, 1985.

[22] Rodney Loudon. *The quantum theory of light*. Oxford university press, second edition, 1983.

[23] Daniel A. Steck. *Quantum and atom optics*, volume 46. University of Oregon, 2007.

[24] C. Gerry and P.S. Knight. *Introductory Quantum Optics*. Cambridge, 2006.

[25] Eugene Wigner. *Group theory: and its application to the quantum mechanics of atomic spectra*, volume 5. Elsevier, 2012.

[26] Hermann Weyl. *The theory of groups and quantum mechanics*. Courier Dover Publications, 1950.

[27] Bartel Leendert Van der Waerden. *Group theory and quantum mechanics*. Springer, 1974.

[28] Michael Tinkham. *Group theory and quantum mechanics*. Courier Dover Publications, 2003.

[29] Jin-Quan Chen, Jialun Ping, and Fan Wang. *Group representation theory for physicists*, volume 7. World Scientific, 1989.

[30] Philip R. Bunker and Per Jensen. *Molecular symmetry and spectroscopy*. NRC Research Press, 1998.

[31] Edgar Bright Wilson. *Molecular vibrations: the theory of infrared and Raman vibrational spectra*. Courier Dover Publications, 1955.

[32] Robert Gilmore. *Lie groups, Lie algebras, and some of their applications*. Courier Dover Publications, 2012.

[33] Leon Cohen. *Time-Frequency Analysis*. Prentice-Hall PTR, New Jersey, 1995.

[34] K. Gröchenig. *Foundations of Time-Frequency Analysis*. Birkhäuser, Boston, 2001.

[35] W. P. Schleich. *Quantum Optics in Phase Space*. Wiley-VCH, 2001.

[36] M.O. Scully and M.S. Zubairy. *Quantum optics*. Cambridge University Press, New York, 1994.

[37] P.W. Milonni. *The Quantum Vacuum: An Introduction to Quantum Electrodynamics*. Academic Press, 1994.

[38] L. Mandel and E. Wolf. *Optical Coherence and Quantum Optics*. Cambridge University Press, 1995.

[39] L.E. de Clercq. Numerical modelling of the excitation of polyatomic molecules by femtosecond laser beams. Master's thesis, University of Stellenbosch, 2011.

[40] A.H. Jaswinski. *Stochastic Processes and Filtering Theory*. Mineola, NY.: Dover Publications, 2007.

[41] Terrence P. McGarty. *Stochastic systems and state estimation*. Wiley, 1974.

[42] Alberto Isidori. *Nonlinear control systems*, volume 1. Springer, 1995.

[43] Robert F. Stengel. *Stochastic optimal control: theory and application*. John Wiley & Sons, Inc., 1986.

[44] Paul Brumer and Moshe Shapiro. Control of unimolecular reactions using coherent light. *Chemical physics letters*, 126(6):541–546, 1986.

[45] P. W. Brumer and M. Shapiro. *Principles of the Quantum Control of Molecular Processes*. New York: Wiley, New York, 1 edition, 2003.

[46] Moshe Shapiro and Paul Brumer. Coherent control of molecular dynamics. *Reports on Progress in Physics*, 66(6):859, 2003.

[47] David J. Tannor and Stuart A. Rice. Control of selectivity of chemical reaction via control of wave packet evolution. *The Journal of Chemical Physics*, 83:5013, 1985.

[48] D. J. Tannor, R. Kosloff, and S. A. Rice. Coherent pulse sequence induced control of selectivity of reactions-exact quantum-mechanical calculations. *Journal of Chemical Physics*, 85:5805, 1986.

[49] Viktor N. Bagratashvili, V.S. Letokhov, A.A. Makarov, and E.A. Ryabov. *Multiple photon infrared laser photophysics and photochemistry*. Harwood Academic Publishers Chur, Switzerland, 1985.

[50] D. J. Tannor and Y. Jin. *Mode selective Chemistry*. Kluwer Academic Publishers, 1991.

[51] Alexander Pechen, Constantin Brif, Rebing Wu, Raj Chakrabarti, and Herschel Rabitz. General unifying features of controlled quantum phenomena. *Physical Review A*, 82(3):030101, 2010.

[52] A.P. Peirce, M.A. Dahleh, and H. Rabitz. Optimal control of quantum-mechanical systems: existence, numerical approximation and applications. *Physics Review A*, 37:4950, 1988.

[53] Herschel Rabitz, Regina de Vivie-Riedle, Marcus Motzkus, and Karl Kompa. Whither the future of controlling quantum phenomena? *Science*, 288(5467): 824–828, 2000.

[54] Richard S Judson and Herschel Rabitz. Teaching lasers to control molecules. *Physical Review Letters*, 68(10):1500, 1992.

[55] L.E. de Clercq, L.R. Botha, E.G. Rohwer, H. Uys, and A. du Plessis. Optimal control of the population dynamics of the ground vibrational state of a polyatomic molecule. In *Proceedings of SPIE*, page 7925. SPIE, 2011.

[56] Max Born and Robert Oppenheimer. Zur Quantentheorie der Molekeln. *Annalen der Physik*, 389(20):457–484, 1927.

[57] Philip M. Morse. Diatomic molecules according to the wave mechanics. II. vibrational levels. *Physical Review*, 34(1):57, 1929.

[58] Gordon M. Barrow. *Introduction to molecular spectroscopy*. McGraw-Hill, 1962.

[59] Nagendra S. Nath. The normal vibrations of molecules having octahedral symmetry. In *Proceedings of the Indian Academy of Sciences, Section A*, volume 1, pages 250–259. Indian Academy of Sciences, 1934.

[60] Fatih Ucun and M Gokhan Sengül. Determination of force constants of octahedral XY_6 molecules by the GF matrix method. *Zeitschrift für Naturforschung. A, A Journal of physical sciences*, 60(11-12):819–822, 2005.

[61] L. Halonen and M.S. Child. Model stretching overtone eigenvalues for SF_6, WF_6, and UF_6. *The Journal of Chemical Physics*, 79(2):559–570, 1983.

[62] Rick Trebino, Kenneth W DeLong, David N Fittinghoff, John N Sweetser, Marco A Krumbügel, Bruce A Richman, and Daniel J Kane. Measuring ultrashort laser pulses in the time-frequency domain using frequency-resolved optical gating. *Review of Scientific Instruments*, 68(9):3277–3295, 1997.

[63] E. Wigner. On the Quantum Correction For Thermodynamic Equilibrium. *Physical Review*, 40:749–759, 1932.

[64] Denis Gabor. Theory of communication. *J. Inst. Elect. Eng.*, 93:429, 1946.

[65] J. Ville. Theorie et Applications de la Notion de Signal Analytique. *Cables et Transmission*, 2:61–74, 1948.

[66] Leon Cohen. Generalized phase-space distribution functions. *Journal of Mathematical Physics*, 7(5):781–786, 1966.

[67] S. Allen Broughton and Kurt M. Bryan. *Discrete Fourier analysis and wavelets: applications to signal and image processing*. Wiley. com, 2011.

[68] L. Cohen. Time-Frequency Distributions-A Review. *Proceedings of the IEEE*, 77(7):941–981, 1989.

[69] Athanasios Papoulis. *Signal analysis*, volume 191. McGraw-Hill New York, 1978.

[70] Athanasios Papoulis and S. Unnikrishna Pillai. *Probability, random variables, and stochastic processes*. Tata McGraw-Hill Education, 2002.

[71] C. Helstrom. An expansion of a signal in Gaussian elementary signals (Corresp.). *Information Theory, IEEE Transactions on*, 12(1):81–82, 1966.

[72] Martin J. Bastiaans. Gabor's expansion of a signal into Gaussian elementary signals. *Proceedings of the IEEE*, 68(4):538–539, 1980.

[73] Martin J. Bastiaans. A sampling theorem for the complex spectrogram, and Gabor's expansion of a signal in Gaussian elementary signals. *Optical Engineering*, 20(4):204597–204597, 1981.

[74] J. Wexler and S. Raz. Discrete Gabor expansions. *Signal processing*, 21(3): 207–220, 1990.

[75] R.S. Orr. Derivation of the finite discrete Gabor transform by periodization and sampling. *Signal Process.*, 34:85, 1993.

[76] R.S. Orr. A Gabor sampling theorem and some time-bandwidth implications. In *Proc. IEEE Int. Conf. on Acoustics, Speech and Signal Processing (ICASSP-94)*, volume 3, pages III/1–III/3. (Piscataway, NJ: IEEE), 1994.

[77] Martin J. Bastiaans and Marc C.W. Geilen. On the discrete Gabor transform and the discrete Zak transform. *Signal processing*, 49(3):151–166, 1996.

[78] A. Shimshovitz and D. J. Tannor. Periodic Gabor Functions with Biorthogonal Exchange: A Highly Accurate and Efficient Method for Signal Compression. *ArXiv e-prints*, 1:1, July 2012.

[79] J. Zak. *Solid State Physics*. Academic, New York, 1972.

[80] John G. Proakis and Dimitris G. Manolakis. *Digital signal processing: principles algorithms and applications*. Macmillan Publishing Company, second edition edition, 1992.

[81] Monson H. Hayes. *Statistical digital signal processing and modeling*. John Wiley & Sons, 2009.

[82] Richard P Feynman. Relativistic cut-off for quantum electrodynamics. *Physical Review*, 74(10):1430, 1948.

[83] Richard Phillips Feynman. Space-time approach to quantum electrodynamics. *Physical Review*, 76(6):769, 1949.

[84] M. Kac. On distributions of certain wiener functionals. *Transactions of American Mathematical Society*, 65:1–13, 1949.

[85] Fabrice Douglas Rouah. The feynman- kac theorem. 2008.

[86] Martin J. Bastiaans. Application of the Wigner distribution function in optics. In *Theory and Applications in Signal Processing*, pages 375–426. Elsevier Science, 1997.

[87] Richard P. Feynman. Negative probability. *Quantum implications: essays in honour of David Bohm*, pages 235–248, 1987.

[88] Marlan O. Scully, Herbert Walther, and Wolfgang Schleich. Feynman approach to negative proabailities. *Physics Review A*, 49(3):1562, 1994.

[89] G.C. Summerfield and P. F. Zweifel. Relationships among Generalized Phase-Space Distributions. *Journal Of Mathematical Physics*, 10(2):233–235, 1969.

[90] K. Husimi. Some Formal Properties of the Density Matrix,. *Proc. Phys. Math. Soc. Jpn.*, 22:264–314, 1940.

[91] J. von Neumann. Die Eindeutigkeit der Schrödingerschen Operatoren. *Math. Ann.*, 104:570, 1931.

[92] M. Boon and J. Zak. Discrete coherent states on the von Neumann lattice. *Physics Review B*, 18:6744–6751, 1978.

[93] J. Zak. von Neumann's hypothesis concerning coherent states. *Journal of Physics A: Mathematical and General*, 36(42):L553, 2003.

[94] Susanne Fechner, Frank Dimler, Tobias Brixner, Gustav Gerber, and David J. Tannor. The von Neumann picture: a new representation for ultrashort laser pulses. *Optics express*, 15(23):15387–15401, 2007.

[95] A. Rodenberg, S. Fechner, F. Dimler, D.J. Tannor, and T. Brixner. Experimental implementation of ultrashort laser pulses in the von Niemann picture. *Applied Physics B*, 93:763–772, 2008.

[96] Frank Dimler, Susanne Fechner, Alexander Rodenberg, Tobias Brixner, and David J. Tannor. Accurate and efficient implementation of the von Neumann

representation for laser pulses with discrete and finite spectra. *New Journal of Physics*, 11(10):105052, 2009.

[97] S. Ruetzel, C. Stolzenberger, S. Fechner, F. Dimler, T. Brixner, and D. J. Tannor. Molecular quantum control landscapes in von Neumann time-frequency phase space. *Journal of Chemical Physics*, 133:164510, 2010.

[98] A. Shimshovitz and D. J. Tannor. Gaussian flexibility with Fourier accuracy: the periodic von Neumann basis set. *ArXiv e-prints*, 1:1, October 2010.

[99] S. Ruetzel, C. Stolzenberger, F. Dimler, D. J. Tannor, and T. Brixner. Adaptive coherent control using the von neumann basis. *Physical Chemistry Chemical Physics*, 13:8627–8636, 2011.

[100] A.M. Smit, L.R. Botha, and E.G. Rohwer. Time-Frequency representations of ultra short laser pulses for coherent control of quantum processes. In *SAIP 57th Annual Conference*, volume 57, page 34. SAIP, University of Pretoria, June 2012.

[101] A. Shimshovitz and D. J. Tannor. Phase Space Approach to Solving the Time-independent Schrödinger Equation. *Physical Review Letters*, 109: 070402, 2012.

[102] A. Shimshovitz and D. J. Tannor. Phase Space Wavelets for Solving Coulomb Problems. *Journal of Chemical Physics*, 137:101103, 2012.

[103] A. Hendriks, H. Uys, A. du Plessis, C. Steenkamp, L.R. Botha, and A.M. Smit. Faster convergence utilizing a combined time-frequency representation in a learning algorithm. In *The Copenhagen Conference on Femtochemistry*, volume 11, page 113. FEMTO11, Rosendahl,DTU, July 2013.

[104] D.J. Tannor, A. Shimsovitz, and N. Takemoto. Phase Space Approach to Quantum Mechanical Calculations for Large Systems: Thinking Inside the Box. In *Proc. CECAM Workshop on Many-dimensional quantum dynamics with (non)classical trajectories*. To be published, 2013.

[105] S Spiegel, Marray Rand Lipschutz. *Mathematcal Handbook of Formulas and Tables*. Schaum's Outline Series. MCGraw-Hill, intenational edition edition, 1996.

[106] Edwin T. Jaynes. *Probability theory: the logic of science*. Cambridge university press, 1996.

[107] L.I. Schiff. *Quantum Mechanics*. McGraw Hill, New York, 1968.

[108] E. Merzbacher. *Quantum Mechanics*. Wiley, New York, 2nd edition, 1970.

[109] S. Fechner, F. Dimler, T. Brixner, G. Gerber, and D. J. Tannor. The von Neumann picture: a new representation for ultrashort laser pulses. *Optics Express*, 15(23,):15387–15401, 2007.

[110] Ahmed H. Zewail et al. Femtochemistry: Past, present, and future. *Pure and applied chemistry*, 72(12):2219–2231, 2000.

[111] Marcos Dantus and Vadim V. Lozovoy. Experimental coherent laser control of physicochemical processes. *Chemical reviews*, 104(4):1813–1860, 2004.

[112] Regina de Vivie-Riedle and Ulrike Troppmann. Femtosecond lasers for quantum information technology. *Chemical reviews*, 107(11):5082–5100, 2007.

[113] Stefan Ruetzel, Christoph Stolzenberger, Frank Dimler, David J. Tannor, and Tobias Brixner. Adaptive coherent control using the von Neumann basis. *Physical Chemistry Chemical Physics*, 13(19):8627–8636, 2011.

[114] Ludwig E. De Clercq, Lourens R. Botha, Erich G. Rohwer, Hermann Uys, and Anton Du Plessis. Optimal control of the population dynamics of the ground vibrational state of a polyatomic molecule. In *SPIE LASE*, pages 79250V–79250V. International Society for Optics and Photonics, 2011.

[115] Szczepan Chelkowski and André D. Bandrauk. Control of vibrational excitation and dissociation of small molecules by chirped intense inflared laser pulses. *Chemical physics letters*, 186(2):264–269, 1991.

[116] D.J. Maas, D.I. Duncan, R.B. Vrijen, W.J. van der Zande, and L.D. Noordam. Vibrational ladder climbing in NO by (sub) picosecond frequency-chirped infrared laser pulses. *Chemical physics letters*, 290(1):75–80, 1998.

[117] Ulrike Troppmann, Carmen M. Tesch, and Regina de Vivie-Riedle. Preparation and addressability of molecular vibrational qubit states in the presence of anharmonic resonance. *Chemical physics letters*, 378(3):273–280, 2003.

[118] T. Witte, T. Hornung, L. Windhorn, D. Proch, R. de Vivie-Riedle, M. Motzkus, and K.L. Kompa. Controlling molecular ground-state dissociation by optimizing vibrational ladder climbing. *The Journal of chemical physics*, 118(5):2021–2024, 2003.

[119] Dmytro Shyshlov and Dmitri Babikov. Complexity and simplicity of optimal control theory pulses shaped for controlling vibrational qubits. *The Journal of chemical physics*, 137(19):194318, 2012.

[120] H. Rabitz, T-S Ho, M. Hsieh, Robert Kosut, and Metin Demiralp. Topology of optimally controlled quantum mechanical transition probability landscapes. *Physical Review A*, 74(1):012721, 2006.

[121] Alexander N. Pechen and David J. Tannor. Are there traps in quantum control landscapes? *Physical review letters*, 106(12):120402, 2011.

[122] Askol'd Mikhailovich Perelomov. On the completeness of a system of coherent states. *Theoretical and Mathematical Physics*, 6(2):156–164, 1971.

[123] O. Christensen. *An Introduction to Frames and Riesz Bases.* Birkhäuser, Boston, 2003.

[124] Sir Michael James Lighthill. *An introduction to Fourier analysis and generalised functions.* Cambridge University Press, 1958.

[125] Athanasios Papoulis. *The Fourier integral and its applications.* McGraw-Hill, 1962.

[126] Ronald Newbold Bracewell. *The Fourier transform and its applications*, volume 31999. McGraw-Hill New York, 1986.

[127] Walter Rudin. *Fourier analysis on groups.* John Wiley & Sons, 2011.

[128] Mary L. Boas. *Mathematical Methods in the Physical Sciences.* John Wiley & Sons., Inc, 2006.

[129] Milton Abramowitz and Irene A. Stegun. *Handbook of mathematical functions: with formulas, graphs, and mathematical tables.* Number 55. Courier Dover Publications, 1972.

[130] Frank W.J. Olver. *NIST handbook of mathematical functions.* Cambridge University Press, 2010.

[131] Gregory Call and Daniel Velleman. Pascal's Matrices. *American Math. Monthly*, 100:1, 1993.

[132] E.D. Potter, J.L. Herek, S. Pedersen, Q. Liu, and A.H. Zewail. Femtosecond laser control of a chemical reaction. *Nature*, 355(6355):66–68, 1992.

[133] A. H. Zewail. Femtochemistry: atomic-scale dynamics of the chemical bond. *J. Phys. Chem. A*, 104:5660, 2000.

[134] A.H. Zewail. *Femtochemistry Atomic scale dynamics of the chemical bond using ultrafast lasers.* Nobel Lectures in Chemistry. Singapore: World Scientific, 2003.

[135] L.R Botha, L.E. de Clercq, A.M. Smit, N. Botha, E. Ronander, and H.J. Strydom. Quantum coherent control of the vibrational dynamics of a polyatomic molecule using adaptive feedback control of a femtosecond laser. In *Proceedings of National Laser Symposium(NLS-21)*, volume 3, pages III/1–III/3. BARC, 2013.

[136] A.M. Weiner. Femtosecond pulse shaping using spatial light modulators. *Review of scientific instruments*, 71(5):1929–1960, 2000.

[137] F. Dimler, S. Fechner, A. Rodenberg, T. Brixner, and D. J. Tannor. Accurate and efficient implementation of the von Neumann representation for laser pulses with discrete and finite spectra. *New J. Phys.*, 11:105052, 2009.

[138] Wolfgang Pauli. The connection between spin and statistics. *Physical Review*, 58(8):716, 1940.

[139] Paul A.M. Dirac. The quantum theory of the emission and absorption of radiation. *Proceedings of the Royal Society of London. Series A, Containing Papers of a Mathematical and Physical Character*, pages 243–265, 1927.

[140] P. Jordan and E. Wigner. Über das Paulische Äquivalenzverbot. *Zeitschrift für Physik*, 47:631, 1928.

[141] Fred L Wilson. Fermi's theory of beta decay. *American Journal of Physics*, 36(12):1150–1160, 1968.

[142] Paul A.M. Dirac. Relativistic quantum mechanics. *Proceedings of the Royal Society of London. Series A*, 136(829):453–464, 1932.

[143] Paul A.M. Dirac. Forms of relativistic dynamics. *Reviews of Modern Physics*, 21(3):392, 1949.

[144] Paul A.M. Dirac. The Hamiltonian form of field dynamics. *Can. J. Math*, 3 (1):1–23, 1951.

[145] J.D. Bjorken and S.D. Drell. *Relativistic quantum fields*. McGraw-Hill, 1965.

[146] Franz Mandl and Graham Shaw. *Quantum field theory*. John Wiley & Sons, second edition, 2010.

[147] Jun John Sakurai. *Advanced quantum mechanics*. Pearson Education India, 2006.

[148] Rodney Loudon. *The quantum theory of light*. Oxford university press, third edition, 2000.

[149] Miguel A. Bandres, Julio C. Gutiérrez-Vega, et al. Ince–Gaussian modes of the paraxial wave equation and stable resonators. *JOSA A*, 21(5):873–880, 2004.

[150] M.O. Scully and M.S. Zubairy. *Quantum Optics*. Cambridge University Press, New York, 1997.

[151] J.K. Klauder and E.C.G. Sudarshan. *Fundamentals of Quantum Optics*. W.A. Benjamin, Inc New York, Amsterdam, 1968.

[152] J David Jackson. *Classical Electrodynamics*. John Wiley and Sons, second edition, 1975.

[153] Paul Lorrain and Dale Corson. *Electromagnetic Fields and Waves*. W.H. Freeman and Company, second edition, 1970.

[154] David J. Griffiths. *Introduction to electrodynamics*. Prentice-Hall, 1999.

[155] Claude Cohen-Tannoudji, Jacques Dupont-Roc, and Gilbert Grynberg. *Atom-photon interactions: basic processes and applications.* Wiley Online Library, 1992.

[156] Charles W. Misner, Kip S. Thorne, and John Archibald Wheeler. *Gravitation*, volume 56. Freeman, San Francisco, CA., 1973.

[157] Enrico Fermi. Quantum theory of radiation. *Reviews of modern physics*, 4 (1):87–132, 1932.

[158] David Griffiths. *Introduction to elementary particles.* John Wiley & Sons, 2008.

[159] R. Hanbury Brown and R.Q. Twiss. Interferometry of th Intensity Fluctuations in Light. I. Basic Theory: The Correltaiton between Photons in Coherent Beams of Radiation. *Proceedings o the Royal Society of London. Series A. Mathematical and Physical Sciences*, 242(1230):300–324, November 1957.

[160] L Mandel and E. Wolf. Correlation in the Fluctuating Outputs from Two Square-Law Detectors Illuminated by Light of Any State of Coherence and Polarization. *Physical Review*, 124(6):1696–1702, December 1961.

[161] E.C.G. Sudarshan. Equivalence of Semiclassical and Quantum Mechanical Descriptions of Statistical Light Beams. *Physical Review Letters*, 10(7):277–279, April 1963.

[162] R.J. Glauber. Photon Correlations. *Physical Review Letters*, 10(3):84–86, February 1963.

[163] R.J. Glauber. Coherent and Incoherent States of the Radiation FIeld. *Physical Review*, 131(6):2766–2788, September 1963.

[164] Roy J. Glauber. The Quantum Theory of Optical Coherence* . *Physical Review*, 130(6):2529–2539, June 1963.

[165] A. Perelomov. *Generalized Coherent States and Their Applications.* Texts and Monographs in Physics. Springer-Verlag, Berlin Heidelberg New York, first edition, 1986.

[166] O.H. Rousseau and P. Blaise. *Quantum Oscillators.* John Wiley & Sons, Inc., Hoboken, New Jersey, 2011.

[167] Jean-Pierre Gazeau. *Coherent States in Quantum Physics.* Wiley-VCH Verlag GmbH & Co. KGaA, 2009.

[168] M. Combescure and D. Robert. *Coherent States and Applications in Mathematical Physics.* Theoretical and Mathematical Physics. Springer, 2012.

[169] R. J. Glauber. *Quantum Theory of Optical Coherence - Selected Papers and Lectures*. Wiley-VCH, 2007.

[170] L Mandel and E. Wolf. Coherence Properties of Optical Fields. *Review of Modern Physics*, 37(2):231–287, 1965.

[171] Paul Busch. The Time-Energy Uncertainty Relation. In J.G. Muga, R.Sala Mayato, and L. Egusquiza, editors, *Time in Quantum Mechanics*, volume 734 of *Lecture Notes in Physics*, pages 73–105. Springer Berlin Heidelberg, 2007. ISBN 978-3-540-73472-7.

[172] Albert Einstein. On the quantum theory of radiation. *Laser Theory*, pages 5–21, 1972.

[173] Francesco Petruccione and Heinz-Peter Breuer. *The theory of open quantum systems*. Oxford Univ. Press, 2002.

[174] Crispin Gardiner and Peter Zoller. *Quantum noise: a handbook of Markovian and non-Markovian quantum stochastic methods with applications to quantum optics*, volume 56. Springer, 2004.

[175] René J. Beerends. *Fourier and Laplace transforms*. Cambridge University Press, 2003.

[176] E. O. Brigham. *The Fast Fourier Transform and its Applications*. Prentice Hall, New Jersey, 1988.

[177] Anders Vretblad. *Fourier analysis and its applications*, volume 223. Springer, 2003.

[178] Brad Osgood. *The Fourier transform and its applications*. Stanford University, 2009.